Inferential Measurement Models for Semi-autogenous Grinding Mills

T.A. APELT

May 2, 2007

A thesis submitted for the degree of
Doctor of Philosophy
of the
University of Sydney

Department of Chemical Engineering
University of Sydney
New South Wales 2006
AUSTRALIA

ABSTRACT

Semi-autogenous grinding (SAG) mill performance is influenced by ball charge, rock charge and feed properties which are difficult to measure directly. The development of inferential measurement models of SAG mill total charge and ball charge levels, feedrate and size distribution, and, mill discharge rate and size distribution and the further development of combined state and parameter estimation for SAG mills are the objectives of this research. Consultation with industry and a review of developments in this area found scope for further contribution. Results of circuit surveys of the Northparkes Mines Module 1 grinding circuit are utilised as reference data for model validation. The comminution models of the Julius Kruttschnitt Mineral Research Centre are utilised as reference for inferential model development.

Inferential models are presented for SAG mill total and ball charge fractions, fresh feedrate and size distribution and discharge rate and size distribution, according to the research objectives. Inferential models are also introduced for the SAG mill recirculating load, rock charge, and total feed rate and size distribution and the primary cyclone underflow split fraction. The inferential models could be utilised in a SAG mill load control strategy, as a measure of SAG mill performance, as an indication of the primary grinding circuit operating conditions, or, any combination of these functions.

Important model parameters are highlighted by sensitivity and uncertainty analyses presented for the inferential models of the SAG mill charge levels, discharge rate and size distribution and the fresh feedrate and size distribution. The results indicate that the mill charge level estimates obtained from the mill weight measurement contain the least uncertainty and are therefore the recommended choice for charge level estimation. Uncertainty may be minimised through the utilisation of the best available mill weight measurement and periodic measurement of mill inside diameter and length. The non-linear nature of the powerdraw model results in a high degree of uncertainty in the total charge estimates obtained from the powerdraw measurement.

Uncertainty in the mill discharge estimates may be minimised by ensuring that the accuracy of the oversize crusher and primary cyclone feed instrumentation is maintained through regular calibration and the periodic measurement of the SAG mill discharge screen aperture size and the process water specific gravity.

Uncertainty in the SAG mill fresh feed estimates may be minimised by ensuring the accuracy of the oversize crusher and primary cyclone feed instrumentation and the crusher gap setting. The SAG mill discharge grate parameters: pebble port size and relative open area fraction of the pebble ports, also strongly influence the size estimates and hence, should be fitted with due care.

Combined state and parameter estimation formulations are developed for the SAG mill, according to the final research objective. The formulations incorporate novel models of the SAG mill ball charge, protective shell lining, mill weight measurement and discharge measurement. The system is detectable although not completely observable. Filter tuning parameter selection is crucial to formulation performance. The results indicate that the superior formulation incorporates a size-by-size SAG mill discharge measurement model, which provides better capacity to estimate important mill discharge grate parameters. The formulations also provide a suitable, positively supportive context for the inferential models presented in this research.

Plant data was sourced and the inferential measurement models are validated against it. The results confirm that the inferential measurement models are valid. Results analysis also reveal the potential for utilisation of the inferential measurement models in a process monitoring/diagnostic capacity.

The models are analysed further in terms of sensitivity and their inherent nature, which illustrates a limitation in the feedsize estimate model that should be noted when dealing with model results. Mill weight and powerdraw contours and a SAG mill operating curve are generated and presented in charge fraction and charge fraction - kilowatt·tonne spaces. The contours and operating curve are discussed in the context of mill charge control.

A multi-variable, model predictive controller simulation is developed that utilises the inferential measurement models for setpoint and constraint-control. The development of the controller incorporates transfer function relationships and the description of the SAG mill variables of powerdraw, weight, rock charge and ball charge as integrating variables. The performance of the controller is documented and assessed.

Further research recommendations centre on further model validation against industrial data, further parameter sensitivity analyses, simulation model development and the investigation of the potential use of the inferential measurement models in a process monitoring capacity. Investigation of the dependence of the operating curve on ore hardness and investigation of control actions of a real controller, in relation to the operating curve, are other key areas to progress the research. Implementation recommendations are particularly relevant to Northparkes Mines but also have relevance for the wider minerals processing community.

Increasing the number of inferential measurement models available to industry and the body of knowledge supporting them adds further impetus to the transition taking the control methods of autogenous grinding circuit supervisory control and the on-line use of phenomenological models from the "active" or "emerging" phase to the "mature" phase.

PREFACE

This Thesis documents a study of inferential measurement models for semiautogeous grinding (SAG) mills. The key contributions contained within are as follows:

- Inferential model of the SAG mill discharge rate and size distribution (including size indicators: T_{80}, T_{60}, T_{40}, T_{20}).
- Inferential model of the SAG mill recirculating load.
- Inferential model of the SAG mill rock charge and size distribution.
- Inferential models of the SAG mill total charge and ball charge levels.
- Inferential model of the SAG mill total feed rate and size distribution.
- Inferential model of the SAG mill fresh feed rate and size distribution (including size indicators: F_{80}, F_{60}, F_{40}, F_{20}).
- Inferential model of the primary cyclone underflow split to the ball mill.
- Sensitivity and uncertainty analyses and assessment of mill discharge, charge level and fresh feed inferential models.
- Sensitivity and uncertainty analyses and assessment of mill breakage rates.
- Dynamic model of the SAG mill ball charge.
- Dynamic model of the SAG mill protective shell.
- One SAG mill weight model.
- Two SAG mill discharge models.
- Two combined state and parameter estimation (CSPE) model formulations for the estimation of thirty six (36) SAG mill states and five (5) parameters, incorporating the SAG mill weight model and both of the SAG mill discharge models.
- Observability and detectability analysis of the two CSPE formulations.
- Assessment of the two CSPE formulations.
- Validation of the inferential measurement models of mill ball, rock and total charges and feed size utilising plant data.
- SAG mill charge and feed size model behaviour discussion and further model sensitivity analysis.
- Construction of a SAG mill operating curve and discussion of its possible utilisation in a mill charge control strategy.
- Development and assessment of an advanced controller structure that utilises the inferential measurement models.

Unless otherwise specifically referenced, all of the work contained within this Thesis is the original work of the author.

The following publications and presentations have been derived from the work covered in this Thesis:

- Romagnoli, J. A., Galan, O. and Apelt, T. A., (1997) "Preliminary Study of SAG Mill Control at Northparkes Mines", Technical Report. ICI Laboratory for Process Systems Engineering. Dept of Chemical Eng, University of Sydney NSW Australia.
- Apelt, T. A., Galan, O. and Romagnoli, J. A. (1998) "Dynamic Environment for Comminution Circuit Operation and Control" In: CHEMECA '98, 26th Australasian Chemical Engineering Conference. CHEMECA. Port Douglas QLD Australia.
- Apelt, T. A. (1998) "Dynamic environment for comminution circuit control, simulation and training", ME(Research) to PhD Upgrade Report, Dept of Chemical Engineering, University of Sydney NSW Australia, 13 November 1998.
- Apelt, T.A., Thornhill, N.F. and Romagnoli, J.A., (2000) "Mineral Grinding Process Modelling in Simulink" In: The Process Applications of MATLAB, Simulink and Stateflow Conference, Cambridge Control Ltd / Mathworks, April 5^{th}, Pope Lecture Theatre, School of Chemical, Environmental and Mining Engineering, University of Nottingham.
- Apelt, T.A., Asprey, S.P. and Thornhill, N.F (2001) "Inferential measurement of SAG mill parameters", Minerals Engineering, Vol. 14, No. 6, 575-591.
- Apelt, T.A., Asprey, S.P. and Thornhill, N.F. (2001) "SAG mill discharge measurement model for combined state and parameter estimation" In: SAG 2001, Vol. IV. pp. 138-149, UBC. Vancouver, B.C., Canada, Third international conference on: Autogenous and Semiautogenous Grinding Technology, Sep 30 - Oct 3, 2001.
- Apelt, T.A., Asprey, S.P. and Thornhill, N.F (2002) "Inferential measurement of SAG mill parameters II: state estimation", Minerals Engineering, Vol. 15, No. 12, 1043-1053.
- Apelt, T.A., Asprey, S.P. and Thornhill, N.F (2002) "Inferential measurement of SAG mill parameters III: inferential models", Minerals Engineering, Vol. 15, No. 12, 1055-1071.
- Apelt, T.A. and Thornhill, N.F (In Press) "Inferential measurement of SAG mill parameters IV: inferential model case study application", Minerals Engineering.

ACKNOWLEDGEMENTS

At the risk of leaving out the names of many who are deserving of thanks, I would like to thank the following people:

Professor Jose Romagnoli for financial assistance with which I was able to obtain the Julius Kruttschnitt Mineral Research Centre Monograph and a personal computer and for the funding to conduct the SAG Control Project at Northparkes Mines.

The Centre for Process Systems Engineering (CPSE), Imperial College London for having me and Professor Nilay Shah for officiating the requisite administrative matters.

The Support Staff at University of Sydney for their friendly, effective day to day management of Departmental affairs, particularly Department Secretary Linda McGill.

Similarly, the Support Staff at the CPSE for their friendly, effective day to day management of Centre affairs.

Northparkes Mines (NPM) for permission to publish the circuit equipment and operating data and the other operation information required by this work.

NPM personnel for assistance in the information gathering and feedback processes undertaken, particularly Rick Dunn, Jim Davis and Tom Pethybridge.

My postgraduate friends at the University of Sydney and at Imperial College for making research life enjoyable when things were going well and bearable when they were not.

James Baird, Chiew Wong and Linda McGill for acting as my proxy at different times at the University of Sydney and made for seamless re-enrollment and thesis submission periods in my absence.

Professor Lester Kershenbaum for the Kalman filter tuning discussions.

Steve Asprey, my deputy Associate Supervisor for his interest and input which was above and beyond the call of duty.

Nina Thornhill, my Associate Supervisor, for her guidance and input, also above and beyond the call of duty. Her tremendous enthusiasm - always appreciated and a crucial research ingredient.

My family and friends outside of university for their patience and understanding, particularly Colin Apelt, my father.

Michael and Donal Scanlan, the Dynamic Askeaton (Co. Limerick) Duo, for some light-hearted moments on my on-project weekends.

My colleagues and friends at the Invensys Stockport office for their continued, more-than-a-passing interest in my revisions' progress, especially Dave Earp, Maria Mackay, Andy Mitchell, Mark Boland, Geoff Lewis and Donna Beirne $\cdots$

Donna Beirne, my wife to be, for her love, patience and support - roll on 07.07.07.

"There are right decisions and there are decisions you make right."

Phil McGraw, PH.D.

REVISED (2^{nd}) EDITION NOTES (March 31, 2005)

The significant revision and changes made to this document in its re-issuing as the second, revised edition are as follows:

- The discussion on error propagation in Section 6.1 was clarified.
- Section 3.2 has been inserted to elaborate on the source of the data utilised for model validation.
- Section 3.5, which considers further model validation of the steady state models on the published data of Gault (1975).
- Chapter 8 is a new Chapter that contains inferential measurement validation on Oct 1997 Northparkes Mines data and explores a simulated plant utilisation of the inferential measurement models.

Minor changes were made throughout the document, chiefly in the Abstract and the concluding chapter, Chapter 9, to reflect these major changes. Section 2.2.4 is a small addition, in the review chapter, about inferential charge measurement from mill motor measurements.

EMENDED (3^{rd}) EDITION NOTES (May 2, 2007)

The major emendations made to this document in its re-issuing as the third, emended edition are as follows:

- Section 3.1 provides an overview of the model development logic and model utilisation. This Section is new which increments the numbers of the other Sections in this Chapter.
- Section 6.1 has been re-written to further clarify the error propagation method employed.
- Sections 7.1.1 and 7.1.2 provide further insight into the formulation and context of the utilisation of the combined state and parameter estimation model and extended Kalman filter.
- Section 8.2, which considers further the behaviour of the inferential SAG mill charge and feed size models. Further comment is made on model sensitivity and characteristics that may be utilised in a mill charge control strategy. This Section is new which increments the numbers of the other Sections in this Chapter.

Minor changes were made throughout the document, chiefly in the Abstract and the concluding chapter, Chapter 9, to reflect these major changes.

Contents

List of Figures

List of Tables

Nomenclature

Greek Symbols

α	efficiency curve parameter: separation sharpness	(–)
β	fraction of charge that is active	(fraction mill total charge)
β	efficiency curve parameter: fine size efficiency boost	(–)
β^*	efficiency curve parameter: d_{50c} preservation	(–)
δf	uncertainty in function f	(fraction)
$\delta\theta_i$	uncertainty in parameter θ_i	(various)
ϵ	porosity of mill grinding charge	(fraction)
γ	mean relative radial position of open area	(fraction)
λ	hindered settling correction term	(–)
ϕ_{fcs}	mill speed	(fraction critical speed)
ϕ_c	experimentally determined fraction of critical mill speed at which centrifuging is fully established	(fraction critical speed)
ρ_b	grinding ball density (specific gravity)	(t/m^3)
ρ_c	mill charge density (specific gravity)	(t/m^3)
ρ_{kidney}	density of active fraction of mill charge (specific gravity)	(t/m^3)
ρ_o	ore density (specific gravity)	(t/m^3)
ϕ	fraction critical mill speed	(fraction)
ψ_e	energy absorption factor of the steel grinding media	(fraction)
ρ_p	cyclone feed pulp (slurry) density	(t/m^3)
ρ_{m_i}	density of grinding media in *size i*	(t/m^3)
ρ_p	SAG mill pulp density	(t/m^3)
σ_f	standard deviation of function f	(fraction)
σ_θ	standard deviation of parameter θ	(various)

θ_{cone}	mill cone angle	(^{o})
θ_S	mill charge shoulder angle	(radians)
θ_{TO}	mill slurry toe angle ($\theta_{TO} = \theta_T$ for grate-discharge mills)	(radians)
θ_T	mill charge toe angle	(radians)
τ	mill residence time	(hr)
θ	CSPE model parameters to be estimated (non-constant)	(−)
θ	cyclone cone full angle	(^{o})
θ_i	$i\,th$ model parameter in error/sensitivity analysis	(−)
θ_I	angle of ball impact at the mill radius	(radians)

Roman Symbols

A	crusher power draw scaling factor	(−)
A	ore impact breakage parameter	(−)
A	state transition matrix that defines the dynamic behaviour of the continuous-time nonlinear system	(−)
A	total discharge grate open area	(m^2)
a	acceleration	(m/s^2)
a	size at which 36.8% (*i.e.*, $100/e$) of particles are retained	(mm)
A_i	crusher model parameters from plant survey	(−)
a_{ij}	appearance function of particles appearing in *size i* (a function of the breakage distribution of particles in sizes $\geq$ *size i*)	(fraction)
$\bar{A}$	discrete-time state transition matrix that defines the dynamic behaviour of the continuous-time nonlinear system	(−)
$ABCD$	stream properties of stream "ABCD"	(−)
$abcd$	size distribution of stream "ABCD"	(% w/w)
$ABCD_i$	mass by size of stream "ABCD"	(t)
a_{he}	high energy appearance function	(fraction)
a_{le}	low energy appearance function	(fraction)
a.m.	*Ante Meridiem*: Latin for "before midday"	(−)
a posteriori	from later (Latin)	(−)
a priori	from what is before (Latin)	(−)
B	control transition matrix that relates the effects of control actions on the continuous-time nonlinear system	(−)
B	crusher breakage distribution function	(fraction)
b	ball diameter	(mm)
b	ore impact breakage parameter	(−)
b	slope of $ln(ln(100/W_r))$ *vs* $ln(x)$ plot	(−)
B_i	crusher model parameters from plant survey	(−)
$\bar{B}$	discrete-control transition matrix that relates the effects of control actions on the continuous-time nonlinear system	(−)
BC	total ball charge mass	(t)
bc_i	mass of balls in ball charge of *size i*	(t)

be_i	balls of *size i* ejecting from the mill	(t/hr)
BEk_i	ball ejection model fitting parameter	(hr^{-1})
bi_i	feed balls in *size i*	(t/hr)
bps	balls per stroke	(−)
bst	ball stroke time	(seconds)
bw_i	mass of balls wearing out of *size i* into *size i* + 1	(t/hr)
BWk_i	ball wear coefficient for balls in *size i*	(Brinnell/hr)
C	$= C(x) =$ crusher probability of breakage function	(fraction)
C	measurement matrix that relates the system states to the process measurements	(−)
C	water recovery to cyclone overflow	(fraction)
c_i	grate classification function for *size i*	(fraction)
$\bar{C}$	discrete-time measurement matrix that relates the system states to the process measurements	(−)
C_s	mill critical speed	(RPM)
$CSPE$	combined state and parameter estimation	(−)
CSS	crusher close side setting	(mm)
C_v	volumetric fraction of solids in feed slurry	(fraction)
CV	Controlled Variable	(−)
CV	Controlled variable	(−)
$C(x)$	probability of breakage	(fraction)
D	direct connection matrix that relates the effects of control actions on the process measurements (usually zero)	(−)
D	mill inside diameter	(m)
d	particle size (diameter)	(mm)
D_m	mill inside diameter	(m)
d_{xm}	mill volumetric discharge of water and solids smaller than x_m	(m^3/hr)
d_0	maximum mill discharge rate constant	(hr^{-1})
$d_{0,\,k}$	discharge rate constant at k^{th} iteration	(hr^{-1})
$d_{0,\,k+1}$	discharge rate constant at k $+^{th}$ iteration	(hr^{-1})
d_{50c}	corrected 50% passing size	(mm)

$\bar{D}$	discrete-time direct connection matrix that relates the effects of control actions on the process measurements (usually zero)	(–)
D_B	ball topsize scaling factor	(–)
D_b	new ball diameter	(mm)
Db_i	diameter of ball of *size i*	(mm)
D/C	discharge	(–)
D_c	cyclone cylinder diameter	(m)
$D/C\,grate$	SAG mill discharge grate weight	(t)
dgt	discharge grate thickness	(mm)
d_i	mill discharge rate for *size i*	(hr^{-1})
D_i	cyclone inlet diameter	(m)
d_i^*	mill discharge rate of *size i* particles normalised to mill residence time, τ	(–)
D_o	cyclone overflow diameter	(m)
$D_{sm\,0}$	SAG mill shell inside diameter	(m)
Dt_{sm}	SAG mill trunnion diameter	(m)
D_u	cyclone underflow diameter	(m)
Ecs_i	specific comminution energy for *size i*	(kWhr/t)
Edc_i	ball ejection efficiency to discharge	(fraction)
e.g.	for example (*Latin* : *exempli gratia*)	(–)
EKF	Extended Kalman Filter	(–)
E_{oa}	classification efficiency to cyclone overflow	(fraction)
ET	crusher eccentric throw	(mm)
et al.	and others (*Latin* : *et alii*)	(–)
f	the CSPE system function	(–)
f	crusher feed by size	(tph)
f_i	feedrate of particles in *size i*	(t/hr)
F_{kW}	mill powerdraw residual function	(kW)
F_{weight}	mill weight residual function	(t)
f	a general function	(–)
FIT	original conditions of fitted ball mill model	(–)

$foag$	discharge grate fraction open area	(fraction)
$FOPTD$	First-order plus time-delay	(–)
f_p	notional fraction pebble port open area:total grate open area ratio	(fraction)
fSA_i	fractional surface area of grinding balls in *size i*	(fraction)
FV	Feed-forward variable	(–)
f_w	feed water addition	(t/hr)
g	the CSPE measurement function	(–)
g	gravitational acceleration	(9.81 m/s^2)
$g_{2...29}(x, \theta, t)$	SAG mill discharge flowrate measurement model	(m^3/hr)
$g_1(x, \theta, t)$	SAG mill weight measurement model	(t)
gms_i	grinding media size class i	(mm)
h	mean drop height	(m)
HB_i	Brinnell Hardness of grinding balls in *size i*	(N/m^2)
hlt	high lifter bar thickness (height)	(mm)
H_2O	water	(–)
i.e.	that is (*Latin* : *id est*)	(–)
J_B	% of total mill volume occupied by grinding balls and associated voids	(%)
J_b	mill fraction occupied by grinding balls including the associated voidage	(fraction mill volume)
JK	Julius Kruttschnitt Mineral Research Centre	(–)
JK	Julius Kruttschnitt Minerals Research Centre	(–)
J_{max}	maximum possible nett fractional grinding media slurry holdup	(fraction)
J_p	nett fractional holdup of slurry in mill	(fraction)
J_{pg}	gross fractional holdup of slurry in mill	(fraction)
J_{pm}	nett fractional holdup of slurry in mill that is contained within the grinding charge interstices	(fraction)
J_{po}	nett fractional slurry holdup in mill 'dead' zone	(fraction)
J_{pt}	nett fractional holdup of slurry in mill that is contained in the slurry pool at the toe of the charge (*i.e.*, slurry outside the grinding charge)	(fraction)
J_t	mill fraction occupied by grinding media (balls plus coarse rocks) including the associated voidage	(fraction mill volume)

K	maximum breakage factor	(mm^{-1})
k	iteration step	(−)
k	mill powerdraw lumped parameter (accounts for heat losses due to internal friction, energy of attrition/abrasion breakage, rotation of the grinding media and inaccuracies in assumptions and charge shape and motion measurements)	(−)
k_{ij}	regression coefficients	(−)
$K1$	particle size below which classification probability is zero, C(x) = 0	(mm)
$K1$	ball size below which hardness equals 250 Brinnell	(mm)
$K2$	particle size above which classification probability is one, C(x) = 1	(mm)
$K2$	ball size above which harness equals 450 Brinnell	(mm)
$K3$	classification function parameter: curve shape	(−)
$K3$	ball hardness curve shape parameter	(−)
k	discharge grate efficiency parameter	(−)
k_g	factor to account for coarse material	(−)
K_{Q0}	ore dependent proportionality constant	(−)
K_{V1}	volumetric flow split to underflow constant	(−)
K_{W1}	water split to underflow constant	(−)
L_{cone}	length (axial) of conical section of mill	(m)
L_m	mill (cylinder) length	(m)
lbw	lifter bar width	(mm)
L_c	cyclone cylinder length	(m)
LF	ball charge fraction, J_b	(fraction)
LHr	crusher liner hours in service	(hrs)
$lining$	SAG mill shell lining weight	(t)
$lining_{DE\ 0}$	installation weight of the discharge end of the shell lining	(t)
$lining_{DE}$	weight of the discharge end of the shell lining	(t)
$lining_{FE\ 0}$	installation weight of the feed end of the shell lining	(t)
$lining_{FE}$	weight of the feed end of the shell lining	(t)
$LLen$	crusher liner length	(mm)
llt	low lifter bar thickness (height)	(mm)
L_m	mill length	(m)

L_{sm}	SAG mill shell length	(m)
M_{kidney}	mass of active fraction of mill charge	(t)
M_{shell}	mill shell weight	(t)
MV_{kW}	mill powerdraw measurement	(kW)
MV_{weight}	mill weight measurement	(t)
$m3ph$	volumetric flow rate	(m^3/hr)
Mb_i	mass of grinding ball in *size i*	(t)
M_i	mass of an ore particle in *size i*	(t)
ΔMV	The change in the MV that causes the change in CV	(−)
MV	Manipulated Variables	(−)
MV	Manipulated variable	(−)
MV_{DC_H2O}	SAG mill discharge water addition flowrate measured variable	(m^3/hr)
MV_{FC_H2O}	SAG mill feed water addition flowrate measured variable	(m^3/hr)
MV_{OSCF}	oversize crusher total feedrate	(t/hr)
MV_{pc_dens}	primary cyclone feed density measured variable	(%solids w/w)
$MV_{PCFD\%sols}$	primary cyclone feed density	(% solids w/w)
MV_{PCFDm3}	primary cyclone feed flowrate	(m^3/hr)
MV_{pc_flow}	primary cyclone feed flowrate measured variable	(m^3/hr)
MV_{scats}	oversize crusher feedrate measured variable	(tph)
$\overline{N}$	mean mill speed	(revolutions per second)
N_m	actual mill speed	(revolutions per second)
N	discharge grate efficiency parameter	(−)
nb_i	number of grinding balls in *size i*	(−)
ndg	number of discharge grate segments	(−)
nhl	number of high lifter bars	(−)
N_i	number of balls in *size i*	(−)
n_i	number of particles in *size i*	(−)
nll	number of low lifter bars	(−)
NPM	Northparkes Mines	(−)
O/S	oversize	(−)

$OSCF_{\%s\,w/w}$ oversize crusher feed solids density (%solids w/w)

$OSCF_{tph\_l}$ oversize crusher liquid feedrate (t/hr)

$OSCF_{tph\_s}$ oversize crusher solids feedrate (t/hr)

$OSCP_{tph\_s}$ solids component of the oversize crusher product (t/hr)

P cyclone inlet pressure (kPa)

p crusher product by size (tph)

p_i mill discharge (product) of particles in *size i* (t/hr)

P_{Charge} mill powerdraw attributable to the contents of the cyclindrical section of the mill (kW)

P_{Cone} mill powerdraw attributable to the contents of the conical (feed) section of the mill (kW)

P_{Gross} power input to the mill motor (metered power) (kW)

P_{Net} mill powerdraw attributable to the contents of the cylindrical section of the mill(kW)

$P_{No\,Load}$ no-load power of mill (empty mill powerdraw) (kW)

p_{xm} volumetric flowrate of water and solids *size* $< x_m$ (m^3/hr)

P_c predicted crusher power draw (kW)

$PCFD_{\%s\,w/w}$ primary cyclone feed density (% solids w/w)

$PCFD_{m3ph\_p}$ primary cyclone feed flowrate (m^3/hr)

MV_{PCFWm3} primary cyclone feed water addition flowrate (m^3/hr)

$(1 - PC_{split})$ fraction of the primary cyclone underflow recycled to the SAG mill (fraction)

PC_{split} fraction of the primary cyclone underflow feeding to the ball mill (fraction)

$PCUF_{tph\_s}$ solids component of the primary cyclone underflow (t/hr)

$PCUS_{tph\_s}$ solids component of the primary cyclone underflow reporting to the SAG mill (t/hr)

$\%sols_{OSCF}$ oversize crusher feed density (% solids w/w)

PI Prediction Interval (time units)

$p.m.$ *P*ost Meridiem: Latin for "afternoon midday" (–)

P_n crusher no-load power (kW)

P_p pendulum power (kW)

p_w water discharge rate (t/hr)

Q_f	cyclone feed flowrate	(m^3/hr)
Q_m	mill discharge flowrate through grinding media	(m^3/hr)
Q_t	mill discharge flowrate through slurry pool at toe of the charge	(m^3/hr)
$\overline{r}$	mean radial position of mill charge	(m)
$R1 \ldots R5$	base breakage rates	(hr^{-1})
r_i	breakage rate of particles in *size i*	(hr^{-1})
r_i	mill charge inner surface radius. (Boundary between the "active" portion of the charge on the mill wall and the "inactive" portion of the charge in free-fall.)	(m)
RPM	actual mill speed	(revolutions per minute)
$RPM_{critical}$	mill critical speed	(revolutions per minute)
$Range_{CV}$	CV range over the vessel volume	(CV units)
$RCE_{i,j,k}$	relative contribution that uncertainty in parameter θ_j makes to the J_k charge estimate uncertainty when utilising residual Equation (i)	(%)
RCL	mill recirculating load	(%)
R_f	water recovery to cyclone underflow	(fraction)
ρ_{liner}	liner density	(t/m^3)
r_n	relative radial position of outermost grate apertures	(fraction)
ROC_{CV}	Rate of change of the CV	(CV units per PI)
$\frac{r_i}{d_i^*}$	ball mill rate/discharge value for *size i* particles	(hr^{-1})
R_r	recycle ratio of $-20 + 4$mm material	(–)
r_{sm}	SAG mill radius	(m)
R_v	volumetric recovery of feed slurry to cyclone underflow	(fraction)
S	mill discharge volumetric solids content	(% solids v/v)
s	distance	(m)
s_i	mill rock charge particles in size i	(t)
s_{xm}	volume of water and solids of $size < x_m$ in the mill	(m^3)
S_a	mill RPM scaling factor	(–)
SA_i	total surface area of grindings ball in *size i*	(m^2)
S_b	mill fraction critical speed scaling factor	(–)
SG_b	grinding ball density	(t/m^3)

SG_l	liquid specific gravity	(t/m^3)
SG_s	ore specific gravity	(t/m^3)
shell	SAG mill shell weight	(t)
sic	Editor note indicating that the quoted material contained the spelling or grammatical error. (*Latin* : *so*, *such*, *that*)	(−)
$_{SIM}$	simulated conditions of ball mill model	(−)
slt	shell liner thickness (height)	(mm)
$SMD50c$	SAG mill discharge screen corrected 50% passing size	(mm)
smdc	SAG mill discharge size distribution (weight retained)	(%retained w/w)
$SMDC_{SGp}$	SAG mill discharge pulp density	(t/m^3)
$SMDC_{tph\_l}$	SAG mill liquid discharge rate	(t/hr)
$SMDC_{tph\_s}$	SAG mill solids discharge rate	(t/hr)
$SMFF_{tph\_s}$	solids component of the SAG mill fresh feed	(t/hr)
smff	SAG mill fresh feed size distribution	(%retained w/w)
smtf	SAG mill total feed size distribution	(%retained w/w)
$SMFF_{tph\_l}$	SAG mill fresh feed liquid feedrate	(t/hr)
$SMFF_{tph\_s}$	SAG mill fresh feed solids feedrate	(t/hr)
$SMIW_0$	initial SAG mill installation weight	(t)
$SMIW$	SAG mill installation weight	(t)
$SMTF_{tph\_l}$	SAG mill total feed liquid feedrate	(t/hr)
$SMTF_{tph\_s}$	SAG mill total feed solids feedrate	(t/hr)
$SMWconst$	SAG mill liner weight constant	(t)
s_w	water in the mill charge	(t)
$s_{xm,\ k}$	mill water and rock charge smaller than x_m at k^{th} iteration	(m^3)
$s_{xm,\ k+1}$	mill water and rock charge smaller than x_m at $k+^{th}$ iteration	(m^3)
t	time	(seconds or hours)
t_c	mean travel time in charge (between toe and shoulder)	(seconds)
t_f	mean travel time in freefall (between shouler and toe)	(seconds)
t_{10}	high energy (impact) t parameter	(%)
t_a	low energy (abrasion) t parameter	(%)

TAGL	Dr. Tim Langrish, Assoc. Professor of Chemical Engineering, Uni of Sydney	(–)
t_{he}	high energy (impact) t parameter	(%)
TimeConversion	Conversion factor for MV time units to PI units	(time over time)
t_{le}	low energy (abrasion) t parameter	(%)
TPH	crusher feedrate	(tph)
tph	mass flow rate	(t/hr)
U	fraction of grinding media voidage occupied by slurry	(fraction)
u	the CSPE system input	(various)
v	velocity	(m/s)
V_{kidney}	volume of active fraction of mill charge	(m^3)
vb_i	the volume of grinding balls in size class i	(m^3)
V_m	mill internal volume	(m^3)
vo_i	the volume of ore in size class i	(m^3)
W_p	material passing *size* x	(% w/w)
wearate	SAG mill shell wearate	(t/hr)
WI	ore work index	(kWh/t)
W_r	material retained at *size* x	(% w/w)
wrt	with respect to	(–)
x	particle size	(mm)
x	ratio of particle size to corrected 50% passing size	(–)
x	the state of the CSPE system	(various)
x_i	target particle *size* i	(mm)
x_g	mill discharge grate aperture size	(mm)
x_m	particle size that behaves like water (in SAG mill)	(mm)
x_m	impact *versus* abrasion breakage boundary particle size (in ball mill)	(mm)
x_p	notional discharge grate pebble port aperture size	(mm)
y	the CSPE system output	(various)
z	mill powerdraw calculation parameter	(–)
1^o	primary	(–)
2^o	secondary	(–)

Chapter 1

Introduction

Autogenous and semiautogenous grinding has progressed a long way since the 1930's when (at South African gold mines) Hadsel first thought of using larger pieces of competent ore to break smaller pieces in a bucket wheel configuration (MacPherson, 1989). Outghred and Hardinge took the idea to North America and utilised it in dry and wet mills, respectively (MacPherson, 1989). Post−WW−II development is credited to Weston who extended the technology to high aspect [1] mills (1959: 22 feet (6.7 m) diameter, 1 MW) (MacPherson, 1989).

Since these early developments the importance of autogenous grinding technology has extended to the present day where 600 mills in 64 nations on 6 continents operate drawing 375,000 hp (260 MW) and mill manufacturers are having to meet evermore demanding specifications (1996: 40 feet (12.2 m) diameter, 20 MW), (Jones Jnr, 2001).

Semi-autogenous grinding (SAG) mill ball charge and rock charge affect mill performance. The size distribution and hardness of the SAG mill feed influence the breakage within the mill and therefore the rock charge that remains after breakage. Throughput and product quality are affected by the conditions inside the mill. The mill inventories and feed properties are therefore important variables and measurement of them opens the way for improved process control and the associated benefits.

Direct measurement of the mill inventories is difficult for various reasons, such as, the rotational motion of the mill and the destructive tumbling action of the charge. Indirect

[1] mill diameter to length ratio

measurement is possible via mill weight and power draw, conductivity probe, microphone, measurements, acoustic spectral analysis and state estimation.

Significant developments have been made in these indirect measurement methods. Industry has generally not been quick on the uptake of these technologies due to the method being in a developmental stage, or being relatively complex (mathematically or conceptually), or being proprietary information (which has cost or confidence implications).

Direct measurement of mill feed size distribution is available through video image analysis of the moving ore stream, *e.g.*, ore on a moving conveyor belt or being dumped from a truck to a crushing facility. This technology is relatively new and its uptake has been limited somewhat by its cost and the poor perceived benefits associated with having such measurement. Larger mining houses and new installations are more likely to acquire this technology. It is gaining wider acceptance with time and a good performance record.

This work focusses on the development of a number of inferential models for SAG mills. Mill power draw and weight measurements are utilised to provide estimates of the mill inventories. Primary cyclone feed and oversize crusher feed measurements are utilised to provide an estimate of the mill discharge rate and size distribution. These indirect measurements are utilised in the estimation of SAG mill fresh feed rate and size distribution. The mill discharge models are further utilised in the formulation of combined state and parameter estimation models of the SAG mill inventories, discharge grate parameters and ore grindability parameters.

A review of the literature and progress in the area of inferential measurement modelling for SAG mills is presented in Chapter 2, where the above points are expanded upon to place this research into context.

Prior to the review, the grinding circuit of interest to this research is introduced below. The operational difficulties of the circuit that are the motivation for this research are discussed, resulting in the Problem Statement in Section 1.3.

1.1 Circuit Description

The circuit under study is the Module 1 grinding circuit at Northparkes Mines (NPM). NPM is a copper-gold mine and concentrator located near Parkes in the Central Western region of New South Wales, Australia.

The design capacity of Module 1 grinding circuit is 245 dry tonnes per hour of low grade copper sulphide ore. Overall, a single coarse ore feed stream is processed into two fine product streams, refer to the process flowsheet in Figure 1.1.

In more detail, rocky run-of-mine ore is drawn from the feed ore stockpile by four vibrating feeders. The fresh feed is conveyed to the semi-autogenous (SAG) mill feed chute. A recycle stream, the oversize crusher product, joins the fresh ore on the feed conveyor. At the SAG mill feed chute, feed dilution water is added in ratio to achieve a solids content of approximately 75% solids (w/w). Another recycle stream, a fraction of the primary cyclone underflow, also reports to the feed chute. The feed mixture enters the SAG mill where size reduction occurs by means of impact breakage (collisions with grinding media - large rocks and steel balls) and abrasion (tumbling action of the mill charge).

The SAG mill discharge grates retain the grinding media while allowing the discharge of water, fine ore particles and middle-sized rocks. SAG mill discharge is presented to a vibrating screen which separates the middle-sized material ("scats") for recycle to the SAG mill via a gyratory cone crusher.

Screen undersize is diluted with the addition of SAG mill discharge water and is pumped to the primary cyclones for further size classification. The SAG mill, SAG mill discharge screen, primary cyclones and oversize crusher constitute the primary grinding circuit. The fine primary cyclone overflow stream reports directly to the ball mill discharge hopper while the coarse cyclone underflow is split between a recycle stream to the SAG mill feed chute and a stream reporting to the ball mill feed chute. The equipment downstream of the primary cyclones (the ball mill, ball mill discharge screen, secondary cyclones and flash flotation cells) constitute the secondary grinding circuit.

Further size reduction occurs within the ball mill by way of the tumbling action of the ball charge. Ball mill discharge reports to a vibrating screen which separates worn grinding balls and any stray coarse particles. The fine screen underflow stream is classified at the secondary cyclones into a fine overflow stream (flotation plant feed) and a coarse underflow stream that is recycled to the ball mill feed chute.

A fraction of the secondary cyclone underflow is processed via the flash flotation circuit before reporting to the ball mill feed chute. The function of the flash flotation cells is to remove any liberated copper mineral particles that have reported to the cyclone underflow due to their relatively high specific gravity.

There are two flash flotation cells, a rougher and a cleaner. The rougher cell performs a coarse separation of the liberated mineral particles from the rock (gangue) particles. The cleaner cell refines the rougher concentrate stream. Cleaner concentrate reports directly to concentrate thickening and filtering. Both the cleaner and rougher tails streams are recycled to the ball mill feed chute. As a means of preventing the over-dilution of the

ball mill feed stream, the larger rougher flash flotation cell is fitted with a water bleed stream. This is an off-take located at approximately three-quarter cell height. At this level the material in the cell is highly dilute and barren of mineral particles. The water bleed is diverted directly to the ball mill discharge hopper, with an optional split to the SAG mill discharge hopper. Further details of the grinding circuit and the other sections of the processing plant may be found elsewhere (Apelt *et al.*, 1998; Freeman *et al.*, 2000*b*; Apelt *et al.*, 2001*a*).

This description corresponds to the circuit as it existed in 1997. The circuit has since undergone some changes that are isolated to the latter part of the secondary grinding circuit[2]. Tertiary grinding has been introduced to process the secondary cyclone overflow (flotation plant feed). However, the tertiary grinding section will not be considered by this research since it is outside the focus of this research and does not affect the research or the findings presented.

1.1.1 Stream Naming Syntax

The circuit stream names have been reduced to a four capitalised-letter abbreviation, *e.g.*, "SAG mill fresh feed" is abbreviated to "$SMFF$", refer to the left-hand-side of Table 1.1. The stream properties on the right-hand-side of Table 1.1 are linked to the abbreviated stream name. The particle size distribution (in weight percent retained format) for each of the streams are linked to the corresponding lowercase four letter abbreviation *e.g.*, "$smff$" represents the size distribution of the $SMFF$ stream.

Whilst convenient, this naming convention introduces some inconsistencies which arise from the multiple properties associated with a single stream name and where single component streams are involved, such as the water addition streams and grinding media streams. Generally however, the meaning of the stream name can be easily deduced from the context of its use (*e.g.*, solids balance/water balance) . Where confusion remains the stream names used will be augmented for clarity. For the water addition streams, the solids mass flowrate is zero and there is no associated size distribution or eighty percent passing size (P_{80}). For the grinding media streams, the solid flows are replaced by steel flows at 100% solids.

1.2 Circuit Operation Challenges

The author was associated with Northparkes Mines immediately prior to the commencement of postgraduate studies at the University of Sydney, holding the post of Plant Metal-

[2]Verbal communication with Northparkes Mines Metallurgical Superintendent - Rick Dunn at *SAG* 2001 conference

Table 1.1: Stream Name Abbreviations and Properties

Abbreviations		*Stream Properties*	
SMFF	SAG mill fresh feed	*tph_s*	solids mass flow (t/hr)
SMTF	SAG mill total feed	*tph_l*	water mass flow (t/hr)
SMFW	SAG mill feed water addition	*tph_p*	total (pulp) mass flow (t/hr)
SMRC	SAG mill rock charge	*%s w/w*	% solids by weight (% w/w)
SMBC	SAG mill ball charge	*%l w/w*	% water by weight (% w/w)
SMDC	SAG mill discharge	*m3ph_s*	volumetric flow of solids (m^3/hr)
SMDW	SAG mill discharge water addition	*m3ph_l*	volumetric flow of water (m^3/hr)
OSCF	Oversize crusher feed	*m3ph_p*	total (pulp) volumetric flow (m^3/hr)
OSCP	Oversize crusher product	*%s v/v*	% solids by volume (% v/v)
PCFD	Primary cyclone feed	*%l v/v*	% water by volume (% v/v)
PCOF	Primary cyclone overflow	*SGp*	pulp specific gravity (t/m^3)
PCUF	Primary cyclone underflow	P_{80}	80% passing size (mm)
PCUS	Primary cyclone underflow to SAG mill		
PCUB	Primary cyclone underflow to ball mill		
BMFD	Ball mill feed		
BMFW	Ball mill feed water addition		
BMDC	Ball mill discharge		
BMDW	Ball mill discharge water addition		
BSOS	Ball mill discharge screen oversize		
BSUS	Ball mill discharge screen undersize		
SCFD	Secondary cyclone feed		
SCOF	Secondary cyclone overflow		
SCUF	Secondary cyclone underflow		

lurgist from May 1995 to June 1997. Included in the duties of Plant Metallurgist was the monitoring and evaluation of grinding circuit operation and performance. In fulfilling this role, various difficulties associated with the operation and control of comminution circuits were identified. The combination of:

- recycle streams
- process interactions
- nonlinear processes
- process measurement constraints
- control system constraints
- unmeasured disturbances (especially feed ore size distribution and hardness),

result in a process that is difficult to control automatically. Consequently, process operators resorted to manual control of many process variables *e.g.*:

- SAG feed dilution water set point
- cyclone feed density set point
- cyclone feed pump speed

During the two year period from mid 1995 to mid 1997, automatic control was generally limited to regulatory control, *e.g.*, PID loops control water flowrates according to the set points entered by the process operator. The utilisation of the control system was effectively remote process operation and monitoring.

In the early stages of this research a small project was proposed and conducted regarding SAG mill control at Northparkes Mines (NPM). Commissioned by NPM, the project report (Romagnoli *et al.*, 1997) presented findings on:

- grinding circuit sensitivity analysis and recommendations on certain operating conditions and strategies
- instrumentation requirements to fully define the circuit mass balance (including SAG mill grinding media mass balance)
- a SAG mill dynamic model and its potential use in a proposed feed-forward, feedback throughput maximisation control loop

The sensitivity analysis results were generated utilising a grinding circuit process model constructed in JKSimMet[3] from circuit surveys conducted in early 1997 (David, 1997). The mass balance definition work was conducted in a Microsoft Excel spreadsheet. The dynamic models were constructed in MATLAB-Simulink which was selected due to its mathematical processing capability, flowsheet manipulation flexibility, and availability.

Communications with NPM have continued since the submission of the project report. Operations personnel indicate that the level of control has advanced considerably since 1997 (Davis, 1999). The improvements are the result of the introduction of rule-based control by NPM personnel.

In early 1997, the SAG mill fresh feedrate was a simple PID loop with a Grinding Technician-entered setpoint that was subject to high and low mill weight alarms and trips and high mill powerdraw alarms and trip. The setpoint would be selected based on the knowledge and experience of the technician, general movement in the powerdraw and mill weight trends, and production targets.

By late 1999, Module 1 feedrate setpoint determination incorporated recycle rate information and a large part of the setpoint determination had been automated. Over 2-3 minute intervals, mill weight, powerdraw and recycle rate are observed. Their current levels and

[3]Commercial simulation software developed by the Julius Kruttschnitt Mineral Research Centre

movement over the interval are subjected to a set of rules to determine required feedrate setpoint changes. Control of Module 2 feedrate was similar except that sound readings (2× microphones) from beneath the mill were used in place of the mill load measurement (which exhibits more signal noise than the Module 1 counter-part).

More recently, the process control team at Northparkes Mines have upgraded the PLC controllers in the grinding circuit. The increased capabilities allowed the site to commission the implementation of mill load constraint-control (Thornton *et al.*, 2005). The control strategy employs the pair of microphones for the audio-indication of charge toe position, manipulating feedrate to control charge level subject to an upper constraint on mill powerdraw. The SAG mill control system has a high degree of operator acceptance (95% utilisation) and can deal with "a wide range of plant disturbances and keep the mill operating at optimal load."

1.3 Problem Statement

Further communications with Northparkes Mines, see Appendix A, revealed that the issues of primary concern are:

- throughput
- product quality (size)
- feed variability (hardness & size)
- SAG mill rock and ball charge control

All of these issues affect or are affected by the SAG mill rock and ball charge but these inventories are not measured at NPM and are generally difficult to measure directly. The lack of measurements around the SAG mill is a primary cause of the problems associated with SAG mill operation.

Inferential measurements for SAG mills is therefore the focus this research. The objective of this research is to develop inferential measurement models for the SAG mill parameters listed below and add to the body of knowledge supporting them.

- ball charge (J_b) and total charge (J_t) levels,
- feed rate and size distribution, and,
- discharge rate and size distribution.

The focus and objectives will be discussed in more detail in Chapter 2.

1.4 Document Outline

In Chapter 2 a review of the literature is presented to provide background and context for this research. Reinforced by the background information, the research focus is re-stated in more detail.

The requisite simulation model development and validation of the comminution circuits unit operations is presented in Chapter 3. The steady state SAG mill model in Chapter 3 is extended into the dynamic models for the rock and water charge in Chapter 4. Dynamic models of the ball charge and protective shell lining are also proposed and validated.

Inferential models of the SAG mill total and ball charge levels, SAG mill feed rate and size distribution, and, SAG mill discharge rate and size distribution are presented in Chapter 5. These inferential models are subjected to sensitivity and error analyses in Chapter 6.

Combined state and parameter estimation for SAG mills is discussed in Chapter 7. Two formulations are presented and compared to the inferential models presented Chapter 5.

The inferential models are validated and assessed on real plant data in Chapter 8. Further analysis of the sensitivity and nature of the models is also described. A SAG mill operating curve is developed and discussed in relation to a mill charge control strategy. The inferential models are also utilised in a multi-variable control simulation.

To highlight the contributions made by this research, the closing sections of Chapters 3 to 8 include a tabulated summary of the innovations arising from that Chapter.

Chapter 9 brings the thesis to a close with a summary of the conclusions of this research and recommendations for future work.

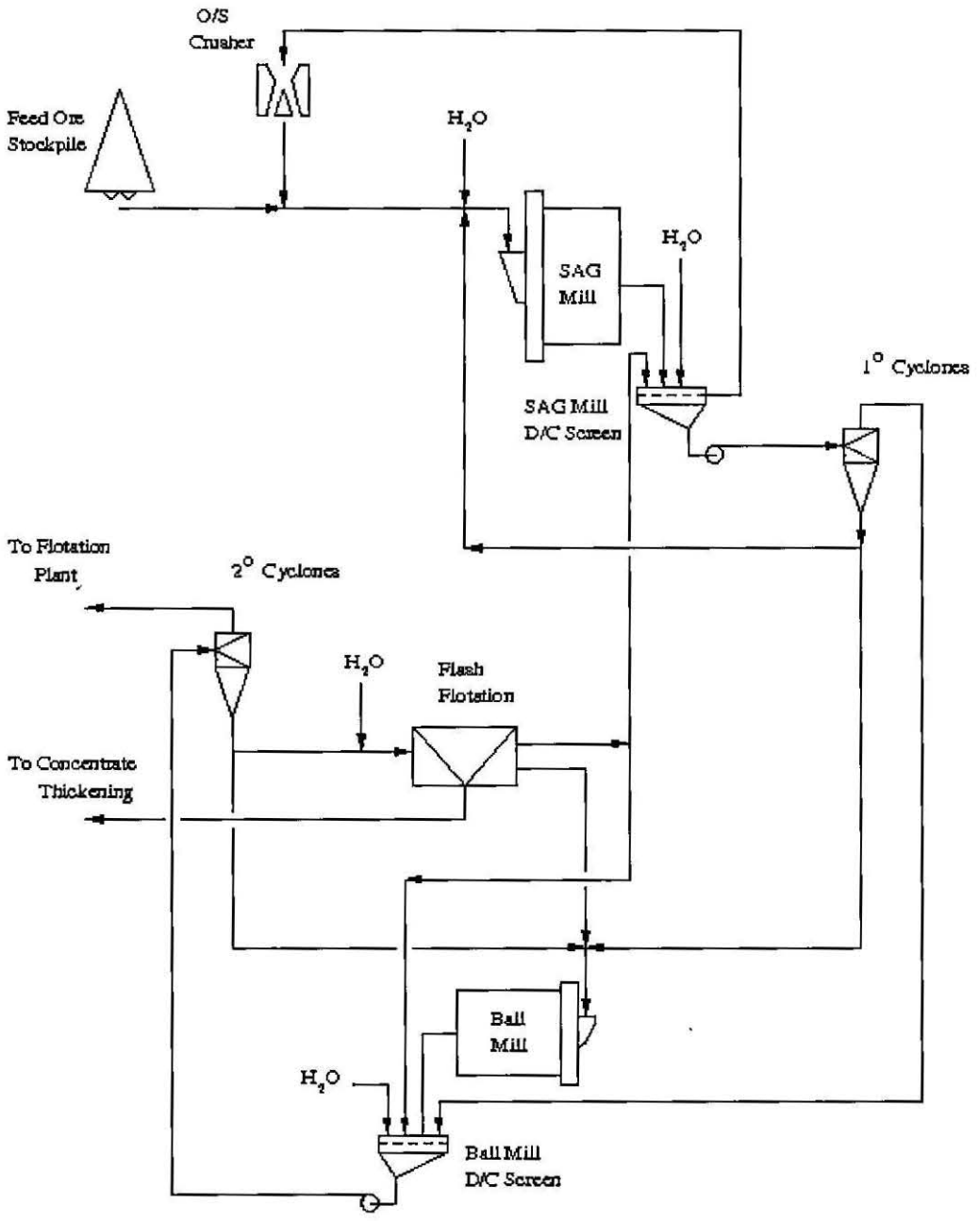

Figure 1.1: Northparkes Mines Module 1 grinding circuit flowsheet

Chapter 2

Background

This Chapter reviews previous research pertinent to the area of inferential measurement modelling of SAG mills and provides the context for this research. The Chapter commences with a general review of SAG mill modelling and control, instrumentation and inferential measurement. The inferential measurement of mill charge levels and discharge are then reviewed in further detail according to the methods employed, namely:

- mill weight and powerdraw measurements
- conductivity probe measurements and energy balance
- acoustic spectral analysis and sound measurement
- state estimation

Further detailed discussion on the measurement of feed size distribution is also presented.

The research focus is then re-stated in the context of this review

2.1 General Review

2.1.1 Modelling and Control

In a review of papers detailing the "state of the art" of automation and control in mineral and metal processing, the "availability of adequate measuring instruments" is observed to have a "major bearing" on the high level of attention required for "the description, characterization and modeling of processes" for control engineering purposes (Hulbert, 2001).

In an earlier review Hulbert (1989) concluded that the "application of models and the effectiveness of automatic control are limited by the availability of on-line measurements" and that "far fewer measurements are available on a real milling circuit than would be required

for the on-line estimation of all the variables and states of a comprehensive mechanistic model of the circuit."

Hodouin *et al.* (2001) report that "essential properties [central in the control of mineral processing operations] such as grindability, ... [and] grinding media size distribution ... are extremely difficult to measure and even to infer from other measurements."

In a review of automation in the minerals processing industry where the implementation of model predictive control is hampered by "lack of precedent applications, high engineering costs and inappropriate control technologies" (Jamsa-Jounela, 2001).

The conclusion of the review of mineral process control (Hodouin *et al.*, 2001) in terms of fields that are 'mature', 'active' or 'emerging' are: "The control fields,[*sic*] which are mature are:

- Expert systems applications
- Steady-state mass balance data reconciliation
- Particle size measurement in the fine size range
- Grinding circuit multivariable stabilizing control
- Flotation circuit multi SISO stabilising control.

The active control areas are mainly:

- Froth image analysis
- Supervisory control of FAG/SAG grinding circuit using a combination of estimators and expert systems
- AI applications to flotation and grinding circuit supervision
- Multivariable non-linear control of flotation systems.

Emerging techniques are appearing in the following domains:

- Fast liberation degree measurement
- Fault detection and isolation
- Integration of comminution and separation control
- Multivariate process monitoring techniques
- Interfacing of mining data and concentrator feed-foward control strategies
- On-line use of phenomenological models."

There are several areas of minerals process control that are considered "mature" and "active". These conclusions are echoed in the findings of a review of SAG mill control techniques (Apelt, 1998) which found that significant work had been conducted in the following areas:

- Expert systems applications
- Grinding circuit multivariable stabilizing control
- Supervisory control of FAG[1]/SAG grinding circuit using a combination of estimators and expert systems

The following five (5) geographic regions feature predominantly in the review:

1. South Africa
2. United States of America
3. Australia
4. Canada
5. Finland and Sweden

These regions are correlated with control methods utilised as presented in Table 2.1 (Table 8 (Apelt, 1998)).

Table 2.1: Control Technique Summary

Advanced Technique	1	2(i)	2(ii)	2(iii)	2(iv)	2(v)	3	4(i)	4(ii)	5	6	7	8	9	10
South Africa				√		√	√			√	√				
USA						√	√			√	√				√
Australia	√		√	√		√	√		√	√	√		√		√
Canada	√	√		√		√	√			√					√
Finland & Sweden				√		√	√			√					√

where:

1	Cascade Control	4(ii)	Neural Networks
2(i)	Delay Compensation	5	Ratio Control
2(ii)	Feed-Forward Control	6	Adaptive and Inferential Control
2(iii)	De-coupling Control	7	Programmable Logic Control
2(iv)	IMC	8	Selective Control/Over-ride Systems
2(v)	MPC / DMC	9	Statistical Quality Control
3	Optimising Control	10	Expert Systems
4(i)	Statistical Process Monitoring		

Although the distinctions are somewhat blurred, the classifications in Table 2.1 that correspond to the areas of expert control, multivariable stabilizing control and supervisory control (with estimators and expert systems) are listed below (with key examples in brackets):

[1]Fully autogenous grinding. Also, 'AG' - autogenous grinding

Expert systems: 10. Expert Systems (Sotelo *et al.*, 1996; Wardell-Johnson *et al.*, 1997).

MVC: 2(iii) Decoupling Control and 2(v) MPC / DMC (Craig *et al.*, 1992*b*; Craig *et al.*, 1992*a*; Niemi *et al.*, 1992; Freeman *et al.*, 1994; Valenzuela *et al.*, 1994; Craig and MacLeod, 1995; Craig and MacLeod, 1996; Flament *et al.*, 1997; Desbiens *et al.*, 1997; Niemi *et al.*, 1997) and more recently (Boulvin *et al.*, 1999).

Supervisory: 3. Optimising Control, 6. Adaptive and Inferential Control and 8. Selective Control/Over-ride Systems (Herbst *et al.*, 1992; Herbst *et al.*, 1993; Morrison, n.d.; Valenzuela *et al.*, 1993; Borell *et al.*, 1996; Hart and Swartz, 1997) also (Samskog *et al.*, 1996) and more recently (Radhakrishnan, 1999).

Current Trends

The current trend in modelling mill load behaviour is primarily through discrete element methods (DEM) (Hodouin *et al.*, 2001). This observation is reinforced by the large number of papers on this topic at *SAG* 2001 the Third International Conference on Autogenous and Semiautogenous Grinding Technology, *e.g.*, Rajamani and Mishra, 2001; Herbst and Pate, 2001; Bwalya and Moys, 2001; Cleary et al., 2001, which indicates that completely satisfactory grinding or load behaviour models have not yet been attained. DEM models of SAG mills have been developing since the mid 1990's (Ranamani and Mishra, 1996). Current models are still based on spring/dash-pot models but now utilise increased computing power to better account for mill and lifter bar geometry, particle shape and the various ball-rock interactions that occur. Refinements to population balance models to account for the mill residence time distribution of rocks and particles are also being progressed (Austin and Cho, 2002).

2.1.2 Instrumentation

Table 2.2 lists the instrumentation requirements for SAG mill control, categorised as 'minimum', 'desirable' and 'ideal' (Fuenzalida *et al.*, 1996). The 'ideal' level of instrumentation "would allow for the incorporation of more detailed process models, unmeasured variable estimations and other support tools; rendering a much more powerful control system, not only for stabilizing purposes but also for overall process performance optimization."
The circuit that Fuenzalida *et al.* (1996) study differs from the NPM circuit in two ways:

1. the SAG and ball mills discharge into a common sump, and,
2. no flash flotation is present.

Table 2.2: SAG Mill Control Instrumentation Requirements

Scale	*Measurements*
minimum	• Fresh feed tonnage measurement and a regulatory PID control loop, controlling feeders. • SAG mill power measurement. • SAG mill bearing pressure measurement. • SAG mill water measurement and a regulatory PID control loop. • Circulating pebbles measurement, if present. • Pebbles crusher power measurement, if present.
desirable	• Ball mill power measurement. • Sump level measurement. • Sump and ball mill water addition measurement and a regulatory PID control loop. • Cyclone feed density measurement. • Cyclone feed pressure measurement.
ideal	• SAG feed particle size measurement. • Independent command upon various ore feeders. • Cyclone feed flowrate measurement. • Cyclone overflow particle size and percent solids measurement. • Variable speed pump. • Cyclone automatic on/off valves.

Constructed in the early 1990's, the NPM circuit is well equipped and has all of the instrumentation listed in Table 2.2 except for:

1. SAG feed particle measurement
2. Primary cyclone overflow particle size and percent solids measurement.

At a more fundamental level, Lynch (1977) states that in "any wet grinding circuit control system the basic sensing instrument requirements are:

(1) measurement and control of all ore and water flow rates to the circuit;

(2) measurement of the pulp level in the sump, so that the sump may be prevented from overflowing or running dry; and

(3) measurement of the circulating load, so that overload may be prevented."

The latter is possible through the cyclone feed density - cyclone feed flowrate measurement combination.

2.1.3 Inferential Measurement

Despite being well equipped in relation to these instrumentation lists (Section 2.1.2), inferential measurement of SAG mill inventories and SAG mill feed and discharge streams at Northparkes Mines is absent.

Indirect measurement of the mill inventories is possible via mill weight and power draw, conductivity probe and microphone measurements, acoustic spectral analysis, energy balance and state estimation. More recently, mill motor measurements have been utilised, in conjunction with other process variables, to infer mill loading, (Pontt, 2004). Direct measurement of mill feed size distribution is available through video image analysis. Hodouin *et al.* (2001) summarise that "video images of flowing [conveyor/truck dumping] particulate material are now processed to extract information on particle size."

The uptake of these technologies has been relatively slow and isolated to larger mining houses and new installations. The lag between development and uptake is reflected in the uptake of model based decision making control (Herbst, 2000). Industry reluctance is due to perceived gap between the technology cost and its benefits and also the performance record of the technology, or its stage of development.

A review of each of these available inferential measurement methods will now follow in Section 2.2. Video image analysis is reviewed in in Section 2.3. A summary of the focus and objectives of this research is contained in Section 2.4.

2.2 Mill Charge and Discharge Measurement

2.2.1 Mill weight and power draw measurements

Significant progress has been made in the area of inferential measurement of SAG mill inventory despite the associated difficulties (harsh operating environment, rotating nature of the mills and a comparatively low number of available measurements to the number of states). "Recent developments have been made in the direct measurement of the total load by the use of conductivity probes set into the mill lining (Moys *et al.*, 1996). Advances

have also been made with the indirect measurement of the mill contents (Herbst and Pate, 1999; Schroder, 2000) using Kalman filters in a combined state and parameter estimation framework" (Apelt *et al.*, 2001a).

Power draw

Several mill power draw models have been developed since the pioneering work of Bond (1961). These models have generally developed from the refinement of the Bond-Allis Chalmers model (Moys, 1993; van Nierop and Moys, 1997*a*; Herbst and Pate, 1999), *e.g.*, Equation (2.1), or via more detailed characterisation of the mill charge (JKTech, 1994; Valery Jnr and Morrell, 1995; Napier-Munn *et al.*, 1996; Valery Jnr., 1998), *e.g.*, Equation (2.2) - which is presented in detail in Chapter 3.

$$P_{Gross} = C3 \sin(\alpha) {D_m}^{0.3} W_C \left(3.2 - 3V^*\right) N^* \left(1 - \frac{0.1}{2^{9-10N^*}}\right) \tag{2.1}$$

$$P_{Gross} = P_{No\,Load} + k\,P_{Charge} \tag{2.2}$$

where

P_{Gross}	=	mill power draw (kW)
$P_{No\,Load}$	=	power draw of empty mill (kW)
P_{Charge}	=	charge contribution to the power draw (kW)
N^*	=	fraction critical speed
W_C	=	charge mass (t) (see the JA Herbst and Associates weight model below)
V^*	=	mill fraction occupied by the charge
α	=	charge angle of repose
$C3$	=	constant

Power draw is a function of mill load (mass and volume). This characteristic may be exploited to estimate mill charge levels. Erickson (1989), for example, generated volumetric ball charge fraction (J_b) curves on a power draw-charge weight grid. The mill rock load is a function of the breakage processes that are occurring. Power draw models have developed in parallel with the development of the mill charge breakage models. Mill weight models have progressed accordingly also.

The characteristic shape of the mill power draw curve (as a function of mill filling) which Equations (2.1) and (2.2) display, is shown Figure 2.1.

Despite the range available of charge dependent power draw models, their utilisation for charge estimation has been limited to total charge level (J_t) estimation for a specified ball

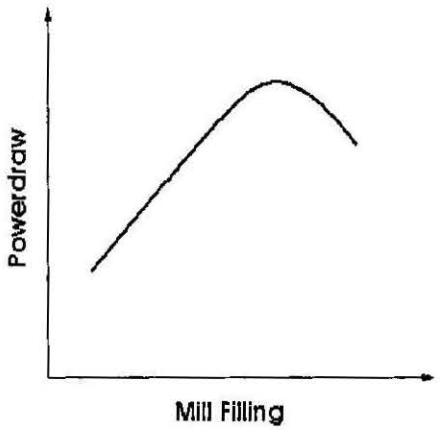

Figure 2.1: Mill power draw *versus* mill filling

charge level (J_b) (Kojovic *et al.*, 2001, Strohmayr and Valery, 2001). Chapter 5 presents the novel use of the "Morrell Power draw Model" for the estimation of ball and total charge levels.

Power draw measurement has also been analysed on a per-mill-revolution scale to determine total charge level. Koivistoinen and Miettunen (1989) found that the entry of the shell lifter bars into the charge caused power draw signal oscillation, the frequency of which is dependent on the number of shell lifter bar rows. The amplitude of oscillation is dependent on the charge volume with higher charge levels having a damping effect. The amplitude *versus* mill filling curve is concave, similar to the power draw *versus* mill filling curve of Figure 2.1. The limited utilisation of the osillation-charge level relationship may be due to a combination of the following:

- A relatively low number of lifter bars (12 in this paper) is required for effective signal filtering. Typical mills have between three and four times this number of lifters (48 in this research, see Chapter 4). Alternative high-lifter, low-lifter arrangements would only increase the filtering difficulties.
- The uncertainty introduced by the concave shape of the amplitude *versus* mill filling curve.
- A lack of awareness of the osillation-charge level relationship or signal filtering expertise amongst operation personnel.

Power draw models have been utilised in several cases in conjuction with mill weight models in a state estimation context, as discussed in Section 2.2.5.

Weight

As mentioned above, mill weight models have progressed in parallel with the mill charge breakage and power draw models. A simple weight model is obtained through linear regression of the mill weight measurement against the internal states (inspection/state estimation) of the mill, see Equation (2.3) (Herbst and Pate, 1999). A more complex model is given in Equation (2.4) which, although also linear, contains complexity in the charge mass (M_{Charge}) term where charge geometry is taken into account. Equation (2.4) is presented in more detail in Chapter 5.

$$M_{Mill} = C2\,(M_{Charge} + M_{Liners}) + C1 \tag{2.3}$$

$$M_{Mill} = M_{Charge} + M_{Shell} \tag{2.4}$$

where

M_{Mill}	=	mill weight (load cell) measurement (t)
M_{Charge}	=	weight of the mill contents (rock, water, media) (t)
M_{Liners}	=	mill liner weight (t)
M_{Shell}	=	mill shell and lining weight (t)
C1, C2	=	intercept and slope constants, respectively

The linear nature of the mill weight function of mill filling, which Equations (2.3) and (2.4) exhibit, is shown Figure 2.2. The curve is monotonically increasing and does not possess the 'looping over' of the power draw curve, see Figure 2.1, which has uncertainty implications in charge estimates from the power draw measurements. This matter is discussed in more detail in Chapter 6.

Mill weight is measured by mill bearing pressure or strain-gauge load cell. In the late 1980's bearing pressure technology meant that bearing pressure was not considered accurate enough for SAG mill control (Mular and Burkert, 1989). In the intervening years bearing pressure measurement has improved, has been adopted widely and is now considered a minimal requirement (Fuenzalida *et al.*, 1996), see Table 2.1.2. Both bearing pressure and load cell measurements are strongly influenced by mill and charge motion. To compensate, recent bearing pressure model developments include the influence of mill charge shape and mill drive forces (Evans, 2001).

Similar to the power draw model utilisation, mill weight models have been utilised to measure the total charge level (J_t) given the ball charge level (J_b), or, used in conjuction

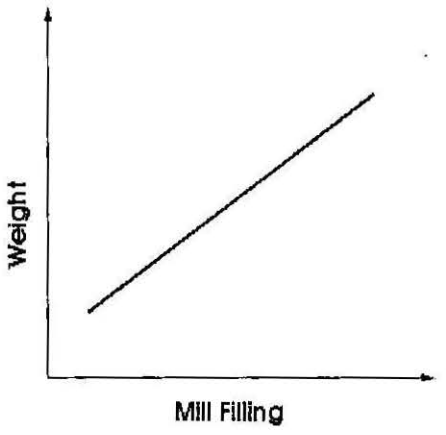

Figure 2.2: Mill weight *versus* mill filling

with mill power draw models in state estimation contexts to estimate both the total and ball charge levels (Herbst and Pate, 1999) and (Apelt *et al.*, 2001b). Chapter 5 presents the novel use of a mill weight model for the estimation of the ball and total charge levels.

2.2.2 Conductivity probe measurements and energy balance

Shell lining and lifter bar components are secured to the inside of the mill shell with bolts. Conductivity probes fixed within the bolts (usually the longer lifter bar bolts) can measure conductivity during a mill revolution to gain information regarding charge. Conductivity is high within the charge, rises on entry at the charge toe and falls on exit at the charge shoulder.

Strain gauges can be utilised in a similar manner. Force is exerted on a lifter bar as it enters at the charge toe and passes through the charge. On exit from the charge at the charge shoulder, the force decreases. Marklund and Oja (1996) utilised conductivity probes for total charge level measurement. The use of conductivity probes was the preferred method of four considered. The three methods eliminated were:

1. Bearing Back Pressure. Recognised as a widely available measurement, its main weakness was said to be the shifts due to temperature and oil circuit valve behaviour.

2. Power Draw Oscillation. Requiring no extra instrumentation or equipment - only signal filtering is necessary, the absence of shoulder position information was considered the main disadvantage.

3. Forces on a Lifter. Able to clearly detect toe position, the slow decay of the strain gauge signal results in an unclear shoulder position.

Moys and colleagues have worked extensively with the conductivity probe technique and have applied and progressed the technology from laboratory-scale through pilot-scale to

industrial scale (Moys, 1985; Moys, 1988; Moys, 1989; van Nierop and Moys, 1996; van Nierop and Moys, 1997*a*; van Nierop and Moys, 1997*b*). The information obtained from the conductivity measurement analysis includes:

- total charge level (J_t)
- charge centrifuging
- mill overload
- charge angle of repose (α)
- slurry pooling at the charge toe angles
- charge shoulder (θ_S) and toe (θ_T) angles (refer to Figure 2.3, which shows these angles for a simplified mill charge geometry)

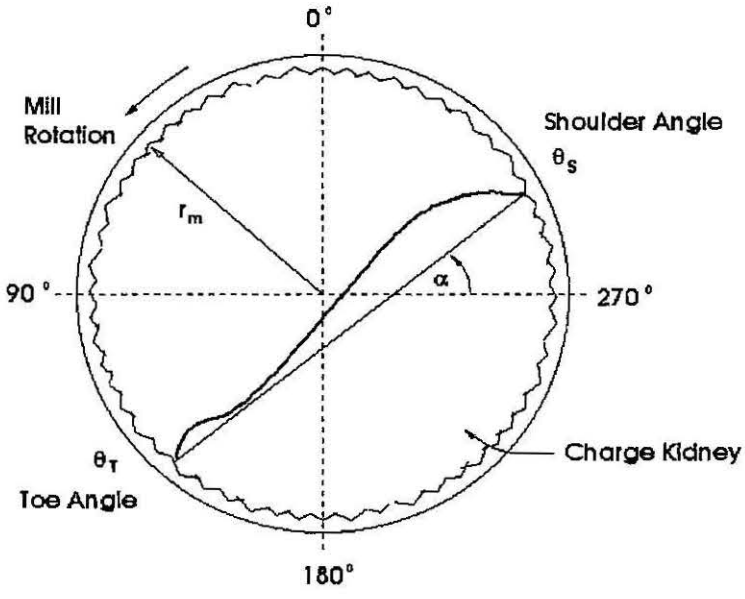

Figure 2.3: Simplified Mill Charge Geometry
(Moys et al., 1996)

To determine the volume of the total charge (J_t) from the conductivity measurements assumptions need to be made regarding the charge geometry. A flat surface between charge toe and shoulder, see Figure 2.3, is a common approximation. Another charge geometry assumption is the BHFU surface (an acronymn of initials of researchers Barth, Hinsley and Fobelets, and, Uggla who defined this hypothetical surface between 1930 and 1968), shown in Figure 2.4. The BHFU charge surface model was utilised for total charge level measurement via conductivity probes in liner bolts (Vermeulen and Schakowski, 1988).

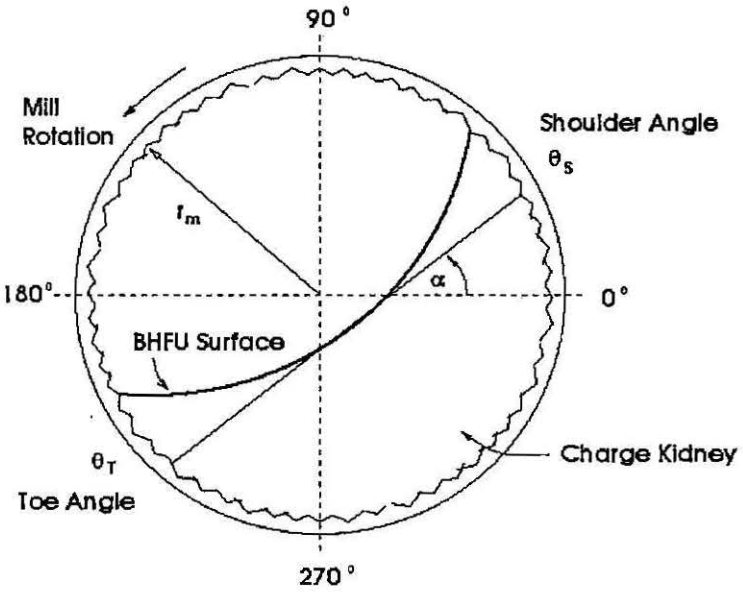

Figure 2.4: BHFU Mill Charge Geometry
(Vermeulen and Schakowski, 1988)

In the absence of flow measurement of SAG mill discharge water addition, Moys and colleagues have used thermocouples to define the energy and mass balances around the mill discharge sump to enable the inferential measurement of the:

- mill discharge water addition rate
- mill discharge density and viscosity
- the mill charge viscosity

(Moys, 1985; Moys *et al.*, 1987; Van Drunick and Moys, 2001)

In summary, conductivity probe measurements have been utilised successfully for total charge level (J_t) measurement. However, individual measurement of ball charge level (J_b) is not possible via this method.

2.2.3 Acoustic spectral analysis and sound measurements

In the 1980's, the use of mill sound for total charge measurement was relatively new and was receiving a mixed review. Mular and Burkert (1989), presumably utilising a microphone, considered it "not useful for control". However, the assessment of the utilisation of a audio probe mounted to the shell of a pilot scale mill saw some potential: "The audio probe measures vibrations from many sources and an expensive transducer and sophisticated techniques of frequency analysis would be required to isolate the signals that come from

sources close to the transducer. A major advantage of such a device is that it would not be subject to wear and would thus require no maintenance " (Moys, 1985). The potential in the use of stereophonic microphones, positioned at angular positions on either side of the charge toe (generally the point of impact) was also recognised for charge level and mill pulp density indication (Moys, 1988). Discussion arising from this paper concluded that:

- a microphone at 6 o'clock and another at 3 or 4 o'clock was a viable mill mass (total charge level) indication option for retrofitting
- the 6 o'clock microphone could also be used for pulp density indication

(Lyon, 1988)

Since the 1980's sound measurement has gained wider acceptance and is used with mill bearing pressure and mill motor windings temperature in a variable speed mill control strategy which manipulates mill feedrate subject to high-low limits on the former three measurements (Perry and Anderson, 1996).

Mill vibrations and acoustic emissions technology has also developed markedly. Digital accoustic signals emitted from laboratory-scale ball mill and transformed to power spectral densities were found to correlate highly with fine particle size distributions (-75μm to 4000 μm) (Aldrich and Theron, 2000).

"Judicious use of signal processing" for improved signal to noise ratio is currently being pursued for the measurement of in-mill variables, particularly charge toe angle, based on physics-based models of charge motion and the various rock-ball-mill shell collisions (Pax, 2001).

Along a similar vein, the measurement of charge position, motion and collisions is being pursued using the processing of surface vibration signals from accelerometers on the mill shell, sent to a fast data acquisition system and interpreted with the aid of a DEM mill model (Spencer *et al.*, 2000; Campbell *et al.*, 2001).

Since the first Edition of this thesis, the process control team at Northparkes Mines have upgraded the PLC controllers in the grinding circuit. The increased capabilities allowed the site to commission the implementation of mill load constraint-control (Thornton et al., 2005). The control strategy employs a pair of microphones for the audio-indication of charge toe position, manipulating feedrate to control charge level subject to an upper constraint on mill powerdraw. The SAG mill control system has a high degree of operator acceptance (95% utilisation) and can deal with "a wide range of plant disturbances and keep the mill operating at optimal load."

In summary, sound measurement is proving a useful indicator for charge toe position and total charge level. More recently, it has been successfully utilised in a mill charge control strategy. The technology of spectral analysis of mill sound and vibrations for toe position,

total charge level and charge motion information is currently emerging and showing good potential. Both techniques give total charge level (J_t) measurement only. Individual measurement of ball charge level (J_b) is not yet possible via these methods.

2.2.4 Mill motor measurements

Pontt (2004) has developed a load filling inferential measurement monitoring device that utilises the load torque reaction produced by the mill charge, stator voltage and excitation current of the large (20MW) synchronous mill-drive motors increasingly employed at large-scale, low-grade operations. Results for a 15,000 Hp SAG mill are presented that exhibited good correlation with visual inspection of mill filling. Utilisation of the MONSAG system increased production by approximately 3.2% and improved specific energy consumption by 3.8%.

2.2.5 State estimation

The comminution process is a typical industrial process in that "the total state vector can seldom be measured and the number of outputs is much less than the number of states" (Ray, 1981). State estimation techniques may be utilised to "provide acceptable estimates of all the state variables (even those not directly measured) in the face of measurement error and process disturbances" (Ray, 1981).

Significant research has been conducted in the use of Kalman filters for comminution process state estimation. Much of the research has been conducted by J.A. Herbst and colleagues whom, over time, have had association with Utah Comminution Centre, Control International (Inc.), GS Industries, JA Herbst and Associates, Svedala (Optimization Services and CISA) and Metso Minerals.

In the 1980's, in adaptive control strategies, the utilisation of a Kalman filter to estimate the current state, model parameters and the predicted state (in the next time step) is discussed (Herbst and Alba J., 1985). In conjunction with the use of a lifter-bolt strain gauge (for charge position indication), mill power draw measurement, and process models of the grinding media and mill shell lining, a Kalman filter was utilised to estimate the ball charge level and wear rate, liner thickness and wear rate (Herbst and Gabardi, 1988). The resulting control was a consistent ball charging rate for ball charge control at maximum mill power draw.

The lack of a rock charge model and the "tumbling mill" terminology in this example indicates that it is a ball mill under scrutiny. The foundation work, from the early 1980's,

is the University of Utah PhD thesis of W.T. Pate who studied a ball mill circuit[2]. Kalman filters were applied to autogenous/semiautogenous (AG/SAG) mills in the late 1980's when estimates of rock (one combined state), ball and water charges, shell liner weight and ore grindability were obtained from a dynamic model-Kalman filter arrangement (Herbst et al., 1989). Mill bearing pressure and power draw were the plant measurements utilised in this instance.

In the 1990's and in more recent years, the work of Herbst and colleagues is essentially the documentation of industrial applications and development of a commercial soft-sensor (Herbst and Pate, 1999; Herbst and Pate, 2001).

NorthEst, a JA Herbst and Associates commercial software product, was installed at Northparkes Mines late 1996 to estimate (and trend) the following unmeasured variables:

- Total charge filling level
- Ball filling level
- Grindability of the ore (t/kWh)
- The fraction greater than 55 mm within the mill (and by difference the fraction less than 55 mm)(Herbst & Associates, 1996)

  (The system consisted of five (5) state estimates (mill hold-up of two rock states ($\pm$55 mm), water, grinding balls and shell liner weight) and two (2) parameter estimates (ore grindability and charge angle of repose))

In its initial "Operator Monitoring" configuration, a 1 - 2% throughput improvement (over baseline) was expected. This target was not achieved due to various factors, such as:

- Configuration. The system was set up for a SAG mill with discharge trommel screen arrangement. Shortly after software installation, the trommel screen (which is attached to the mill itself) was removed and replaced by a (detached) vibrating screen, thus upsetting the mill weight calibration.
- Expertise. The system required the attention of a engineer trained-up on the software. Personnel movements and re-allocations at that time left the system without a "champion".
- Mistrust. Comprehension of the system and its functioning and capabilities was less than ideal. This lack of knowledge brought a degree of mistrust of the system which was not further utilised beyond the first commissioning stage.

A Kalman filter has been used on a iron ore pebble mill to "allow on-line estimation of filling levels, charge angle of repose, particle grinding rates, pebble wear and product size" (Herbst and Pate, 1996). Herbst and Pate (1999) describe a generic softsensor with examples of

- ore grindability estimation for a ball mill

[2]Discussion with WT Pate at SAG 2001 Conference, Vancouver, Sep 30 - Oct 3, 2001

- estimation of mill filling (ore, balls and water), dynamic angle of repose and ore grindability for a SAG mill

The Svedala Cisa OCS© optimising control system package for AG/SAG mills includes a softsensor module (Broussaud et al., 2001). Applications on minimally and comprehensively instrumented plants are described. The softsensor "continuously computes a mass balance and estimates mill charge (mass of solids, simplified size distribution and percent solids in the mill), cyclone feed, circulating load and cyclone overflow (particle size and percent solids)." The following "guideline for defining a proper level of instrumentation" is given in Table 2.3 (and correlates well with the list given earlier in Table 2.2).

Table 2.3: Guideline for defining a proper level of instrumentation

1. The *minimum level* which should be installed regardless of the size of the plant and other conditions, consists of:
   - feed rate measurement (weigh scales) and control,
   - all water additions measurement (flowmeters) and control valves),
   - mill power draw (all mills),
   - sump level (ultrasonic level sensors) and pump speed if there is a sump and variable speed pump,
   - DCS or PLC controls.
2. The next priority should be given to instruments which help the OCS© EKF and model to more accurately predict overload trends, and operate the process close to the circulating load limits:
   - mill charge: bearing pressure (when properly used), or load cells provide initial, inexpensive and valuable information. It comes systematically with state of the art mills,
   - weigh scale(s) on the pebbles crusher circuit,
   - magnetic flowmeter and nuclear density gauge on cyclone feed,
   - automatic valves for opening and closing cyclones in the classification circuit.
3. The need for installation of additional instrumentation should be assessed specifically for each plant when ore properties are variable. The following measurements are recommended and expected to become almost standard in the future:
   - Visual feed size analysis. The SAG mill feed size distribution can be measured on the feed belt via camera connected to a computer. Advanced dedicated image analysis system like Svedala TVis accounts for particle overlap and segregation on the belt and generates 3D distribution$_{[sic]}$. This information adds value to an optimizing control system. When OCS© soft sensor and predictor optimizer are in operation, real time information on feed size improves the accuracy of estimates of ore hardness or grindability, and makes it possible to better anticipate overload trends and opportunities to increase feedrate or power.
   - CCM: Continuous Charge Monitoring - Svedala has developed an advanced sensor for directly measuring mill load in rubber lined mills. CCM provides information which is complementary to bearing pressure or load cells since it may discriminate between liquid and solids, or rocks and fine ore and contains information about charge location and in some cases conditions of lifters.
   - Sound sensors: The nature and location of the sound generated by impacts within the mill contain an enormous amount of information about what is happening inside the mill.
4. When the downstream process is highly sensitive to particle size (like iron ore pelletizing or some flotation processes), a direct measurement of product fineness is appropriate. Such measurement may be either a measurement of particle size or something more specific - such as Blaine specific surface in iron ore pellet plants for instance.

(Broussaud et al., 2001)

The application of Kalman filters to SAG mill state estimation is clearly well progressed. In the "mature, active, emerging" terminology of Hodouin et al., (2001) due to the lack of widespread adoption it is should be considered an "active" area. This assessment is reinforced by the following points:

- Broussaud et al. (2001) assess that the on-line "estimation of the ball load and wear rate in a SAG mill remains a major difficulty in most plants. Ball addition is almost never perfectly controlled in SAG mills, essentially because there is no fully operational commercial ball addition system yet. Control systems have some difficulty finding the relative contribution of ore and balls to mill power draw. In the future a combination of CCM and good control of ball addition should allow a closer on-line optimization of the ball load and further improve SAG mill performance."
- The Herbst and Pate application of a Kalman filter for the estimation of mill rock and ball hold-up is recognised in a review of automation in the minerals processing industry where the implementation of model predictive control is hampered by "lack of precedent applications, high engineering costs and inappropriate control technologies" (Jamsa-Jounela, 2001).
- Research into state estimation for SAG mills is also currently being progressed at the Julius Kruttschnitt Mineral Research Centre where a Kalman filter is utilised to predict ore hardness, mill total charge and mill discharge factors (Schroder, 2000). An open-loop plant trial gave good correlation and tracking performance.

Although some difficulties are experienced, state estimation of mill rock charge, ball charge (J_b), water charge and thus total charge (J_t) is possible. In Chapter 7 combined state and parameter estimation for SAG mills is discussed further with the presentation of two formulations including the presentation of novel measurement models, one of which has already been placed in the public domain (Apelt et al., 2001b).

2.3 Feed Size Distribution Measurement

Feed size distribution measurement is generally considered important but not crucial, see Tables 2.2 and 2.3. Online image analysis is generally the accepted method for size measurement. The technology has been developing since the 1980's from the one-dimensional Autometrics MSD 95 instrument which used "photo-detectors to detect the shadows between the rocks along a probe line in the centre of the conveyor belt. These shadow data are then converted to size measurements" (Lange, 1988). Moving to a two dimensional image analysis instrument for improved size distribution estimation required a digital camera

(with high shutter speed) and further image processing developments to account for following important characteristics (which affect the stereology[3]):

"(a) The rocks overlap (occlude) and hide portions of one another.

(b) Occasionally a large rock looks like a group of small rocks, and groups of small rocks look like large single rocks.

(c) The surfaces of these rocks range from very smooth to very rough. The rocks can be described generally as having convex surfaces but they may have many ridges, indentations, and other features on their surfaces.

(d) Although not apparent in the images presented, the colour and intensities of these rocks also vary greatly, not only from rock to rock, but within a single rock.

(e) The rocks are 'randomly' oriented, but there are packing patterns.

(f) Some form of classification occurs on the conveyor belts. Small rocks may fall to the bottom or the rocks may be sorted across the width of the belt during loading from the hopper."

(Lange, 1988)

A good software-hardware match is required for practical instrument and despite blurring from belt speed and segregation on the belt, the "measurement is acceptable for use in milling control"(Lyon, 1988).

Since the 1980's the image methods have progressed to the point that numerous commercial instruments are available, including:

- *OOS* : An instrument developed in Australia that analyses contours that parallel laser beams make on rock laden conveyor belts (Fimeri, 1997) and best able to detect relative size changes on industrial conveyor belts (Davies et al., 2000).
- *SPLIT / Split – Online* : An image analysis system used to estimate the size distribution of blasted rock piles and moving streams. Arising from research at the University of Arizona, the *Split Engineering* product is now associated with the Julius Kruttschnitt Mineral Research Centre (Morrison, 2000). Image transformation is either by fragment delineation or a circular feature identification (circle centres and radii) algorithm (Girdner et al., 2001).

[3]The transformation that relates two-dimensional information to three-dimensional structure

- $T-VIS$: An instrument that analyses digital video frames of laden conveyor belts or truck-dumping points using software developed at the University of Utah to transform linear chord length distributions to volumetric distributions (Herbst and Blust, 2000). The actual sizing *versus* the $T-VIS$ sizing for a given example was "very close". The stereology accounts for particle overlap and segregation on the belt and generates 3D distribution (Broussaud *et al.*, 2001).

- *WipFrag* : An instrument that analyses images from a camera source. Originally developed to measure the size distribution of blasted rock with a "roving camera" (Maerz and Palangio, 2000). Inherent limitations of optical image analysis constrains measurement accuracy. However, the instrument has high precision and hence its output can be "used as a process control instrument, focusing on very small changes in measured size" (Maerz, 2001).

An alternative to the above dimensional image processing methods is a texture based image processing algorithm (Petersen et al., 1998). Mill feed systems exhibit a wide variety of conditions, *e.g.*, "order-of-magnitude ranges in particle size, the presence of mud and water, and concealment of particles" which can be better accommodated for by a textural approach (two-dimensional grey level (range and variance) assessment *versus* pattern recognition). In a developmental stage, this technology gave average particle size measurements to better than 90% accuracy.

With feed size measurement technology, particularly pattern recognition methods, reaching a high level of maturity, opportunities now exist to manipulate AG/SAG mill feed size distribution through stockpile feeder operation and blast pattern selection (Morrell and Valery, 2001) and through blasting practice optimisation (Sherman, 2001).

Despite these advances in size measurement there is scope for development of model-based means. Chapter 5 presents a novel model-based method for the inferential measurement of the feed size distribution which could be utilised as an alternative where capital or installation costs of the pattern and textural instrumentation are prohibitive.

2.4 Research Focus and Objectives

2.4.1 Focus

Recall from Section 1.3 that the lack of measurements around the SAG mill is a primary cause of the problems associated with SAG mill operation at Northparkes Mines . Hence, the area of inferential measurement modelling for SAG mills was stipulated as the focus of this research. The review of the literature and the relevant research in the area finds that:

Mill Inventories : Significant advances in this area have been made. The literature review has shown that developments in the concurrent estimation of both the ball charge level (J_b) and total charge level (J_t) is limited to state estimation formulations. Mill weight and power draw measurements have been utilised to estimate the total charge level (J_t) for a specified ball charge level (J_b). These measurements are generally available and there is scope to utilise them for the simultaneous estimation of the charge levels (J_t & J_b).

Feed Size : Image analysis instruments are gaining wider acceptance in industry. A primary concern of such instruments is the error introduced during the image analysis. The cost of these instruments is also prohibitive in some cases. Hence, there is scope to investigate a model-based alternative for inferential mill feed size measurement.

SAG Mill Discharge : Measurement of SAG mill discharge has generally been restricted to the direct measurement of cyclone feed flow and density. These measurements have also been inferred from mass and energy balances in the absence of flow meters and density gauges. The mill discharge measurement is a bulk flow measurement (solid, liquid and pulp). There is scope to investigate a size by size mill discharge inferential measurement which could provide insight into SAG mill performance.

State Estimation : Much work has been conducted in the area of state estimation for comminution circuits. However, widespread acceptance of this technology in the minerals processing industry is not evident. There is scope to add to the body of SAG mill state estimation knowledge which could assist in the transition from an 'active' to a 'mature' technology.

2.4.2 Objectives

In view of the findings of the review and the research focus, the objectives of this research are:

1. **Mill Inventories** : To develop and assess inferential models capable of the concurrent estimation of both of the SAG total charge (J_t) and ball charge (J_b) filling levels from mill weight or mill power draw measurements.

2. **Feed Size** : To develop and assess an alternative model-based inferential measurement of the SAG mill feed size distribution. The inferential measurement of the SAG mill feed rate and solids content is integral to the development of the inferential size measurement. Therefore, "to develop and assess an inferential model of the feed rate" is a further objective of this research.

3. **SAG Mill Discharge** : To develop and assess an inferential model of the SAG mill discharge rate and size distribution based on other plant measurements and equipment specifications.

4. **State Estimation** : To develop a combined state and parameter estimation formulation that utilises the SAG mill discharge models proposed by this research such that comparison may be made to the mill inventory inferential models and information supporting SAG mill state estimation may be added to the body of knowledge.

The research area of inferential measurement modelling for SAG mills is not on a "control method" in itself. However, using the terminology of Hodouin *et al.* (2001), the focus of this research falls in the "active" and "emerging" areas. The control method classifications into which this research falls generally are:

- Supervisory control of FAG/SAG grinding circuit using a combination of estimators and expert systems
- On-line use of phenomenological models.

In contributing to this area, by adding to the number of inferential measurement models available to industry and to the information available about the models, this research aims to assist the transition that takes a control method from an "active" or "emerging" phase to a "mature" phase.

Chapter 3

Steady State Model Development and Validation

In this Chapter the development and validation of steady state models of various comminution unit operations and the Northparkes Mines grinding circuit are described. Discussion of the steady state models is required as they are the foundation of the developments detailed in Chapters 4 through 7, especially the models of the SAG mill, oversize crusher, primary cyclones and SAG mill discharge screen. The source of the data utilised for model validation is detailed in Section 3.2. The development and validation of the unit operation models in isolation is described in Section 3.3. The linking of the unit operation models to form the Northparkes Mines grinding circuit and the circuit model validation are described in Section 3.4. Further model validation, against published data (Gault, 1975), is presented in Section 3.5.

The foundation of the modelling work in this Chapter and those that follow is that of the Julius Kruttschnitt Mineral Research Centre, which has studied and modelled autogenous (AG) and semi-autogenous grinding (SAG) mills for over twenty (20) years (Morrell and Delboni Jnr, 1996). Their "Variable Rates" AG/SAG model (utilised in this work) is "arguably ... the only one that is widely used ... for design, pilot mill scale-up and optimisation" (Morrell et al., 2001), which reflects the quality and depth of their research programme. These models are gaining wider acceptance and are being utilised for mill scale-up, design and optimisation (Morrell, 2004).

3.1 Model Development Logic

This Section provides an overview of logic behind the development and utilisation of the models presented in Chapters 3, 4 and 5.

In Chapter 3, the steady state models of the unit operations that make up the grinding circuit at Northparkes Mines are described. The basis of the steady state models is the extensive modelling work conducted by the Julius Kruttschnitt Mineral Research Centre.

The models are realised in the MATLAB-Simulink environment in the model development sections. This development serves two purposes. Firstly, replicating the results of commercially-available software demonstrates that the models have been correctly coded in the MATLAB-Simulink environment. Secondly, sufficient confidence in the steady state model coding allowed the progression of the research towards the final goal of the development of inferential measurement models.

The physics behind the steady-state models is not described in detail in this Thesis. Such description is beyond the scope of this research. Furthermore, the model physics is described in detail elsewhere (Whiten, 1974), (Lynch, 1977), (JKTech, 1994), (Morrell and Delboni Jnr, 1996), (Napier-Munn et al., 1996), (Valery Jnr., 1998), *etc.*

Dynamic models of the SAG mill ball charge, rock charge, water charge and mill liner weight are presented in Chapter 4. The SAG mill ball charge and mill liner models are novel to this research and the associated physics and logic are presented alongside the development of the model equations.

The SAG mill rock and water charge models are dynamic extensions of the steady state models presented in Chapter 3 and draw heavily from the work of Valery, (Valery Jnr and Morrell, 1995) and (Valery Jnr., 1998), who was conducting research at the Julius Kruttschnitt Mineral Research Centre at that time.

The presentation and development of dynamic models was required for their utilisation in the Combined State and Parameter Estimation model formulations presented in Chapter 7 and described in one of the the journal papers resulting from this research: Apelt et al. (2002a).

Chapter 5 describes the inferential measurement models of the SAG mill inventories, fresh feedrate and discharge rate and the corresponding size estimates. The development of these inferential models was a key objective of this research. The inferential models have been described in two further journal papers resulting from this research: Apelt et al. (2001a) and Apelt et al. (2002b).

The models are subjected to model validation, sensitivity analysis (also detailed in these two journal papers) and case-study type applications in Chapters 5, 6 and 8, respectively. The model demonstration on plant data, construction of a SAG mill operating curve and MVC development and simulation constitute the content of the next journal installment (Apelt and Thornhill, In Press).

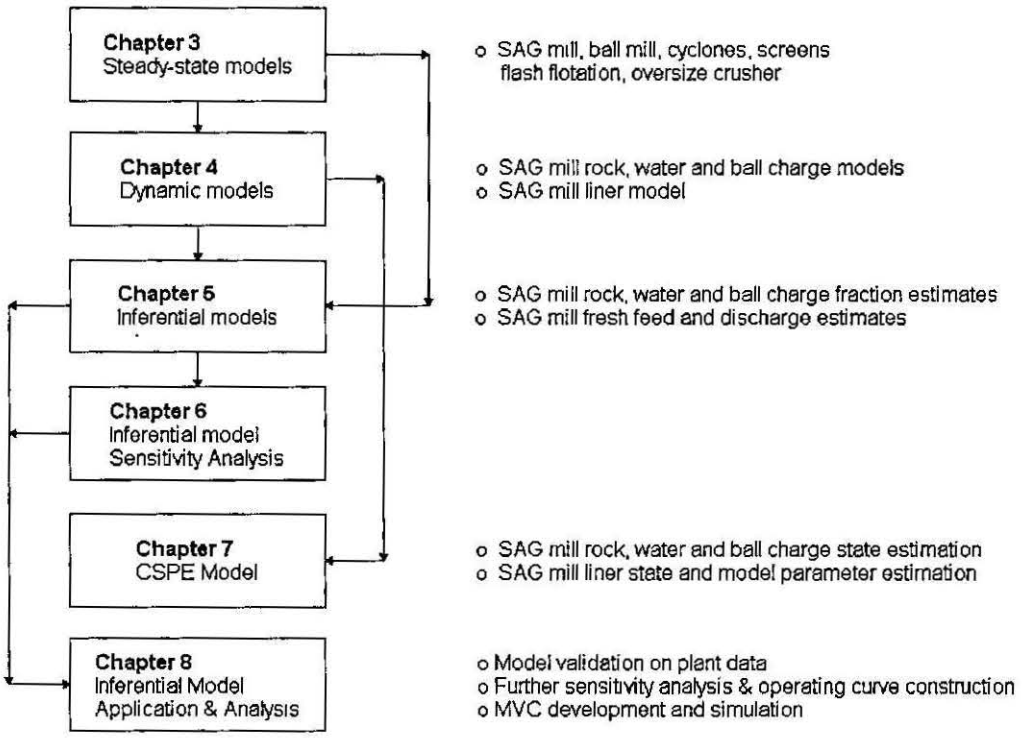

Figure 3.1: Model development logic, illustrating how the steady-state models form the foundation from which the dynamic, inferential and state-estimation are developed.

3.2 Model Validation Data Source

The data utilised for model validation originates from the results of detailed grinding circuit surveys conducted in early 1997 (David, 1997). A consultant from JKTech[1] attended site and co-ordinated the surveying of Module 1 and 2 grinding circuits with site personnel, including the author. Duplicate steady-state surveys of each grinding module were completed. The surveys were conducted for steady state model generation purposes.

The on-site survey procedure entailed:

1. **Setup:** Operating parameters conducive to steady-state grinding circuit operation were established a number of hours (nominally 4 hours in this case) prior to the target circuit survey start time. These operating parameters were maintained to allow the circuit to reach steady-state.

2. **Sampling:** Once steady-state conditions were prevalent, sampling of the circuit commenced. Fifteen−minute samples were taken of the primary and secondary cyclone feed, overflow and underflow streams, the SAG mill discharge screen undersize stream and the ball discharge stream over a two-hour period. Circuit operating parameters were monitored and recorded during this two-hour period to ensure steady-state conditions were maintained.

   The slurry-stream samples were collected using slotted, sampling scoops and collected in buckets. Cyclone feed sampling was effected by the utilisation of the periodic opening of the knife-gate valve feeding to a spare cyclone with a blanked-off overflow. This configuration allowed the taking of a feed sample via the cyclone spigot while the knife-gate valve was open.

3. **SAG mill crash-stop:** At the end of the two-hour survey period, the SAG mill was crashed-stopped. Once the SAG mill, SAG mill feed conveyor and the oversize crusher feed conveyor had been electrically isolated, belt-cut samples were taken and a mill inspection was completed to determine mill rock and ball loading. The belt-cut samples were collected into sealed, 44-gallon drums.

All of the samples were dispatched to The Julius Kruttschnitt Mineral Research Centre for size and moisture analysis. The results obtained were then utilised to generate *JKSimMet*[2] models for each of the processing unit operations, using the model-fitting functionality incorporated in *JKSimMet*. The individual models were then linked up to

[1] JKTech is the commercial division of the Julius Kruttschnitt Mineral Research Centre (JKMRC)

[2] Steady state mineral processing simulation software developed at the JKMRC and distributed by JKTech

match the topology of the Northparkes Mines grinding circuits. These circuit models were then used to simulate various operating conditions and process configuration alterations so that informed decisions regarding production targets were possible. The findings were documented in the report by David (1997), which was the main project deliverable.

The base-case simulation circuit model for Module 1 Grinding Circuit presented in the report represents the as-surveyed circuit model. It is this model that is used as the reference case for model validation in this document. As mentioned previously, the JKSimMet Module 1 circuit model results are detailed in Appendix B.

3.3 Steady State Model Development

This Section details steady state models of the following comminution unit operations:

- SAG mill
- hydrocyclones
- oversize crusher
- mill discharge screens
- ball mill
- flash flotation cells

The unit operation models have been coded into MATLAB-Simulink. The models are based on those developed by the Julius Kruttschnitt Mineral Research Centre (Morrell and Morrison, 1989; JKTech, 1994; Morrell and Delboni Jr, 1996; Morrell and Morrison, 1996; Napier-Munn *et al.*, 1996; Valery Jnr., 1998) with the model parameters being drawn from the survey models (David, 1997), see Appendix B.

The JKSimMet simulation model of the Module 1 grinding circuit is the basis of the model constructed in MATLAB-Simulink. The JKSimMet simulation results, model parameters and other grinding circuit survey data are contained in Appendix B. The JKSimMet simulation results also form the basis of the MATLAB-Simulink model validation.

In this Section, the unit operation models are firstly described with model validation of each unit operation in isolation. In Section 3.4 the units are linked together to simulate the Northparkes Mines Module 1 grinding circuit and validated against the survey information in Appendix B.

3.3.1 SAG Mill

A simplified cross-sectional view of the charge within a rotating SAG mill is shown in Figure 3.2. Lifter bars on the mill shell lift the charge to the shoulder from where the material is thrown or rolls (cataracts) towards the charge toe. The throwing, cataracting and general rubbing that occurs within the charge causes high energy (impact) and low energy (abrasion & attrition) breakage.

The rotating charge with the mill forms a kidney shape across which a velocity profile exists. At the 'eye' of the kidney the velocity is zero. The charge inner radius, r_i, delineates the "active" and "inactive" regions of the charge. Most breakage occurs within the active part of the charge and it is the active part of the charge that may be used in the modelling of mill weight and mill powerdraw.

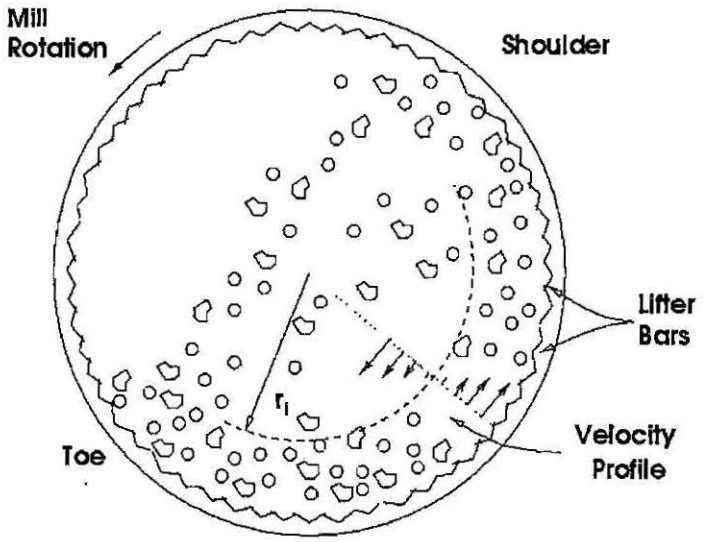

Figure 3.2: Simplified mill charge cross-section

The SAG mill model is comprised of:

1. solids balance
2. water balance
3. ball charge model
4. powerdraw model
5. impact zone model

The solids and water balances are inter-related and are integral to the perfectly mixed mill model described below. The ball charge model is independent of these mass balances.

However, the ball charge influences the solids balance via the breakage rates. The powerdraw and impact zone models are utilised once the mass balances and ball charge have been specified.

SAG Mill Charge/Product Model Algorithm

To further clarify the relationships between the mass balance and ball charge models, the calculation sequence for the perfectly mixed SAG mill model is presented below. Diagrammatic representation of this algorithm is given elsewhere (Napier-Munn *et al.*, 1996), (Valery Jnr., 1998).

1. Read input data
    - mill specifications
    - discharge grate specifications
    - general appearance function database
    - initial estimate of rock charge
    - ball charge
    - feedrate and size distribution
    - ore breakage characteristics
    - breakage rates
2. Make initial estimates of mill slurry holdup and mill discharge
3. Calculate low and high energy appearance functions and the combined appearance function
4. Apply the steady state perfectly mixed mill model
5. Compare the new estimates of mill slurry holdup with intial estimate
6. If error acceptable, stop
7. Else, adjust maximum discharge rate and return to Step 4.

Solids Balance

The solids mass balance for the SAG mill is based on the Whiten perfect mixing model (Whiten, 1974), which is an independently developed, special case of the general population balance model described elsewhere (Austin et al., 1987). On a size by size basis, the solids

may be stated as follows (Valery and Morrell, 1995), (Napier-Munn *et al.*, 1996):

$$\begin{aligned} Accumulation &= In - Out + Generation - Consumption \\ \frac{ds_i}{dt} &= f_i - p_i + \sum_{j=1}^{i-1} r_j s_j a_{ij} - (1 - a_{ii}) r_i s_i \qquad (3.1) \\ Accumulation &= 0 \; at \; steady \; state \\ 0 &= f_i - p_i + \sum_{j=1}^{i-1} r_j s_j a_{ij} - (1 - a_{ii}) r_i s_i \qquad (3.2) \end{aligned}$$

where

s_i = mill rock charge particles in *size* i (t)

f_i = feedrate of particles in *size* i (t/hr)

p_i = mill discharge (product) of particles in *size* i (t/hr)

r_i = breakage rate of particles in *size* i (hr^{-1})

a_{ij} = appearance function of particles appearing in *size* i (a function of the breakage distribution of particles in sizes $\geq$ *size* i) (fraction)

The feed component in Equation (3.1) requires no further discussion except that it is assumed to be known *e.g.*, from sizings of conveyor belt samples taken during a grinding survey. The product, generation and consumption components will now be discussed further.

Product

The mill product, p_i, (the SAG mill discharge stream, $SMDC$) is calculated as follows:

$$p_i = d_0 c_i s_i \qquad (3.3)$$

where

d_0 = maximum mill discharge rate constant (hr^{-1})

c_i = grate classification function for *size* i (fraction)

= probability of a *size* i particle passing through mill discharge grate

Referring to Equation (3.4) and Figure 3.3, the grate classification function, c_i, is equal to unity for particle sizes less than the size that behaves like water, x_m ($x < x_m$) and equal to zero for particle sizes greater than the notional pebble port aperture size, x_p ($x > x_p$). For particles sizes greater than the water-like size but less than or equal to the grate aperture size, x_g ($x_m < size \leq x_g$), the classification function, c_i, decreases linearly to the point

(x_g, f_p) where there is a change in gradient. From this point, the classification function, c_i, decreases linearly to the point $(x_p,0)$. The fitted model parameter f_p is the notional open area of the pebble ports as a fraction of the total grate open area (JKTech, 1994).

$$\begin{aligned} c_i &= 0.0 && \text{for } x \geq x_p \\ c_i &= \frac{x_p - x}{x_p - x_g} f_p && \text{for } x_g < x < x_p \\ c_i &= \frac{x - x_m}{x_g - x_m}(f_p - 1) + 1.0 && \text{for } x_m < x \leq x_g \\ c_i &= 1.0 && \text{for } x \leq x_m \end{aligned} \tag{3.4}$$

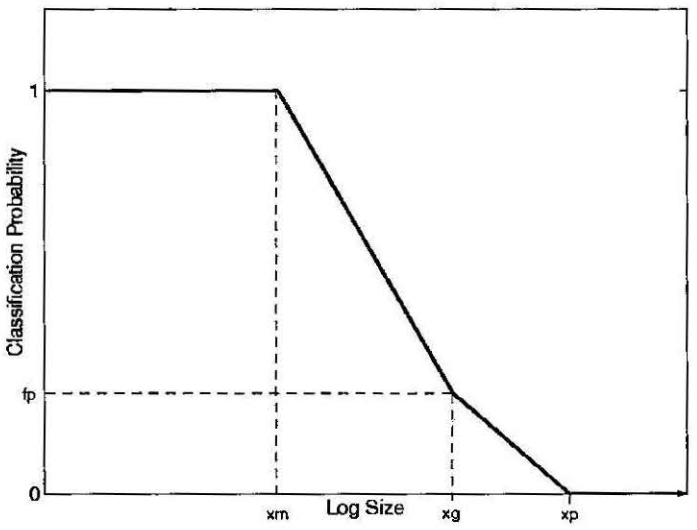

Figure 3.3: Grate Classification Function

The mill ore charge, s_i, product, p_i, and maximum mill discharge rate constant, d_0 are determined in an iterative manner given the initial estimate of the ore charge and x_m, the particle size which behaves effectively as water in the mill.

From the initial estimates of the SAG mill rock charge properties ($SMRC$) and size distribution ($smrc$) the volumetric fraction of the grinding charge occupied by slurry, J_{pm}, is determined which can then be utilised to determine the volumetric discharge from the mill, Q.

$$Q = Q_m + Q_t \tag{3.5}$$

$$Q_m = 6100\, J_{pm}^2 \gamma^{2.5} A \phi^{-1.38} D^{0.5} \tag{3.6}$$

$$Q_t = 935\, J_{pt} \gamma^2 A\, D^{0.5} \tag{3.7}$$

where

Q_m = mill discharge flowrate through grinding media (m^3/hr)

Q_t = mill discharge flowrate through slurry pool at toe of the charge (m^3/hr)

A = total discharge grate open area (m^2)

D = mill inside diameter (m)

γ = mean relative radial position of open area (fraction)

ϕ = fraction critical mill speed (fraction)

$$J_{max} = 0.5\, J_t - J_{po} \tag{3.8}$$

= maximum possible nett fractional grinding media slurry holdup (fraction)

$$J_p = J_{pg} - J_{po} \tag{3.9}$$

$$= J_{pm} \text{ (for } J_p \leq J_{max}) \tag{3.10}$$

$$= J_{pt} + J_{pm} \text{ (for } J_p > J_{max}) \tag{3.11}$$

= nett fractional holdup of slurry in mill (fraction)

J_{pm} = nett fractional holdup of slurry in mill that is contained within the grinding charge interstices (fraction)

J_{pt} = nett fractional holdup of slurry in mill that is contained in the slurry pool at the toe of the charge (fraction) (*i.e.*, slurry outside the grinding charge)

J_{pg} = gross fractional holdup of slurry in mill (fraction)

$$J_{po} = 0.33(1 - r_n) \tag{3.12}$$

= nett fractional slurry holdup in mill 'dead' zone (fraction) (*i.e.*, fraction of mill volume outside outermost grate apertures)

$$J_{pt} = J_p - J_{max} \tag{3.13}$$

J_t = mill volume fraction occupied by the grinding charge (balls + coarse rocks + interstices) (fraction)

r_n = relative radial position of outermost grate apertures (fraction)

The initial estimates of volumetric mill discharge and rock charge are used to determine the the maximum mill discharge rate, d_0 (Valery Jnr., 1998),

$$d_0 = \frac{Q_m + Q_t}{(J_{pm} + J_{pt}) \cdot V_m} \tag{3.14}$$

where

V_m = mill internal volume (m^3)

Napier-Munn *et al.* (1996) state that the charge toe angle, θ_T, and the slurry toe angle, θ_{TO}, are equal for grate discharge mills, *i.e.*,

$$\theta_{TO} = \theta_T \tag{3.15}$$

This implies that no slurry pool exists and the nett fractional hold up of slurry is less than the media maximum holdup capacity, *i.e.*, $J_p \leq J_{max}$, and reduces Equation (3.14) to

$$d_0 = \frac{Q_m}{J_{pm} \cdot V_m} \tag{3.16}$$

and mill volumetric discharge may then be calculated from Q_m only (Equation (3.6)). (Section 3.3.1 discusses charge toe and slurry toe angle in more detail.)

Recognising the the mill volumetric discharge, Q_m, is in fact the mill product which consists of water and water-like solids ($size < x_m$), *i.e.*,

$$p_{xm} = k_g Q_m \tag{3.17}$$

allows the calculation of an initial estimate of the maximum discharge rate constant, d_0, and the volume of solids of $size < x_m$, s_{xm}, from

$$d_{xm} = \frac{p_{xm}}{s_{xm}} \tag{3.18}$$

where

$$\begin{aligned} d_{xm} &= d_0 \qquad (3.19)\\ &= \text{mill discharge rate for water and solids of size} < x_m \ (\text{hr}^{-1})\\ &= \text{maximum mill discharge rate constant} \ (\text{hr}^{-1})\\ s_{xm} &= J_{pg}\, \pi \frac{{D_m}^2}{4} L_m \qquad (3.20)\\ &= \text{volume of water and solids of size} < x_m \text{ in the mill} \ (m^3)\\ k_g &= \text{factor to account for coarse material} \ (-) \end{aligned}$$

The steady state mass balance, Equation (3.1), is then applied and solved for the rock load, $SMRC/smrc$. The corresponding volume of rock load smaller than x_m is then calculated

and compared to the initial estimate. The maximum discharge rate, d_0, is adjusted by Equation (3.21) until agreement is satisfactory.

$$d_{0,\,k+1} = d_{0,\,k} \cdot \frac{s_{xm,\,k+1}}{s_{xm,\,k}} \tag{3.21}$$

where

$d_{0,\,k+1}$	=	discharge rate constant at $k + 1^{th}$ iteration (hr^{-1})
$d_{0,\,k}$	=	discharge rate constant at k^{th} iteration (hr^{-1})
$d_{0,\,k+1}$	=	discharge rate constant at $k + 1^{th}$ iteration (hr^{-1})
$s_{xm,\,k+1}$	=	mill water and rock charge smaller than x_m at $k + 1^{th}$ iteration (m^3)
$s_{xm,\,k}$	=	mill water and rock charge smaller than x_m at k^{th} iteration (m^3)
k	=	iteration step

In summary, the calculation sequence for the maximum mill discharge rate constant (d_0) is as follows:

1. Given
   - initial estimates of the rock charge, $SMRC/smrc$
   - particle size that behaves effectively as water, x_m

   determine
   - volumetric fraction of grinding charge voidage occupied by slurry, J_{pm}
   - the mill volumetric discharge (product), $k_g Q_m = p_{xm}$
   - the volume of slurry within the mill, s_{xm}
   - the discharge rate for water and sub x_m size solids (maximum discharge rate constant), $d_{xm} = d_0$
2. apply steady state mass balance and solve for mill rock charge, s_i
3. recalculate s_{xm} and compare to initial estimate
4. if agreement is within tolerance, stop
5. else, adjust d_0 and goto Step 2.

Consumption and Generation

Both the generation and consumption components have a dependence on the breakage rate function, r_i, and the appearance function, a_{ij}.

Breakage Rate Function, r_i : The "variable rates model" (JKTech, 1994) and (Morrell and Morrison, 1996) is a set of five pairs of "knot" sizes and base breakage rates. The knot sizes are selected to encompass the size distribution and capture important features of the breakage rate curve, *e.g.*, the slower breaking rates of the critically sized material (which is discharged from the mill via pebble ports and recycled to the oversize crusher). The breakage rate for each particle size is determined by interpolation. The base breakage rates are as follows (JKTech, 1994) and (Morrell and Morrison, 1996):

$$ln(R1) \doteq \frac{(k_{11} + k_{12}ln(R2) - k_{13}ln(R3) + J_B(k_{14} - k_{15}F_{80}) - D_B)}{S_b} \tag{3.22}$$

$$ln(R2) = k_{21} + k_{22}ln(R3) - k_{23}ln(R4) - k_{24}F_{80} \tag{3.23}$$

$$ln(R3) = S_a + \frac{(k_{31} + k_{32}ln(R4) - k_{33}R_r)}{S_b} \tag{3.24}$$

$$ln(R4) = S_b\left((k_{41} + k_{42}ln(R5) + J_B\left(k_{43} - k_{44}F_{80}\right)\right. \tag{3.25}$$

$$ln(R5) = S_a + S_b\left(k_{51} + k_{52}F_{80} + J_B\left(k_{53} - k_{54}F_{80}ln(R4)\right) - 3D_B\right) \tag{3.26}$$

where

$R1 \ldots R5$ = base breakage rates (hr^{-1})

k_{ij} = regression coefficients

J_B = mill volume occupied by grinding balls and associated voids (%)

$$S_a = ln(\frac{RPM}{23.6}) \tag{3.27}$$

= mill RPM scaling factor

$$S_b = ln(\frac{N_{fcs}}{0.75}) \tag{3.28}$$

= mill fraction critical speed scaling factor

$$D_B = ln(\frac{D_{ball}}{90}) \tag{3.29}$$

= ball topsize scaling factor

$$R_r = \frac{\text{tph recycled material } -20 + 4 \text{ mm}}{(\text{tph fresh feed} + \text{tph recycled material } -20 + 4 \text{ mm})} \tag{3.30}$$

= recycle ratio of $-20 + 4$ mm material

Regression coefficients, k_{ij}, are given in Table 3.1 and are based on data collected by the Julius Kruttschnitt Mineral Research Centre. From inspection of Equations (3.22) through (3.30) it is evident that the breakage rates are a function of:

- equipment parameters (mill speed and ball size)
- parameters (regression coefficients)
- operating conditions (feed size, recycle ratio and ball charge level, J_b)

Detail of the effects of ball load, feed size, recycle load, mill speed and ball size on the breakage rates can be found elsewhere (Morrell and Morrison, 1996).

Table 3.1: Breakage Rate Regression Coefficients, k_{ij}

j	k_{1j}	k_{2j}	k_{3j}	k_{4j}	k_{5j}
1	2.504	4.682	3.141	1.057	1.894
2	0.397	0.468	0.402	0.333	0.014
3	0.597	0.327	4.632	0.171	0.473
4	0.192	0.0085	-	0.0014	0.002
5	0.002	-	-	-	-

Appearance Function, a_{ij} : The appearance function, a_{ij}, is a matrix of column vectors that describe:

1. the amount of material in a give size that is "selected" for breakage, and,
2. the distribution that remains after breakage has occurred

Each particle size has its own vector and thus, the appearance function matrix is a square matrix of dimension (no. of sizes × no. of sizes). Since there is no particle growth, the appearance function matrix is a lower-triangular matrix.

Each appearance function vector is a weighted average of high-energy (impact) breakage and low-energy (abrasion) breakage appearance functions:

$$a_{ij} = \frac{t_{le}a_{le} + t_{he}a_{he}}{t_{le} + t_{he}} \tag{3.31}$$

where

a_{he} = high energy appearance function, (fraction)
a_{le} = low energy appearance function (fraction)
t_{he} = high energy (impact) t parameter (%)
t_{le} = low energy (abrasion) t parameter (%)

The t parameters are size distribution data identifiers, *i.e.*, a look-up table reference point for data in a Julius Kruttschnitt Mineral Research Centrereference database. The high energy t parameter is also known as the "$t10$" or "t_{10}" parameter and the low energy t parameter is also known as the "ta" or "t_a" parameter. That is,

$$\begin{aligned} t_{10} &= t_{he} \\ t_a &= t_{le} \end{aligned} \tag{3.32}$$

Breakage due to abrasion is assumed to be independent of size. For a given ore type a t_a value is determined from laboratory abrasion tests. The t_a is the cummulative percent (by weight) of material passing $\frac{1}{10}th$ of the original particle size after low energy breakage has occurred. For example, a 30mm particle with a $t_a = 1\%$ is subjected to a low energy breakage event after which 1% of the material is < 3 mm in size. That is, mostly large particles remain, as expected for abrasion breakage. A complete distribution is obtained from a single t_a value from Table 3.3.1.

Table 3.2: Low Energy Appearance Function

Particle Size (t value)	Cummulative % Passing (t_a scaling factor)
$t_{1.25}$	$2.687 \cdot t_a$
$t_{1.5}$	$1.631 \cdot t_a$
t_{10} (t_a)	$1.0 \cdot t_a$
t_{100}	$0.9372 \cdot t_a$
t_{250}	$0.8070 \cdot t_a$
t_{500}	$0.6365 \cdot t_a$

p A-74 Appendix A9 (JKTech, 1994)

The cummulative percent passing distribution of the particle sizes of interest are determined by interpolation. Conversion to a weight fraction retained format results in the low energy appearance function.

Breakage due to impact is dependent on ore type and on the particle size (by way of the breakage energy that is exerted on particles of that size). Therefore, each size fraction has a unique t_{10} value.

A t_{10} value is the cummulative percent (by weight) of material passing $\frac{1}{10}th$ of the original particle size after high energy breakage has occurred. A complete distibution is obtained from a single t_{10} value from a database of t_{10} *versus* [t_{75}, t_{50}, t_{25}, t_4, t_2] data. Again, the cummulative percent passing distribution of the particle sizes on interest are determined by interpolation.

The ore dependancy is determined from laboratory test work and is reported as two impact breakage parameters, A and b. The breakage energy dependancy is through a specific comminution energy, Ecs, parameter. The t_{10} values for each size fraction is determined

using these three parameters (A, b, Ecs) as follows:

$$t_{10_i} = A(1 - e^{-b\,Ecs_i}) \tag{3.33}$$

where

A	=	ore impact breakage parameter (−)
b	=	ore impact breakage parameter (−))
Ecs_i	=	specific comminution energy for *size* i (kWhr/t)

The specific comminution energy, Ecs_i, is a vector of the amount of energy available for impact breakage of the $i\,th$ particle size and is determined as follows (Valery Jnr., 1998):

$$Ecs_i = \frac{\psi_e\, gms_i\, \rho_{m_i}\, g\, h}{SG_s\, x_i\, 3.6 \times 10^3} \tag{3.34}$$

where

ψ_e	=	energy absorption factor of the steel grinding media (fraction)
gms_i	=	grinding media size class i (mm)
ρ_{m_i}	=	density of grinding media in *size* i (t/m^3)
g	=	gravitational acceleration (m/s^2)
h	=	mean drop height (m)
SG_s	=	ore specific gravity (t/m^3)
x_i	=	target particle *size* i (mm)
3.6×10^3	=	$\frac{kWhr}{t}$ conversion factor

The mean drop height, h, is determined from charge geometry information as follows:

$$h = \frac{(r_{sm} + r_i)}{2}\,(sin(\theta_S) - sin(\theta_T)) \tag{3.35}$$

where

r_{sm}	=	SAG mill radius (m)
r_i	=	SAG mill charge inner radius (m)
θ_S	=	SAG charge shoulder angle (radians) (see Section 3.3.1)
θ_T	=	SAG charge toe angle (radians) (see Section 3.3.1)

The target particle size, x_i, is the geometric mean of the size distribution intervals, *i.e.*,

$$x_i = \frac{(size_{i-1} + size_i)}{2} \tag{3.36}$$

The density of grinding media in *size i*, ρ_{m_i}, is calculated as follows (Valery Jnr., 1998):

$$\rho_{m_i} = \frac{(\frac{1}{2}\, vo_i \;+\; \sum_{i=1}^{i-1} vo_i)\, SG_s \;+\; (\sum_{i=1}^{n} vb_i)\, SG_b}{\frac{1}{2}\, vo_i \;+\; \sum_{i=1}^{i-1} vo_i \;+\; \sum_{i=1}^{n} vb_i} \tag{3.37}$$

where

i = $\sqrt{2}$ size class
- $i = 1$: largest size
- $i = n$: smallest ball size
- $i = q$: smallest rock size (16 mm)
- $i = z$: smallest particle size

vo_i = the volume of ore in size class i (m^3)

vb_i = the volume of grinding balls in size class i (m^3)

SG_b = grinding ball density (t/m^3)

Grinding balls and ore larger than fifty 50 mm constitutes grinding media. Fifty percent of rock in *size i* is larger than the remaining fifty percent and can theoretically cause breakage within the size fraction. All rocks greater in size than *size i* and all of the grinding balls can cause breakage. Therefore, the grinding media size that is effective on *size i*, gms_i, is calculated as follows (Valery Jnr., 1998):

$x_i \geq 50\,mm$

$$gms_i = \left(\frac{\frac{1}{2}\, n_i\, x_i^2 \;+\; \sum_{j=1}^{i-1} n_j\, x_i^2 \;+\; \sum_{j=1}^{z} nb_j\, x_j^2}{\frac{1}{2}\, n_i \;+\; \sum_{j=1}^{i-1} n_j \;+\; \sum_{j=1}^{z} nb_j} \right)^{0.5} \tag{3.38}$$

$x_i < 50\,mm$

$$gms_i = gms_{i-1}$$

where

$$n_i = \frac{SMRC_i}{M_i} \tag{3.39}$$

$= $ number of particles in *size i*

$SMRC_i$ = SAG mill rock charge mass in *size i* (t)

$$M_i = \frac{\pi}{6} \left(\frac{size}{1 \times 10^3} \right)^3 SG_s \tag{3.40}$$

$= $ mass of an ore particle in *size i* (t)

$$nb_i = \frac{SMBC_i}{Mb_i} \tag{3.41}$$

$= $ number of grinding balls in *size i*

$SMBC_i$ = SAG mill ball charge mass in *size i* (t)

$$Mb_i = \frac{\pi}{6} \left(\frac{size}{1 \times 10^3} \right)^3 SG_b \tag{3.42}$$

$= $ mass of grinding ball in *size i* (t)

The energy absorption factor of the steel grinding media, ψ_e, which reduces the energy imparted to rock breakage due to the elastisticity of the grinding balls, is determined as follows (Valery Jnr., 1998):

$$\psi_e = \frac{(\sum_{i=1}^{z} vb_i)\, SG_b + (\sum_{i=1}^{q} vo_i)\, SG_s}{(\sum_{i=1}^{q} vo_i)\, SG_s} \tag{3.43}$$

In summary, the determination of the appearance function, a_{ij}, involves the following steps:

1. Laboratory determination of A, b and t_a
2. Calculation of the abrasion appearance function by interpolation of the particle size distribution into the data in Table 3.3.1
3. Calculation of the impact appearance function by calculating:
   (a) the specific comminution energy, Ecs_i, from Equation (3.34) through Equation (3.43)
   (b) the t_{10} values for each size fraction from Equation (3.33)
   (c) the impact appearance function for each size fraction by interpolation against Julius Kruttschnitt Mineral Research Centre data
   (d) the appearance function in fraction retained format
4. Calculation of the (combined) appearance function, a_{ij}, - a weighted average of the high and low energy appearance functions - from Equation (3.31)

With the appearance function, a_{ij}, and the breakage rates, r_i, determined, the generation and consumption terms of the solids mass balance, Equation (3.1), may be calculated.

Consumption, $(1 - a_{ii})r_i s_i$: Recalling that the appearance function, a_{ij} is in a mass fraction retained format, the diagonal of the appearance function, a_{ii}, indicates (by difference) how much of the material in a given size is broken and distributed into the size fractions below (according to the appearance function for that given parent size).

Generation, $\sum_{j=1}^{i-1} r_j s_j a_{ij}$: Summation of the product of the rock charge mass in the size fractions above *size i*, s_j, and their respective breakage rates, r_j, and the fraction appearing into *size i* from the breakage occurring above, a_{ij}, results in the generation term for *size i*.

The feed, product, consumption and generation terms are now determined and the mass balance, Equation (3.1), is now defined.

Water Balance

As is evident from the discussion about mill product, p_i, earlier in this Section, the solids and water balance are interlinked via the volumetric discharge flowrate (Q_m) and the maximum discharge rate constant (d_0). With zero consumption and generation, the water mass balance is as follows:

$$\begin{aligned} Accumulation &= In - Out \\ \frac{ds_w}{dt} &= f_w - p_w \end{aligned} \tag{3.44}$$

where

s_w = water in the mill charge (t)

f_w = feed water addition (t/hr)

p_w = water discharge rate (t/hr)

$$= d_0\, s_w \tag{3.45}$$

The water balance calculation sequence is as follows:

1. the feedwater addition rate is specified
2. the water discharge rate is calculated from Equation (3.45), and,
3. the mill water charge is calculated from Equation (3.44).

Ball Charge Model

The ball charge model is essentially a user specified ball charge volume and size distribution. There are no "In", "Out", "Generation", "Consumption", or, "Accumulation" terms. The user specifies the:

- ball charge volumetric load, J_b
- ball topsize
- ball size distribution (four size fractions)

  see Table 3.3 for example.

Table 3.3: SAG Mill Ball Charge Model

Ball Load Fraction, J_b	(fraction)	0.14
Ball Top Size	(mm)	125
Size 1: Top Size$\times\frac{1}{\sqrt{2}}$	(%)	50
Size 2: Top Size$\times\frac{1}{2}$	(%)	35
Size 3: Top Size$\times\frac{1}{2\sqrt{2}}$	(%)	15
Size 4: Top Size$\times\frac{1}{4}$	(%)	0

Powerdraw Model

According to the Morrel powerdraw model (Morrell, 1994), the mill powerdraw, P_{Gross}, is as follows:

$$P_{Gross} = P_{No\,Load} + kP_{Charge} \tag{3.46}$$

where

$P_{No\,Load}$ = no-load power of mill (empty mill powerdraw) (kW)

P_{Charge} = mill powerdraw attributable to the entire contents of the mill (kW)

k = mill powerdraw lumped parameter (accounts for heat losses due to internal friction, energy of attrition/abrasion breakage, rotation of the grinding media and inaccuracies in assumptions and charge shape and motion measurements (dimensionless)

The no-load component of the mill powerdraw, $P_{No\,Load}$ is,

$$P_{No\,Load} = 1.68\left({D_m}^{2.5}\phi_{fcs}\left(0.667\,L_{cone} + L_m\right)\right)^{0.82} \tag{3.47}$$

where

D_m = mill inside diameter (m)

ϕ_{fcs} = mill fraction critical speed (fraction)

L_{cone} = length of the conical section of the mill (m)

The powerdraw component attributable to mill charge contents, P_{Charge}, consists of components of powerdraw attributable to material in the conical feed end section of the mill

and the material in the cylindrical section of the mill, as shown in Equation (3.48).

$$P_{Charge} = P_{Net} + P_{Cone} \tag{3.48}$$

where

P_{Net} = mill powerdraw attributable to the contents of the cylindrical section of the mill (kW)

P_{Cone} = mill powerdraw attributable to the contents of the conical (feed) section of the mill (kW)

The powerdraw attributable to the cylindrical and conical sections of the mill are determined by Equation (3.49) and Equation (3.50), respectively.

$$\begin{aligned} P_{Net} = & \frac{\pi\, g L_m N_m r_m \left(2 {r_m}^3 - 3\, z {r_m}^2 r_i + {r_i}^3 (3\, z - 2)\right) \left(\rho_c \left(\sin(\theta_S) - \sin(\theta_T)\right)\right)}{3\, r_m - 3\, z r_i} \\ & + \frac{\pi\, g L_m N_m r_m \left(2 {r_m}^3 - 3\, z {r_m}^2 r_i + {r_i}^3 (3\, z - 2)\right) \left(\rho_p \left(\sin(\theta_T) - \sin(\theta_{TO})\right)\right)}{3\, r_m - 3\, z r_i} \\ & + \frac{L_m \rho_c {N_m}^3 {r_m}^3 \pi^3 \left((r_m - z r_i)^4 - {r_i}^4 (z-1)^4 \right)}{(r_m - z r_i)^3} \end{aligned} \tag{3.49}$$

$$\begin{aligned} P_{Cone} = & \frac{\pi\, g L_{cone} N_m \left({r_m}^4 - 4\, r_m {r_i}^3 + 3\, {r_i}^4\right) \left(\rho_c \left(\sin(\theta_S) - \sin(\theta_T)\right)\right)}{3\, (r_m - r_t)} \\ & + \frac{\pi\, g L_{cone} N_m \left({r_m}^4 - 4\, r_m {r_i}^3 + 3\, {r_i}^4\right) \left(\rho_p \left(\sin(\theta_T) - \sin(\theta_{TO})\right)\right)}{3\, (r_m - r_t)} \\ & + 2\, \frac{2\, \pi^3 N_m L_{cone} \rho_c \left({r_m}^5 - 5\, r_m {r_i}^4 + 4\, {r_i}^5\right)}{5\, (r_m - r_t)} \end{aligned} \tag{3.50}$$

where

g = gravitational acceleration (9.81 m/s^2)

L_{cone} = length (axial) of conical section of mill (m)

L_m = length of the cylindrical section of the mill (m)

N_m = actual mill speed (revolutions per second)

P_{Cone} = mill powerdraw attributable to the contents of the conical (feed) section of the mill (kW)

r_i = mill charge surface inner radius (m)
r_m = mill radius (m)
r_t = mill trunnion radius (m)
z = mill powerdraw calculation parameter (−)
ρ_c = mill charge density (specific gravity) (t/m^3)
ρ_p = mill pulp density (specific gravity) (t/m^3)
θ_S = mill charge shoulder angle (radians), see Figure 3.4
θ_T = mill charge toe angle (radians), see Figure 3.4
θ_{TO} = mill slurry toe angle (radians), see Figure 3.4

The mill pulp density, ρ_p, is assumed to be equal to the mill discharge pulp density:

$$\rho_p = SMDC_{SGp} \tag{3.51}$$

where

ρ_p = SAG mill pulp density (t/m^3)
$SMDC_{SGp}$ = SAG mill discharge pulp density (t/m^3)

Mill cone length is determined as follows:

$$L_{cone} = \frac{(D_m - D_t)}{2} \tan(\frac{\pi}{180}\theta_{cone}) \tag{3.52}$$

where

L_{cone} = length (axial) of conical section of mill (m)
D_m = mill inside diameter (m)
θ_{cone} = mill cone angle (^{o})

Figure 3.4 shows a simplified mill charge geometry (is cross-section). The 'C' or kidney shape describes the surface of the "active" part of the charge where particle breakage occurs. Figure 3.4 also shows the charge shoulder angle (θ_S), charge toe angle (θ_T), and the charge inner surface radius (r_i) which define the charge geometry.

The angle of the mill charge shoulder, θ_S, is given by:

$$\theta_S = \frac{\pi}{2} - (\theta_T - \frac{\pi}{2})\left((0.3386 + 0.1041\,\phi_{fcs}) + (1.54 - 2.5673\,\phi_{fcs})\,J_t\right) \tag{3.53}$$

The angle of the mill charge toe, θ_T is given by:

$$\theta_T = 2.5307\,(1.2796 - J_t)\left(1 - e^{-19.42\,(\phi_c - \phi_{fcs})}\right) + \frac{\pi}{2} \tag{3.54}$$

Since the SAG mill is a grate discharge mill, the angle of the mill charge slurry toe, θ_{TO} is equal to the charge to angle:

$$\theta_{TO} = \theta_T \tag{3.55}$$

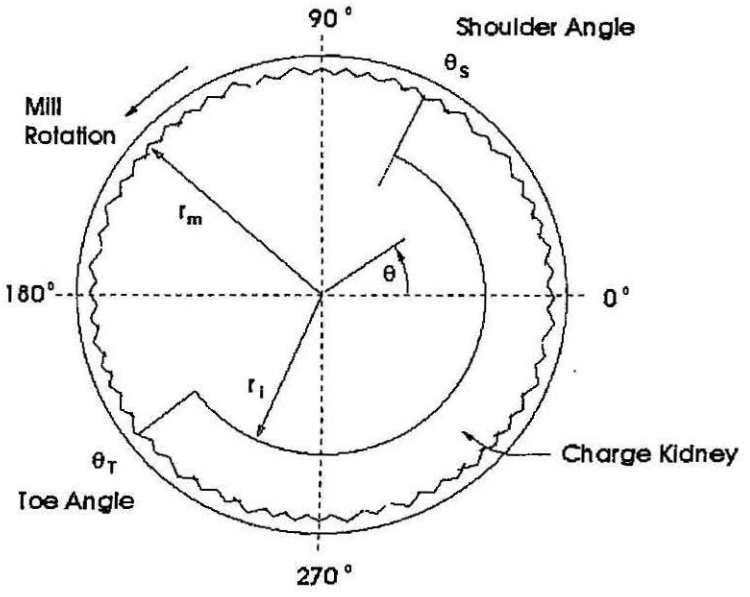

Figure 3.4: Simplified mill charge geometry

The powerdraw calculation parameter, z, is given by:

$$z = (1 - J_t)^{0.4532} \tag{3.56}$$

Mill critical speed, $RPM_{critical}$, (the rotational speed where angular acceleration is equal to gravitational acceleration) is as follows:

$$RPM_{critical} = \frac{60}{2\pi}\sqrt{\frac{2g}{D_m}} \tag{3.57}$$

The actual mill speed, represented as a fraction of the critical speed, ϕ_{fcs}:

$$\phi_{fcs} = \frac{RPM}{RPM_{critical}} \tag{3.58}$$

where

RPM = actual mill speed (revolutions per minute)

The actual mill speed in revolutions per second, N_m is:

$$N_m = \frac{RPM}{60} \tag{3.59}$$

The mean rotational rate, $\overline{N}$, is given by:

$$\overline{N} = \frac{N_m}{2} \tag{3.60}$$

The mill charge density, ρ_c, is determined as follows:

$$\rho_c = \frac{\left(J_t\,\rho_o\,\left(1-\epsilon+\epsilon U\frac{S}{100}\right)+J_b\,\left(\rho_b-\rho_o\right)\left(1-\epsilon\right)+J_t\,\epsilon U\left(1-\frac{S}{100}\right)\right)}{J_t} \tag{3.61}$$

where

J_b	=	mill fraction occupied by grinding balls including the associated voidage (fraction mill volume)
S	=	mill discharge volumetric solids content (% solids v/v)
ϵ	=	mill charge porosity (fraction)
ρ_b	=	grinding ball density (specific gravity) (t/m^3)
ρ_c	=	mill charge density (specific gravity) (t/m^3)
ρ_o	=	ore density (specific gravity) (t/m^3)

The fraction of grinding media voidage occupied by the slurry, U, is:

$$U = \frac{J_{pm}}{\epsilon J_t} \tag{3.62}$$

The remaining variables yet to be defined are: ϕ_c, t_c, t_f, β, $\overline{r}$ and r_i.

The experimentally determined fraction of critical mill at which centrifuging is fully established, ϕ_c, is calculated as follows:

$$\phi_c = 0.35\,(3.364 - 0.35\,J_t) \tag{3.63}$$

The mean travel time for material in the charge (from the charge toe to the charge shoulder), t_c, is:

$$t_c = \frac{2\,\pi - \theta_T + \theta_S}{2\pi\,\overline{N}} \tag{3.64}$$

The mean travel time for material in free fall (from the charge shoulder to the charge toe), t_f, is:

$$t_f = \left(\frac{2\overline{r}\,\left(\sin(\theta_S) - \sin(\theta_T)\right)}{g}\right)^{0.5} \tag{3.65}$$

The fraction of charge that is active, β, is determined as follows:

$$\beta = \frac{t_c}{t_f + t_c} \tag{3.66}$$

The mean radial position of the mill charge, $\overline{r}$, is calculated as follows:

$$\overline{r} = \frac{r_m}{2}\left(1 + \left(1 - \frac{2\pi J_t}{2\pi - \theta_T + \theta_S}\right)^{0.5}\right) \tag{3.67}$$

The radial position of the mill charge inner surface, r_i, can then be determined:

$$r_i = r_m\left(1 - \frac{2\pi\beta J_t}{2\pi - \theta_T + \theta_S}\right)^{0.5} \tag{3.68}$$

All parameters and variables in the model are now specified and mill powerdraw may now be calculated by Equation (3.46).

Impact Zone Model

Although the mill considered in this research is a fixed speed mill, variable speed mills are becoming increasingly popular. The mill speed affects the

1. breakage rates, r_i (see Equations (3.22) to (3.26))
2. volumetric discharge, Q_m (see Equation (3.6))
3. mill powerdraw, P_{Gross} (see Equations (3.49) & (3.50))
4. charge shape as defined by the
   - toe angle, θ_T (see Equation (3.54))
   - shoulder angle, θ_S (see Equation (3.53))
   - active charge radius, r_i (see Equation (3.68))

An important implication of the charge shape is the location of the impact zone. For a fixed speed mill, the impact zone is designed to be on the toe of the charge. When the mill is powered by a variable speed drive, the impact zone can move between a point within the charge to a point beyond the toe of the charge. In the latter case, damage to the mill liners and lifter bars is caused by the direct impact of grinding balls.

Since such conditions are undesirable, a model for locating the impact zone has been included in the SAG mill model. Although a ball trajectory model is not part of the DOS based JKSimMet simulation software (Version 4), a trajectory model has since been incorporated into the succeeding Microsoft Windows based version (Schroder, 2000). The exact details of the model were not available at the time of coding the MATLAB-Simulink models, however, it is believed to be based on the equations for projectile motion. Thus, a simple model for the point of impact is proposed here that utilises projectile motion equations.

Projectile Motion Equations

The equations governing the motion of projectiles are those of constant acceleration (Alonso and Finn, 1969):

$$v_1 = v_0 + at \tag{3.69}$$

$$s_1 = s_0 + v_0 t + \frac{1}{2}at^2 \tag{3.70}$$

where

a	=	acceleration (m/s^2)
v	=	velocity (m/s)
s	=	distance (m)
t	=	time (sec)
$_0$	=	initial conditions
$_1$	=	conditions at time t

The motion is analysed in the horizontal plane (where acceleration is zero, *i.e.*, $a_h = 0$), denoted with a subscript 'h', and the vertical plane (where acceleration is due to gravity, *i.e.*, $a = -g = -9.81$ m/s^2), denoted with a subscript 'v'. The analysis is divided into the upward the downward motion. The initial conditions of the motion in this instance are those of the charge shoulder and are denoted with a subscript zero, *e.g.*, v_{0h} for initial horizontal velocity. The end of the upward journey and beginning of the downward journey is denoted with a subscript one, *e.g.*, v_{1h} for horizontal velocity at maximum projectile height. The final conditions of the downward journey, at the point of impact, are denoted with a subscript two, *e.g.*, v_{2h} for horizontal velocity at the point of impact with the mill shell.

Using the central axis of the mill as the reference point and the horizontal axis positive sense pointing to the side of the mill ofthe charge shoulder, the equations of motion are

UP

Horizontal

$$v_{0,h} = -\frac{RPM}{60} 2r_m\pi\cos(\theta_S) \tag{3.71}$$

$$v_{1,h} = v_{0,h} \tag{3.72}$$

$$s_{0,h} = r_m\cos(\theta_S) \tag{3.73}$$

$$s_{1,h} = s_{0,h} + v_{0,h}t_1 + \frac{1}{2}a_h t_1^2 = s_{0,h} + v_{0,h}t_1 \ (a_h = 0) \tag{3.74}$$

Vertical

$$v_{0,v} = \frac{RPM}{60} 2r_m\pi\sin(\theta_S) \tag{3.75}$$

$$v_{1,v} = 0 = v_{0,v} + a_v t_1 = v_{0v} - gt_1 \tag{3.76}$$

$$s_{0,v} = r_m\sin(\theta_S) \tag{3.77}$$

$$s_{1,v} = s_{0,v} + v_{0,v}t_1 - \frac{1}{2}gt_1^2 \tag{3.78}$$

Solving Equation (3.76) for the upward journey time, t_1,

$$t_1 = \frac{v_{0v}}{g} = \frac{RPM}{60\,g} 2r_m\pi\sin(\theta_S) \tag{3.79}$$

allows the solution of the upward journey system, Equation (3.71) to (3.78).

DOWN

Horizontal

$$v_{1,h} = -\frac{RPM}{60} 2r_m\pi\cos(\theta_S) \tag{3.80}$$

$$v_{2,h} = v_{1,h} \tag{3.81}$$

$$s_{1,h} = s_{0,h} + v_{0,h}t_1 \tag{3.82}$$

$$s_{2,h} = s_{1,h} + v_{1,h}t_2 = s_{0,h} + v_{0,h}(t_1 + t_2) \tag{3.83}$$

Vertical

$$v_{1,v} = 0 \tag{3.84}$$

$$v_{2,v} = v_{1,v} + a_v t_2 \tag{3.85}$$

$$s_{1,v} = s_{0,v} + v_{0,v}t_1 - \frac{1}{2}gt_1^2 \tag{3.86}$$

$$s_{2,v} = s_{1,v} + v_{1,v}t_2 - \frac{1}{2}gt_2^2 = s_{1,v} - \frac{1}{2}gt_2^2 \tag{3.87}$$

$$= s_{0,v} + v_{0,v}t_1 - \frac{1}{2}g(t_1^2 + t_2^2) \tag{3.88}$$

The point of impact (or apparent impact) is at the mill shell, *i.e.*,

$$r_m^2 = s_{2,h}^2 + s_{2,v}^2 \tag{3.89}$$

Inspection of Equations (3.83) and (3.88), reveal that Equation (3.89) is a function of one unknown - t_2 - which may therefore be determined. This allows the solution of the downward journey system, Equation (3.80) to (3.88), and the determination of the impact angle:

$$\theta_I = \arctan\left(\frac{s_{2,v}}{s_{2,h}}\right) \tag{3.90}$$

where

θ_I = angle of ball impact at the mill radius (radians)

When the impact angle is outside the toe angle ($\theta_I < \theta_T$), impact with the mill shell occurs.

When the impact angle is within or equal to the toe angle ($\theta_I \geq \theta_T$), impact is at the charge toe or within the boundaries of the charge.

SAG mill model validation

Table 3.4 contains results of the validation of the SAG mill model (in isolation) by way of the stream properties of the rock load and the mill discharge streams. The reference case is the JKSimMet simulation results from the model constructed from the grinding circuit survey (David, 1997), see Appendix B. The feed stream and the columns headed with "JK" is the reference data. The columns headed "model" and "error" are the results from this work and the absolute, relative error between this work and the reference data.

The mill discharge stream shows good agreement with no results further than 3% from the reference case. Although excellent, the agreement in the rock charge results is somewhat misleading. The JKSimMet SAG mill model is intrinsically steady state in nature. The steady state form of Equation (3.1) is solved simultaneously with Equation (3.3) to give a rock load and discharge that satisfies the mass balance. The calculated rock charge is specified as the initial conditions for the rock charge. Since steady state conditions are being simulated, the rock load does not change and thus, agreement is "perfect".

Another SAG mill result of importance is the mill powerdraw. The validation results are in the lower part of Table 3.4 and illustrate good agreement once again.

At this point the SAG mill model was judged valid.

Table 3.4: SAG Mill model validation

Stream	Total	Rock Load			Mill Discharge		
Properties	Feed	JK	model	error (%)	JK	model	error (%)
tph_s	252.1	45.7	45.7	0.0	252.1	252.1	0.01
tph_l	80.0	2.1	2.1	0.0	80.0	80.0	0.07
tph_p	332.1	47.7	47.7	0.0	332.1	332.1	0.01
%s w/w	75.9	95.7	95.7	0.0	75.9	75.9	0.02
%l w/w	24.1	4.3	4.3	0.0	24.1	24.1	0.06
m3ph_s	95.1	17.2	17.2	0.0	95.1	95.1	0.01
m3ph_l	80.0	2.1	2.1	0.0	80.0	80.0	0.07
m3ph_p	175.2	19.3	19.3	0.0	175.2	175.1	0.03
%s v/v	54.3	89.3	89.3	0.0	54.3	54.3	0.03
%l v/v	45.7	10.7	10.7	0.0	45.7	45.7	0.04
SGp	2.25	2.58	2.58	0.0	2.25	2.25	0.01
P_{80}	84.0	87.3	87.3	0.0	16.7	16.4	2.0
Powerdraw (kW)		2863	2866	0.1			

3.3.2 Hydrocyclones

The Nageswararao model, which is detailed in Napier-Munn *et al.* (1996), is used to model the primary (and secondary) cyclones. The model is comprised of several equations that are functions of cyclone geometry, feed flowrate and solids density, and, feed ore characteristics.

Cyclone pressure, P, is calculated from the following flowrate equation,

$$Q_f = K_{Q1} {D_c}^2 \left(\frac{P}{\rho_p}\right)^{0.5} \left(\frac{D_o}{D_c}\right)^{0.68} \left(\frac{D_i}{D_c}\right)^{0.45} \theta^{-0.1} \left(\frac{L_c}{D_c}\right)^{0.2} \tag{3.91}$$

where

$$K_{Q1} = K_{Q0} D_c^{-0.1} \tag{3.92}$$

K_{Q0} = ore dependent proportionality constant

D_i = inlet diameter (m)

D_o = overflow diameter (m)

D_u = underflow diameter (m)

D_c = cyclone cylinder diameter (m)

L_c = cyclone cylinder length (m)

θ = cone full angle (°)

P = cyclone inlet pressure (kPa)

ρ_p = feed pulp (slurry) density (t/m^3)

Q_f = cyclone feed flowrate (m^3/hr)

Cyclone corrected 50% passing size, d_{50c}, is predicted from:

$$\frac{d_{50c}}{D_c} = K_{D1} \left(\frac{D_o}{D_c}\right)^{0.52} \left(\frac{D_u}{D_c}\right)^{-0.47} \lambda^{0.93} \left(\frac{P}{\rho_p g D_c}\right)^{-0.22} \left(\frac{D_i}{D_c}\right)^{-0.5} \left(\frac{L_c}{D_c}\right)^{0.2} \theta^{0.15} \tag{3.93}$$

where

$$K_{D1} = K_{D0} D_c^{-0.65} \tag{3.94}$$

K_{D0} = ore dependent proportionality constant

d_{50c} = corrected 50% passing size (mm)

g = gravitational acceleration (9.81 m/s^2)

The water recovery to cyclone underflow, R_f, is

$$R_f = K_{W1}\left(\frac{D_o}{D_c}\right)^{-1.19}\left(\frac{D_u}{D_c}\right)^{2.40}\left(\frac{P}{\rho_p g D_c}\right)^{-0.53}\lambda^{0.27}\left(\frac{D_i}{D_c}\right)^{-0.50}\theta^{-0.24}\left(\frac{L_c}{D_c}\right)^{0.22} \quad (3.95)$$

where

K_{W1} = water split to underflow constant

$$\lambda = \frac{10^{1.82\,C_v}}{(8.05[1-C_v]^2)} \quad (3.96)$$

= hindered settling correction term

C_v = volumetric fraction of solids in feed slurry (fraction)

The volumetric recovery of feed slurry to cyclone underflow, R_v, is

$$R_v = K_{V1}\left(\frac{D_o}{D_c}\right)^{-0.94}\left(\frac{D_u}{D_c}\right)^{1.83}\left(\frac{P}{\rho_p g D_c}\right)^{-0.31}\left(\frac{D_i}{D_c}\right)^{-0.25}\theta^{-0.24}\left(\frac{L_c}{D_c}\right)^{0.22} \quad (3.97)$$

where

K_{V1} = constant to be estimated from data

The size classification function is described by the efficiency to overflow, E_{oa}, equation:

$$E_{oa} = C\left(\frac{(1+\beta\beta^* x)(e^{\alpha}-1)}{e^{\alpha\beta^* x}+e^{\alpha}-2}\right) \quad (3.98)$$

where

$$C = 1 - R_f \quad (3.99)$$

= water recovery to cyclone overflow (fraction)

$$x = \frac{d}{d_{50c}} \quad (3.100)$$

= ratio of particle size to corrected 50% passing size

d = particle size (mm)

α = efficiency curve parameter: separation sharpness

β = efficiency curve parameter: fine size efficiency boost

β^* = efficiency curve parameter: d_{50c} preservation

The cyclone model calculation sequence is as follows:

1. Given the
   - cyclone dimensions
   - model parameters (α, β, β^*, K_{D0}, K_{Q0}, K_{V1} and K_{W1}) as determined from plant surveys

- feed flowrate and size distribution

2. Calculate cyclone operating pressure from Equation (3.91)
3. Calculate corrected 50% passing size from Equation (3.93)
4. Calculate water recovery to underflow from Equation (3.95)
5. Calculate the separation efficiency to overflow from Equation (3.98)
6. Conduct a mass balance around the cyclone to determine the overflow and underflow streams and size distributions

Cyclone model validation

Table 3.5 contains results of the validation of the primary cyclone model (in isolation) by way of the stream properties of the overflow and underflow streams. The reference case is the JKSimMet simulation results from the model constructed from the grinding circuit survey (David, 1997), see Appendix B. The feed stream and the columns headed with "JK" is the reference data. The columns headed "model" and "error" are the results from this work and the absolute, relative error between this work and the reference data.

Generally, the model results show good agreement with the reference data, with errors of less than 0.2%. The P_{80} result for the overflow stream exhibits a 16% error which is distinctly worse than the other results. This error is attributed to the interpolation method used to arrive at the P_{80} result, *i.e.*, linear interpolation of cumulative weight percent passing *versus* particle size distribution. The Rosin-Rammler distribution function (Napier-Munn *et al.*, 1996) suggests some variation of a log-linear interpolation may be more accurate. However, since the model size distributions were fixed by the points (0.001 mm, 0%passing) and (180.76 mm, 100%passing), a linear extrapolation (*versus* a smoothing spline extrapolation), of the P_{80} point was utilised for consistency. Good agreement was generally obtained except for the finely-sized streams, such as the cyclone overflows.

Another primary cyclone result of importance is the cyclone operating pressure. The validation results are in the lower part of Table 3.5 and illustrate good agreement once again.

Table 3.5: Primary cyclone model validation

Stream Properties	1° Cyclone Feed	1° Cyclone O/F JK	1° Cyclone O/F model	1° Cyclone O/F error (%)	1° Cyclone U/F JK	1° Cyclone U/F model	1° Cyclone U/F error (%)
tph_s	185.0	34.3	34.3	0.15	150.7	150.7	0.03
tph_l	179.3	117.0	117.0	0.03	62.4	62.3	0.06
tph_p	364.3	151.3	151.3	0.01	213.0	213.0	0.01
%s w/w	50.8	22.7	22.7	0.13	70.7	70.7	0.03
%l w/w	49.2	77.3	77.3	0.04	29.3	29.3	0.06
m3ph_s	69.8	13.0	12.9	0.15	56.9	56.9	0.03
m3ph_l	179.3	117.0	117.0	0.03	62.4	62.3	0.06
m3ph_p	249.1	129.9	129.9	0.01	119.2	119.2	0.01
%s v/v	28.0	10.0	10.0	0.16	47.7	47.7	0.05
%l v/v	72.0	90.0	90.0	0.02	52.3	52.3	0.04
SGp	1.84	1.37	1.37	0.04	2.17	2.17	0.02
P_{80}	2.64	0.06	0.07	15.8	3.24	3.24	0.09
Pressure (kPa)		57.3	57.2	0.17			

Table 3.6: Secondary cyclone model validation

Stream Properties	2° Cyclone Feed	2° Cyclone O/F JK	2° Cyclone O/F model	2° Cyclone O/F error (%)	2° Cyclone U/F JK	2° Cyclone U/F model	2° Cyclone U/F error (%)
tph_s	1099	181.5	181.5	0.0	918	918	0.0
tph_l	564	305	305	0.0	259	259	0.0
tph_p	1663	486	486	0.0	1177	1177	0.0
%s w/w	66.1	37.3	37.3	0.01	78.0	78.0	0.01
%l w/w	33.9	62.7	62.7	0.01	22.0	22.0	0.02
m3ph_s	415	68.5	68.5	0.01	346	346	0.0
m3ph_l	564	305	305	0.01	259	259	0.02
m3ph_p	979	373	373	0.0	605	605	0.01
%s v/v	42.4	18.3	18.3	0.02	57.2	57.2	0.01
%l v/v	57.6	81.7	81.7	0.0	42.8	42.8	0.01
SGp	2.09	1.62	1.62	0.0	2.29	2.29	0.0
P_{80}	0.42	0.09	0.08	6.9	0.50	0.50	0
Pressure (kPa)		150.2	150.2	0.02			

Table 3.6 contains results of the validation of the secondary cyclone model (in isolation) by way of the stream properties of the overflow and underflow streams. The reference case is the JKSimMet simulation results from the model constructed from the grinding circuit survey (David, 1997), see Appendix B. The feed stream and the columns headed with "JK" is the reference data. The columns headed "model" and "error" are the results from this work and the absolute, relative error between this work and the reference data.

Generally, the model results show good agreement with the reference data, with errors of less than 0.02%. As for the primary cyclone overflow, the P_{80} result for the secondary cyclone overflow stream exhibits a larger error ($\approx$ 7%) which is attributed to linear interpolation errors at the fine sizes.

The secondary cyclone operating pressure, in the lower part of Table 3.6, shows good agreement also.

At this point the cyclone model was considered valid.

3.3.3 Oversize Crusher

The model for the oversize crusher is comprised of:

- a particle classification/selection for breakage function
- a breakage distribution function
- a power draw prediction function

Again, it is based on the models developed at the Julius Kruttschnitt Mineral Research Centre, (Whiten, 1972), (Napier-Munn *et al.*, 1996) and (JKTech, 1994).

Crusher Classification Function

The classification function is a selection for breakage function (the Whiten classification model (Napier-Munn *et al.*, 1996)) and provides the probability of breakage *versus* particle size as follows:

$$\begin{aligned} C(x) &= 0.0 && \text{for } x < K1 \\ C(x) &= 1.0 - \left(\frac{K2 - x}{K2 - K1}\right)^{K3} && \text{for } K1 \leq x \leq K1 \\ C(x) &= 1.0 && \text{for } x > K2 \end{aligned} \tag{3.101}$$

where

$C(x)$ = probability of breakage (fraction)

$$K1 = A_0 \cdot CSS + A_1 \cdot TPH + A_2 \cdot F_{80} + A_3 \cdot LLen + A_4 \tag{3.102}$$

= particle size below which C(x) = 0 (mm)

$$K2 = B_0 \cdot CSS - B_1 \cdot TPH + B_2 \cdot F_{80} + B_3 \cdot LHr + B_4 \cdot ET + B_5 \tag{3.103}$$

= particle size above which C(x) = 1 (mm)

$K3$ = C_0usually 2.3 (3.104)

= classification function parameter: curve shape

(3.105)

A_i = model parameters from plant survey

B_i = model parameters from plant survey

CSS = crusher close side setting (mm)

TPH = crusher feedrate (tph)

F_{80} = crusher feed 80% passing size (mm)

$LLen$ = crusher liner length (mm)

LHr = crusher liner hours in service (hrs)

ET = crusher eccentric throw (mm)

The oversize crusher probability of breakage function ($C(x)$) is shown in Figure 3.5.

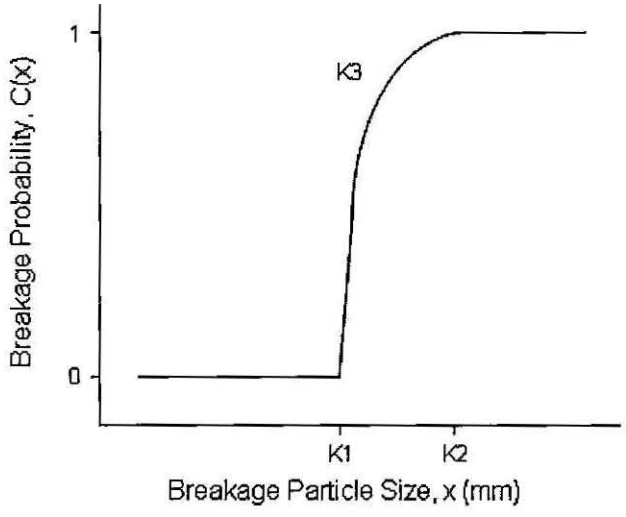

Figure 3.5: Crusher Probability of Breakage Function
(p 141 Napier-Munn et al. (1996))

Breakage Distribution Function

Laboratory ore tests give a crusher breakage parameter, t_{10}, which is a size distribution data identifier, *i.e.*, a look-up table reference point for data in a Julius Kruttschnitt Mineral Research Centre reference database (as described in Section 3.3.1 for the SAG mill appearance function discussion). For the ore in question, the distribution after breakage

is obtained from the database and the fraction of material retained in the size fractions of interest are determined by interpolation. The oversize crusher product is then determined as follows:

$$p = (1 - C) \cdot (1 - BC)^{-1} \cdot f \tag{3.106}$$

where

p = crusher product by size (tph)

f = crusher feed by size (tph)

B = crusher breakage distribution function (fraction)

C = = C(x) = crusher probability of breakage function (fraction)

Equation (3.106) is the crusher mass balance equation which is implicitly steady state, *i.e.*,

- no accumulation (feed tph = product tph)
- any water in the feed reports to product

Crusher Power draw Prediction

The oversize crusher power draw is determined as follows:

1. for the ore specific crusher t_{10} parameter, the specific comminution energy, *Ecs* (kWh/t), *versus size* relationship is determined by interpolation against a Julius Kruttschnitt Mineral Research Centre database
2. the *Ecs* for the size fractions of interest are determined by interpolation against the result from Step 1.
3. the pendulum power, P_p, is determined by Equation (3.107)
4. predicted crusher power draw, P_c, is then determined by Equation (3.108)

$$P_p = \sum Ecs_i C_i f_i \tag{3.107}$$

$$P_c = A P_p + P_n \tag{3.108}$$

where

P_p = pendulum power (kW)

P_c = predicted crusher power draw (kW)

P_n = crusher no-load power (kW)

Ecs_i = specific comminution energy by size (kWh/t)

C_i = crusher probability of breakage function (fraction)

f_i = crusher feedrate by size (tph)

A = dimensionless scaling factor

Oversize crusher model validation

Table 3.7 contains results of the validation of the oversize crusher model (in isolation) by way of the stream properties of the crusher product stream. The reference case is the JKSimMet simulation results from the model constructed from the grinding circuit survey (David, 1997), see Appendix B. The feed stream and the columns headed with "JK" is the reference data. The columns headed "model" and "error" are the results from this work and the absolute, relative error between this work and the reference data.

Generally, the model results show excellent agreement with the reference data. As for the cyclone overflow streams, the P_{80} result for the crusher product stream exhibits a larger error (12%) which is attributed to linear interpolation errors at the fine sizes.

The crusher powerdraw, in the lower part of Table 3.7, shows good agreement also.

At this point the oversize crusher model was judged valid.

Table 3.7: O/S Crusher model validation

Stream Properties	O/S Crusher Feed	O/S Crusher Product JK	model	error (%)
tph_s	67.1	67.1	67.1	0
tph_l	0.05	0.05	0.05	0
tph_p	67.1	67.1	67.1	0
%s w/w	99.9	99.9	99.9	0
%l w/w	0.1	0.1	0.1	0
m3ph_s	25.3	25.3	25.3	0
m3ph_l	0.05	0.05	0.05	0
m3ph_p	25.4	25.4	25.4	0
%s v/v	99.8	99.8	99.8	0
%l v/v	0.2	0.2	0.2	0
SGp	2.65	2.65	2.65	0
P_{80}	42.9	34.0	37.9	11.5
Powerdraw (kW)		42.8	41.9	1.9

3.3.4 Mill Discharge Screens

The mill discharge screens are modelled as a simple efficiency curve, similar to the efficiency to overflow, E_{oa}, curve used for the primary cyclones, see Equation (3.98). The corrected 50% passing size, d_{50c}, and water recovery to underflow, R_f, are calculated in the case of the cyclone model. However, in the discharge screen model these two parameters are specified (as determined from surveyed screen performance).

Screen model validation

Table 3.8 contains results of the validation of the SAG mill discharge screen model (in isolation) by way of the stream properties of the oversize and undersize streams. The reference case is the JKSimMet simulation results from the model constructed from the grinding circuit survey (David, 1997), see Appendix B. The feed stream and the columns headed with "JK" is the reference data. The columns headed "model" and "error" are the results from this work and the absolute, relative error between this work and the reference data.

Generally, the model results show good agreement with the reference data, with errors of less than 0.3%, including the P_{80} results. The largest errors occur in the water balance ($\approx$ 6%). This is due to the screen oversize being virtually dry. Small errors in the water content of the stream translate to larger relative errors.

Table 3.9 contains results of the validation of the ball mill discharge screen model (in isolation) by way of the stream properties of the oversize and undersize streams. The reference case is the JKSimMet simulation results from the model constructed from the grinding circuit survey (David, 1997), see Appendix B. The feed stream and the columns headed with "JK" is the reference data. The columns headed "model" and "error" are the results from this work and the absolute, relative error between this work and the reference data.

Generally, the model results show good agreement with the reference data, with errors of less than 0.1%. The largest error, $\approx$ 2%, is in screen oversize P_{80} estimate.

At this point the screen model was considered valid.

Table 3.8: SAG mill discharge screen model validation

Stream	SAG mill	Screen Oversize			Screen Undersize		
Properties	Screen feed	JK	model	error (%)	JK	model	error (%)
tph_s	252.1	67.1	67.1	0.03	185.0	185.0	0.01
tph_l	94.9	0.05	0.06	6.15	95.0	94.9	0.06
tph_p	347.0	67.1	67.1	0.02	280.0	279.9	0.01
%s w/w	72.6	99.9	99.9	0.0	66.1	66.1	0.02
%l w/w	27.4	0.1	0.1	6.1	33.9	33.9	0.05
m3ph_s	95.1	25.3	25.3	0.03	69.8	69.8	0.01
m3ph_l	94.9	0.05	0.06	6.1	95.0	94.9	0.06
m3ph_p	190.1	25.4	25.4	0.01	164.8	164.7	0.03
%s v/v	50.0	99.8	99.8	0.01	42.4	42.4	0.04
%l v/v	50.0	0.2	0.2	6.1	57.6	57.6	0.03
SGp	2.20	2.65	2.65	0.0	2.09	2.09	0.01
P_{80}	16.7	42.9	42.9	0.05	2.64	2.65	0.20

Table 3.9: Ball mill discharge screen model validation

Stream	Ball mill	Screen Oversize			Screen Undersize		
Properties	Screen feed	JK	model	error (%)	JK	model	error (%)
tph_s	1068	3.4	3.4	0.1	1065	1065	0.0
tph_l	336	0.0	0.0	0.0	336	336	0.0
tph_p	1405	3.4	3.4	0.1	1401	1401	0.0
%s w/w	76.1	99.3	99.3	0.0	76.0	76.0	0.0
%l w/w	23.9	0.7	0.7	0.09	24.0	24.0	0.01
m3ph_s	403	1.3	1.3	0.06	402	402	0.0
m3ph_l	336	0.02	0.02	0.0	336	336	0.01
m3ph_p	739	1.3	1.3	0.07	738	738	0.01
%s v/v	54.5	98.2	98.2	0.0	54.5	54.5	0.0
%l v/v	45.5	1.8	1.8	0.08	45.5	45.5	0.0
SGp	2.26	2.64	2.64	0.0	2.25	2.25	0.0
P_{80}	0.44	11.6	11.3	2.3	0.43	0.43	0.05

3.3.5 Ball Mill

The ball mill model is similar to the SAG mill model, described in Section 3.3.1, and consists of:

- solids balance
- water balance
- ball charge model
- power draw model

Mass Balances

Water : The steady state water balance for the ball mill is simply

$$Water\ In\ =\ Water\ Out \tag{3.109}$$

Solids : The steady state solids mass balance for the ball mill (Valery Jnr and Morrell, 1995) and (Napier-Munn *et al.*, 1996) is:

$$\begin{aligned} 0 &= \text{In - Out + Generation - Consumption} \\ 0 &= f_i - p_i + \sum_{j=1}^{i-1} r_j s_j a_{ij} - (1 - a_{ii}) r_i s_i \end{aligned} \tag{3.110}$$

where

s_i	=	mill rock charge particles in *sizei* (t)
f_i	=	feedrate of particles in *size i* (t)
p_i	=	mill discharge (product) of particles in *size i* (t)
r_i	=	breakage rate of particles in *size i* (hr^{-1})
a_{ij}	=	appearance function of particles appearing in *size i* (a function of the breakage distribution of particles in sizes $\geq$ *size i*) (fraction)

The feed component in Equation (3.110) is obtained by the summation of the:

- primary cyclone underflow to the ball milll,
- secondary cyclone underflow to the ball mill, and,
- the flash flotation tails stream.

The ball mill product, generation and consumption components are dealt with differently to the SAG mill. These terms will now be discussed further.

Product

The ball mill product, p_i, (the ball mill discharge stream, $BMDC$) is calculated as follows:

$$p_i = d_i s_i \tag{3.111}$$

where

$$d_i = d_i^* \left(\frac{4Q}{D_m^2 L_m} \right) = d_i^* \frac{1}{\tau} \tag{3.112}$$

d_i = mill discharge rate of *size* i particles (hr^{-1})

d_i^* = mill discharge rate of *size* i particles normalised to mill residence time ($-$)

$$\frac{D_m^2 L_m}{4Q} = \tau = \text{mill residence time (hr)} \tag{3.113}$$

$$\frac{1}{\tau} = \text{mill space velocity } (\text{hr}^{-1}) \tag{3.114}$$

D_m = mill inside diameter (m)

L_m = mill length (m)

Rearranging Equation (3.111) for s_i and substituting into Equation (3.110) yields Equation (3.115) which can be solved for mill product, p_i, once the appearance function, a_{ij}, and the rate/discharge function, $\frac{r_i}{d_i^*}$, have been specified.

$$0 = f_i - p_i + \tau \sum_{j=1}^{i-1} \frac{r_j}{d_j^*} p_j a_{ij} - (1 - a_{ii}) \tau \frac{r_i}{d_i^*} p_i \tag{3.115}$$

where

$\frac{r_i}{d_i^*}$ = ball mill rate/discharge value for *size* i particles (hr^{-1})

Generation and Consumption

As mentioned above, the ball mill appearance function, a_{ij}, and the rate/discharge function, $\frac{r_i}{d_i^*}$ function are specified in the ball mill model and are determined by laboratory scale ore ball milling tests.

Appearance Function, a_{ij} : Similar to the the SAG mill appearance function, the ball mill appearance function is a matrix of vectors that describe:

1. the amount of material in a given size that is "selected" for breakage, and,

2. the distribution that remains after breakage has occurred

Similar to the SAG mill appearance function matrix, the ball mill appearance function matrix is a square matrix of size (no. of sizes $\times$ no. of sizes). Also, since there is no particle growth, the appearance function matrix is a lower-triangular matrix. Unlike the SAG mill, the appearance vector is the same for each particle size. This is a result of type of breakage occurring in the mill. Only abrasion (low energy) breakage occurs in a ball mill and the resulting breakage distribution is independent of size.

Rate/Discharge Function, $\frac{r_i}{d_i^*}$: The rate/discharge function is determined from data obtained during plant surveys and by a model fitting process. The full function for a given ball mill is condensed to a set of four (4) ("knot size", $ln(\frac{r}{d^*})$) pairs. The knot sizes are selected to encompass the size distribution and capture important features,such as the maximum breakage rates of intermediately sized particles. The rate/discharge values for each particle size is determined by interpolation.

Ball Charge Model

The ball mill ball charge model simply consists of:

1. a specified ball charge level, J_b
2. a specified ball top size (in mm)

Both of these parameters are specified by plant survey data.

Model Scaling

To increase the utility of the ball mill model, a number of scaling factors are used to adjust the rate/discharge function values according to the prevailing operating conditions (*wrt*

the conditions for which the original model was developed), see Equation (3.116).

$$\frac{\left(\frac{r}{d^*}\right)_{SIM}}{\left(\frac{r}{d^*}\right)_{FIT}} = \left(\frac{D_{SIM}}{D_{FIT}}\right)^{0.5}\left(\frac{1-LF_{SIM}}{1-LF_{FIT}}\right)\left(\frac{LF_{SIM}}{LF_{FIT}}\right)\left(\frac{C_{s\,SIM}}{C_{s\,FIT}}\right)\left(\frac{WI_{SIM}}{WI_{FIT}}\right)^{0.8} \tag{3.116}$$

where

$$\begin{aligned} D &= \text{mill inside diameter (m)} \\ LF &= J_b = \text{ball charge fraction } (J_b) \text{ (fraction)} \\ C_s &= \frac{42.3}{\sqrt{D}} = \text{mill critical speed (RPM)} \\ WI &= \text{ore work index (kWh/t)} \\ FIT &= \text{original conditions of fitted model} \\ SIM &= \text{simulated conditions} \end{aligned} \tag{3.117}$$

Model scaling on account of ball size is divided around size x_m, the size below which, abrasion breakage predominates and above which, impact breakage predominates, see Equation (3.118).

$$x_m = K \cdot b^2 \tag{3.118}$$

where

$$\begin{aligned} K &= \text{maximum breakage factor } (\text{mm}^{-1}) \\ b &= \text{ball diameter (mm)} \\ x_m &= \text{impact } \textit{versus} \text{ abrasion breakage boundary particle size (mm)} \end{aligned}$$

For particle sizes, $x \leq x_m$,

$$\frac{\left(\frac{r}{d^*}\right)_{SIM}}{\left(\frac{r}{d^*}\right)_{FIT}} = \frac{b_{FIT}}{b_{SIM}} \tag{3.119}$$

For particle sizes, $x > x_m$,

$$\frac{\left(\frac{r}{d^*}\right)_{SIM}}{\left(\frac{r}{d^*}\right)_{FIT}} = \left(\frac{b_{SIM}}{b_{FIT}}\right)^2 \tag{3.120}$$

Power draw Model

The ball mill power draw model is the same as that detailed for SAG mill power draw in Section 3.3.1.

Ball mill model validation

Table 3.10 contains results of the validation of the ball mill model (in isolation) by way of the stream properties of the ball mill discharge stream. The reference case is the JKSimMet simulation results from the model constructed from the grinding circuit survey (David, 1997), see Appendix B. The feed stream and the columns headed with "JK" is the reference data. The columns headed "model" and "error" are the results from this work and the absolute, relative error between this work and the reference data.

Generally, the model results show excellent agreement with the reference data with all errors less than 0.6%. The reference data lacked a ball mill powerdraw figure. The ball mill is rated to 3000 kW. The model power parameter, k, can be adjusted so that the agreement is better than the tabulated 5%. Therefore this aspect of the model is considered valid also.

At this point the ball mill model was judged valid.

Table 3.10: Ball mill model validation

Stream	Ball mill	O/S Ball mill discharge		
Properties	Feed	JK	model	error (%)
tph_s	1069	1068	1069	0.0
tph_l	321	321	321	0.0
tph_p	1390	1390	13890	0.0
%s w/w	76.9	76.9	76.9	0.01
%l w/w	23.1	23.1	23.1	0.02
m3ph_s	403	403	403	0.01
m3ph_l	321	321	321	0.03
m3ph_p	724	724	724	0.02
%s v/v	55.7	55.7	55.7	0.01
%l v/v	44.3	44.3	44.3	0.01
SGp	2.27	2.27	2.27	0.0
P_{80}	0.64	0.44	0.44	0.5
Powerdraw (kW)		$\approx$ 3000	3148	4.9

3.3.6 Flash Flotation Cells

At the time of the grinding circuit surveys (early 1997) the flash flotation cells were either being installed or commissioned. As a result, the flash flotation cells were not in operation during the surveys. Furthermore, a detailed model was not developed for the NPM flash flotation cells by the JKTech personnel. Therefore, to achieve a full circuit model, a simplified model would need to be utilised for the flash flotation cells. The model proposed for such utilisation is a simple efficiency curve, similar to that utilised for the SAG mill discharge screen, see Section 3.3.4. Again, the corrected 50% passing size, d_{50c}, and water recovery to underflow (tails), R_f, are specified model parameters (that would have to be determined by plant survey).

In the absence of operating data, or, a reference JKSimMet simulation case, validation of a flash flotation model is not feasible. Therefore, the flash flotation cells have been omitted from the full circuit model.

3.4 Steady State Circuit Model Validation

Once the individual equipment models were constructed and validated they were joined together to form the full circuit as per the grinding circuit survey (David, 1997). Operating conditions characteristic of the survey are:

- zero recycle of primary cyclone underflow to the SAG mill
- flash flotation cells not operating

Table 3.11 through Table 3.14 show the comparative error between the model simulation results and the base case data (David, 1997), see Appendix B. For brevity, comparative Stream Properties results only are shown here. Appendix C contains the reference data and the simulation results in full. The Appendix B survey data was simulated on a unit by unit basis by the MATLAB-Simulink models to produce the reference data in Appendix C. Table C.1 through Table C.4 contains the stream properties and size distribution information for the reference data. Table C.5 through Table C.8 contains the stream properties and size distribution information for the full circuit MATLAB-Simulink simulation model results. The size distribution information for these two cases (and the inferential model case) are shown graphically in Figure C.1 through Figure C.8[8].

Referring again to Tables 3.11 to 3.14, the agreement is generally acceptable with many of the results exhibiting errors of $< 1\%$. There are a number of results which exhibit errors significantly larger and these will now be addressed in more detail.

Table 3.11 contains the results for the "front-end" of the primary grinding circuit and Table 3.12 contains the results for the "back-end" of the primary grinding circuit. Again, agreement is generally acceptable at $< 1\%$. It should be noted that the SAG mill fresh feed and rock charge, $SMFF$ & $SMRC$, respectively, are specified information. Further details are as follows:

- The oversize crusher feed ($OSCF$) and product ($OSCP$) exhibit $\approx 6\%$ error in the water flow. These are essentially dry streams. Therefore, small differences in water flowrates correspond to larger relative errors.
- The SAG mill and oversize crusher powerdraw and the primary cyclone pressure estimates exhibit good agreement.
- A number of the eighty percent passing size (P_{80}) results show significant deviation from the base case information. These deviations are attributed to interpolation errors combined with minor model approximations. The commercial simulation package (JKSimMet) utilises splines to describe size distributions and for interpolation. Linear description and interpolation (fixed by the points (0.001 mm, 0%passing) and (180.76 mm, 100%passing)) are considered sufficiently accurate in this research and thus are utilised in the MATLAB-Simulink models.

Furthermore, for fine streams, such as the primary cyclone overflow ($PCOF$) and underflow ($PCUF$), where the reference data is of the order of 10^1 to 10^3 μm, small differences between simulation and reference data are simply relatively larger.

The P_{80} measure is also an attempt at a single point measure of a full size distribution. Relative movement in the P_{80} measurement over time is the most important consideration rather than the absolute value of the measurement itself (Davies *et al.*, 2000) .

The difference in interpolation methods is one of the minor model approximations. Manual fitting of model parameters was utilised predominantly in the model development phase. In the JKSimMet software, model fitting, using least squares minimisation techniques, is conducted prior to conducting simulations. Manual model parameter fitting was considered sufficiently accurate in this research and proved insightful regarding model sensitivity.

Considering these points, the simulation results, including the P_{80} results, are considered acceptable.

Table 3.13 contains the results for the "front-end" of the secondary grinding circuit and Table 3.14 contains the results for the "back-end" of the secondary grinding circuit. Here the level of agreement is lower than the for the primary circuit and there is also a wider range in the results. These features are due to the propagation of errors from upstream information combined with model parameter influences. Certain parameters were selected to achieve close agreement for the grinding circuit product stream (secondary cyclone overflow, $SCOF$) at the expense of lower agreement levels for some streams internal to the circuit,*e.g.*, secondary cyclone underflow, $SCUF$. Further points of discussion are:

- The P_{80} remarks above regarding interpolation methods and model approximations apply here also.
- The "dry stream" comments above apply for the ball mill screen oversize ($BSOS$) here.
- Water results throughout the secondary survey are strongly influenced by the circulating water in the secondary cyclone underflow ($SCUF$) stream which is a result of model parameter influences mentioned above.
- Ball mill powerdraw and secondary cyclone pressure estimates display good agreement.

In conclusion, these results (Table 3.11 through Table 3.14) and those in Appendix C display satisfactory agreement with the reference data outright, especially once the propagation of errors and the influence of model parameters have been considered. Therefore, at this point the steady state grinding circuit model is deemed valid.

Table 3.11: Simulation Errors: Primary Circuit - SAG mill

Stream Properties	SMFF	OSCP	SMTF	SMRC	SMDC
tph_s	0.0	0.1	0.0	0.0	0.0
tph_l	0.0	6.0	0.0	0.0	0.1
tph_p	0.0	0.1	0.0	0.0	0.0
%s w/w	0.0	0.0	0.0	0.0	0.0
%l w/w	0.0	5.9	0.0	0.0	0.1
m3ph_s	0.0	0.1	0.0	0.0	0.0
m3ph_l	0.0	6.0	0.0	0.0	0.1
m3ph_p	0.0	0.1	0.0	0.0	0.0
%s v/v	0.0	0.0	0.0	0.0	0.0
%l v/v	0.0	5.9	0.0	0.0	0.0
SGp	0.0	0.0	0.0	0.0	0.0
P_{80}	0.0	20.0	0.0	0.0	2.0
Power				2.2	
Pressure					

Table 3.12: Simulation Errors: Primary Circuit - Screen/Crusher/Cyclones

Stream Properties	SMDC	OSCF	OSCP	PCFD	PCUF	PCOF
tph_s	0.0	0.1	0.1	0.0	0.0	0.1
tph_l	0.1	6.0	6.0	0.1	0.0	0.1
tph_p	0.0	0.1	0.1	0.0	0.0	0.1
%s w/w	0.0	0.0	0.0	0.0	0.0	0.0
%l w/w	0.1	5.9	5.9	0.0	0.0	0.01
m3ph_s	0.0	0.1	0.1	0.0	0.0	0.1
m3ph_l	0.1	6.0	6.0	0.1	0.0	0.1
m3ph_p	0.0	0.1	0.1	0.1	0.0	0.1
%s v/v	0.0	0.0	0.0	0.0	0.0	0.0
%l v/v	0.0	5.9	5.9	0.0	0.0	0.0
SGp	0.0	0.0	0.0	0.0	0.0	0.0
P_{80}	2.0	34	20	95	90	36
Power			5.2			
Pressure				0.3		

Table 3.13: Simulation Errors: Secondary Circuit - Ball mill/Screen

Stream Properties	PCUF	SCUF	BMFD	BMDC	BSOS	BSUS
tph_s	0.0	0.1	0.1	0.1	3.8	0.1
tph_l	0.0	45	36	36	34	34
tph_p	0.0	9.9	8.	8.4	3.6	8.3
%s w/w	0.0	8.9	7.7	7.7	0.3	7.6
%l w/w	0.0	32	25	26	39	24
m3ph_s	0.0	0.1	0.1	0.1	3.8	0.1
m3ph_l	0.0	45	36	36	34	34
m3ph_p	0.0	19	16	16	3.1249	16
%s v/v	0.0	16.0	13.7	13.7	0.7	13.5
%l v/v	0.0	21.4	17.2	17.3	39	16.2
SGp	0.0	0.1	0.1	0.1	0.1	0.1
P_{80}	90	41	38	34	48	33
Power				≤ 10		
Pressure						

Table 3.14: Simulation Errors: Secondary Circuit - Cyclones

Stream Properties	BSUS	PCOF	SCFD	SCUF	SCOF
tph_s	0.1	0.1	0.1	0.1	0.0
tph_l	34	0.1	20.5	45	0.0
tph_p	8.4	0.1	7.0	9.9	0.0
%s w/w	7.6	0.0	6.5	8.9	0.1
%l w/w	24.1	0.0	12.6	32	0.
m3ph_s	0.1	0.1	0.1	0.1	0.0
m3ph_l	34	0.1	20.5	45	0.1
m3ph_p	15.7	0.1	11.9	19.2	0.0
%s v/v	13.5	0.0	10.5	16.0	0.1
%l v/v	16.1	0.0	7.7	21.4	0.0
SGp	0.1	0.0	0.1	0.1	0.0
P_{80}	33	36	32	41	49
Power					
Pressure			0.1		

3.5 Supplementary Model Validation: Gault Data

3.5.1 Process Description

The steady state models discussed above were further validated against data published in a University of Queensland PhD Thesis, (Gault, 1975). The results of the base case of the Kambalda Nickel Operation (KNO) rock-pebble mill circuit, shown in Figure 3.6, were selected as reference for further model validation.

The fresh ore (−9.5 mm) is fed to a rock mill, which is periodically charged with rock media (+127 to −203 mm). Rock mill discharge is presented to a DSM sieve bend, which recycles screen oversize to the rock mill and feeds screen undersize to a Krebs D20B cyclone[3]. Cyclone overflow represents the circuit product, which reports to the flotation plant. Cyclone underflow is fed to a pebble mill, which is periodically charged with pebble media (+76 to −127 mm). Pebble mill discharge joins the rock mill discharge stream reporting to the DSM sieve bend. Table 3.15 contains the key details of the processing units within the KNO circuit and the modelling parameters utilised. The DSM Screen was modelled as an efficiency curve.

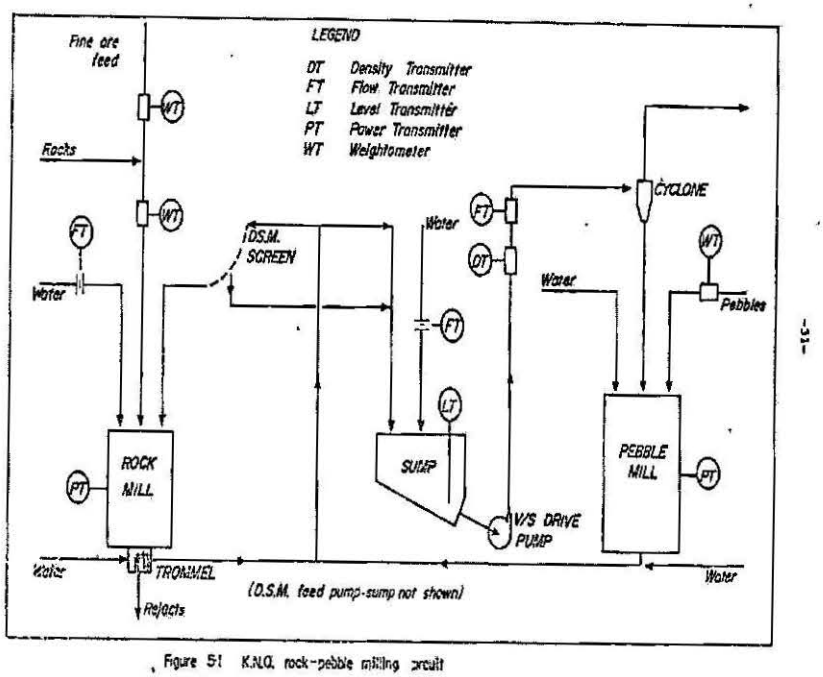

Figure 3.6: KNO Grinding Circuit

[3]Cyclone dimensions taken from the supplementary information manual of the *JKSimMet* Manual (JKTech, 1994)

The SAG mill model requires numerous parameters, such as ore hardness and breakage parameters (A, b and ta), an initial estimate of the SAG mill rock charge, discharge grate characteristics (fractional grate open area, relative open area of the pebble ports, relative radial position of open area and relative radial position of outer grate) and numerous others. These parameters were not presented by Gault (1975), presumably because the SAG model was not at its current stage of development. Educated guess-work could be used to estimate a number of the parameters. However, determination of all of the required parameters and the full definition of the SAG mill model is not possible. Therefore, the SAG mill was modelled as a ball mill to fulfill the objective of obtaining a full circuit model.

A major consequence of this simplification was that simulation of the dynamic tests conducted by Gault (1975) were not possible to replicate. However, this unfortunate development did not compromise the model validation objective. The results presented below reinforce the validation of the steady state models. Regarding the further validation of the inferential measurement models developed in Chapter 5, fortuitously, Northparkes Mines data was sourced from the time of the *SAG Control Project* (Romagnoli *et al.*, 1997) , which was able to be utilised for this purpose. Section 8.1 details this further validation of the inferential models.

3.5.2 Validation Results

Figure 3.7 shows the simulation model Rock Mill discharge presented alongside the KNO Rock Mill discharge. Visual inspection shows a good match between the simulation results and the Gault reference data. These results reinforce the validity of the simulation models utilised in this research, especially considering minimal, manual model fitting was conducted. The in-built model-fitting functionality of *JKSimMet* is not a feature of the models utilised in this research. The latter two points apply throughout the following discussion.

The Pebble Mill discharge results are shown in Figure 3.8. The close fit of the Rock Mill discharge is not evident here. However, the fit between the simulation model and the Gault data was considered satisfactory, which reinforced the validity of the ball mill model utilised in this research.

Table 3.15: KNO Process Units

Unit	Dimensions
Rock Mill	Mill Diameter, D_{mill} = 3.20 m Mill Length, L_{mill} = 4.10 m Frac. Critical Speed, N_{fcs} = 78 % Cone Angle, $\theta = 15\ ^o$ Trunnion Diameter, D_t = 0.75 m
Trommel Screen	Aperture = 7.9 mm
DSM Screen	Aperture = 5 mm
Pebble Mill	Mill Diameter, D_{mill} = 3.81 m Mill Length, L_{mill} = 5.79 m Frac. Critical Speed, N_{fcs} = 67 % Cone Angle, $\theta = 15\ ^o$ Trunnion Diameter, D_t = 0.75 m
Cyclone	Krebs D20B Cyclone Diameter, D_c = 0.508 m Inlet Diameter, D_i = 0.157 m Outlet Diameter, D_o = 0.203 m Underflow Diameter, D_u = 0.152 m Cylinder Length, L_c = 0.32 m Cone Angle, $\theta = 20\ ^o$

Figures 3.9, 3.10 and 3.11 illustrate the simulation model results *versus* the Gault data for the DSM sieve bend, Rock Mill trommel screen and cyclone, respectively. The DSM sieve bend results, Figure 3.9, are mixed. There is excellent agreement for the fine undersize stream, while there is a lesser degree of agreement for the coarse oversize stream. This latter diversion is attributed to the low degree of separation effected by the DSM sieve bend.

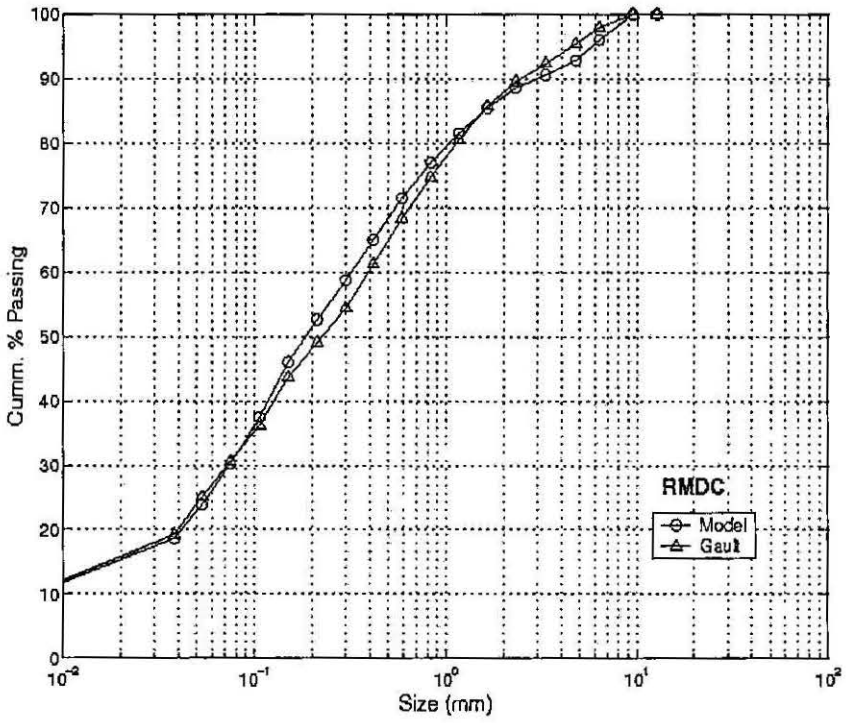

Figure 3.7: KNO Rock Mill Discharge

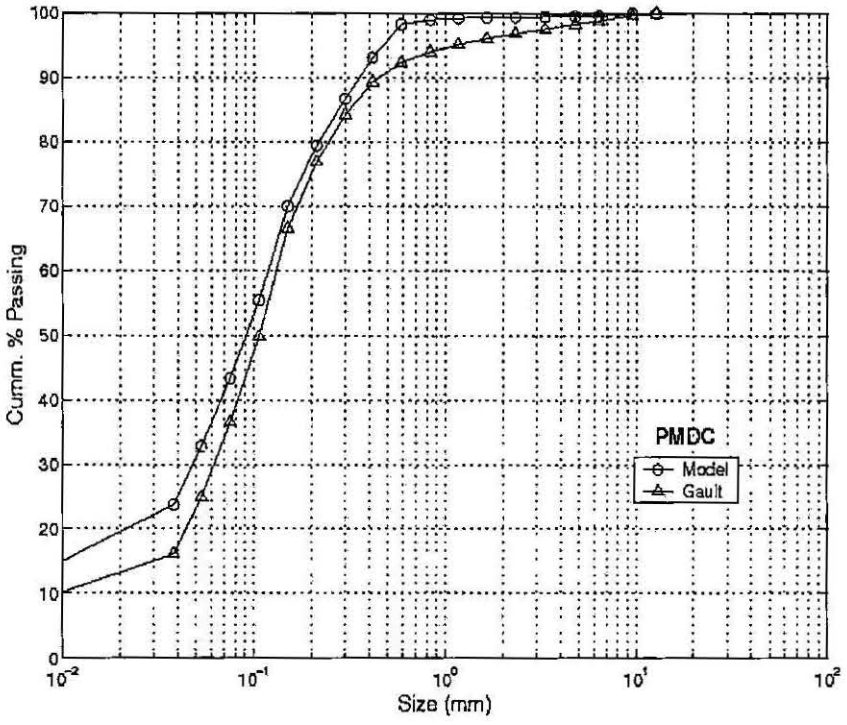

Figure 3.8: KNO Pebble Mill Discharge

The undersize stream distribution is similar to the feed distribution. Small modelling inaccuracies are emphasized in the stream that is extracted from the bulk material, the coarse stream in this instance. The model fitting effort was limited by time constraints. Furthermore, the relative, perceived insignificance of supplementary model validation of a DSM sieve bend curtailed further model fitting. The results for the DSM sieve bend as they stand, and considering the latter points, are considered sufficient to deem the sieve bend model valid.

The Rock Mill trommel screen results are shown in Figure 3.10. There is good agreement at the top and bottom of the distribution. There is lesser agreement mid-distribution. The discrepancies in the results are attributed to the sharp separation required to model the narrow trommel oversize distribution. Such a sharp separation requires thorough model-fitting, which was not afforded to this problem on account of time constraints and the relative insignificance of the trommel screen modelling task. The results were considered sufficiently satisfactory and the trommel screen model, therefore, was considered valid.

Figure 3.11 illustrates the cyclone stream results. There is a relatively low degree of separation occurring at the cyclone, with the cyclone underflow being not altogether dissimilar to the cyclone feed. This is a contributing factor to the errors evident in the results. Other contributing factors are related to the cyclone dimensions and the cyclone modelling parameters.

The cyclone is a *Krebs D20B* cyclone, the dimensions or which are not detailed by Gault (1975). The dimensions listed in Table 3.15 were sourced, as previously mentioned, from the supplementary information booklet of the *JKSimMet* Manual (JKTech, 1994). There is no way to ascertain the applicability of these dimensions to the KNO cyclone.

The Nageswararao cyclone model, detailed in Napier-Munn *et al.* (1996) and utilised in this research relies on numerous cyclone dimension, ore property and efficiency curve parameters. As mentioned, the cyclone dimensions utlised contain a degree on uncertainty. Best estimates of the ore-property parameters were sourced from the supplementary information booklet of the *JKSimMet* Manual (JKTech, 1994). Time constraints and research focus curtailed the model-fitting effort. Considering these points, the model-fit achieved was considered sufficient to prove the validity of the cyclone models utilised in this research.

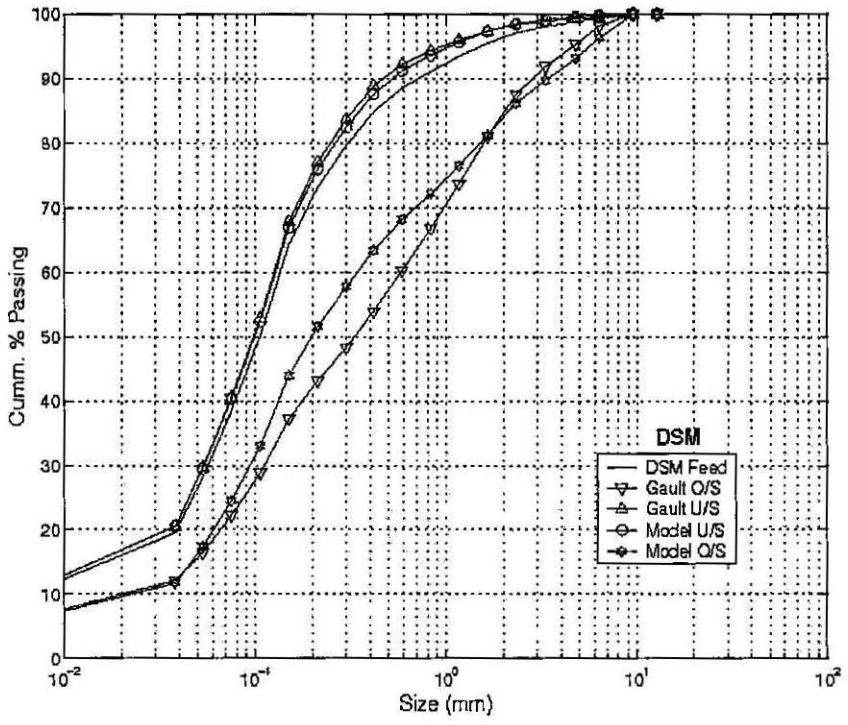

Figure 3.9: KNO DSM Screen Streams

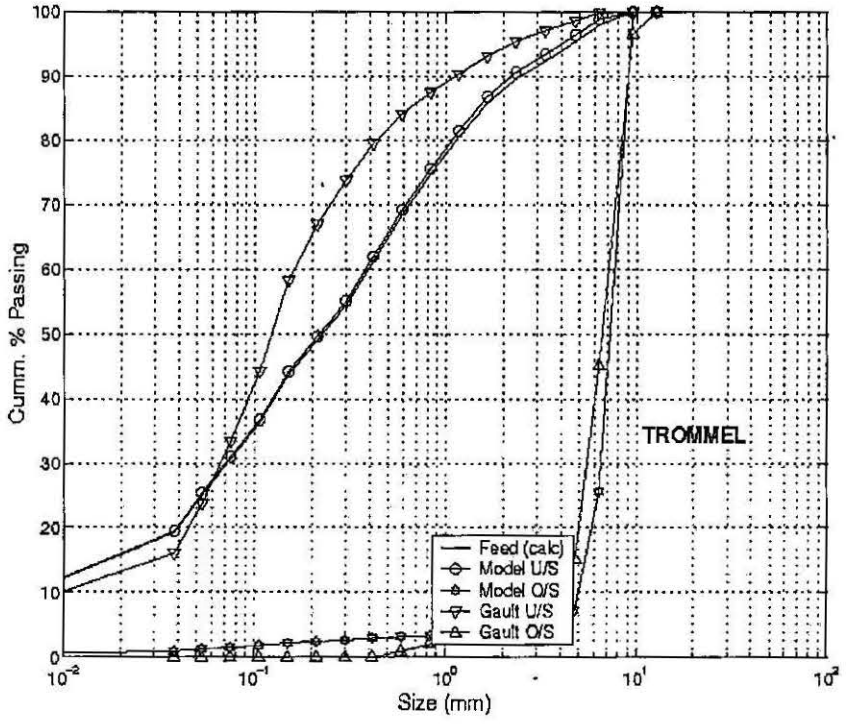

Figure 3.10: KNO Trommel Screen Streams

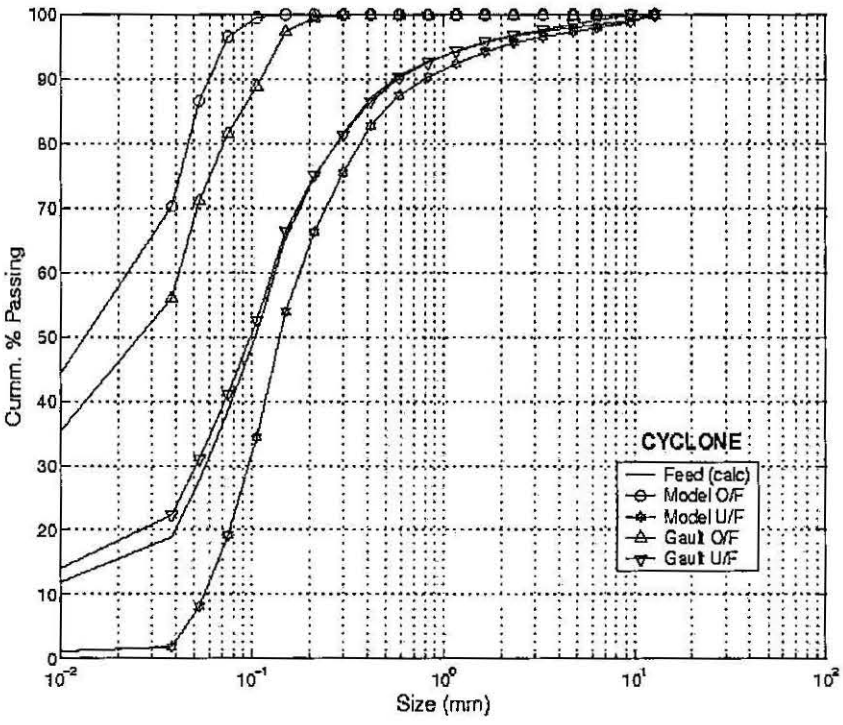

Figure 3.11: KNO Cyclone Streams

In conclusion, the supplementary model validation, based on the data published in Gault (1975) and presented in summary by way of Figures 3.7 through 3.11, reinforce the conclusions of Sections 3.3 and 3.4 that the steady state unit process models and the steady state grinding circuit model are valid.

The model validation conducted in this Chapter has been the comparison of the MATLAB-Simulink model results to the results generated by JKSimMet (the commercially available software) for the same circuit. This degree of validation was dictated by access to the process and the independent nature of this research, *i.e.*, comminution research without the support of a comminution research resource-base, such as the Julius Kruttschnitt Mineral Research Centre. Therefore, model validation at a pilot plant or full scale level was not feasible. The research independence has resulted in certain freedom in the techniques employed and model assessments presented.

Model validation at the simulation model level was considered sufficient towards the achievement of the objectives of the research - the development of the SAG mill inferential models. This level of validation also leaves the simulation models in a state of readiness for further research and development.

3.6 Summary

In this Chapter, steady state models of the comminution circuit unit operations and the full circuit have been programmed into the MATLAB-Simulink environment and validated against industrial plant survey data, see Appendix B and Appendix C. Further supplementary validation was conducted against published data (Gault, 1975).

Generally, the models presented in this Chapter are those described in the Julius Kruttschnitt Mineral Research Centre Monograph (Napier-Munn *et al.*, 1996) and the JKSimMet User Manual (JKTech, 1994) and thus do not represent innovations of this research. One exception is the impact zone model developed independently in the course of this research, see Section 3.3.1, as indicated in Table 3.16, the Innovation Summary for this Chapter.

Table 3.16: Chapter 3 Innovation Summary

Section	Innovation
Section 3.3.1	SAG mill impact zone model

Chapter 4

Dynamic Model Development

To investigate state estimation for SAG mills a number of dynamic models are required. In this Chapter dynamic models are developed for the following:

- SAG mill ball charge (*size* by *size*)
- SAG mill rock charge (*size* by *size*)
- SAG mill water charge
- SAG mill liner weight

The ball charge model is detailed in Section 4.1, the rock and water charge models are described in Section 4.2, and the shell weight model is presented in Section 4.3.

4.1 SAG mill ball charge

The dynamic ball charge model proposed by this work is as follows:

$$\begin{aligned} \text{Accumulation} &= \text{In - Out + Generation - Consumption} \\ \frac{dbc_i}{dt} &= bi_i - be_i + bw_{i-1} - bw_i \end{aligned} \tag{4.1}$$

where

bc_i = mass of balls in ball charge of *size* i (t)

bi_i = feed balls in *size* i (t/hr)

be_i = balls of *size* i ejecting from the mill i (t/hr)

bw_i = mass of balls wearing out of *size* i into *size* $i + 1$ (t)

4.1.1 Ball Feed

The ball feed to the SAG mill, bi_i, can be determined from operating conditions. Assuming that the feed balls are of a single diameter, D_b, the ball feed is as follows:

$$bi_i = \frac{\pi}{6}\left(\frac{D_b}{1000}\right)^3 SG_b\, bps\, \frac{3600}{bst} \tag{4.2}$$

where

bps	=	balls per stroke
bst	=	ball stroke time (seconds)
D_b	=	new ball diameter (mm)
SG_b	=	ball specific gravity (t/m^3)

Some points to clarify balls per stroke, *bps*, and ball stroke time, *bst*, are:

- grinding balls are fed to the Northparkes Mines SAG mill via a hopper discharging onto the fresh feed conveyor
- grinding ball feed rate is controlled by the stroke rate of the feeding ram
- the ram is set to stroke every x seconds, *i.e.*, ball stroke time, *bst*, and discharges y balls onto the feed conveyor, *i.e.*, balls per stroke, *bps*

4.1.2 Ball Wear

The overall ball wear rate may be determined from operating data. If the ball charge level is being maintained at a constant level, the ball wear rate is equal to the ball feed rate. The overall ball wear rate translates to ball wear rates by size. These ball wear rates by size (bw_i) are proposed here to be proportional to the fractional surface area and the ball mass in *size i* and inversely proportional to ball hardness, *i.e.*,

$$bw_i \propto fSA_i \frac{1}{HB_i} SMBC_i \tag{4.3}$$

where

bw_i	=	ball wear of grinding balls in *size i* (t/hr)
fSA_i	=	fractional surface area of grinding balls in *size i* (fraction)
HB_i	=	Brinnell Hardness of grinding balls in *size i* (N/m^2)
$SMBC_i$	=	mass of grinding balls in *size i* (t)

The total surface area of grinding balls in *size i*, SA_i, is the product of the number of balls in *size i*, N_i, and the surface area of a ball of *size i*, *i.e.*,

$$SA_i = N_i\, \pi\, Db_i^2 \tag{4.4}$$

The number of balls in *size i*, N_i, is determined from the mass fraction of the total ball charge in *size i* and the mass of a ball of *size i*, *i.e.*,

$$N_i = \frac{\frac{smbc_i}{100} BC}{\frac{\pi}{6}\left(\frac{Db_i}{1000}\right)^3 SG_b} \tag{4.5}$$

where

BC = total ball charge mass (t)

Db_i = diameter of ball of *size i* (mm)

$smbc_i$ = mass percent of balls in *size i* (%)

The fractional surface area of the ball charge in *size i*, fSA_i, is

$$fSA_i = \frac{SA_i}{\sum SA_i} = \frac{\frac{smbc_i}{Db_i}}{\sum_{i=1}^{n} \frac{smbc_i}{Db_i}} \tag{4.6}$$

The ball hardness model proposed here is based on the findings of Banisi *et al.*(2000), *i.e.*, that the ball hardness of 80 mm balls drops significantly when the ball wears to less than 65 mm in size ($\approx$ 81% original size). In this work the original ball diameter is 125 mm and it is assumed that the hardness decreases markedly at the 95 mm mark (76% original size).

Assuming hardness of 450 and 250 Brinnell for the outside layer and the inner layer of the balls, respectively, (estimated from data in *Perry's*, (Perry et al., 1984)) and that the variation of hardness across ball diameter can be described by a Whiten classification model type relationship, (Whiten, 1972), (Napier-Munn *et al.*, 1996)(also refer to Section 3.3.3), the ball hardness, HB_i, can be described as follows:

$$\begin{aligned} HB(Db_i) &= 250 && \text{for } Db_i \leq K1 \\ HB(Db_i) &= 450 - \left(\frac{K2 - Db_i}{K2 - K1}\right)^{K3} && \text{for } K1 < Db_i < K2 \\ HB(Db_i) &= 450 && \text{for } Db_i \geq K2 \end{aligned} \tag{4.7}$$

(4.8)

where

$HB(Db_i)$ = ball hardness as a function of ball diameter (Brinnell)

$K1$ = $0.76\,D_b$ = 95 mm

= ball size below which hardness falls to 250 Brinnell (mm)

$K2$ = D_b = 125 mm

= ball size where hardness is 450 Brinnell (initial ball diameter) (mm)

$K3$ = 2.3

= curve shape parameter

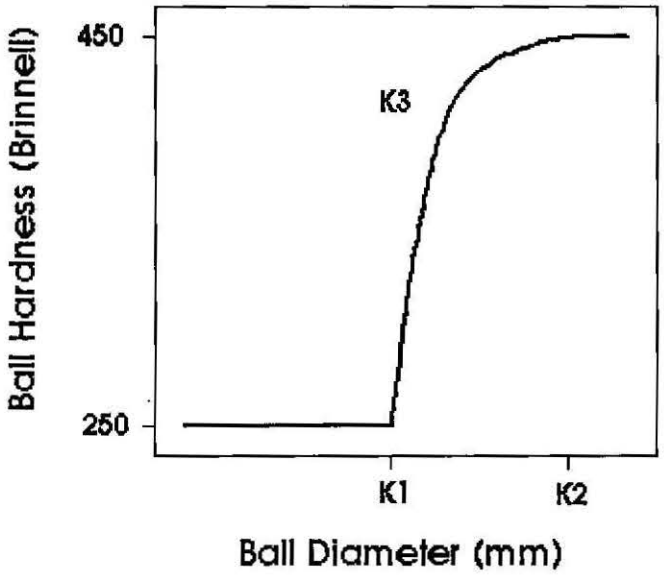

Figure 4.1: Ball Hardness Model

The ball hardness model is illustrated in Figure 4.1. The model can be adjusted to suit a given set of operating conditions by the introduction of a ball wear coefficient, BWk_i, which can be fitted to operating data. For mass balance consistency, the units of the ball wear coefficient are (Brinnel/hr). The ball wear model can now be stated as follows:

$$bw_i = BWk_i\, fSA_i \frac{1}{HB_i} SMBC_i \tag{4.9}$$

4.1.3 Ball Ejection

The model of ejection of balls from the SAG mill proposes that the SAG mill discharge grate behaves as a vibrating screen which can be modelled by an efficiency to oversize model, (Napier-Munn *et al.*, 1996). Ball ejection of *size i*, be_i, can then be stated as follows:

$$be_i = BEk_i\, Edc_i\, SMBC_i \tag{4.10}$$

where

Edc_i = ball ejection efficiency to discharge of *size i* (fraction)
be_i = ejection rate for balls of *size i* (t/hr)
BEk_i = ball ejection model fitting parameter (hr^{-1})

The efficiency model utilised here is taken from Napier-Munn *et al.* (1996) and is expressed in terms of efficiency to undersize since the ejected balls are screen "undersize".

$$Edc_i = 1 - \exp\left(-N\, foag \left[1 - \frac{Db_i}{x_p}\right]^k\right) \tag{4.11}$$

where

N = 1 = discharge grate efficiency parameter
$foag$ = discharge grate fraction open area (fraction)
Db_i = ball diameter of *size i* (mm)
x_p = discharge grate pebble port size (mm)
k = 2 = discharge grate efficiency parameter

4.1.4 Model Fitting and Validation

With limited scope for model validation against operating data, the model was validated by fitting the model parameters of:

- ball wear model parameters, BWk_i, and
- ball ejection model parameters, BEk_i,

such that the ball charge model agreed with the steady state operating conditions of the survey, (David, 1997), *i.e.*, $\frac{dbc_i}{dt} = 0$, see Equation (4.1) and Table 3.3.

4.2 SAG Mill Rock and Water Charges

The dynamic models of the SAG mill rock and water charge are obtained by taking the models presented in Chapter 3 and relaxing the imposed steady state conditions.

4.2.1 Solids Balance

Recall the solids balance from Equation (3.1):

$$\begin{aligned} Accumulation &= In - Out + Generation - Consumption \\ \frac{ds_i}{dt} &= f_i - p_i + \sum_{j=1}^{i-1} r_j s_j a_{ij} - (1 - a_{ii}) r_i s_i \end{aligned} \tag{4.12}$$

where

s_i = mill rock charge particles in *size i* (t)

f_i = feedrate of particles in *size i* (t)

p_i = mill discharge (product) of particles in *size i* (t)

r_i = breakage rate of particles in *size i* (hr^{-1})

a_{ij} = appearance function of particles appearing in *size i* (a function of the breakage distribution of particles in sizes $\geq$ *size i*) (fraction)

Recall also that the mill product stream from Equation (3.3):

$$p_i = d_0 c_i s_i \tag{4.13}$$

where

d_0 = maximum mill discharge rate (hr^{-1})

c_i = grate classification function for *size i* (fraction)

= probability of *size i* particle passing through mill discharge grate

In the case of the steady state model:

1. the LHS of Equation (4.12) is set to zero, and,
2. the maximum discharge rate parameter, d_0, is fitted to satisfy the steady state mass balance.

For the dynamic solids mass balance:

1. the LHS of Equation (4.12) is allowed to vary, and,
2. the maximum discharge rate parameter, d_0, is governed by Equation (4.14) below.

$$d_0 = \frac{Q_m}{J_{pm} \cdot V_m} \tag{4.14}$$

J_{pm} = nett fractional holdup of slurry in mill that is contained within the grinding charge interstices (fraction)

V_m = mill internal volume (m^3)

The volumetric discharge from the mill (through the media), Q_m, is

$$Q_m = 6100\, J_{pm}^2 \gamma^{2.5} A \phi^{-1.38} D^{0.5} \tag{4.15}$$

where

Q_m = mill discharge flowrate through grinding media (m^3/hr)

A = total discharge grate open area (m^2)

D = mill inside diameter (m)

γ = mean relative radial position of open area (fraction)

ϕ = fraction critical mill speed (fraction)

4.2.2 Water Balance

Recall the SAG mill water balance from Chapter 3, Equation (3.44):

$$\begin{aligned} Accumulation &= In - Out \\ \frac{ds_w}{dt} &= f_w - p_w \end{aligned} \tag{4.16}$$

where

s_w = water in the mill charge (t)

f_w = feed water addition (t/hr)

The water feedrate to the mill, f_w, is known, therefore the water balance can be determined by calculation of the mill discharge water flowrate, p_w, as follows:

$$p_w = d_0\, s_w \tag{4.17}$$

The water charge accumulation term may then be determined from Equation (4.16).

4.2.3 Model Fitting and Validation

The steady state models of the SAG mill rock charge and water charge were validated in Chapter 3. In the absence of dynamic plant data, the corresponding dynamic models were validated by verifying their satisfactory behaviour at the steady state conditions of the plant survey (David, 1997), see Appendix B.

In this development and validation phase of the dynamic model of the SAG mill a high degree of model sensitivity to the SAG mill breakage rates, r_i, was encountered. Small variations in the calculated breakage rates, r_i, resulted in the SAG mill rock charge diverging in an un-bounded fashion from the initial steady state conditions.

This behaviour may be attributed in part to errors introduced during the model fitting stage of this research, including the utilisation of linear interpolation methods instead of higher order methods. The behaviour is also likely to be characteristic of the breakage rate model itself since researchers at the Julius Kruttschnitt Mineral Research Centre have experienced similar behaviour ("room for improvement" exists in the "key sub-process" of "breakage rate relationships") and have utilised a Kalman filter to estimate parameters to continually tune the model against on line data (Morrell *et al.*, 2001). Currently, the Julius Kruttschnitt Mineral Research Centre dynamic SAG mill model is currently undergoing validation[1] and is projected to be utilised widely by industry over the next 10 years (Lynch and Morrison, 1999).

A detailed study of the breakage rate calculation is beyond the scope of this work. However, in Section 6.5, the breakage rate "knot" equations, Equations (3.22) to (3.30) in Section 3.3.1, are included in a sensitivity analysis that studies the relative influence various model parameters have on the breakage rates. The effect of the breakage rates on the fresh feedsize inferential model are described in Section 8.2.2.

4.3 SAG Mill Liner Weight

The SAG mill installation weight, $SMIW$, can be considered a sum of a number of constituents:

$$SMIW = shell + lining + D/C\,grate \tag{4.18}$$

where

$SMIW$	=	SAG mill installation weight (t)
$shell$	=	SAG mill shell weight (t)
$lining$	=	SAG mill shell lining weight (t)
$D/C\,grate$	=	SAG mill discharge grate weight (t)

The mill shell remains intact throughout the operational life of the mill. Therefore, the mill shell weight ($shell$) is a constant. The $lining$ is the internal shell protective lining and is subject to wear through direct contact with the mill contents. The SAG mill discharge

[1] As discussed with Dean David, Manager, JKTech Consulting, JKTech, at SAG 2001 Conference.

grate is internal to the mill also and is subject to wear. Periodic change out of the mill protective lining and discharge grate occurs to accommodate the wear of these internal components.

From plant experience, the shell lining wear occurs predominantly at discharge end. Therefore, the *lining* term can be broken up into a feed end and a discharge end term:

$$SMIW = (shell + lining_{FE}) + (lining_{DE} + D/C\,grate) \tag{4.19}$$

where

$lining_{DE}$ = weight of the discharge end of the shell lining (t)

$lining_{FE}$ = weight of the feed end of the shell lining (t)

Combining the feed end lining terms and a constant (to accommodate mill weight instrument offset), $SMWconst$ (t), allows the model to we rewritten as follows

$$SMIW = SMWconst + lining_{DE} + D/C\,grate \tag{4.20}$$

The dynamic SAG mill liner wear model may then focus on the grouped mill discharge end terms and may be written as follows:

$$\frac{dSMIW}{dt} = -wearate \tag{4.21}$$

where

$wearate$ = SAG mill discharge end wearate (t/hr)

Integrating Equation (4.21) with respect to time, t, yields

$$SMIW = SMIW_0 - wearate \cdot t \tag{4.22}$$

where

$SMIW_0$ = initial SAG mill installation weight (Equation (4.20) evaluated at initial conditions) (t)

t = time (hr)

4.3.1 Wear Rate

The mill liner wear rate, *wearate*, can determined from:

- the change-out frequency, and,
- the relative change in weight of the discharge grate and discharge end shell lining at change-out time

Based on plant experience, the change-out frequency is approximately 6 weeks, or 1,008 hours (6 × 7 × 24), and the change-out liner weight is approximately half the liner installation weight, *i.e.*,

$$wearate = \frac{\frac{1}{2}(lining_{DE\,0} + D/C\,grate_0)}{1008} \tag{4.23}$$

where

$lining_{DE\,0}$ = installation weight of the discharge end of the shell lining (t)
$lining_{FE\,0}$ = installation weight of the feed end of the shell lining (t)

The shell lining is a series of alternating low lifter and high lifter bars separated by shell lining pieces. The installation weight of the discharge end shell lining, $lining_{DE\,0}$, is calculated as follows:

$$\begin{aligned} lining_{DE\,0} = {} & \frac{1}{2} L_{sm}\, \rho_{liner}\, nhl\, \frac{lbw}{1000} \frac{(hlt - slt)}{1000} \\ & + \frac{1}{2} L_{sm}\, \rho_{liner}\, nll\, \frac{lbw}{1000} \frac{(llt - slt)}{1000} \\ & + \frac{\pi}{2} \rho_{liner}\, L_{sm} \{ D_{sm\,0} \frac{slt}{1000} - \left[\frac{slt}{1000}\right]^2 \} \end{aligned} \tag{4.24}$$

where

ρ_{liner} = liner density (t/m^3)
nhl = number of high lifter bars
nll = number of low lifter bars
lbw = lifter bar width (mm)
hlt = high lifter bar thickness (height) (mm)
llt = low lifter bar thickness (height) (mm)
slt = shell liner thickness (height) (mm)
$D_{sm\,0}$ = SAG mill shell inside diameter (m)
L_{sm} = SAG mill shell length (m)

In Equation (4.24), the third term represents the weight of an annular piece of shell lining of thickness slt, defined by the shell inside diameter, $D_{sm\,0}$, and extending to half the mill length, L_{sm}. The first and second terms are the weight of portion of high and low lifter bars, respectively, that protrude above the shell lining.

The installation weight of the discharge grate, $D/C\,grate_{\,0}$, is calculated as follows:

$$\begin{aligned} D/C\,grate_{\,0} = {} & \rho_{liner} \left(\pi \frac{{D_{sm}}^2}{4} \frac{dgt}{1000} (1 - foag) - \pi \frac{{Dt_{sm}}^2}{4} \frac{dgt}{1000} \right. \\ & \left. + ndg \frac{lbw}{1000} \frac{(hlt - slt)}{1000} (D_{sm} - Dt_{sm}) \right) \end{aligned} \tag{4.25}$$

where

dgt	=	discharge grate thickness (mm)
ndg	=	number of discharge grate segments
	=	(conceptually similar to pieces of pie)
$foag$	=	fraction grate open area (fraction)
Dt_{sm}	=	SAG mill trunnion diameter (m)

In Equation (4.25), the first and second terms represent the weight of the large flat disc (that constitutes the discharge grate) of thickness, dgt, *less* the apertures in the grates (area fraction $foag$) and the absent central piece of diameter Dt_{sm}. The third term represents the weight of the portion of the discharge end lifter bars that protrude above the surface of the discharge grate. The discharge grate lifter bars are of thickness (height) hlt and of length $(D_{sm} - Dt_{sm})$.

4.3.2 Shell Thickness

The assumption that all mill lining wear occurs in the discharge end of the mill allows the mill liner model to be simplified. Subtracting the mill weight constant ($SMWconst$) from both sides of Equation (4.22) yields:

$$(lining_{DE} + D/C\,grate) = (lining_{DE} + D/C\,grate)_0 - wearate \cdot t \tag{4.26}$$

Assuming that wear is uniform throughout the discharge end of the mill, the wear thickness, wt, (the amount (mm) of lining component that has been worn away) can be determined as follows:

1. Take all terms in Equation (4.26) to one side of the equation:

$$0 = (lining_{DE} + D/C\,grate)_0 - wearate \cdot t - (lining_{DE} + D/C\,grate) \tag{4.27}$$

2. Express $(lining_{DE} + D/C\,grate)$ in terms of wear thickness, wt, by the substitution of $(slt - wt)$ for slt in Equation (4.24) and Equation (4.25):

$$
\begin{aligned}
& & & \frac{1}{2} L_{sm}\, \rho_{liner}\, nhl\, \frac{lbw}{1000} \frac{(hlt\ -\ (slt\ -\ wt))}{1000} \\
& lining_{DE} & & + \frac{1}{2} L_{sm}\, \rho_{liner}\, nll\, \frac{lbw}{1000} \frac{(llt\ -\ (slt\ -\ wt))}{1000} \\
+ & & = & + \frac{\pi}{2} \rho_{liner}\, L_{sm} \{ D_{sm\,0} \frac{(slt\ -\ wt)}{1000} - \left[\frac{(slt\ -\ wt)}{1000} \right]^2 \} \\
& D/C\, grate & & + \rho_{liner} \left(\pi \frac{{D_{sm}}^2}{4} \frac{dgt}{1000} (1\ -\ foag) - \pi \frac{{Dt_{sm}}^2}{4} \frac{dgt}{1000} \right. \\
& & & \left. + ndg \frac{lbw}{1000} \frac{(hlt\ -\ (slt\ -\ wt))}{1000} (D_{sm}\ -\ Dt_{sm}) \right)
\end{aligned}
\tag{4.28}
$$

3. Solve Equation (4.27) for wt - the root of the equation, *e.g.*, with $fzero$, the MATLAB scalar nonlinear zero finding function

4. Determine the current lining thickness, $(slt\ -\ wt)$

4.3.3 Model Validation

The mill specifications and other data relevant to this model are contained in Table 4.1. Utilising this data yields the results contained in Table 4.2 which translate to 38 tonnes (43 mm) of discharge end liner wear occurring over a six (6) week period. These results are plausible. In the absence of detailed operating data, further model validation was not possible but is recommended at or prior to an implementation stage.

Table 4.1: Mill Lining Specifications

ITEM	VALUE
SAG mill installation weight (initial), $SMIW_0$ (t)	338
number of high lifter bars, nhl	24
number of low lifter bars, nll	24
lifter bar width, lbw (mm)	200
high lifter bar thickness (height), hlt (mm)	180
low lifter bar thickness (height), llt (mm)	75
shell liner thickness (height), slt (mm)	50
SAG mill shell inside diameter, $D_{sm\,0}$ (m)	7.32
SAG mill shell inside length, $L_{sm\,0}$ (m)	3.73
SAG mill shell length, L_{sm} (m)	3.53
discharge grate thickness, dgt (mm)	100
number of discharge grate segments, ndg	24
fraction grate open area, $foag$ (fraction)	0.179
SAG mill trunnion diameter, Dt_{sm} (m)	1.6
liner density, ρ_{liner} (t/m^3)	7.8

Table 4.2: Mill Liner Model Results

ITEM	VALUE
Initial discharge end lining weight, $lining_{DE\,0}$ (t)	26.0
Initial discharge grate weight, $D/C\,grate_0$ (t)	51.8
Wear rate, $wearate$, (t/hr)	0.038
Wear thickness, wt (mm/hr)	0.043
(= thickness worn away each hour)	

4.4 Summary

In this Chapter, dynamic models of the SAG mill rock, water and ball charges and the mill protective lining were developed and presented. Each model was programmed into the MATLAB-Simulink environment and validated against steady state industrial plant survey data, see Appendix B.

The rock and water charge models presented in this Chapter are extensions of the steady state models of Chapter 3 and have been presented previously by Julius Kruttschnitt Mineral Research Centre personnel and thus do not represent innovations of this research. However, the discussion surrounding the rock charge model sensitivity to the breakage rates, in Section 4.2.3, represents independent commentary.

The dynamic ball charge and protective lining models presented in Sections 4.1 and 4.3, respectively, are innovations resulting from this research. Further model validation is recommended at or prior to an implementation stage. The innovations of this Chapter are summarised in Table 4.3.

Table 4.3: Chapter 4 Innovation Summary

Section	Innovation
Section 4.1	Dynamic SAG mill ball charge model
Section 4.3	Dynamic SAG mill protective lining model
Section 4.2.3	Comments on the sensitivity of the rock charge model to the breakage rates

Chapter 5

Inferential Model Development

With the foundation steady state and dynamic modelling presented, focus now turns to the primary grinding circuit, refer to Figure 5.1, and the inferential measurement of the SAG mill inventories, SAG mill fresh feed rate and size distribution and SAG mill discharge rate and size distribution. This Chapter discusses the development of these inferential models. In Section 5.1, the inferential models are presented following an overview of the calculation sequence involved. In Section 5.2, the models are validated against the reference data and the simulation data.

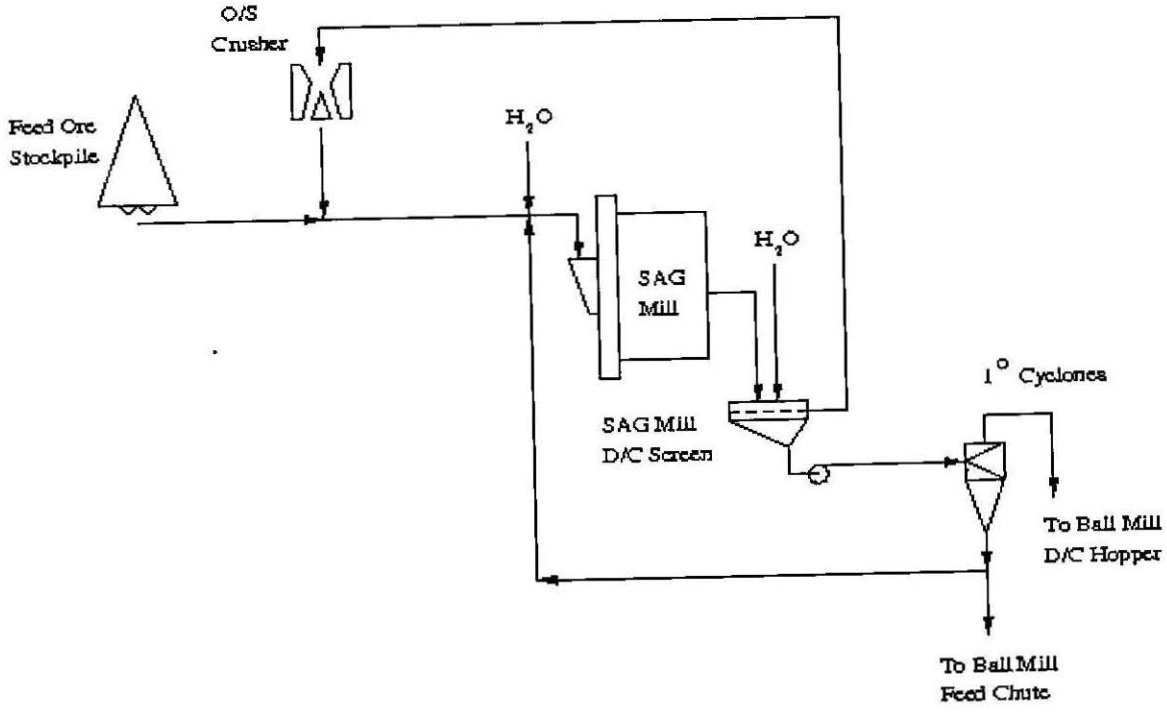

Figure 5.1: Primary grinding circuit flowsheet

5.1 Model Overview

Inferential measurement of the SAG mill inventories, feed rate and sizing and mill discharge rate and sizing requires the development of suitable models. Section 5.1.1 through Section 5.1.6 details the development and utilisation of the inferential measurement models. An overview of the model utilisation and calculation sequence is as follows:

1. The oversize crusher feed ($OSCF$) and primary cyclone feed ($PCFD$) streams are calculated from the *scats* feedrate, primary cyclone feed flowrate and density data and assumptions about the size distributions (based on SAG mill grate size and discharge screen aperture size). The addition of $OSCF$ and $PCFD$ *less* the discharge water addition yields the SAG mill discharge stream ($SMDC$). The mill discharge size distribution ($smdc$) and passing sizes ($T_{80} \ldots T_{20}$) are calculated in the process.

2. The SAG mill rock charge ($SMRC$) is calculated by SAG mill discharge function model inversion.

3. SAG mill fractional total filling, J_t, and ball filling, J_b, are determined by solving the powerdraw or mill weight equations given mill power draw or weight process measurements as inputs.

4. SAG mill total feed ($SMTF$) is then calculated by mill model inversion after making assumptions about the ball charge size distribution.

5. Oversize crusher product ($OSCP$) and primary cyclone underflow ($PCUF$) are calculated by the direct application of the crusher and cyclone models.

6. SAG mill fresh feed ($SMFF$) is calculated by subtracting $OSCP$ and the primary cyclone underflow to SAG mill ($PCUS$) from the $SMTF$ stream. The fresh feed size distribution ($smff$) and passing sizes ($F_{80} \ldots F_{20}$) are calculated in the process.

5.1.1 Oversize Crusher Feed, Primary Cyclone Feed and SAG Mill Discharge

Oversize Crusher Feed, $OSCF/oscf$

The oversize crusher feed properties ($OSCF$) and size distribution ($oscf$) are estimated based on the following combination of measured variables, model parameters and assumptions:

Measured Variable	oversize crusher feedrate (tph), MV_{scats}.
Model Parameter	SAG mill discharge grate pebble port size, $x_p = 74.11$ mm
Model Parameter	SAG mill discharge screen corrected 50% Passing size, $D_{50c} = 9.82$ mm
Assumption	$OSCF$ solids content is 99.9 %solids w/w (based on the screen oversize component being relatively dry)
Assumption	$oscf$ can be approximated by a Rosin-Rammler distribution

The oversize crusher feed mass flowrates and stream properties ($OSCF$) are calculated as follows:

$$OSCF_{tph\_s} = MV_{scats}\, OSCF_{\%s\, w/w} \tag{5.1}$$

$$OSCF_{tph\_l} = MV_{scats}\, \frac{(100 - OSCF_{\%s\, w/w})}{100} \tag{5.2}$$

where

$OSCF_{tph\_s}$ = oversize crusher solids feedrate (t/hr)

$OSCF_{tph\_l}$ = oversize crusher liquid feedrate (t/hr)

$OSCF_{\%s\, w/w}$ = oversize crusher feed solids density (%solids w/w)

The Rosin-Rammler size distribution function is given in Equation (5.3) and has been selected for its convenience and since it "has been found to fit many size distributions very well" (Napier-Munn *et al.*, 1996)[1].

$$W_r = 100\, e^{-\left(\frac{x}{a}\right)^b} \tag{5.3}$$

where

W_r = cummulative weight percent of material retained at *size* x (cummulative %retained w/w)

x = particle size (mm)

a = size at which 36.8% (*i.e.*, $100/e$) of particles are retained (mm)

b = slope of $ln\left(ln\left(\frac{100}{W_r}\right)\right)$ *versus* $ln(x)$

Since it is conventional in mineral processing to represent size distributions in cummulative percent passing format, Equation (5.3) is more useful in such a format, as given in Equation (5.4). The values of a and b for $oscf$ are estimated.

$$W_p = 100 - 100\, e^{-\left(\frac{x}{a}\right)^b} \tag{5.4}$$

[1]Section A3.3

where

W_p = cummulative weight percent of material passing *size* x (Cummulative %Retained w/w)

Primary Cyclone Feed, $PCFD/pcfd$

The basis for the primary cyclone feed stream properties ($PCFD$) and size distribution ($pcfd$) estimates is as follows:

Measured Variable	primary cyclone feed flowrate (m^3/hr), MV_{pc_flow}
Measured Variable	primary cyclone feed density (%solids w/w), MV_{pc_dens}
Model Parameter	SAG mill discharge screen corrected 50% Passing size, D_{50c} = 9.82 mm
Assumption	$pcfd$ can be approximated by a Rosin-Rammler distribution

The primary cyclone feed properties ($PCFD$) are calculated from the plant measured variables of cyclone feed flowrate, $PCFD_{m3ph\_p}$ (MV_{pc_flow}), and feed solids density, $PCFD_{\%s\,w/w}$ (MV_{pc_dens}). A mass balance yields,

$$PCFD_{tph\_s} = \frac{PCFD_{m3ph\_p}\,PCFD_{\%s\,w/w}\,SG_l\,SG_s}{PCFD_{\%s\,w/w}\,SG_l + (100 - PCFD_{\%s\,w/w})\,SG_s} \tag{5.5}$$

$$PCFD_{tph\_l} = PCFD_{tph\_s}\frac{100 - PCFD_{\%s\,w/w}}{PCFD_{\%s\,w/w}} \tag{5.6}$$

where

$PCFD_{m3ph\_p}$ = primary cyclone feed flowrate (m^3/hr)

$PCFD_{\%s\,w/w}$ = primary cyclone feed density (% solids w/w)

Equation (5.5) may also be derived from a flow-density-pulp specific gravity combination of measurements (Wills, 1989). The primary cyclone feed size distribution ($pcfd$) is estimated in a similar manner as the oversize crusher feed stream. That is, $pcfd$ is approximated by a Rosin-Rammler distribution, see Equation (5.4), with estimated values of a and b.

SAG Mill Discharge, $SMDC/smdc$

The SAG mill discharge properties ($SMDC$) and size distribution ($smdc$) are estimated by the addition of the estimated primary cyclone feed and oversize crusher feed streams

less the SAG mill discharge water flowrate.

$$SMDC_{tph\_s} = OSCF_{tph\_s} + PCFD_{tph\_s} \tag{5.7}$$

$$SMDC_{tph\_l} = OSCF_{tph\_l} + PCFD_{tph\_l} - MV_{DC\_H2O}\, SG_l \tag{5.8}$$

$$smdc = \frac{OSCF_{tph\_s}}{SMDC_{tph\_s}}\, oscf + \frac{PCFD_{tph\_s}}{SMDC_{tph\_s}}\, pcfd \tag{5.9}$$

where

$SMDC_{tph\_s}$	=	SAG mill solids discharge rate (t/hr)
$SMDC_{tph\_l}$	=	SAG mill liquid discharge rate (t/hr)
$smdc$	=	SAG mill discharge size distribution (weight retained) (%retained w/w)
SG_l	=	process water specific gravity (t/m^3)

The only additional measured variable, model parameter, or, assumption is:

Measured Variable SAG mill discharge water addition flowrate measured variable (m^3/hr), MV_{DC_H2O}

Potential now exists to utilise the SAG mill discharge inferential measurement as a measure of SAG mill performance. Control objectives and strategies could be formulated centering on this measurement.

Recirculating Load, *RCL*

One of the "basic requirements" of a grinding circuit control system is the "measurement of the circulating load, so that overload may be prevented" (Lynch, 1977). For a closed-loop mill-cyclone arrangement, the circulating load is generally defined as the ratio of the solids mass flow in the cyclone underflow to the solids feed to the mill (Wills, 1989).

In this case, where there are two recycle streams (oversize crusher feed, $OSCF$, and a proportion of the primary cyclone underflow, $(1 - PC_{split})\, PCUF$), the amount of solid material recirculating is the difference between the mill discharge and the fresh feed. Therefore, the recirculating load, RCL, is

$$RCL = \frac{(SMDC_{tph\_s} - SMFF_{tph\_s})\, 100\%}{SMFF_{tph\_s}} \tag{5.10}$$

Equation (5.10) can be solved utilising the SAG mill discharge solids flow, $SMDC_{tph\_s}$, from Equation (5.7) and the SAG mill fresh feed solids flow, $SMFF_{tph\_s}$, calculated in Section 5.1.6.

Potential now also exists to utilise the recirculating load inferential measurement as a measure of SAG mill performance. Control objectives and strategies could be also formulated incorporating this measurement.

5.1.2 SAG Mill Rock Charge

The SAG mill rock charge properties ($SMRC$) and size distribution ($smrc$) are estimated by the reverse-application of the SAG mill grate discharge function on the SAG mill discharge stream estimate, incorporating a size distribution assumption.

Solids : Recalling, from Equation (3.6), that mill discharge flowrate is equal to the flowrate through the mill charge, $Q = k_g Q_m$ (for SAG mills the charge toe angle and charge slurry pool angle are equal, $\theta_T = \theta_{TO}$), is a function of the nett fractional slurry holdup in the grinding media, J_{pm}, allows the calculation of the holdup term:

$$J_{pm} = \left(\frac{Q_m}{6100\,\gamma^{2.5}\,A\,\phi^{-1.38}\,D^{0.5}} \right)^{0.5} \tag{5.11}$$

It is now possible to calculate

- J_{pg} and J_{po} from Equation (3.9), Equation (3.10) and Equation (3.12)
- s_{xm} from Equation (3.20)
- d_0 from Equation (3.18) and Equation (3.19)

With the maximum discharge rate, d_0, the mill product, p_i ($SMDC/smdc$), and the following simplified version of the classification function, c_i, (also see Figure 5.2)

$$\begin{aligned} c_i &= 0.0 && \text{for } x \geq x_g \\ c_i &= \frac{x_g - x}{x_g - x_m} && \text{for } x_m < x < x_g \\ c_i &= 1.0 && \text{for } x \leq x_m \end{aligned} \tag{5.12}$$

the calculation of mill rock charge, s_i ($SMRC/smrc$), is then possible by manipulation of Equation (3.3), *i.e.*,

$$s_i = \frac{p_i}{d_0 c_i} \tag{5.13}$$

Equation (5.13) provides no information about the material in the rock charge larger than the grate aperture size (x_g). This proportion of the rock charge is estimated by

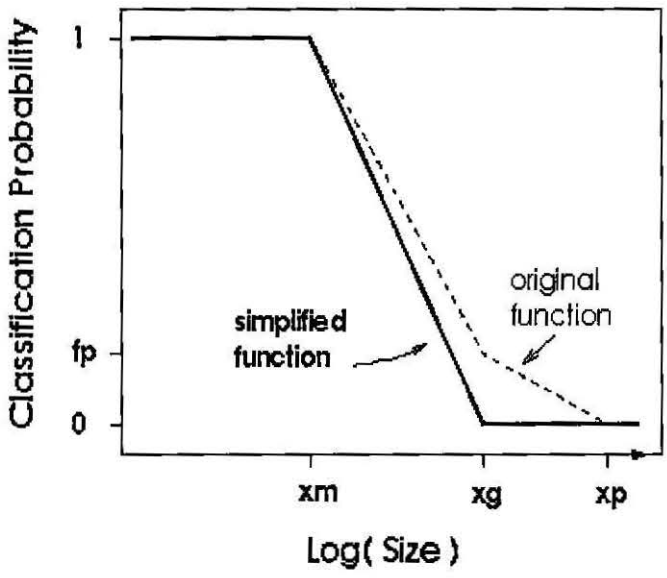

Figure 5.2: Grate Classification Function

assuming that it can be approximated by a Rosin-Rammler distribution and then solving the following system of q cummulative weight retained equations:

$$\frac{\sum_{j=1}^{q} s_j}{\sum_{i=1}^{q} s_i + \sum_{i=q+1}^{z} s_i} 100 = 100\, e^{-\left(\frac{x}{a}\right)^b} \tag{5.14}$$

where

x	=	particle size (mm)
i	=	particle size class
		$i = 1$: largest size
		$i = q$: smallest rock size (16 mm)
		$i = z$: smallest particle size
a, b	=	Rosin-Rammler distribution parameters
$\sum_{i=q+1}^{z} s_i$	=	summation of the material less than 16mm in size. Determined from interpolating the rock charge information obtained from Equation (5.13)

The values of a and b for *smrc* are estimated with reference to the following points:

- the total charge (J_t) and ball charge (J_b) level estimates from the next step are determined independent of this step and provide information on the amount of material in the rock charge larger than 50 mm (J_r), *i.e.*,

$$J_r = J_t - J_b \tag{5.15}$$

- the coarse end of the distribution is bounded by the point (180.76, 100%Passing).

Water : The mill water charge (s_w) may be calculated by manipulation of Equation (3.45), *i.e.*,

$$s_w = \frac{p_w}{d_0} \tag{5.16}$$

where

p_w = SAG mill discharge water mass flowrate (t/hr)

For the SAG mill rock charge estimate, the only additional measured variable, model parameter, or, assumption is:

Assumption *smrc* can be approximated by a Rosin-Rammler distribution

5.1.3 Total Charge and Ball Charge Filling Levels

The fractional total filling, J_t, and ball filling, J_b, are estimated independently solving the mill powerdraw and mill weight equations. There is considerable 'over-lap' of the equations utilised, however, two independent estimates of the mill inventories result. Both estimates consist of one residual equation in two unknowns (J_t & J_b) and a inequality constraint that imposes the practical reality that the ball charge must be less than or equal to the total charge ($J_b \leq J_t$). The calculation involved for each of these estimates will now be detailed.

Estimates from Powerdraw

Close inspection of Equations (3.46) through (3.68) yields that given:

- mill discharge
- mill specifications
- mill model parameters
- measured mill powerdraw

the mill powerdraw model can be reduced to one function of two unknowns, *i.e.*, volumetric ball charge fraction, J_b, and total charge volumetric fraction, J_t. The inspection will now be summarised.

Powerdraw Model Inspection

The equations that contain J_t and J_b explicitly are:

					Equation
U	$=$	$f(J_t)$			(3.62)
z	$=$	$f(J_t)$			(3.56)
ϕ_c	$=$	$f(J_t)$			(3.63)
θ_T	$=$	$f(J_t, \phi_c)$	$\rightarrow$	$f(J_t)$	(3.54)
θ_S	$=$	$f(J_t, \theta_T)$	$\rightarrow$	$f(J_t)$	(3.53)
$\overline{r}$	$=$	$f(J_t, \theta_S, \theta_T)$	$\rightarrow$	$f(J_t)$	(3.67)
r_i	$=$	$f(J_t, \beta, \theta_S, \theta_T)$	$\rightarrow$	$f(J_t)$	(3.68)
ρ_c	$=$	$f(J_b, J_t, U)$	$\rightarrow$	$f(J_b, J_t)$	(3.61)

The remaining equations are either functions of these functions (*i.e.*, implicit functions of J_b and/or J_t) or simply functions of plant data and/or equipment specifications.

The equations that are implicit functions of the ball charge fraction (J_b) and/or the total charge fraction (J_t) are:

					Equation
θ_{TO}	$=$	$f(\theta_T)$	$\rightarrow$	$f(J_t)$	(3.55)
t_c	$=$	$f(\theta_S, \theta_T)$	$\rightarrow$	$f(J_t)$	(3.64)
t_f	$=$	$f(\overline{r}, \theta_S, \theta_T)$	$\rightarrow$	$f(J_t)$	(3.65)
β	$=$	$f(t_c, t_f)$	$\rightarrow$	$f(J_t)$	(3.66)
P_{Net}	$=$	$f(r_i, z, \rho_c, \theta_S, \theta_T, \theta_{TO})$	$\rightarrow$	$f(J_b, J_t)$	(3.49)
P_{Cone}	$=$	$f(r_i, \rho_c, \theta_S, \theta_T, \theta_{TO})$	$\rightarrow$	$f(J_b, J_t)$	(3.50)
P_{Charge}	$=$	$f(P_{Net}, P_{Cone})$	$\rightarrow$	$f(J_b, J_t)$	(3.48)
P_{Gross}	$=$	$f(P_{Charge})$	$\rightarrow$	$f(J_b, J_t)$	(3.46)
F_{kW}	$=$	$f(P_{Gross})$	$\rightarrow$	$f(J_b, J_t)$	(5.17)

The equations that are simple functions of plant data and/or equipment specifications are:

	Equation
L_{cone}	(3.52)
$RPM_{critical}$	(3.57)
ϕ_{fcs}	(3.58)
N_m	(3.59)
$\overline{N}$	(3.60)
p_{xm}	(3.17)
J_{pm}	(5.11)
J_p	(3.9)
J_{po}	(3.12)
J_{pg}	(3.9), (3.10) & (3.12)
s_{xm}	(3.20)
d_{xm}	(3.18)
$P_{No\,Load}$	(3.47)

The mill inventory estimates from mill powerdraw data are determined by the solution of Equation (5.17) which determines values for the total charge level (J_t) and ball charge level (J_b) such that the calculated mill powerdraw, P_{Gross}, equates with the actual mill powerdraw MV_{kW}, and therefore satisfying the residual equality ($F_{kW} = 0$).

$$F_{kW} = MV_{kW} - P_{Gross} = 0 \tag{5.17}$$

F_{kW} = mill powerdraw residual function (kW)
MV_{kW} = mill powerdraw measurement (kW)

Estimates from Mill Weight

A second residual, similar to Equation (5.17), can be obtained by the utilisation of several mill weight equations which will now be introduced. Since the material in the inactive part of the charge is in 'freefall' and forms a poorly defined surface, the mill weight may be approximated by the summation of the mill shell weight and the weight of the material in the charge kidney (the active portion of the mill charge resting on the mill shell and forming a surface that is more easily defined), refer to Figure 5.3. The weight of the kidney, M_{kidney}, is the product of the kidney density, ρ_{kidney}, and volume, V_{kidney},

$$M_{kidney} = V_{kidney}\,\rho_{kidney} \tag{5.18}$$

The volume of the kidney is

$$V_{kidney} = \pi L_m \left({r_m}^2 - {r_i}^2\right) \frac{(2\,\pi - \theta_T + \theta_S)}{2\,\pi} \tag{5.19}$$

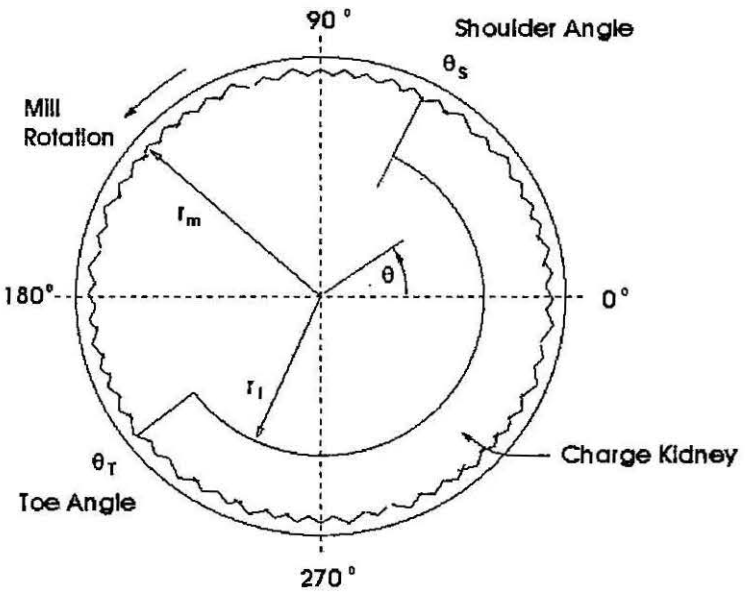

Figure 5.3: Simplified mill charge geometry

Assuming kidney density is equal to the charge density, see Equation (3.61), *i.e.*,

$$\rho_{kidney} = \rho_c \tag{5.20}$$

the kidney mass (M_{kidney}) may be calculated.

The dependence of Equations (5.20) and (5.19) on θ_T, θ_S, r_i and ρ_c, introduces the functional dependence on J_t and J_b and also the 'over-lap' with the independent powerdraw estimates. The additional equations for the estimates of mill inventory based on mill weight are all implicit functions of ball charge level (J_b) and/or total charge level (J_t) and are listed below:

					Equation
ρ_{kidney}	=	$f(\rho_c)$	→	$f(J_b, J_t)$	(5.20)
V_{kidney}	=	$f(r_i, \theta_S, \theta_T)$	→	$f(J_t)$	(5.19)
M_{kidney}	=	$f(V_{kidney}, \rho_{kidney})$	→	$f(J_b, J_t)$	(5.18)
F_{weight}	=	$f(M_{kidney})$	→	$f(J_b, J_t)$	(5.21)

The mill inventory estimates from mill weight data are determined by the solution of Equation (5.21) which determines values for J_t and J_b that equate the calculated mill weight, $M_{shell} + M_{kidney}$, with the actual mill weight measurement MV_{weight} and therefore satisfying the mill weight residual equality ($F_{weight} = 0$).

$$F_{weight} = MV_{weight} - M_{shell} - M_{kidney} \tag{5.21}$$

In Chapter 7 the uncertainty in the mill inventory estimates from mill powerdraw and mill weight is analysed and assessed. Potential now exists to utilise the SAG mill volumetric charge inferential measurements as a measure of SAG mill performance and an indication of the prevailing conditions within the mill. Control objectives and strategies could be formulated incorporating these measurements.

5.1.4 SAG Mill Total Feed

Solids Balance

The solids component of the SAG mill total feed ($SMTF/smtf$) is estimated by the inversion of the steady state perfectly mixed mill model, Equation (3.2). Rearranging terms yields,

$$f_i = p_i - \sum_{j=1}^{i-1} r_j s_j a_{ij} + (1 - a_{ii}) r_i s_i \tag{5.22}$$

The estimate of total feed to the SAG mill, $SMTF/smtf$, is determined as follows:

(a) the mill product, p_i, and mill rock charge, s_i, are known from Steps 1 and 2, respectively

(b) assuming a ball charge size distribution and using the rock charge and ball charge information from Steps 2 and 3, allows the determination of the specific comminution energy, Ecs_i, the breakage parameter, t_{10_i}, and the appearance function, a_{ij}, refer to the Consumption and Generation section of Chapter 3 (Section 3.3.1)

(c) the breakage rate function, r_i, is determined from the ball charge information from Step 3 and the estimate of the recycle ratio of $-20 + 4$ mm material from the previous time step, again refer to Section 3.3.1

(d) using the information from (a) to (c), the total feed estimate, f_i, is determined by solving Equation (5.22)

The use of the steady state perfectly mixed mill model is valid since the mill charge and discharge estimates are determined from the prevailing operating conditions regardless of whether the mill contents are increasing, decreasing or at steady-state. A valid estimate of the total mill feed is possible providing the calculation time between the discharge and charge estimates and the total mill feed estimate is relatively short.

Water Balance

SAG mill total feed water is determined by the steady state balance for the water:

$$Water\ In\ =\ Water\ Out$$

The water entering the mill is equal to the water in the SAG mill discharge stream, determined in Step 1.

5.1.5 Oversize Crusher Product and Primary Cyclone Underflow

The estimate of the oversize crusher product, $OSCP/oscp$, is determined by applying the crusher model, as detailed in Section 3.3.3, to the estimate of the oversize crusher feed, $OSCF/oscf$, determined in Step 1.

The estimate of the primary cyclone underflow, $PCUF/pcuf$, is determined by applying the cyclone model, as detailed in Section 3.3.2, to the estimate of the primary cyclone feed, $PCFD/pcfd$, determined in Step 1.

The primary cyclone overflow, $PCOF/pcof$, may also be estimated by applying cyclone model to the primary cyclone feed. The cyclone overflow stream is a slurry of fine particles. Particle size measurement technology for such streams is well developed, there are instruments available on the market that use either ultrasound, laser diffraction or physical size measurement. Inferential measurement of slurries of fine particles is an alternative to these direct measurements. Focus on the inferential measurement of the cyclone overflow size distribution is outside the scope of this research. However, it is interesting to note that a cyclone model has been utilised, in conjuntion with cyclone feed flowrate and density, cyclone underflow angle and overflow density, in an inferential measurement model of the percent passing 75 μm size of the cyclone overflow (Smith and Swartz, 1999).

5.1.6 SAG Mill Fresh Feed

The estimate of the SAG mill fresh feed (the new feed from the stockpile), $SMFF/smff$, is determined by subtracting (from the SAG mill total feed $SMTF/smtf$), the SAG feed water addition, the estimate of the oversize crusher product, $OSCP/oscp$, and the recycled

component of the primary cyclone underflow, $(1 - PC_{split}) \cdot PCUF$ & $pcuf$:

$$SMFF_{tph\_s} = SMTF_{tph\_s} - OSCP_{tph\_s} - (1 - PC_{split})PCUF_{tph\_s} \quad (5.2$$

$$SMFF_{tph\_l} = SMTF_{tph\_l} - OSCP_{tph\_l} - (1 - PC_{split})\,PCUF_{tph\_l} - MV_{FD\_H2O}\,SC \quad (5.2$$

$$smff = \frac{SMTF_{tph\_s}\,smtf - OSCP_{tph\_s}\,oscp - (1 - PC_{split})\,PCUF_{tph\_s}\,pcuf}{SMTF_{tph\_s} - OSCP_{tph\_s} - (1 - PC_{split})\,PCUF_{tph\_s}} \quad (5.2$$

where

$SMFF_{tph\_s}$	=	SAG mill fresh feed solids feedrate (t/hr)
$SMFF_{tph\_l}$	=	SAG mill fresh feed liquid feedrate (t/hr)
$smff$	=	SAG mill fresh feed size distribution (weight retained) (%retained, w/w)
$SMTF_{tph\_s}$	=	SAG mill total feed solids feedrate (t/hr)
$SMTF_{tph\_l}$	=	SAG mill total feed liquid feedrate (t/hr)
$smtf$	=	SAG mill total feed size distribution (weight retained) (%retained, w/w)
SG_l	=	process water specific gravity (t/m^3)

The additional measured variables, model parameters, or, assumptions are as follows:

Measured Variable	SAG mill feed water addition flowrate measured variable (m^3/hr), MV_{FD_H2O}.
Model Parameter	Primary cyclone underflow split proceeding to the ball mill, PC_{split}

If PC_{split} is the fraction of $PCUF$ fed to the ball mill, the fraction to recycled to the SAG mill is $(1 - PC_{split})$.

- In the steady state model, PC_{split} is a specified operating parameter.
- In the inferential model, PC_{split} is a specified operating parameter.
- In the state estimation model, PC_{split} can be detemined from mass balance, or can be a specified operating parameter.

Fresh Feed Passing Sizes

The estimate of the SAG mill fresh feed eighty percent passing size, F_{80}, is determined by interpolation of the estimate of the size distribution, $smff$, at the 80% mark. Similarly, the sixty, forty and twenty percent passing sizes (F_{60}, F_{40} & F_{20}) can be determined.

Potential now exists to utilise the SAG mill fresh feed size inferential measurements as a measure of crusher or blasting performance and of feed size disturbances reporting to the mill.The fresh feed solids inferential measurement could be utilised for metallurgical accounting purposes. Control objectives and strategies could be formulated incorporating these measurements.

5.2 Model Validation - Simulation and Reference Data

The inferential model results have two reference points for comparison:

1. The simulation model results
2. The reference data from the plant survey

The following results assessment is once again on a comparative basis. Appendix C contains the reference data, simulation results and the inferential model results in full. Specifically:

Table C.1 - Table C.4:	Reference Data (Stream Properties and Size Distribution)
Table C.5 - Table C.8:	Simulation Model (Stream Properties and Size Distribution)
Table C.9 - Table C.12:	Inferential Model (Stream Properties and Size Distribution)
Figure C.1 - Figure C.8:	Graphical representation of all stream size distribution data for the Reference Data, Simulation Model and Inferential Model.

5.2.1 Inferential - Simulation Comparison

Table 5.1 through Table 5.4 show the comparative error between the inferential model results and the simulation model results. For brevity, Stream Properties results only are shown here. Appendix C contains the inferential and the simulation results in full.

Table 5.1 contains the results for the "front-end" of the primary grinding circuit and Table 5.2 contains the results for the "back-end" of the primary grinding circuit. Generally, the agreement is acceptable with most of the results exhibiting errors of $< 5\%$. There are a number of results which exhibit errors significantly larger:

- The oversize crusher feed ($OSCF$) and product ($OSCP$) exhibit $\approx$ 18% error in the water flow. These are essentially dry streams. Therefore, small differences in flowrates correspond to larger relative errors.

- A number of the eighty percent passing size (P_{80}) results show significant deviation from the simulation model information. These deviations are attributed to interpolation errors combined with minor model approximations, discussed in Section 3.4. Furthermore, the results comparison is to the simulation model results which contained there own errors. With respect to the reference data the results comparison of many streams improved. Also, the error levels are of the same order of magnitude as the steady state circuit validation results, Table 3.11 and Table 3.12. Considering these points, the P_{80} results are considered acceptable.

Table 5.3 contains the results for the "front-end" of the secondary grinding circuit and Table 5.4 contains the results for the "back-end" of the secondary grinding circuit. Here the level of agreement is lower than the for the primary circuit and there is also more "spread" in the results. These features are due to the propagation of errors from upstream information combined with model parameter influences, namely, model parameters being selected on the basis of achieving satisfactory internal stream results and good grinding circuit output stream (secondary cyclone overflow) results. Further points of discussion are:

- The P_{80} remarks above also apply here.
- The "dry stream" comments above apply for the ball mill screen oversize ($BSOS$) here.
- Water results throughout the secondary survey are strongly influenced by the recycling water in the secondary cyclone underflow ($SCUF$) stream which is a result of model parameter selection.
- Ball mill powerdraw and secondary cyclone pressure estimates display good agreement.

5.2.2 Inferential - Reference Comparison

Table 5.5 through Table 5.8 show the comparative error between the inferential model results and the reference data. Again, Stream Properties results only are shown here for brevity. Appendix C contains the reference data and the inferential model results in full.

As in the inferential model *versus* simulation model results comparison above, the agreement displayed here is acceptable. The stream comparison results for the primary grinding circuit here, Table 5.5 and Table 5.6, are comparable to those of the previous comparison. Differences appear in the oversize crusher feed, $OSCF$, and product, $OSCP$, streams. The points raised regarding the predominantly solid streams apply here.

Table 5.1: Inferential v Simulation: Primary Circuit - SAG mill

Stream Properties	SMFF	OSCP	SMTF	SMRC	SMDC
tph_s	0.1	0.0	0.1	5.1	0.0
tph_l	3.9	18.0	0.2	29.4	0.1
tph_p	0.1	0.0	0.1	6.1	0.0
%s w/w	0.1	0.0	0.0	1.0	0.0
%l w/w	3.7	18.0	0.1	21.9	0.1
m3ph_s	0.1	0.0	0.1	5.1	0.0
m3ph_l	3.9	18.0	0.2	29.4	0.1
m3ph_p	0.3	0.0	0.1	7.7	0.0
%s v/v	0.2	0.0	0.1	2.4	0.0
%l v/v	3.6	18.0	0.1	20.1	0.0
SGp	0.1	0.0	0.0	1.4	0.0
P_{80}	25.2	38	27.1	65	3.1
Power				0.0	
Pressure					

Table 5.2: Inferential v Simulation: Primary Circuit - Screen/Crusher/Cyclones

Stream Properties	SMDC	OSCF	OSCP	PCFD	PCUF	PCOF
tph_s	0.0	0.0	0.0	0.0	3.0	13.4
tph_l	0.1	18.0	18.0	0.0	0.0	0.0
tph_p	0.0	0.0	0.0	0.0	2.2	3.0
%s w/w	0.0	0.0	0.0	0.0	0.9	10.1
%l w/w	0.1	18.0	18.0	0.0	2.2	2.9
m3ph_s	0.0	0.0	0.0	0.0	3.0	13.4
m3ph_l	0.1	18.0	18.0	0.0	0.0	0.0
m3ph_p	0.0	0.0	0.0	0.0	1.5	1.3
%s v/v	0.0	0.0	0.0	0.0	1.6	11.9
%l v/v	0.0	18.0	18.0	0.0	1.5	1.3
SGp	0.0	0.0	0.0	0.0	0.7	1.7
P_{80}	3.1	54	38	51	47	1.0
Power			3.9			
Pressure				0.0		

Table 5.3: Inferential v Simulation: Secondary Circuit - Ball mill/Screen

Stream Properties	PCUF	SCUF	BMFD	BMDC	BSOS	BSUS
tph_s	3.0	1.5	1.7	1.7	19.7	1.8
tph_l	0.0	0.1	0.1	0.1	0.1	0.1
tph_p	2.2	1.1	1.2	1.2	19.6	1.3
%s w/w	0.9	0.4	0.5	0.5	0.2	0.5
%l w/w	2.2	1.0	1.2	1.2	16.4	1.2
m3ph_s	3.0	1.5	1.7	1.7	19.7	1.8
m3ph_l	0.0	0.1	0.1	0.1	0.1	0.1
m3ph_p	1.5	0.8	0.9	0.9	19.2	0.9
%s v/v	1.6	0.7	0.9	0.9	0.4	0.9
%l v/v	1.5	0.7	0.8	0.8	16.2	0.8
SGp	0.7	0.4	0.4	0.4	0.2	0.4
P_{80}	47	0.5	7.7	0.4	47	0.4
Power				0.0		
Pressure						

Table 5.4: Inferential v Simulation: Secondary Circuit - Cyclones

Stream Properties	BSUS	PCOF	SCFD	SCUF	SCOF
tph_s	1.8	13.4	1.3	1.5	0.4
tph_l	0.1	0.0	0.0	0.1	0.0
tph_p	1.3	3.0	0.8	1.1	0.1
%s w/w	0.5	10.0	0.5	0.4	0.2
%l w/w	1.2	2.9	0.8	1.0	0.1
m3ph_s	1.8	13.4	1.3	1.5	0.4
m3ph_l	0.1	0.0	0.0	0.1	0.0
m3ph_p	0.9	1.3	0.5	0.8	0.1
%s v/v	0.9	11.9	0.8	0.7	0.3
%l v/v	0.8	1.3	0.5	0.7	0.1
SGp	0.4	1.7	0.4	0.4	0.1
P_{80}	0.4	1.0	0.5	0.5	0.5
Power					
Pressure			1.3		

Table 5.5: Inferential v Reference: Primary Circuit - SAG mill

Stream Properties	SMFF	OSCP	SMTF	SMRC	SMDC
tph_s	0.1	0.1	0.0	5.1	0.0
tph_l	3.9	25.1	0.1	29.4	0.1
tph_p	0.1	0.1	0.0	6.1	0.0
%s w/w	0.1	0.0	0.0	1.0	0.0
%l w/w	3.7	25.0	0.1	21.9	0.1
m3ph_s	0.1	0.1	0.0	5.1	0.0
m3ph_l	3.9	25.1	0.1	29.4	0.1
m3ph_p	0.3	0.1	0.1	7.7	0.1
%s v/v	0.2	0.1	0.1	2.4	0.1
%l v/v	3.6	25.0	0.1	20.1	0.1
SGp	0.1	0.0	0.0	1.4	0.0
P_{80}	25.2	10.8	27.1	65	1.0
Power				2.1902	
Pressure					

Table 5.6: Inferential v Reference: Primary Circuit - Screen/Crusher/Cyclones

Stream Properties	SMDC	OSCF	OSCP	PCFD	PCUF	PCOF
tph_s	0.0	0.1	0.1	0.0	3.0	13.2
tph_l	0.1	25.1	25.1	0.1	0.0	0.1
tph_p	0.0	0.1	0.1	0.0	2.2	2.9
%s w/w	0.0	0.0	0.0	0.0	0.9	10.0
%l w/w	0.1	25.0	25.0	0.0	2.2	2.9
m3ph_s	0.0	0.1	0.1	0.0	3.0	13.2
m3ph_l	0.1	25.1	25.1	0.1	0.0	0.1
m3ph_p	0.1	0.1	0.1	0.1	1.5	1.2
%s v/v	0.1	0.6	0.6	0.0	1.6	11.9
%l v/v	0.1	25.0	25.0	0.0	1.4	1.3
SGp	0.0	0.0	0.0	0.0	0.7	1.7
P_{80}	1.0	1.3	10.8	3.3	0.8	34
Power			1.4			
Pressure				0.3		

Table 5.7: Inferential v Reference: Secondary Circuit - Ball mill/Screen

Stream Properties	PCUF	SCUF	BMFD	BMDC	BSOS	BSUS
tph_s	3.0	1.4	1.6	1.6	15.2	1.7
tph_l	0.0	45	36	36	34	34
tph_p	2.2	8.7	7.1	7.1	15.3	7.0
%s w/w	0.9	9.3	8.1	8.1	0.1	8.1
%l w/w	2.2	33	27.0	27.0	16.5	25.6
m3ph_s	3.0	1.4	1.6	1.6	15.2	1.7
m3ph_l	0.0	45	36	36	34	34
m3ph_p	1.5	18.3	15.0	15.0	15.5	14.7
%s v/v	1.6	16.6	14.5	14.5	0.3	14.3
%l v/v	1.4	22.2	18.2	18.2	16.3	17.16
SGp	0.7	0.3	0.3	0.3	0.1	0.4
P_{80}	0.8	41	43	34	118	33
Power				10.0		
Pressure						

Table 5.8: Inferential v Reference: Secondary Circuit - Cyclones

Stream Properties	BSUS	PCOF	SCFD	SCUF	SCOF
tph_s	1.7	13.2	1.2	1.4	0.3
tph_l	34	0.1	20.4	44.6	0.1
tph_p	7.0	2.9	6.1	8.7	0.1
%s w/w	8.1	10.0	6.9	9.3	0.2
%l w/w	25.6	2.9	13.5	33	0.1
m3ph_s	1.7	13.2	1.2	1.4	0.3
m3ph_l	34	0.1	20.4	45	0.1
m3ph_p	14.7	1.2	11.3	18.3	0.1
%s v/v	14.3	11.9	11.2	16.6	0.2
%l v/v	17.1	1.3	8.2	22.2	0.0
SGp	0.4	1.7	0.3	0.3	0.0
P_{80}	33	34	32	41	49
Power					
Pressure			0.6		

As mentioned above, many of the errors in the eighty percent passing sizes in this comparison are less than those for the Inferential - Simulation model comparison. This is due to a degree of independent model fitting of the inferential models to the reference data. That is, the inferential models were tuned to match the reference data rather than the simulation model results.

The secondary grinding circuit results, Table 5.7 and Table 5.8, exhibit noticeably larger deviations. Model parameters in the secondary circuit were (manually) adjusted to obtain the best results for the secondary cyclone overflow, $SCOF$, which represents the product of the grinding circuit whilst maintaining a satisfactory secondary grinding circuit solids mass balance. Errors present in the secondary cyclone underflow, $SCUF$, are "recycled" through the ball mill, the ball mill screen and once again to the secondary cyclones. This recycling of error strongly influenced the secondary grinding circuit water balance.

Overall the agreement displayed between the inferential model and the reference data and the simulation model results was deemed sufficient for the inferential model to be considered valid. Further model validation would be required prior to, or, at an implementation stage.

5.3 Summary

In this Chapter, inferential models of the SAG mill inventories, SAG mill fresh feed rate and size distribution and SAG mill discharge rate and size distribution have been presented. Each model was programmed into the MATLAB-Simulink environment and validated against steady state industrial plant survey data, see Appendix C.

These models are innovations of this research, as summarised in Table 5.9. Further model validation is recommended at or prior to an implementation stage.

Table 5.9: Chapter 5 Innovation Summary

Section	Innovation
	The development of inferential models of:
Section 5.1.1	• SAG mill discharge rate and size distribution - Equations (5.7) to (5.9)
Section 5.1.2	• SAG mill rock charge and size distribution - Equations (5.13), (5.14) & (5.16)
Section 5.1.3	• SAG mill inventory levels - Equations (5.17) & (5.21)
Section 5.1.4	• SAG mill total feed rate and size distribution - Equation (5.22)
Section 5.1.6	• SAG mill fresh feed rate and size distribution - Equations (5.23) to (5.25)

Chapter 6

Inferential Model Error and Sensitivity Analyses

The inferential models developed in Chapter 5 for the SAG mill discharge rate and sizing, the SAG mill inventories and the SAG mill fresh feed rate and sizing were demonstrated to be valid in that they showed good agreement with the reference data and the simulation model results. In this Chapter an analysis of the errors in the the inferential models is presented. The influence of uncertainties in the parameters on the model uncertainties is also analysed. These analyses required the symbolic (algebraic) manipulation of the inferential models. To facilitate this the inferential models were coded into Maple V Release 5.1.

6.1 Error Propagation

The general formula for error propagation (Taylor, 1982) for a function in several variables is:

$$\delta f = \sqrt{\sum_{i=1}^{N} \left(\frac{\partial f}{\partial \theta_i} \delta \theta_i \right)^2} \tag{6.1}$$

where

f	=	a general function
θ_i	=	$i\,th$ model parameter in error/sensitivity analysis
δf	=	uncertainty in f
$\delta \theta_i$	=	uncertainty in θ_i
N	=	number of parameters

Here it is assumed that the parameter uncertainties are independent, random and normally distributed. Utilising a given level of confidence in the parameter uncertainties, $\delta\theta$, translates to a corresponding level of confidence in the estimate of the function uncertainty, δf. If the parameter uncertainty utilised is one standard deviation of the error in the parameter, σ_θ, then the estimated error in the function represents one standard deviation, σ_f, see Equation (6.2).

$$\sigma_f = \sqrt{\sum_{i=1}^{N} \left(\frac{\partial f}{\partial \theta_i} \sigma_{\theta_i} \right)^2} \tag{6.2}$$

It follows then that if the parameter uncertainty utilised is six (6) standard deviations of the error in the parameters, $6\,\sigma_\theta$, - a 99% confidence interval, than the estimated error in the function also represents six standard deviations, $6\,\sigma_f$.

The data and parameters associated with the inferential models developed in this research were available only in single-value form which required the estimation of their uncertainty. The uncertainty estimates were determined on a 99% confidence interval basis, *i.e.*, $\pm 3\sigma_{\theta_i}$. Utilising this level of parameter uncertainty in Equation (6.2), and assuming no parameter–interdependence, yields an estimate of the uncertainty in f also with a 99% level of confidence, *i.e.*, $\pm 3\sigma_f$.

Prior to detailing the results of the uncertainty and sensitivity analyses, recall the inferential model calculation sequence described in Chapter 5 which is summarised as follows:

Estimate the,

1. the oversize crusher and primary cyclone feed streams
2. SAG mill discharge stream estimate
3. SAG mill rock charge
4. SAG mill total and ball volumetric loads
5. SAG mill total feed stream
6. SAG mill fresh feed stream

This calculation sequence means that parameters in Step 1 influence the results of the ensuing Steps. Additional parameters introduced in the intermediate Steps, whilst having no bearing on the preceding Steps, influence the results of remaining Steps.

Parameters were selected and analysed on an inferential model case by case basis, namely:

1. SAG mill total and ball volumetric loads,
2. SAG mill discharge sizing, and,
3. SAG mill fresh feed sizing

Results for Cases 1 through 3 are presented in Sections 6.2 through 6.4, respectively.

6.2 SAG Mill Charge Estimates

Recall from Section 5.1.3 the residual equations which constitute the inferential models for the SAG mill total charge and ball charge volumetric filling, J_t and J_b, respectively:

$$F_{kW} = MV_{kW} - P_{Gross} = 0 \tag{6.3}$$

$$F_{weight} = MV_{weight} - M_{shell} - M_{kidney} = 0 \tag{6.4}$$

where

F_{kW}	=	mill power draw residual function (kW)
F_{weight}	=	mill weight residual function (t)
MV_{kW}	=	mill power draw measurement (kW)
MV_{weight}	=	mill weight measurement (t)
M_{shell}	=	mill shell weight (t)
M_{kidney}	=	calculated mass of active fraction of mill charge (t), see Equation (5.18)
P_{Gross}	=	calculated mill power draw (kW), see Equation (3.46)

The inferential mill charge level models, Equations (6.3) and (6.4) are functions of the volumetric filling fractions and a number of parameters θ (recall the constituent equations of these residuals, Section 3.3.1 and Section 5.1.3, and the functional dependancy analysis, Section 5.1.3), and hence may be written as follows:

$$F_{kW} = f(J_t, J_b, \theta) \tag{6.5}$$

$$F_{weight} = f(J_t, J_b, \theta) \tag{6.6}$$

If each of the parameters, θ, are specified, both Equation (6.5) and (6.6) reduce to a function of two unknowns, J_b and J_t, which may be solved by the application of a constrained nonlinear optimisation technique[1].

[1] *e.g.*, *fmincon* function in the MATLAB optimisation toolbox

The results, figures and discussion of this Section draw extensively from those presented by the author and colleagues in the *Minerals Engineering* journal (Apelt *et al.*, 2001). An analysis was conducted on Equations (6.5) and (6.6) and on another two equivalent residual equations that utilise, as their basis, mill power draw and mill weight models from another recognised source (JA Herbst and Associates). The paper concluded that while each equation could be utilised to estimate the total charge and ball charge volumetric filling fractions, J_t and J_b, respectively, the most dependable (least uncertain) results were those obtained from the weight residual, Equation (6.6). Despite this conclusion, the power draw residual, Equation (6.5), will be included in the analysis here due to its utilisation in the SAG mill model for estimating the mill power draw and to provide a contrast to the analysis of the mill weight residual. The charge estimate results from the other source (JA Herbst and Associates) will not be further analysed here.

Table 6.1 contains the solutions of the constrained nonlinear optimisation for Equations (6.5) and (6.6), which show good agreement with the nominal conditions (shown in brackets).

Table 6.1: Total (J_t) and Ball (J_b) Charge Level Estimates

Inferential Measurement (actual)	Model	Value (vol. fraction)	Error wrt actual (%)
J_t (0.230)	F_{kW}	0.230	0.0
	F_{weight}	0.233	1.3
J_b (0.142)	F_{kW}	0.133	6.5
	F_{weight}	0.145	1.8

Figure 6.1 depicts the contours (solutions) of Equation (6.5) and (6.6) with the point results from Table 6.1 indicated. Significant lengths of the contours lie in the feasible region bounded by:

$J_b \leq J_t$ (ball charge can never be greater than total charge), and,

$J_t = 0.36$ (maximum charge before the mill contents begin to block the feed trunnion).

The point estimates show good agreement with the nominal conditions. However, the contours illustrate that there is a range of solutions that are feasible. Therefore, the uncertainty of the point estimates requires assessment.

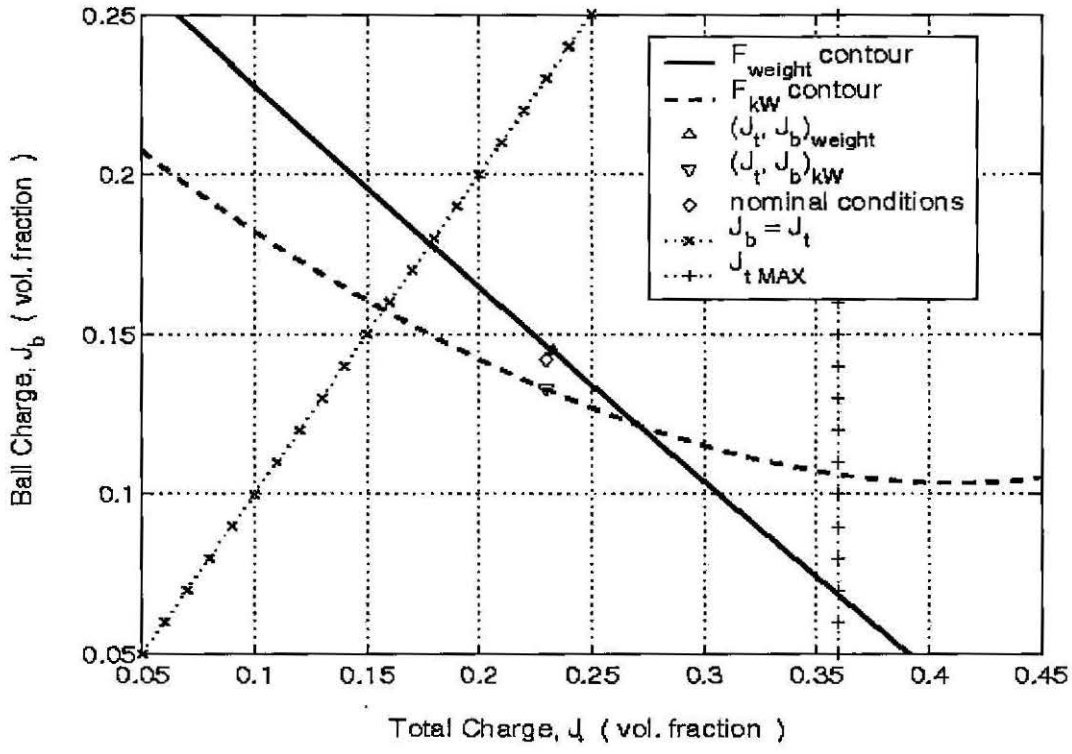

Figure 6.1: Inferential Model Contours

6.2.1 Sensitivity Analysis

If we define the $\frac{\partial f}{\partial \theta}$ term in Equation (6.1) as the sensitivity of the charge estimate to a given parameter, then the sensitivity can be determined by applying the Differentiation of Composite Function rule to Equation (6.5) and (6.6). The Differentiation of Composite Function rule is as follows (Perry *et al.*, 1984)

Given $F_i(J_t, J_b, \theta_j) = 0$ then (for $\partial F_i/\partial J_k \neq 0$),

$$\frac{\partial J_k}{\partial \theta_j} = -\frac{\partial F_i/\partial \theta_j}{\partial F_i/\partial J_k} \tag{6.7}$$

where

i = kW or $weight$ = residual indicator, *i.e.*, Equation (6.5) or (6.6), respectively

j = $1 \ldots 17$ = parameter indicator

k = t or b = estimate indicator, *i.e.*, total charge or ball charge, respectively

Seventeen (17) parameters, θ_j, were considered in the sensitivity analysis of the total charge and ball charge estimates. These parameters are listed in Table 6.2. The *Value* column lists the nominal value of the parameter. The *Error* and the % *Error* columns list the estimate of the error and absolute relative error in the parameter (to $\approx 99\%$ confidence), respectively.

Table 6.2: Mill Charge Level Model Parameters, θ_j

j	Parameter, θ_j	Value	Error	%Error
1.	k, Julius Kruttschnitt Mineral Research Centre mill power draw lumped parameter (dimensionless)	1.39	0.15	11
2.	D_{mill}, mill diameter (m)	7.12	0.15	2
3.	L_{mill}, mill length (m)	3.53	0.15	4
4.	θ_{cone}, mill cone angle (^{o})	15	2.00	13
5.	D_t, mill trunnion diamter (m)	1.6	0.10	6
6.	RPM, mill speed (RPM)	12.014	0.50	4
7.	SG_s, ore specific gravity (t/m^3)	2.65	0.10	4
8.	SG_b, ball specific gravity (t/m^3)	7.80	0.20	3
9.	ϵ, charge voidage (fraction)	0.4	0.015	4
10.	$SMDC_{tph\_s}$, mill solids throughput (tph)	252.1	10.00	4
11.	$SMDC_{\%sw/w}$, discharge density, (%sols w/w)	75.93	3.00	4
12.	γ, relative radial position of open area (fraction)	0.8031	0.05	6
13.	$foag$, discharge grate fractional open area (fraction)	0.179	0.02	11
14.	MV_{wt}, mill weight measurement (t)	176	10.00	6
15.	M_{shell}, mill shell weight (t)	64	5.00	8
16.	MV_{kW}, mill power draw measurement (kW)	2800	200.00	7
17.	r_n, relative radius of outermost grate (fraction)	0.972	0.028	3

The sensitivity (absolute value) of the estimates to the parameters are shown in the following Figures, according to the following schedule:

Figure No.	*Description*
(6.2)	Ball charge level estimate from F_{kW} (Equation (6.5)) sensitivity
(6.3)	Ball charge level estimate from F_{weight} (Equation (6.6)) sensitivity
(6.4)	Total charge level estimate from F_{kW} (Equation (6.5)) sensitivity
(6.5)	Total charge level estimate from F_{weight} (Equation (6.6)) sensitivity

These Figures draw attention to the following parameters on account of the charge estimate sensitivities:

j	θ_j	*Description*
1	k	Julius Kruttschnitt Mineral Research Centre mill power draw lumped parameter (dimensionless)
2	D_{mill}	mill diameter (m)
3	L_{mill}	mill length (m)
9	ϵ	charge voidage (fraction)
12	γ	relative radial position of open area (fraction)
13	$foag$	discharge grate fractional open area (fraction)

The sensitivity results for several parameters are zero or effectively zero. This is due to one or a combination of the following:

a) the parameter was included in the analysis in anticipation of it being relevant to the ensuing inferential model Steps

b) the parameter was included to investigate its importance in the estimates

c) the $\partial F_i/\partial J_k$ term in Equation (6.7) is very much larger than the $\partial F_i/\partial \theta_j$ term

The sensitivity results in each Figure cannot be compared directly since each (bar chart) bar has its own units (*mill fraction per [parameter unit]*). Although an intermediate step in the error analysis, the sensitivity analysis for the mill charge level estimates are included in this Section for the following reasons:

- The relative importance of the parameters differs markedly between the sensitivity analysis and the error analysis (discussed in Section 6.2.2). Inclusion of the sensitivity analysis results aids the illustration of this point.
- The (bar chart) bars can be compared between figures (for a specific parameter) since the units are consistent in this case. Inspection of the four figures reveals that the sensitivity results are generally of the same order of magnitude except for the sensitivities in Figure 6.4 - the total charge estimate from the power draw residual (Equation (6.5)). Further discussion of this point will take place in the error analysis in Section 6.2.3.

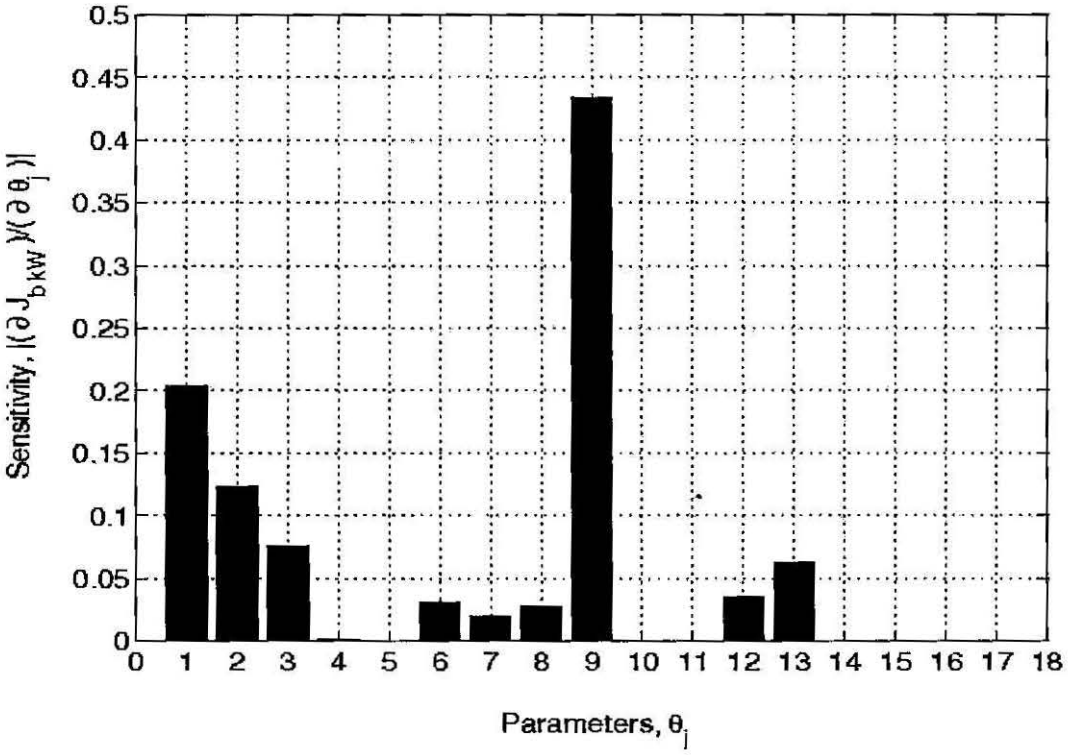

Figure 6.2: Power draw Ball Charge Estimate Sensitivity

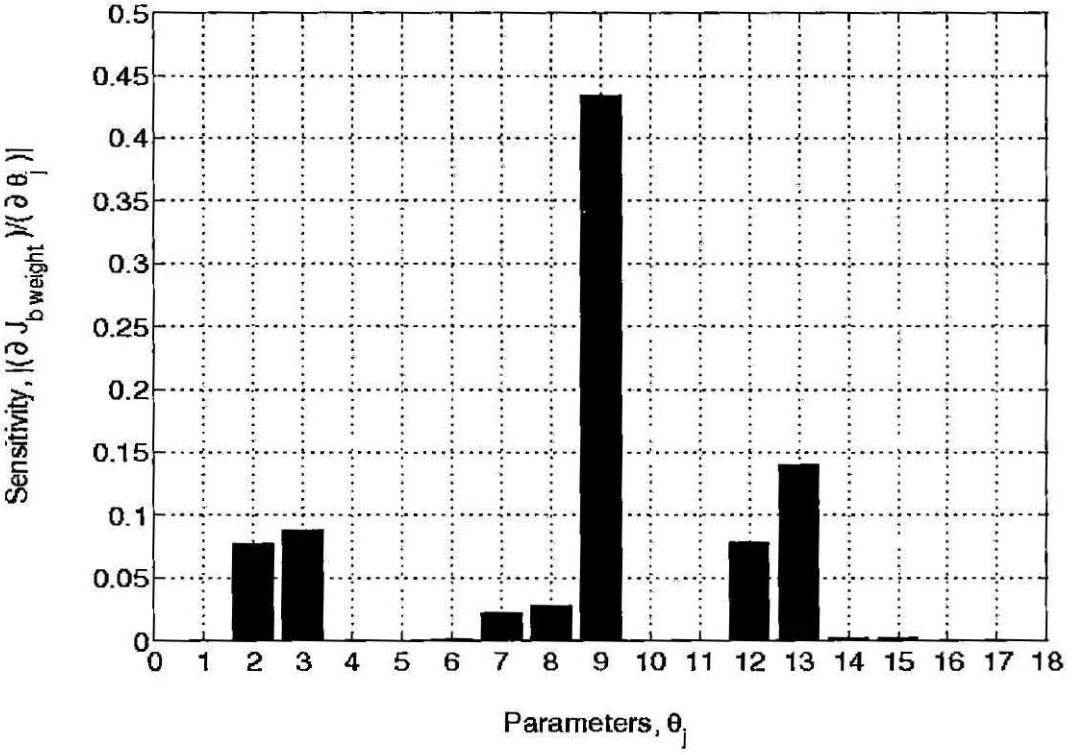

Figure 6.3: Mill Weight Ball Charge Estimate Sensitivity

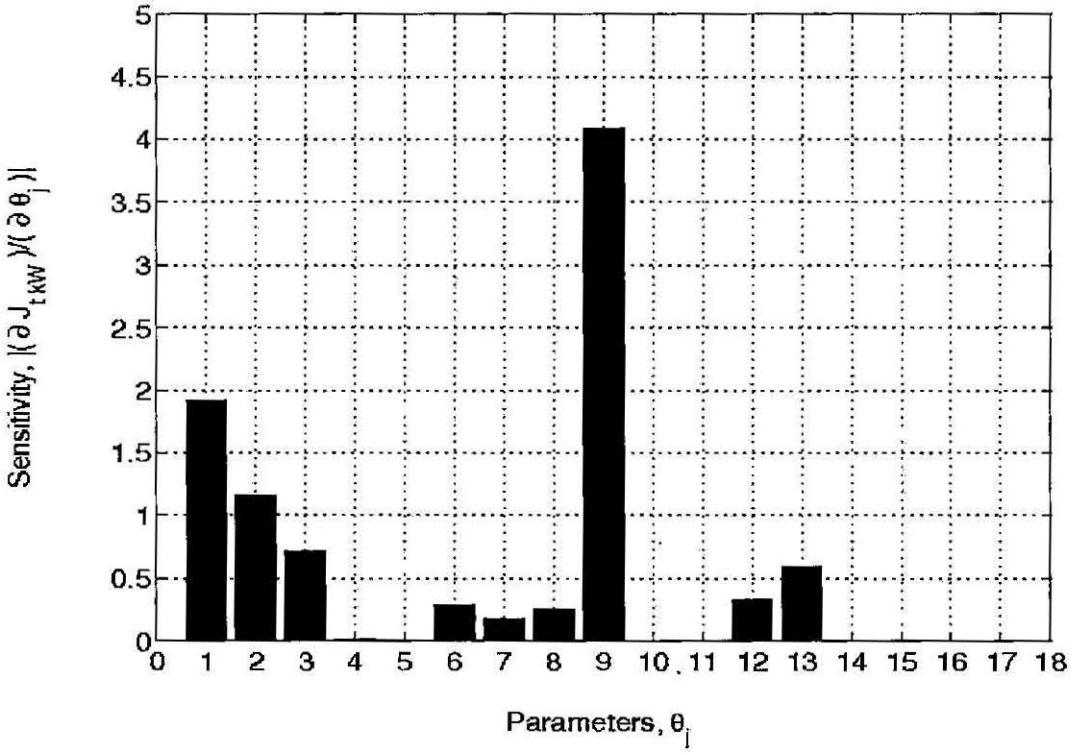

Figure 6.4: Power draw Total Charge Estimate Sensitivity

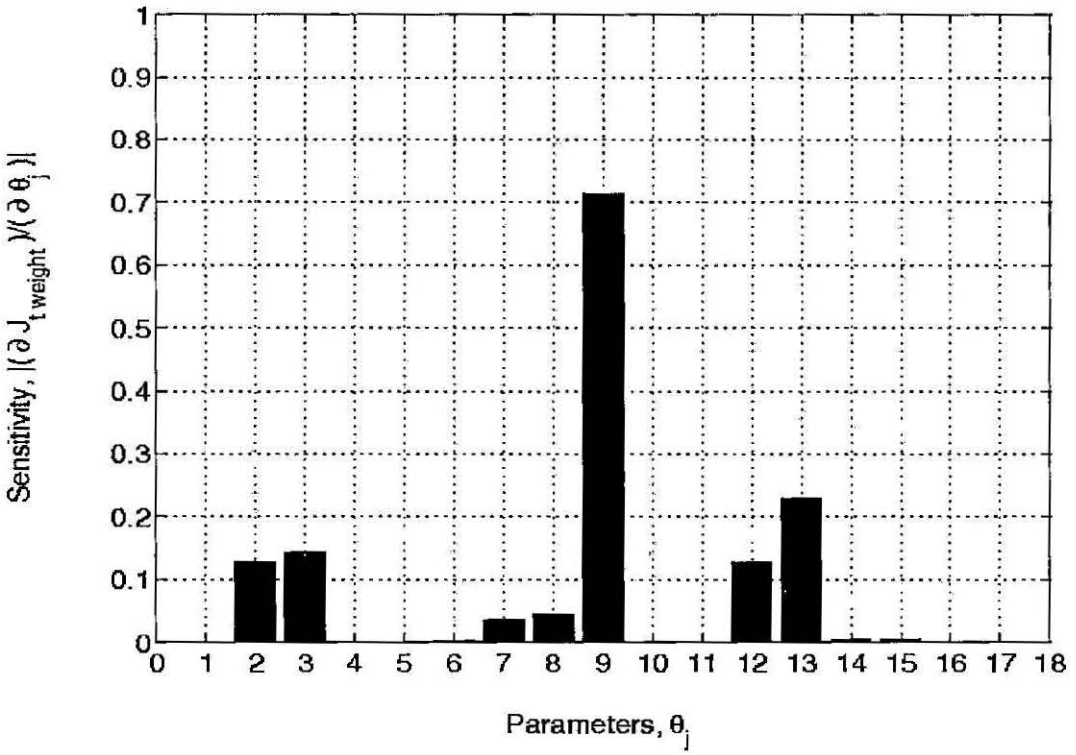

Figure 6.5: Mill Weight Total Charge Estimate Sensitivity

6.2.2 Error Analysis

Equation (6.1) was applied to each of the inferential models, Equations (6.5) and (6.6) to estimate the uncertainty in the mill inventory estimates obtained from them, *i.e.*,

$$\delta J_{k,i} = \sqrt{\sum_{j=1}^{N} \left(\frac{\partial J_{k,i}}{\partial \theta_j} \delta \theta_j \right)^2} \tag{6.8}$$

where

$\delta J_{k,i}$ = the uncertainty in charge estimate J_k obtained when using residual Equation i

$\delta \theta_j$ = uncertainty in θ_j

$\frac{\partial J_k}{\partial \theta_j}$ = the sensitivity of charge estimate J_k to parameters θ_j

N = total number of parameters (17)

Table 6.3 contains the results for the error analysis. Overall, the uncertainty in the estimates is acceptable ($\leq$ 33%). However, despite good agreement between estimate and the nominal condition, the total charge estimate (J_t) from the power draw residual, Equation (6.5), contains a high level of uncertainty ($>$ $\pm$ 180%).

Table 6.3: Mill Charge Estimate Uncertainty Analysis Summary

Inferential Measurement (actual)	Model	Value (vol. fraction)	Error wrt actual (%)	Uncertainty	
				absolute (vol frac)	relative (%)
J_t (0.230)	F_{kW}	0.230	0.0	0.42	181
	F_{weight}	0.233	1.3	0.06	26
J_b (0.142)	F_{kW}	0.133	6.5	0.04	33
	F_{weight}	0.145	1.8	0.04	26

The findings lead to the following conclusions:

1. Despite good agreement, the total charge level estimate (J_t) from the power draw model, Equation (6.3), contains a high degree of uncertainty.
2. The power draw model, Equation (6.3), yields a good ball charge level estimate (J_b) with reasonable certainty.
3. The weight model, Equation (6.4), gives good estimates of both the total charge level (J_t) and ball charge level (J_b) with reasonable certainty and is therefore the recommended model for charge estimation.

The seventeen (17) parameters considered in this analysis are a subset of the large number of parameters available for consideration. The parameters were selected drawing from industrial experience and simulation model familiarity. Analysis of a comprehensive set of parameters would generate a prohibitively large problem. The results presented here are therefore estimates of the uncertainty only.

Relative Contribution to Estimate Errors

If the relative contribution to the estimate error, RCE, is defined as the relative contribution that the uncertainty in a parameter makes to the uncertainty in a charge estimate, then RCE may be utilised to assess the relative influence a parameter has on the uncertainty of a charge estimate. According to this definintion, RCE is calculated as follows:

$$RCE_{i,j,k} = \frac{\left(\frac{\partial J_k}{\partial \theta_j}\,\delta\theta_j\right)^2}{\sum_{j=1}^{N}\left(\frac{\partial J_k}{\partial \theta_j}\,\delta\theta_j\right)^2}\cdot 100\% \tag{6.9}$$

where

$RCE_{i,j,k}$ = relative contribution that uncertainty in parameter θ_j makes to the J_k charge estimate uncertainty when utilising residual Equation (i) (%)

The relative contribution to estimate error (RCE) was determined for charge estimate uncertainties given in Table 6.3. The results are presented graphically in Figures (6.6) to (6.9) according to the following schedule:

Figure No.	*Description*
(6.6)	Ball charge estimate from F_{kW} (Equation (6.5)) error analysis
(6.7)	Ball charge estimate from F_{weight} (Equation (6.6)) error analysis
(6.8)	Total charge estimate from F_{kW} (Equation (6.5)) error analysis
(6.9)	Total charge estimate from F_{weight} (Equation (6.6)) error analysis

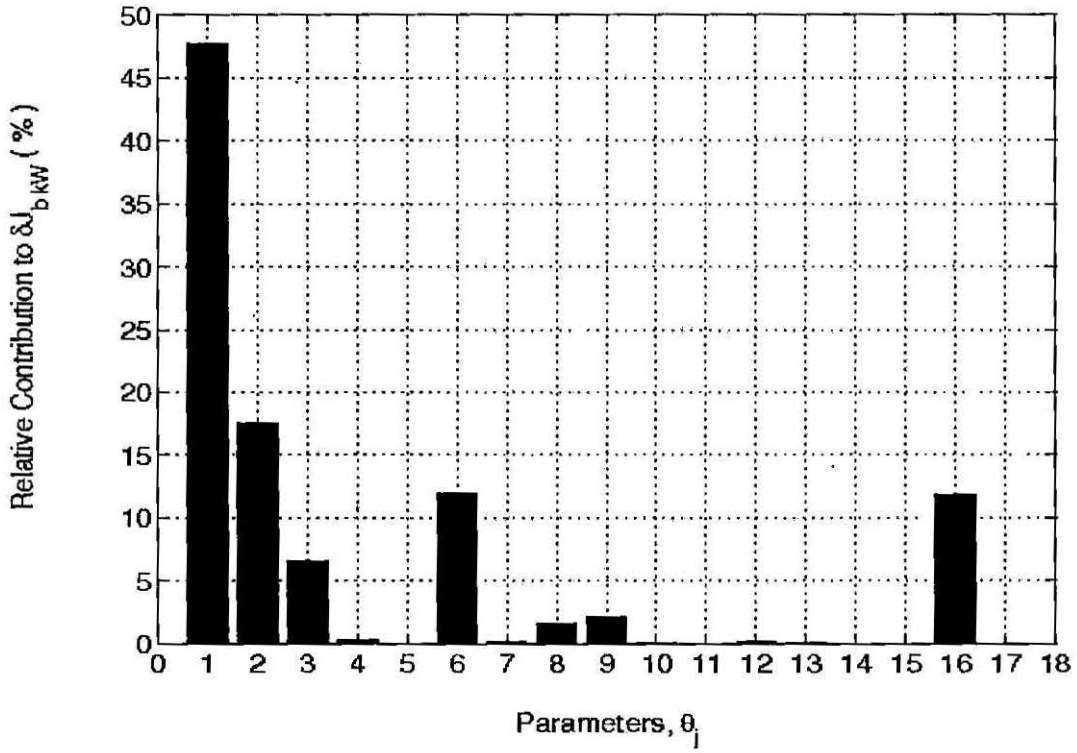

Figure 6.6: Power draw Ball Charge Estimate Uncertainty

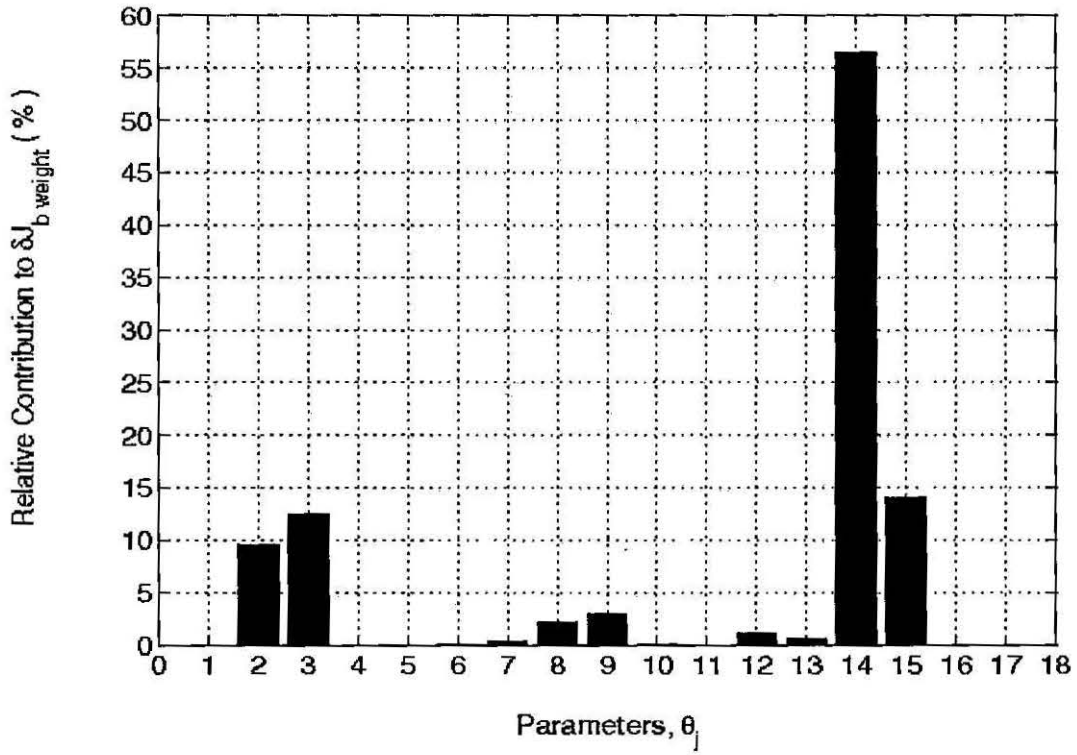

Figure 6.7: Mill Weight Ball Charge Estimate Uncertainty

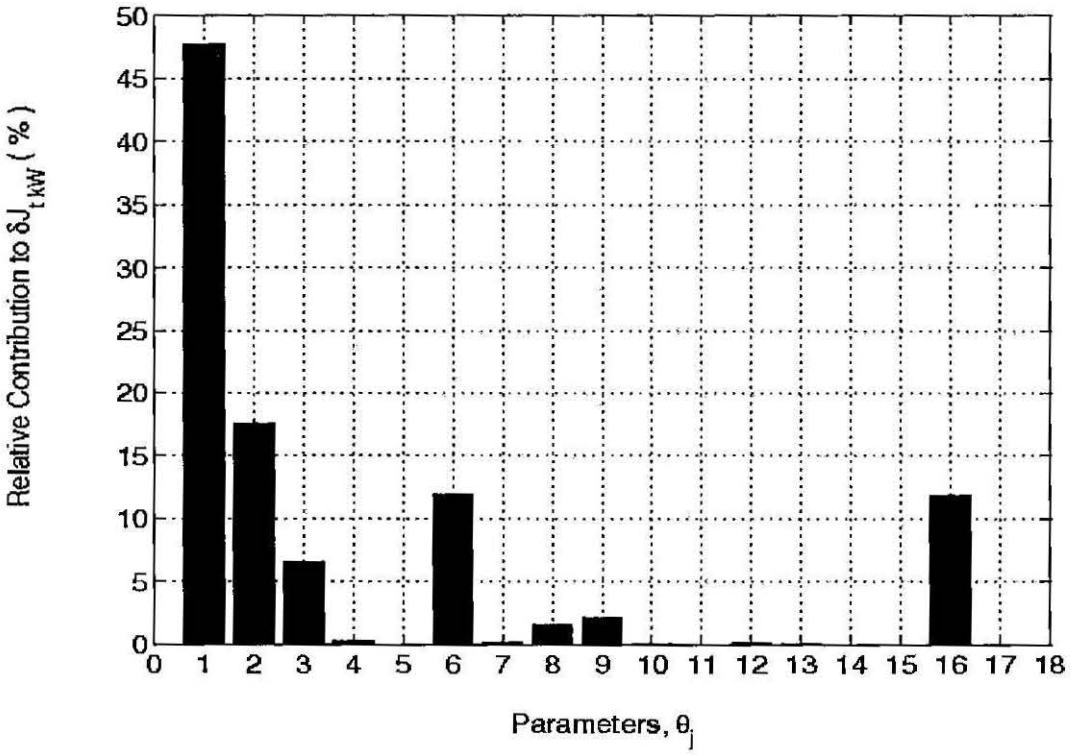

Figure 6.8: Power draw Total Charge Estimate Uncertainty

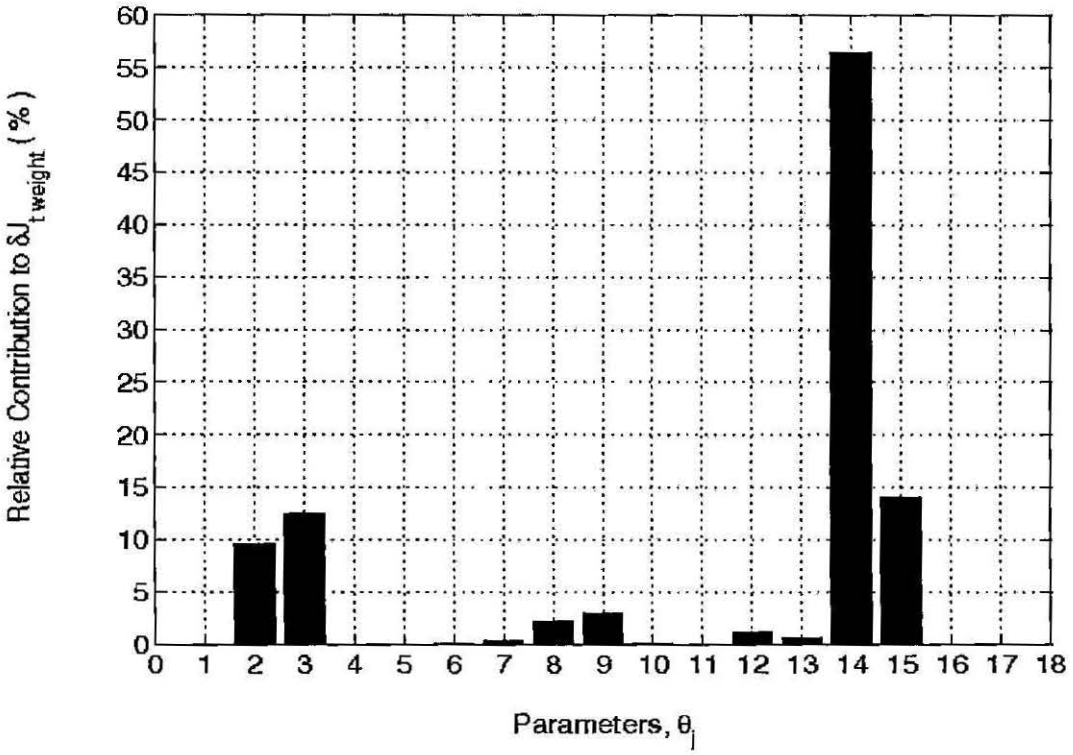

Figure 6.9: Mill Weight Total Charge Estimate Uncertainty

On a residual by residual basis, a number of observations may be made regarding the error analysis results:

***E*stimates from mill power draw, Equation (6.5)**

- The parameters that have the largest influence on the estimate uncertainties are:

j	θ_j	*Description*
1	k	Julius Kruttschnitt Mineral Research Centre mill power draw lumped parameter (dimensionless)
2	D_{mill}	mill diameter (m)
6	RPM	mill speed (RPM)
16	MV_{kW}	mill power draw measurement (kW)

- Julius Kruttschnitt Mineral Research Centremill power draw lumped parameter, k, contributes the highest relative amount of uncertainty, higher than the combination of the uncertainties from the mill diameter, D_{mill}, the mill speed, RPM and the mill power draw measurement, MV_{kW}.

- The parameters flagged in the sensitivity analysis that have little or no influence on the estimate uncertainties are:

j	θ_j	*Description*
3	L_{mill}	mill length (m)
9	ϵ	charge voidage (fraction)
13	$frac_{OA}$	discharge grate fractional open area (fraction)

- The mill power draw measurement (MV_{kW}) is an influential parameter. The sensitivity analysis did not, however, highlight its importance.

These observations lead to the following conclusions:

- fitting of the power draw lumped parameter, k, should be conducted with due care since it accounts for $\approx 50\%$ of the uncertainty in the charge estimates.

- the best available measurements of mill power draw, MV_{kW}, and speed, RPM, should be utilised.

- mill diameter, D_{mill}, should be measured at regular intervals to account for shell liner wear.

- measurements of mill diameter, D_{mill}, could be supplemented by and utilised to tune a dynamic mill liner model, *e.g.*, the model proposed in Chapter 5.

Estimates from mill weight, Equation (6.6)

- The parameters that have the largest influence on the estimate uncertainties are:

j	θ_j	*Description*
2	D_{mill}	mill diameter (m)
3	L_{mill}	mill length (m)
14	MV_{wt}	mill weight measurement (t)
15	M_{shell}	mill shell weight (t)

- Mill weight measurement, MV_{wt}, contributes the highest relative amount of uncertainty, higher than the combination of the uncertainties from the mill length, L_{mill}, the mill diameter, D_{mill} and the mill shell weight, M_{shell}.

- The parameters flagged in the sensitivity analysis that have little or no influence on the estimate uncertainties are:

j	θ_j	*Description*
9	ϵ	charge voidage (fraction)
12	rrp_{OA}	relative radial position of open area (fraction)
13	$frac_{OA}$	discharge grate fractional open area (fraction)

- The mill weight measurement (MV_{wt}) and shell weight (M_{shell}) are influential parameters. The sensitivity analysis did not, however, highlight their importance.

These observations lead to the following conclusions which echo those published elsewhere (Apelt *et al.*, 2001a):

- the best possible measurement of mill weight, MV_{wt}, should be utilised. This requirement could help justify the installation of a load cell or bearing pressure measurement as an initial or secondary mill weight measurement.

- mill diameter, D_{mill}, and mill length, L_{mill}, should be measured at regular intervals to account for shell liner wear.

- measurements of mill diameter, D_{mill}, could be supplemented by and utilised to tune a dynamic mill liner model, *e.g.*, the model proposed in Chapter 5.

Further to the sensitivity points raised in Section 6.2.1, comparison of the relative contribution to the error (RCE) results and the sensitivity analysis ($\delta J/\delta\theta$) results illustrates how the relative importance of the parameters differs between the sensitivity analysis and the error analysis.

For example, comparison of Figures 6.2 and 6.6 reveals that the sensitivity analysis of the ball charge estimate from the power draw residual did not highlight the importance of the mill power draw measurement towards the estimate uncertainty.

Similarly, comparison of Figures 6.5 and 6.9 reveals that the sensitivity analysis of the total charge estimate from the weight residual did not highlight the importance of the mill weight measurement or mill shell weight towards the estimate uncertainty.

These examples highlight the importance of utilising the relative contribution to the error (RCE) for assessment of parameter influence in estimate uncertainty.

Whilst the relatively large sensitivities for the total charge estimate from the power draw residual are raised in discussion, in Section 6.2.3, the further utilisation of sensitivity assessment for the remaining inferential nmodels will not be pursued.

6.2.3 Further Discussion

Relative Contribution to the Error Similarities

Inspection of the relative contribution to the error Figures reveals

- Figures (6.6) and (6.8) are the same, and,
- Figures (6.7) and (6.9) are the same.

These similarities have a mathmatical explanation not detailed by Apelt *et al.* (2001a). Recall the Differentiation of Composite Function rule:

Given $F_i(J_t,\, J_b,\, \theta_j) \;=\; 0$ then (for $\partial F_i/\partial J_k \;\neq\; 0$),

$$\frac{\partial J_k}{\partial \theta_j} \;=\; -\frac{\partial F_i/\partial \theta_j}{\partial F_i/\partial J_k} \tag{6.10}$$

Recall also the definition for relative contribution to the estimate error (RCE):

$$RCE_{i,\,j,\,k} \;=\; \frac{\left(\frac{\partial J_k}{\partial \theta_j}\;\delta\theta_j\right)^2}{\sum_{j=1}^{N}\left(\frac{\partial J_k}{\partial \theta_j}\;\delta\theta_j\right)^2}\cdot 100\% \tag{6.11}$$

Substitution of Equation (6.10) into Equation (6.11) yields:

$$RCE_{i,j,k} = \frac{\left(\frac{\partial F_i}{\partial \theta_j}\frac{\partial J_k}{\partial F_i}\,\delta\theta_j\right)^2}{\sum_{j=1}^{N}\left(\frac{\partial F_i}{\partial \theta_j}\frac{\partial J_k}{\partial F_i}\,\delta\theta_j\right)^2} \tag{6.12}$$

Recognising that $\frac{\partial J_k}{\partial F_i}$ is a constant that may be factored out yields:

$$RCE_{i,j} = \frac{\left(\frac{\partial F_i}{\partial \theta_j}\,\delta\theta_j\right)^2}{\sum_{j=1}^{N}\left(\frac{\partial F_i}{\partial \theta_j}\,\delta\theta_j\right)^2} \tag{6.13}$$

This means that the the relative contribution to estimate error, $RCE_{(i,j)}$, is now independent of the volumetric charge level being estimated, J_t or J_b, and is dependent only on the residual equation i being considered and the parameters θ_j. This renders the results for the total charge,J_t, and the ball charge, J_b, estimates equivalent for a given residual as demonstrated in Figures (6.6) to (6.9) .

Residual Contour Plot Tangents

For residual i, substituting Equation (6.10) into Equation (6.8) yields:

$$\delta J_{t,i} = \frac{\partial J_{t,i}}{\partial F_i}\sqrt{\sum_{j=1}^{N}\left(\frac{\partial F_i}{\partial \theta_j}\,\delta\theta_j\right)^2} \tag{6.14}$$

and

$$\delta J_{b,i} = \frac{\partial J_{b,i}}{\partial F_i}\sqrt{\sum_{j=1}^{N}\left(\frac{\partial F_i}{\partial \theta_j}\,\delta\theta_j\right)^2} \tag{6.15}$$

Dividing Equation (6.15) by Equation (6.14) yields:

$$\frac{\delta J_{b,i}}{\delta J_{t,i}} = \frac{\partial J_{b,i}}{\partial J_{t,i}} \tag{6.16}$$

The right hand side of Equation (6.16) is the slope of the contour of residual Equation (i). This means that visual inspection of the contours indicates how the uncertainties in the estimates compare and how their comparative uncertainty changes along the contour.

Inspection of the mill weight residual in Figure 6.1 indicates that the uncertainty in the total charge estimate, δJ_t, remains relatively constant with respect to the the uncertainty in the ball charge estimate, δJ_b, *i.e.*, constant slope. In contrast to this, for the mill power draw residual case, the uncertainty in the total charge estimate, δJ_t, increases with respect to the the uncertainty in the ball charge estimate, δJ_b the higher the total charge

is above the the ball charge, *i.e.*, decreasing slope. This is attributed the concave nature of the power draw *versus* charge curve, *i.e.*, beyond some total load level, the power draw passes through a maximum and begins to decrease. Hence, two load conditions are feasible for a range of high power draw readings. Recall from Chapter 2 that mill power draw 'loops-over', see Figure 6.10 (whereas the weight curve is a monotonically increasing function of mill filling). Uncertainty is introduced since over a range of the curve, a single power draw reading corresponds to two mill filling levels.

Table 6.4 contains the gradients of the residuals calculated by Equation (6.16) and by visual inspection of the contours in Figure 6.1. The expected agreement is evident for the weight residual. However, a discrepancy is evident for the power draw residual. A thorough investigation into the root of this discrepancy was considered outside the scope of this research. However, it is attributed to the following:

1. **Large Sensitivities.** Referring to Figure 6.4, the sensitivities of the total charge estimate, J_t, to the parameters in the power draw residual are an order of magnitude large than the sensitivities of the other charge estimates. This highlights the non-linearity in J_t of the power draw residual and also the relative prominence J_t plays in the power draw residual Equation (6.3).

   Total charge fraction, J_t, features extensively in the residual whereas the ball charge estimate, J_b, occurs linearly in the charge density term, ρ_c. These characteristics would be expected to give an over-estimate of the uncertainty in the total charge estimate, J_t, and thus, result in an underestimate of the slope of the power draw residual contour when utilising Equation (6.16).

2. **Compensating Errors.** When a function involves any variable more than once, compensating errors may occur and a step by step calculation may over-estimate the uncertainty (Taylor, 1982). This is indeed the case here as mentioned in the previous point. The complexity of the residual equation means that the one-step uncertainty calculation advised by Taylor (1982) for an accurate uncertainty estimate was not feasible despite the symbolic manipulation capability of Maple. The complex nature of the residual equation required the utilisation of the rules for the (partial) differentiation of sums and products and the chain rule (Perry *et al.*, 1984).

3. **Residual Non-linearity.** The error estimates are based on partial derivatives which are linear estimates of the gradient of the non-linear function. The more non-linear the function, the more approximate the estimate. The power draw is highly non-linear, thus, the uncertainty estimate is an over-estimation.

One method to improve the agreement is to reduce the size of the errors in the parameters, $\delta\theta_j$. This was tested by reducing all of the errors in Table 6.2 by half. The uncertainties in the total charge estimate, δJ_t, and the ball charge estimate, δJ_b, both reduced by approximately a half. The corresponding slope of 0.14 (by Equation (6.16)) represents only a slight improvement in the estimate of the slope in Figure 6.1.

4. **Power draw Curve.** The points of residual non-linearity and large sensitivity are inter-related with the power draw model itself which has a range where a single power draw reading corresponds to two mill filling levels, refer to Figure 6.10 above. This uncertainty is exacerbated with the use of variable speed drives (which are gaining increasing acceptance (Barratt and Brodie, 2001)) which shift the power draw curve up the power draw axis with increasing mill speed.

The presence of compensating errors introduces the possibility of uncertainty over-estimation in the case of the total charge estimate (J_t) from the power draw residual, Equation (6.5). However, the large sensitivities, residual non-linearity and power draw curve shape, reinforce the high level of uncertainty. Therefore, the total charge estimate (J_t) from the power draw residual, Equation (6.5), continues to be considered less reliable than the estimate from the mill weight residual, Equation (6.6).

Table 6.4: Residual Slope Comparison

Contour	Gradient Equation (6.16)	Gradient Figure 6.1
Power draw Equation (6.5)	0.10	0.38
Weight Equation (6.6)	0.67	0.67

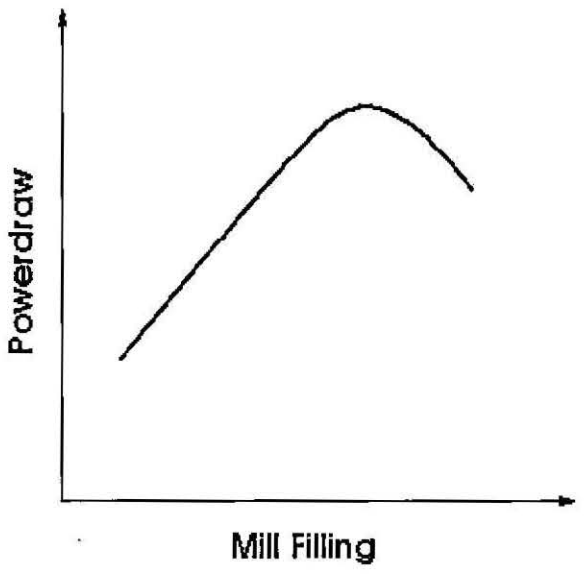

Figure 6.10: Mill power draw *versus* mill filling

6.2.4 Mill Charge Level Model Summary

The sensitivity and error analysis results and discussion have found in favour of the utilisation the mill weight residual, Equation (6.6), for estimating the total charge fraction, J_t, and the ball charge fraction, J_b. The estimates from this residual contain the least uncertainty. Therefore, the mill weight residual should be utilised in preference to the mill power draw residual.

To minimise uncertainty in the charge estimates from the mill weight residual, the best available mill weight measurement, MV_{wt}, should be utilised and mill diameter, D_{mill}, and mill length, L_{mill}, should be measured at regular intervals to account for shell liner wear. The mill diameter, D_{mill}, measurements could be supplemented by and utilised to tune a dynamic mill liner model, *e.g.*, the model proposed in Chapter 5.

6.3 SAG Mill Discharge Estimate

Based on plant measurements of the feed rate to the oversize crusher, the flow rate and density of the primary cyclone feed and estimates of the size distributions reporting to the oversize crusher and the primary cyclones, the SAG mill discharge rate ($SMDC$) and size distribution ($smdc$) may be estimated.

Size

The SAG mill discharge size distribution, $smdc$, may be indicated by way of the T_{80}, T_{60}, T_{40} and T_{20} measurements (the 80%, 60%, 40% and 20% w/w passing sizes of the mill discharge material, respectively). The "T" designation is for "$transfer$" size, *i.e.*, the size distribution of the SAG mill discharge stream indicates the size distribution of material being transferred from the primary grinding circuit to the secondary grinding circuit. Multiple passing size estimates are necessary to define the size distribution where a single point indication (*e.g.*, T_{80} only) is insufficient (McKen et al., 2001).

The results of the inferential measurement of the SAG mill discharge size distribution are shown in Figure 6.11. The good agreement for the P_{80} (T_{80}) size of 1 - 3% error between the inferential model and the reference data (Table 5.5) and simulation model results (Table 5.1), respectively, is evident here also. Recall that details of the stream information for reference data, simulation and inferential model results can be found in Appendix C.

Table 6.5: Inferential Mill Discharge Size Distribution Indication ($smdc$)

$SMDC$ % Passing	Passing Size		
	actual (mm)	model (mm)	error (%)
T_{80}	16.7	16.9	1
T_{60}	2.9	6.4	120
T_{40}	0.6	2.6	277
T_{20}	0.1	0.4	319

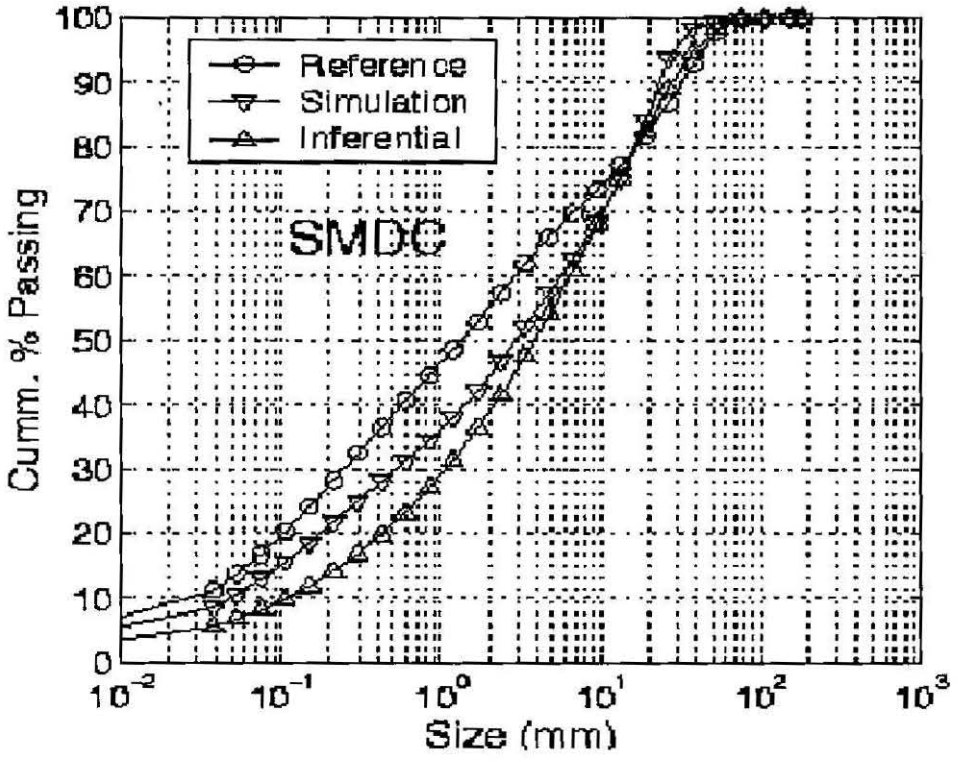

Figure 6.11: Inferential Mill Discharge Size Distribution Results (*smdc*)

Overall the inferential model predicts a size distribution that is more narrow and more coarse than the "actual" size distribution, *i.e.*, the Reference Data. This feature is also evident in the results of the inferential size distribution indication, given in Table 6.5.

The estimates for T_{60}, T_{40} and T_{20} contain relatively larger errors. Section 3.4 described the sources of error in the T_{80} (P_{80}) calculations, *i.e.*, the error in the size distribution is attributed to interpolation errors (particularly at fine sizes) combined with minor model approximations. Furthermore, as the transfer (and passing) size indicators are obtained from the cummulative percent passing format of the size distribution, errors in the coarse end of the distribution impact on the estimates at the fine end of the distribution. However, since the relative movement in the P_{80} measurement over time is considered most important rather than the absolute value of the measurement (Davies *et al.*, 2000), these size indicators are considered a satisfactory means of SAG mill discharge size indication.

Rate and Density

The results for the inferential model estimates of SAG mill solids discharge rate and density are shown in Table 6.6 and exhibit good agreement to the Reference Data. Therefore, a satisfactory inferential measurement of the SAG mill discharge rate and density, based on

plant measurements of the oversize crusher feed rate, primary cyclone feed flowrate and density and feedwater addition rate, is possible.

Table 6.6: Inferential Mill Discharge Rate and Density Results ($SMDC$)

item	$SMDC_{tph\_s}$	$SMDC_{\%s\,w/w}$
Reference	252.1	75.9
Inferential	252.1	75.9
Error (%)	0.0	0.0

6.3.1 Sensitivity and Error Analyses

Sensitivity and error analyses similar to those conducted on the mill charge inferential models, see Section 6.2.1, were conducted on the SAG mill discharge size, rate and density inferential models. Nine (9) parameters are considered in the analysis, see Table 6.7. These parameters differ from those considered for the total volumetric charge (J_t) and the ball charge (J_b), Section 6.2.1, since the discharge model is independent and upstream of the charge models in the calculation sequence.

Size

Equation (6.1) was applied to the mill discharge inferential model to estimate the uncertainty in the transfer size estimates. Table 6.8 contains the uncertainty estimates for the transfer size indicators which range from 74% to 415%. Although feasible, considering the high levels of relative error, this estimated level of uncertainty is not considered an accurate reflection of the actual uncertainty. The high uncertainty is attributed to an over-estimation due to *compensating errors*.

The discharge inferential model is in Step 1 of the inferential model calculation sequence. Therefore, a relatively straight forward uncertainty calculation could be expected. However the calculation required the utilisation of the rules for the (partial) differentiation of sums and products and the chain rule (Perry *et al.*, 1984) despite the symbolic manipulation capabilities of Maple, which may result in an uncertainty over-estimate (Taylor, 1982), as discussed for the powerdraw residual in Section 6.2.3.

Table 6.7: Inferential Mill Discharge Model Parameters, θ_j

j	Parameter, θ_j	Value	Error	%Error
1.	$OSCF_{tph\_p}$, oversize crusher feedrate (t/hr) (Measured Variable)	67.1	7	10
2.	$OSCF_{\%s\ w/w}$, oversize crusher density (%sols w/w) (Assumption)	99.9	1	1
3.	x_p, pepple port diameter (mm)	74.1	7	10
4.	$PCFD_{m3ph\_p}$, primary cyclone feed flowrate (m^3/hr) (Measured Variable)	243	24	10
5.	$PCFD_{\%s\ w/w}$, primary cyclone feed density (%sols w/w) (Measured Variable)	50.8	5	10
6.	$SMD50c$, SAG mill discharge screen corrected 50% passing size (mm)	5.0	3	60
7.	$PCFW_{m3ph\_l}$, primary cyclone feed water addition flowrate (m^3/hr) (Measure Variable)	99.2	10	10
8.	SG_s, ore specific gravity (t/m^3)	2.65	0.3	10
9.	SG_l, process water specific gravity (t/m^3)	1.00	0.1	10

It is considered here that an uncertainty over-estimation is evident. However, further investigation of the uncertainty estimation was deemed beyond the scope of this research.

Table 6.8: Mill Discharge Size Estimate Uncertainty Summary

$SMDC$ % Passing	Passing Size			
	actual (mm)	model (mm)	error (%)	uncertainty (%)
T_{80}	16.7	16.9	1	225
T_{60}	2.9	6.4	120	74
T_{40}	0.6	2.6	277	209
T_{20}	0.1	0.4	319	415

Presentation of the relative contribution to the estimate error (RCE) is considered useful despite concerns regarding uncertainty over-estimation. Figures (6.12) to (6.15) contain the relative contribution to the error, RCE, for the T_{80}, T_{60}, T_{40} and T_{20} mill discharge size indicators, respectively.

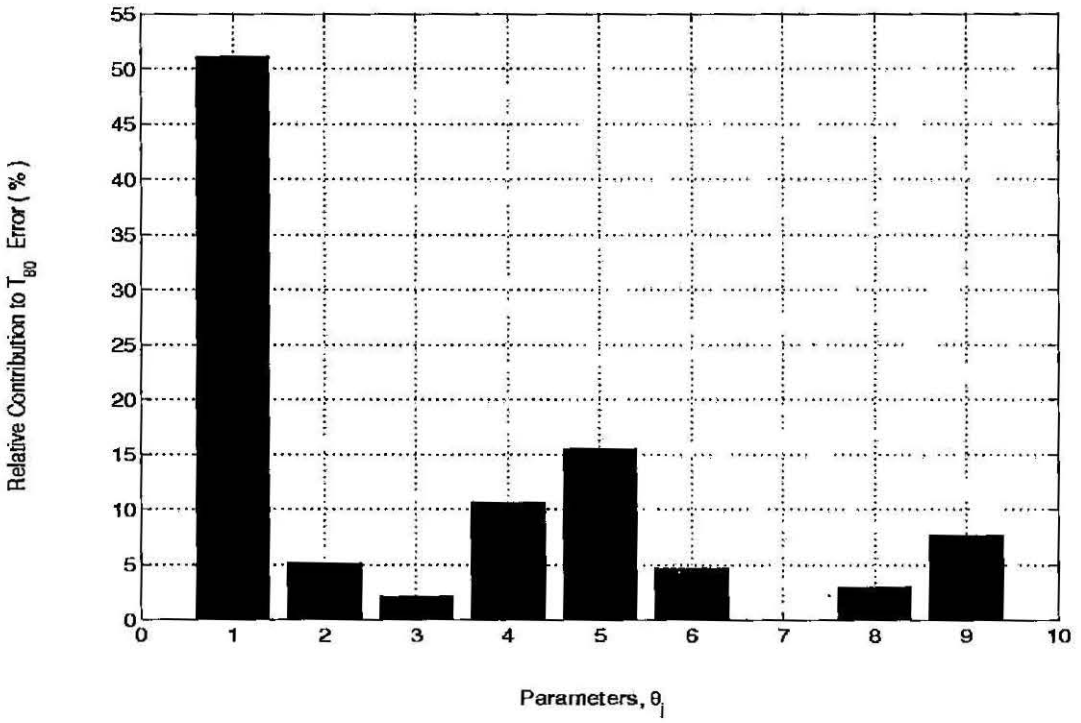

Figure 6.12: SAG Mill Discharge 80% Passing Size Indication Uncertainty (T_{80})

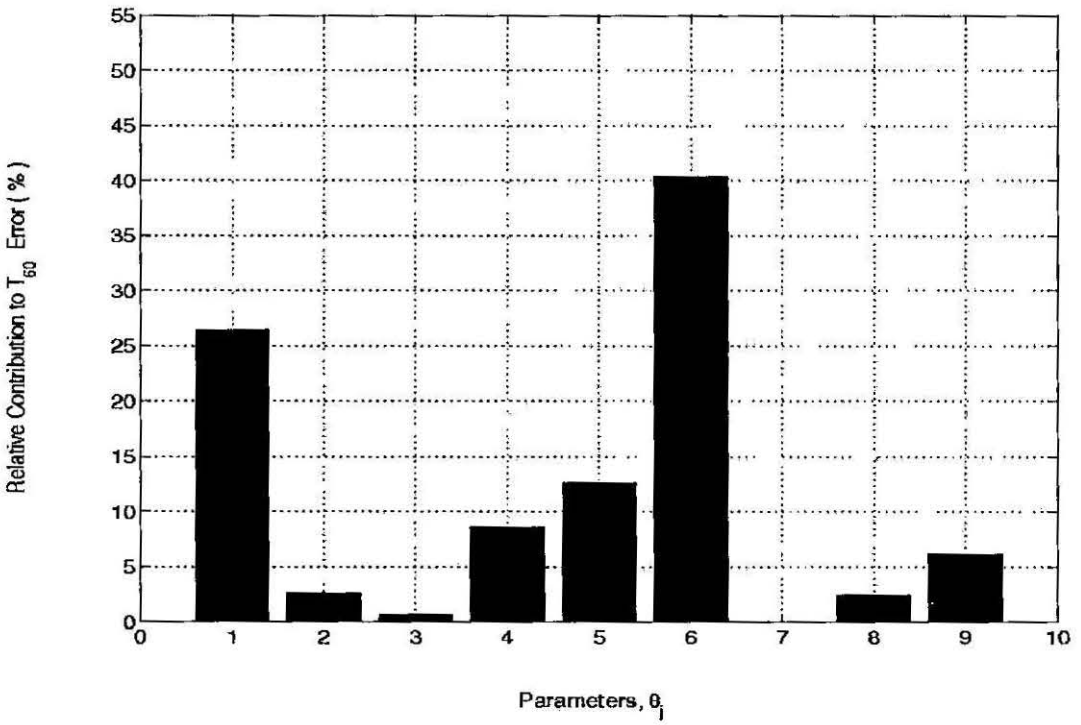

Figure 6.13: SAG Mill Discharge 60% Passing Size Indication Uncertainty (T_{60})

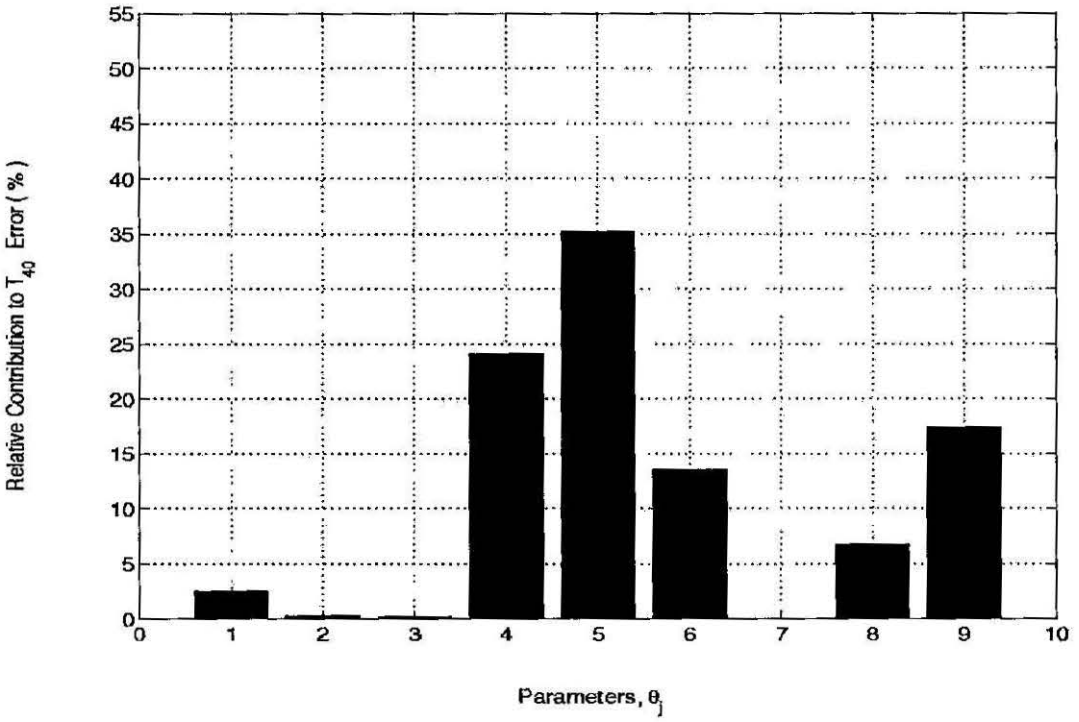

Figure 6.14: SAG Mill Discharge 40% Passing Size Indication Uncertainty (T_{40})

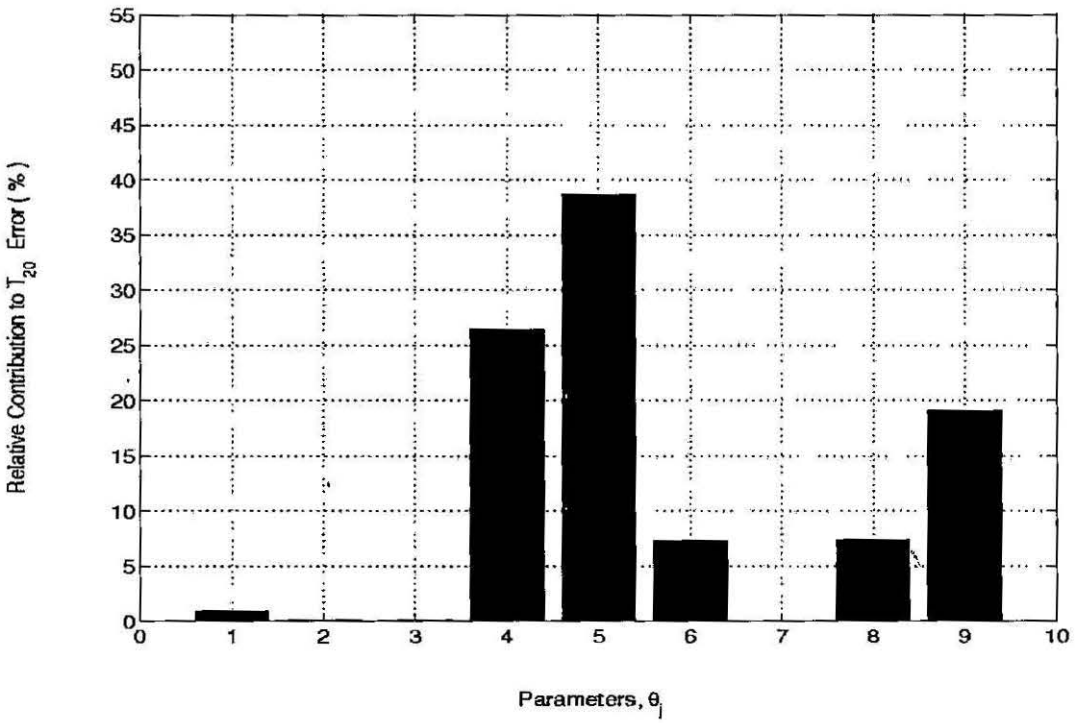

Figure 6.15: SAG Mill Discharge 20% Passing Size Indication Uncertainty (T_{20})

From Figure 6.12 through Figure 6.15, the parameters that have the most influence on the uncertainty in the inferential SAG mill discharge size distribution measurement are listed in Table 6.9.

Table 6.9: Influential Parameters: SAG Mill Discharge Size Estimate (*smdc*)

j	θ_j	Description
T_{80}		
1	$OSCF_{tph\_p}$	oversize crusher feedrate (t/hr) (Measured Variable)
4	$PCFD_{m3ph\_p}$	primary cyclone feed flowrate (m^3/hr) (Measured Variable)
5	$PCFD_{\%s\ w/w}$	primary cyclone feed density (%sols w/w) (Measured Variable)
T_{60}		
1	$OSCF_{tph\_p}$	oversize crusher feedrate (t/hr) (Measured Variable)
5	$PCFD_{\%s\ w/w}$	primary cyclone feed density (%sols w/w) (Measured Variable)
6	$SMD50c$	SAG mill discharge screen corrected 50% passing size (mm)
T_{40}		
4	$PCFD_{m3ph\_p}$	primary cyclone feed flowrate (m^3/hr) (Measured Variable)
5	$PCFD_{\%s\ w/w}$	primary cyclone feed density (%sols w/w) (Measured Variable)
6	$SMD50c$	SAG mill discharge screen corrected 50% passing size (mm)
9	SG_l	process water specific gravity (t/m^3)
T_{20}		
4	$PCFD_{m3ph\_p}$	primary cyclone feed flowrate (m^3/hr) (Measured Variable)
5	$PCFD_{\%s\ w/w}$	primary cyclone feed density (%sols w/w) (Measured Variable)
9	SG_l	process water specific gravity (t/m^3)

Referring to Figures (6.12) to (6.15) and Table 6.9, the influence of parameters differs with SAG mill discharge size estimate. This is due to the relative importance that the oversize crusher feed (coarse stream) and primary cyclone feed (fine stream) estimates play in the respective discharge size estimates. Therefore, the coarse mill discharge estimates (T_{80} & T_{60}) are influenced most by parameters utilised in the oversize crusher feed estimate and the fine mill discharge estimates (T_{40} & T_{20}) are influenced most by parameters utilised in the primary cyclone feed estimate.

Rate and Density

Equation (6.1) was applied to the mill discharge inferential model to estimate the uncertainty in the rate and density estimates. Table 6.10 contains the uncertainty estimates for the rate (14%) and density (8%) estimates. In contrast to the size estimate uncertainties, this level of uncertainty is acceptable. The overall mass balance calculations are simple in comparison to the size by size balances involved in the size distribution estimate. Therefore, over-estimation due to *compensating errors* is not evident. Figure 6.16 and Figure 6.17

Table 6.10: Mill Discharge Rate and Density Uncertainty Summary

item	$SMDC_{tph\_s}$	$SMDC_{\%s\ w/w}$
Reference	252.1	75.9
Inferential	252.1	75.9
Error (%)	0.0	0.0
Uncertainty (%)	14	8

contain the relative contribution to the error, RCE, for the SAG mill solids discharge rate ($SMDC_{tph\_s}$) and density ($SMDC_{\%s\ w/w}$) indicators, respectively. The parameters that have the most influence on the uncertainty in the inferential SAG mill discharge rate and density measurement are listed in Table 6.11.

Table 6.11: Influential Parameters: SAG Mill Discharge Rate & Density Estimates ($SMDC$)

j	θ_j	Description
4	$PCFD_{m3ph\_p}$	primary cyclone feed flowrate (m^3/hr) (Measured Variable)
5	$PCFD_{\%s\ w/w}$	primary cyclone feed density (%sols w/w) (Measured Variable)
7	$PCFW_{m3ph\_l}$	primary cyclone feed water addition flowrate (m^3/hr) (Measure Variable)
9	SG_l	process water specific gravity (t/m^3)

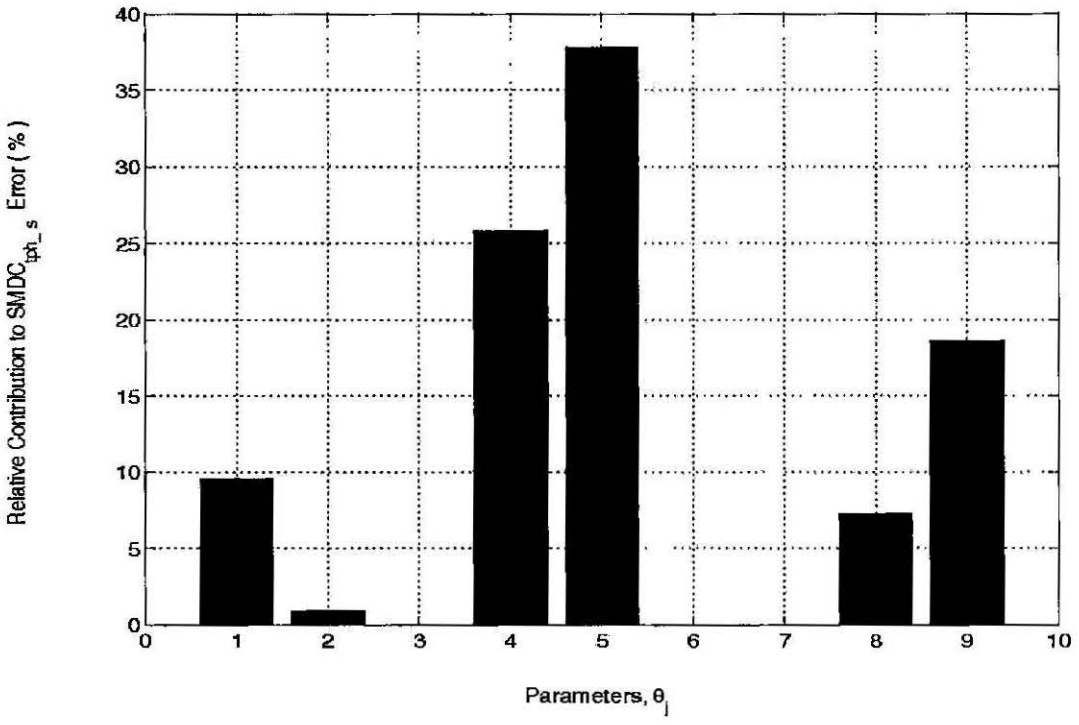

Figure 6.16: SAG Mill Solids Discharge Rate Indication Uncertainty

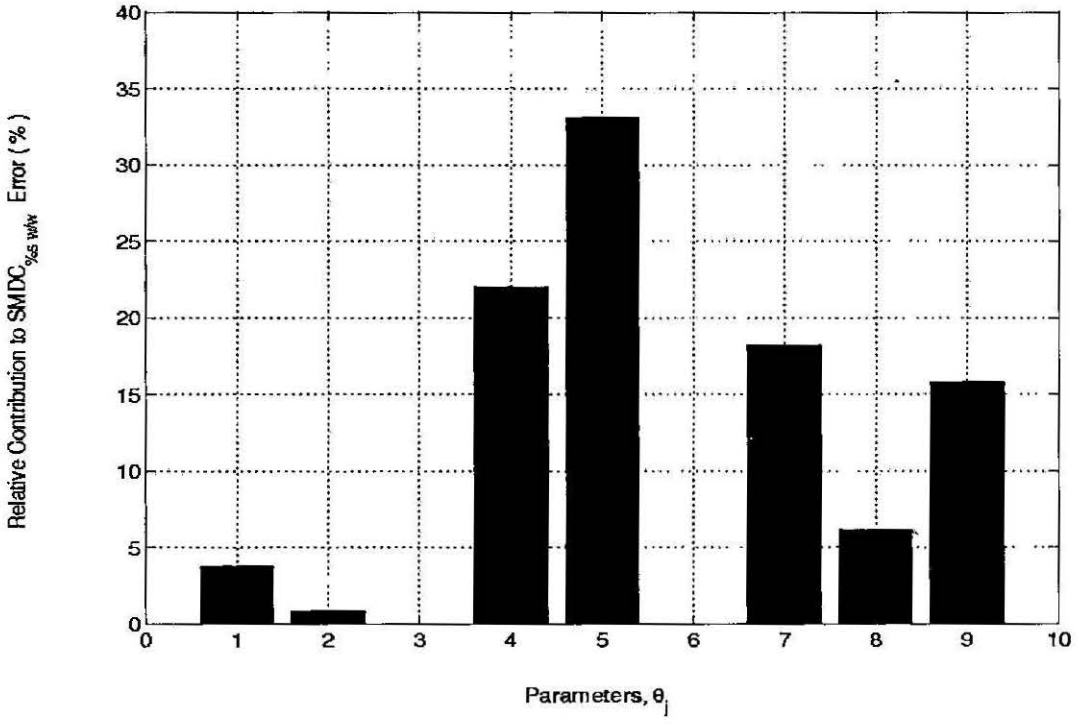

Figure 6.17: SAG Mill Discharge Density Indication Uncertainty

Referring to Figures (6.16) to (6.17) and Table 6.11, the parameters that most strongly influence the uncertainty in the SAG mill solids discharge rate and density are three of the parameters that affect the uncertainty in the size indicators, *i.e.*,

- primary cyclone feed flowrate, $PCFD_{m3ph\_p}$,
- primary cyclone feed density, $PCFD_{\%s\ w/w}$, and,
- process water specific gravity, SG_l.

The primary cyclone feed water addition flowrate, $PCFW_{m3ph\_l}$, also strongly influences the uncertainty in the density estimate.

6.3.2 Mill Discharge Model Summary

From the observations of Section 6.3.1 it is possible to conclude that the inferential model of the SAG mill discharge provides satisfactory indication of discharge rate, density and size distribution. Also, due to the influence that the process measurements, the discharge screen aperture and the process water specific gravity have on the uncertainty of the mill discharge estimates, it is possible to conclude that to minimise uncertainty in the inferential mill discharge size indicators, SAG mill solids discharge rate and density:

- the accuracy of the oversize crusher feed rate, $OSCF_{tph\_p}$, should be checked periodically, *e.g.*, by calibration checks and belt-cuts.
- calibration checks of the primary cyclone feed density gauge measurement, $PCFD_{\%s\ w/w}$, and flow meter, $PCFD_{m3ph\_p}$, and primary cyclone feed water addition flowrate, $PCFW_{m3ph\_l}$, should be conducted regularly to ensure accuracy.
- the SAG mill discharge screen aperture size should be monitored and measured regularly to ensure the corrected fifty percent passing size, $SMD50c$, may be adjusted as required.
- the specific gravity of the process water, SG_l, should be checked periodically.

6.4 SAG Mill Fresh Feed Estimate

Recall from the beginning of the Chapter that once estimates of the SAG mill discharge $SMDC$, SAG mill rock charge $SMRC$, and SAG mill ball charge, $SMBC$ have been obtained, it is possible to estimate the total and fresh SAG mill feed streams, $SMTF$ and $SMFF$, respectively. Fresh feed size distribution indication by way of the F_{80}, F_{60}, F_{40} and F_{20} measurements (the 80%, 60%, 40% and 20% w/w passing sizes of the feed ore material, respectively) can then be obtained from the fresh feed size distribution estimate, $smff$.

Size

The results of the inferential measurement of the SAG mill fresh feed size distribution is shown in Figure 6.18. The 25% error in the P_{80} size for the inferential model indicated in Table 5.1 and Table 5.5 is also evident here. As mentioned in Chapter 3 and Chapter 5, details of the stream information for reference data, simulation and inferential model results can be found in Appendix C. Overall the inferential model predicts a finer, more narrowly sized distribution than the reference data. This feature is also evident in the results of the inferential size distribution indication given in Table 6.12.

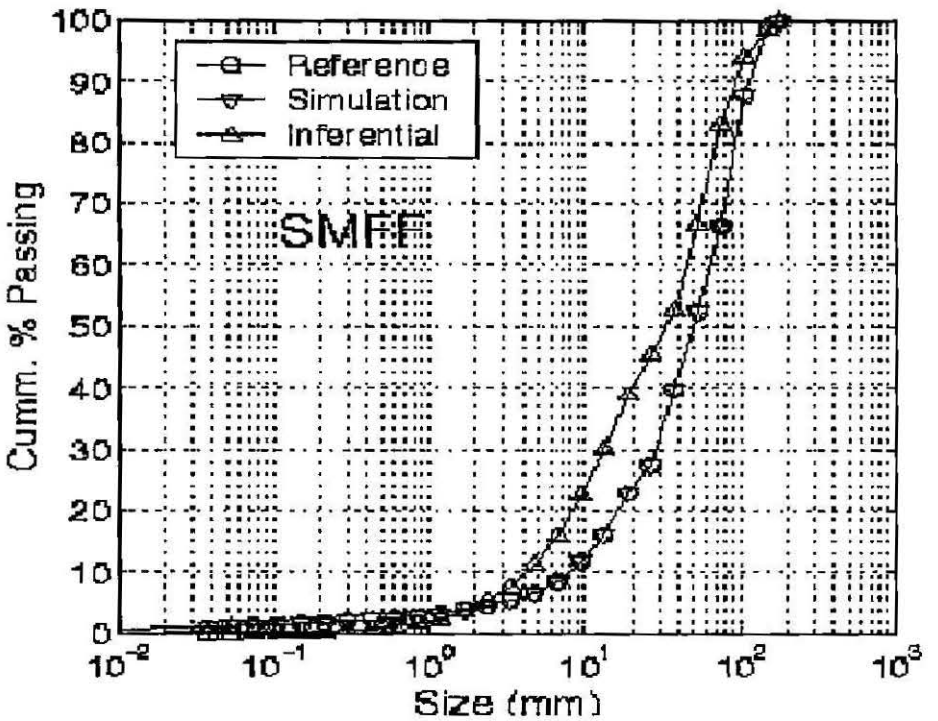

Figure 6.18: Mill Feed Size Distribution Results ($smff$)

Table 6.12: Inferential Mill Feed Size Distribution Results ($smff$)

Feed % Passing	Passing Size		
	actual (mm)	model (mm)	error (%)
F_{80}	95	71	25
F_{60}	65	46	30
F_{40}	38	20	46
F_{20}	16	8	49

As mentioned in Sections 3.4 and 5.2 for the P_{80} (F_{80}) measurement, the error in the size distribution is attributed to interpolation errors combined with minor model approximations. Also, the relative movement in the P_{80} measurement over time is considered the most important rather than the absolute value of the measurement itself, a conclusion echoed by Davies *et al.*, (2000). Furthermore, regarding the level of error increasing with decreasing size (F_{80}... F_{20}), the feed (passing) size indicators are obtained from the cummulative percent passing format of the size distribution, hence, errors in the coarse end of the distribution impact on the estimates at the fine end of the distribution. Considering these points, the size indicators are considered a satisfactory means of SAG mill feed size indication.

Table 6.13 contains the results of the plant evaluation of the commercially available *Online Ore Sizing* system (OOS) and a restatement of inferential model results of this research. The range of error for exhibited by the OOS is 8-34%. For the inferential size indication the error range is 25-49%. The comparison is favourable on the counts of validation and size range.

Validation:

The OOS would have been undergone extensive validation and evaluation in proceeding from concept to commercially available product whereas this inferential model has undergone limited validation due to resource and data availability constraints.

Size Range:

The error trends increase with decreasing particle size for both measurement methods. The feed ore studied in this research is finer than that evaluated with the OOS. Consequently, the errors are comparatively larger.

Table 6.13: Size Measurement Comparison

Feed % Passing	*OOS* System			Inferential Model		
	Passing Size	Size Error		Passing Size	Size Error	
	(mm)	(%)	(mm)	(mm)	(%)	(mm)
F_{80}	136	8.3	11.3	95	25.2	23.9
F_{60}	90	20.4	18.4	65	29.7	19.3
F_{40}	55	24.2	13.3	38	46.1	17.5
F_{20}	34	34.4	11.7	16	49.0	7.8

Rate and Density

The results for the inferential model estimates of SAG mill fresh solids feed rate and density are shown in Table 6.14 and exhibit good agreement to the Reference Data and hence deemed satisfactory. The SAG mill fresh feed rate (total) is one of the measured variables available on the plant. As a result it could be perceived that the solids feedrate estimate has a lesser importance than the other estimates presented here (especially considering the dry nature of the fresh feed stream). However, it is an important estimate since:

a) production targets are set on a (dry) solids basis, and,

b) it is an integral component of the fresh feed density estimate which is required to determine the (dry) solids production targets and, at an operational level, is a characteristic for which indiction is desirable.

Table 6.14: Inferential Model Rate and Density

item	$SMFF_{tph\_s}$	$SMFF_{\%s\,w/w}$
Reference	185.0	98.0
Inferential	184.9	98.1
Error (%)	0.0	0.0

One parameter of importance to the fresh feed density estimate but omitted from the analysis is the SAG mill feed water addition, $SMFW$, which is one of the measured variables available on the plant. The analysis for the SAG mill fresh feed density was conducted again with the SAG mill feed water addition included. The analysis showed that the feed water addition had a relative contribution to error level of 0.003% and thus was not considered further.

6.4.1 Sensitivity and Error Analyses

Sensitivity and error analyses similar to those conducted on the mill charge inferential models, see Section 6.2.1, were conducted on the SAG mill feed inferential model. Forty one (41) parameters are considered in this analysis, see Table 6.16. The effects of the total volumetric charge (J_t) and the ball charge (J_b) were studied here in lieu of considering approximately half of the parameters studied for the mill charge inferential models, see Table 6.2. The additional parameters here are either unique or relatively important to the feed rate and size models.

Size

Equation (6.1) was applied to the mill feed inferential model to estimate the uncertainty in the passing size estimates. Table 6.15 contains the uncertainty estimates for the feed size indicators which range from 2 to 7×10^6 %. These extraordinarily high uncertainty estimates are attributed to *compensating errors*. The fresh feed stream is the final step in the inferential model calculation sequence (Step 6). The prevalent utilisation of the rules for the (partial) differentiation of sums and products and the chain rule have resulted in an over-estimation of the feed size distribution uncertainty. Considering the current symbolic manipulation capabilities of Maple, this method for uncertainty calculation appears unsuitable for this model. Further investigation of other methods for uncertainty estimation was deemed beyond the scope of this research.

Table 6.15: Mill Feed Size Uncertainty Summary

Feed % Passing	Passing Size			
	actual (mm)	model (mm)	error (%)	uncertainty (%)
F_{80}	95	71	25	2×10^6
F_{60}	65	46	30	4×10^6
F_{40}	38	20	46	5×10^6
F_{20}	16	8	49	7×10^6

Table 6.16: SAG Mill Fresh Feed Model Parameters, θ_j

j	Parameter, θ_j	Value	Error	%Error
1.	$OSCF_{tph\_p}$, oversize crusher feedrate (t/hr) (Measured Variable)	67.12	6.7	10
2.	$OSCF_{\%s\ w/w}$, oversize crusher density (%sols w/w) (Assumption)	99.92	1.0	1
3.	x_p, pebble port diameter (mm)	74.11	7.4	10
4.	$PCFD_{m3ph\_p}$, primary cyclone feed flowrate (m^3/hr) (Measured Variable)	243	24.3	10
5.	$PCFD_{\%s\ w/w}$, primary cyclone feed density (%sols w/w) (Measured Variable)	50.8	5.1	10
6.	$SMD50c$, SAG mill discharge screen corrected 50% passing size (mm)	5.0	3.0	60
7.	$PCFW_{m3ph\_l}$, primary cyclone feed water addition flowrate (m^3/hr) (Measure Variable)	99.25	9.9	10
8.	SG_s, ore specific gravity (t/m^3)	2.65	0.26	10
9.	SG_l, water specific gravity (t/m^3)	1.00	0.10	10
10.	x_m, SAG mill model fine size (mm)	0.5427	0.054	10
11.	r_n, relative radius of outermost grate (fraction)	0.9720	0.029	3
12.	$foag$, fraction open area (fraction)	0.1790	0.0215	12
13.	D_{mill}, SAG mill diameter (m)	7.12	0.14	2
14.	L_{mill}, SAG mill length (m)	3.53	0.14	4
15.	γ, relative radial position of the open area (fraction)	0.8031	0.05	6
16.	RPM, mill speed (RPM)	12.014	0.6	5
17.	f_p, pebble port relative open area (fraction of the open area)	0.011	0.011	100
18.	SG_b, ball specific gravity (t/m^3)	7.8	1.56	20
19.	ϵ, charge voidage (fraction)	0.40	0.04	10
20.	J_b, volumetric ball charge (fraction)	0.142	0.028	20

j	Parameter, θ_j	Value	Error	%Error
21.	D_b, ball diameter (mm)	125	12.5	10
22.	$smbc_2$, ball charge size distribution - weight retained in *size* 2 (%)	1	0.1	10
23.	$smbc_3$, ball charge size distribution - weight retained in *size* 3 (%)	50	5.0	10
24.	$smbc_4$, ball charge size distribution - weight retained in *size* 4 (%)	35	3.5	10
25.	$smbc_5$, ball charge size distribution - weight retained in *size* 5 (%)	14	1.4	10
26.	$smbc_6$, ball charge size distribution - weight retained in *size* 6 (%)	0	1	
27.	$smbc_7$, ball charge size distribution - weight retained in *size* 7 (%)	0	1	
28.	J_t, total volumetric charge (fraction)	0.2298	0.046	20
29.	A, ore impact breakage parameter	78.5	7.85	10
30.	b, ore impact breakage parameter	0.45	0.045	10
31.	ta, re abrasion breakage parameter	0.13	0.013	10
32.	$ln(R0)$, logarithm of breakage rate R0	0	0.50	
33.	$ln(R1)$, logarithm of breakage rate R1	1.781	0.53	30
34.	$ln(R2)$, logarithm of breakage rate R2	3.800	0.19	5
35.	$ln(R3)$, logarithm of breakage rate R3	3.996	0.20	5
36.	$ln(R4)$, logarithm of breakage rate R4	2.544	0.51	20
37.	$ln(R5)$, logarithm of breakage rate R5	2.458	0.25	10
38.	$ln(R6)$, logarithm of breakage rate R6	2.458	0.25	10
39.	$F_{80\,i-1}$, F_{80} from the previous time step	70.7	21	30
40.	$RecRatio_{i-1}$, ratio of the $-20 + 4mm$ material in the oversize crusher product to similarly sized material in the mill feed from the previous time step (fraction)	0.144	0.014	10
41.	PC_{split}, primary cyclone underflow split to ball mill (fraction)	0.9995	0.1	10

Again, despite the uncertainty over-estimation, the relative contribution to the estimate error (RCE) is considered insightful and worth presenting. Figure 6.19 contains the relative contribution to the error, RCE, for the F_{80} feed size indicator. The RCE graphs for the F_{60} to F_{20} feed size indicators are the same as the RCE curve for the F_{80} size indicator, for all intents and purposes. This means that although different magnitudes of error are present in the size indicators, the sources of error and their relative contribution to the estimate error are the same.

From Figure 6.19, the parameters that have the most influence on the uncertainty in the inferential SAG mill fresh feed size distribution measurement are:

j	θ_j	Description
1	$OSCF_{tph\_p}$	oversize crusher feedrate (t/hr) (Measured Variable)
3	x_p	pepple port diameter (mm)
5	$PCFD_{\%s\ w/w}$	primary cyclone feed density (%sols w/w) (Measured Variable)
17	f_p	pebble port relative open area (fraction of the open area)

Rate and Density

Equation (6.1) was applied to the mill feed inferential model to estimate the uncertainty in the rate and density estimates. Table 6.17 contains the uncertainty estimates for the rate and density estimates. Whilst not as high as the estimated uncertainty in the feed size estimates, the levels estimated here (600 to 3,000%) are considered an over-estimation of the uncertainty. The *compensating errors*, attributed to the recurrent presence of variables in this and preceding calculation steps of the inferential model calculation sequence, has resulted in uncertainty over-estimation. Once again, considering the current symbolic manipulation capacity of Maple, this method for uncertainty calculation appears unsuitable for this model. Again, further investigation of other methods for uncertainty estimation was deemed beyond the scope of this research.

For insight into parameter influence on the estimate uncertainty, Figure 6.20 contains the relative contribution to the error, RCE, for the SAG mill fresh feed density, $SMFF_{\%s\,w/w}$, estimate. The SAG mill fresh solids feedrate, $SMFF_{tph\_s}$, is not shown since it is the same as Figure 6.20, for all intents and purposes.

Table 6.17: Mill Feed Rate and Density Uncertainty Summary

item	$SMFF_{tph\_s}$	$SMFF_{\%s\,w/w}$
Reference	185.0	98.0
Inferential	184.9	98.1
Error (%)	0.0	0.0
Uncertainty (%)	3×10^3	6×10^2

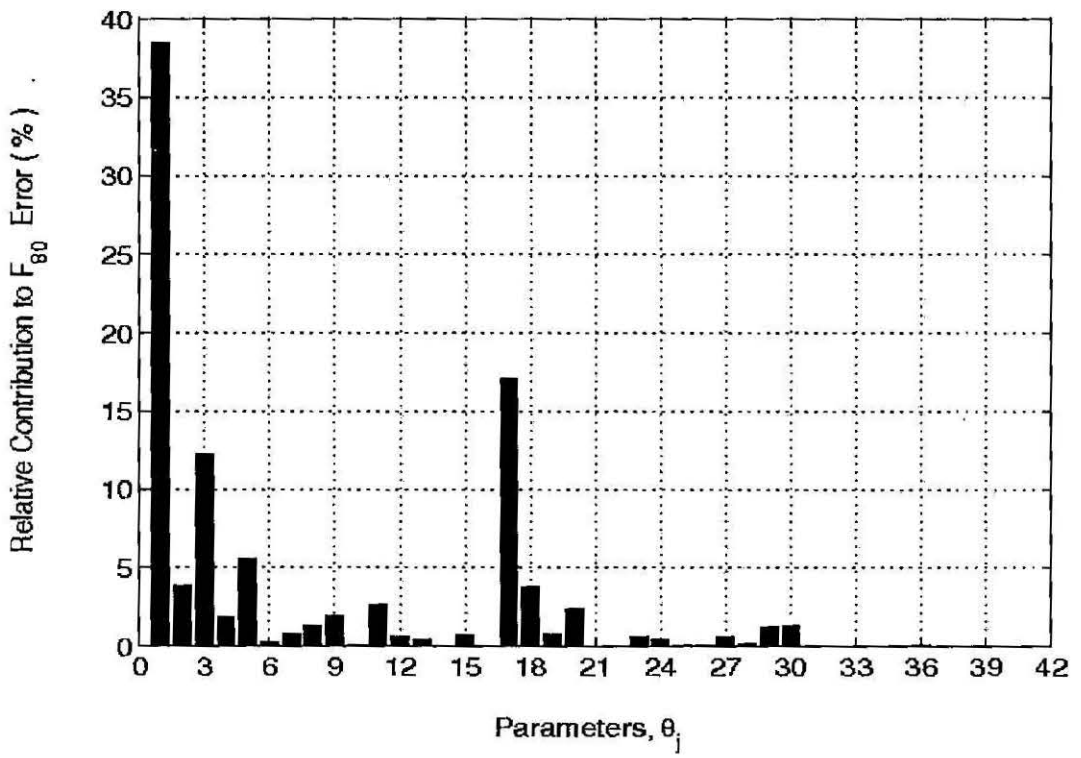

Figure 6.19: SAG Mill Fresh Feed Size Indication Uncertainty

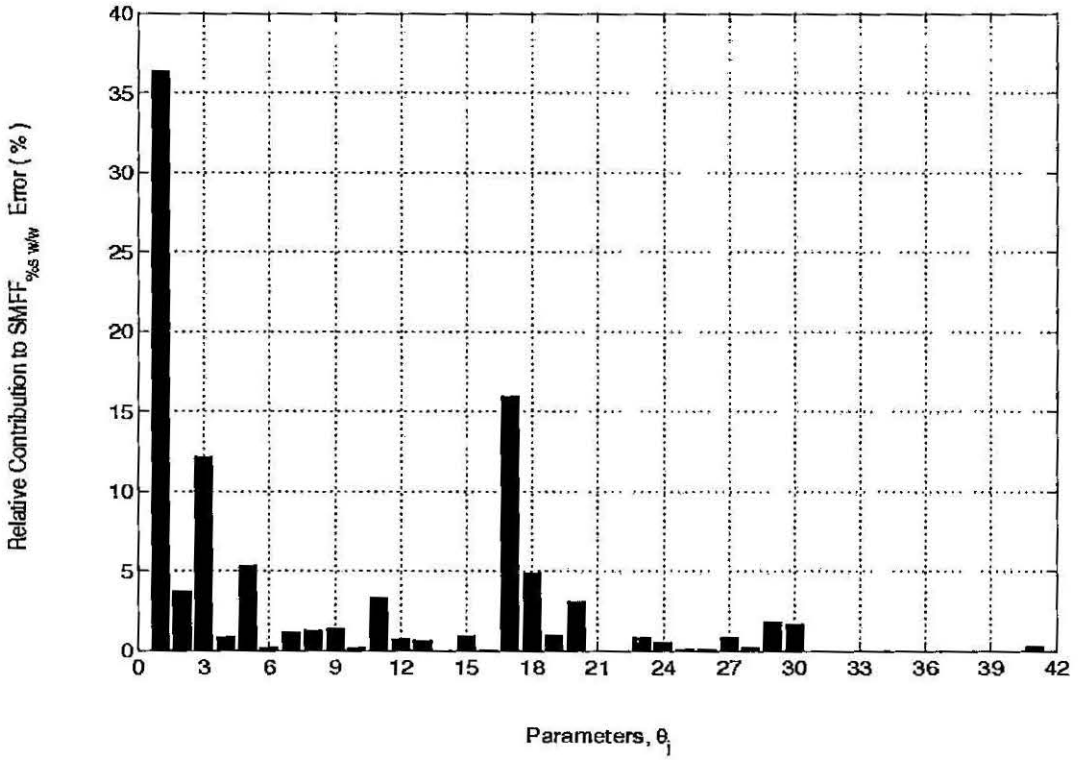

Figure 6.20: SAG Mill Fresh Feed Density Indication Uncertainty

On the comparison of Figure 6.20 with Figure 6.19 it is evident that the parameters that most influence the uncertainty of the SAG mill fresh feed solids rate and density are exactly those that strongly influence the SAG mill fresh feed size indicators, namely,

- oversize crusher feedrate, $OSCF_{tph\_p}$
- pebble port diameter, x_p
- primary cyclone feed density, $PCFD_{\%s\,w/w}$
- pebble port relative open area, f_p

6.4.2 SAG Mill Fresh Feed Model Summary

From the observations made in Section (6.4.1), it is possible to conclude that the inferential model of the SAG mill fresh feed provides satisfactory indication of fresh feed rate, density and size distribution. Also, due to the influence that the process measurements, the oversize crusher product and the SAG mill discharge grate parameters have on the uncertainty of the mill discharge estimates, it is possible to conclude that to minimise uncertainty in the inferential feed size indicators and the solids rate and feed density estimates:

- the accuracy of the oversize crusher feed rate, $OSCF_{tph\_p}$, should be checked regularly, *e.g.*, by calibration checks and belt-cuts.
- due to the implicit importance of the oversize crusher product size (via $OSCF_{tph\_p}$), the accuracy of the crusher gap setting should be checked regularly, *e.g.*, by dipping the crusher with a lead bob.
- calibration checks of the primary cyclone feed density gauge measurement, $PCFD_{\%s\ w/w}$, should be conducted regularly to ensure accuracy.
- the SAG mill discharge grate parameters, x_p and f_p, should be fitted with due care.

6.5 Breakage Rates Analysis

In the development and validation of the dynamic model of the SAG mill, see Section 4.2.3, a high degree of model sensitivity to the SAG mill breakage rates, r_i, was encountered. These rates are determined by interpolation of a number of key "knot" points - $ln(R1)$ to $ln(R5)$, see Equations (3.22) to (3.26) in Section 3.3.1. These SAG mill breakage rate parameters either did not feature at all, or, did not feature prominently in the uncertainty analysis of the SAG mill feed size inferential measurement.

However, to investigate which are the influential parameters in the determining the breakage rates, the model parameters $ln(R1)$ to $ln(R6)$ (Equations (3.22) to (3.26) and a bounding term) were considered in an uncertainty analysis. Table 6.18 contains the results of this analysis. These results were utilised in uncertainty analysis of the inferential measurement of the SAG mill fresh feed size, see Table 6.16. The results of the relative contribution to error (RCE) analysis are shown in Figure 6.21 and Figure 6.22.

Table 6.18: Breakage Rate Uncertainty Results

Parameter		Value	Error	%Error
$ln(R1)$	logarithm of breakage rate R1	1.78	0.53	30
$ln(R2)$	logarithm of breakage rate R2	3.80	0.19	5
$ln(R3)$	logarithm of breakage rate R3	4.00	0.20	5
$ln(R4)$	logarithm of breakage rate R4	2.54	0.51	20
$ln(R5)$	logarithm of breakage rate R5	2.46	0.25	10
$ln(R6)$	logarithm of breakage rate R6	2.46	0.25	10

The breakage rates are influenced by the following six parameters:

j	θ_j	Description
13	D_{mill}	SAG mill diameter (m)
* 16	RPM	mill speed (RPM)
* 20	J_b	volumetric ball charge (fraction)
21	D_b	ball diameter (mm)
* 39	$F_{80\,i-1}$	F_{80} from the previous time step
40	$RecRatio_{i-1}$	ratio of the $-20 + 4mm$ material in the oversize crusher product to similarly sized material in the mill feed from the previous time step (fraction)

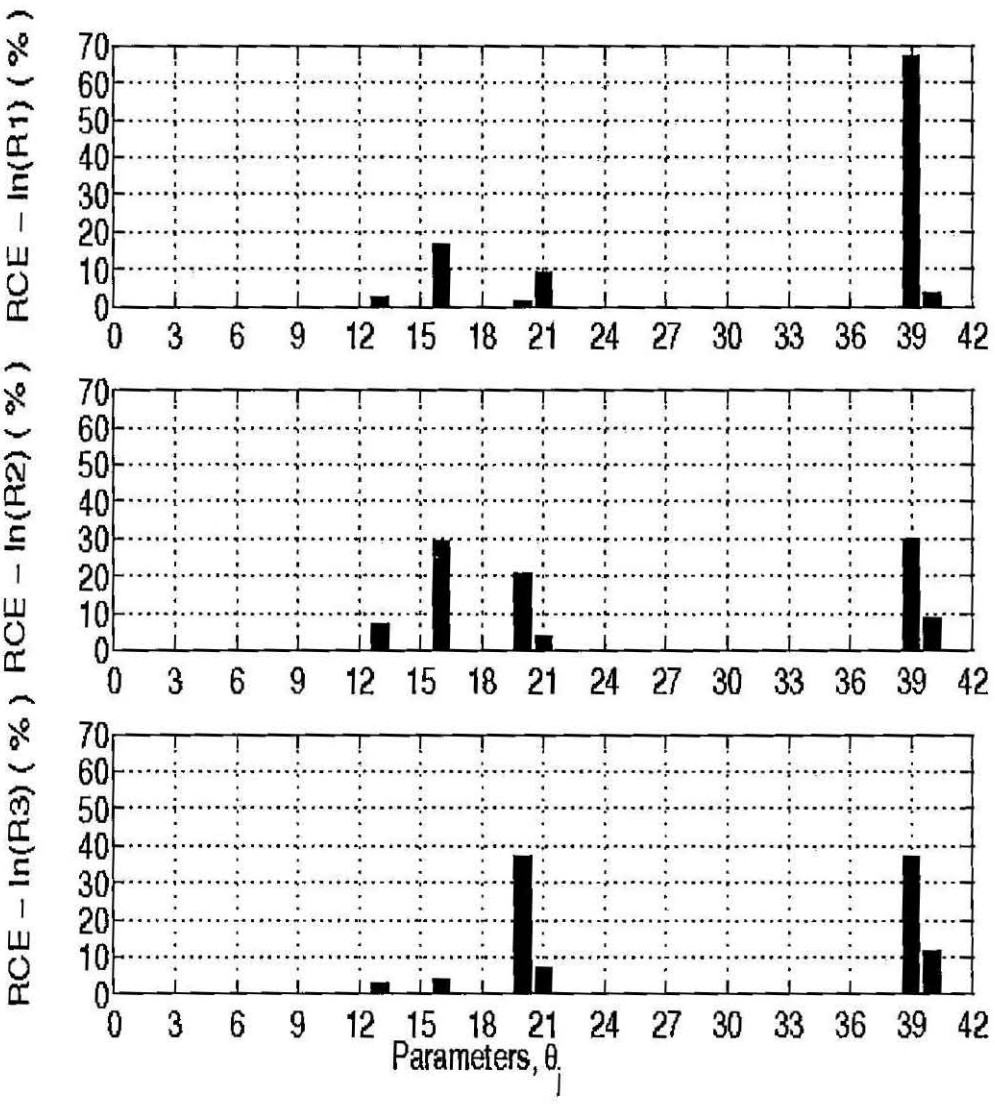

Figure 6.21: SAG Mill Breakage Rates ($ln(R1 - R3)$) Uncertainty

The three parameters that have the most influence on the uncertainty in the breakage rates are those marked with an asterisk (*), namely, mill speed (RPM), volumetric ball charge level (J_b) and F_{80} from the previous time step ($F_{80\,i-1}$).

The ball charge level, J_b, and feed eighty percent passing size, F_{80}, are of particular interest here considering they are two of the inferential measurements discussed earlier in this Chapter. The recycle ratio of material in the size range of $-20 + 4$ mm, $RecRatio_{i-1}$, is also topical since it is based on the fresh feed size distribution, $smff$, whose estimate is discussed in the previous Sections. It is also based on the oversize crusher product, $oscp$, which is the product of oversize crusher's treatment of the oversize crusher feed estimate, $oscf$, see Chapter 5.

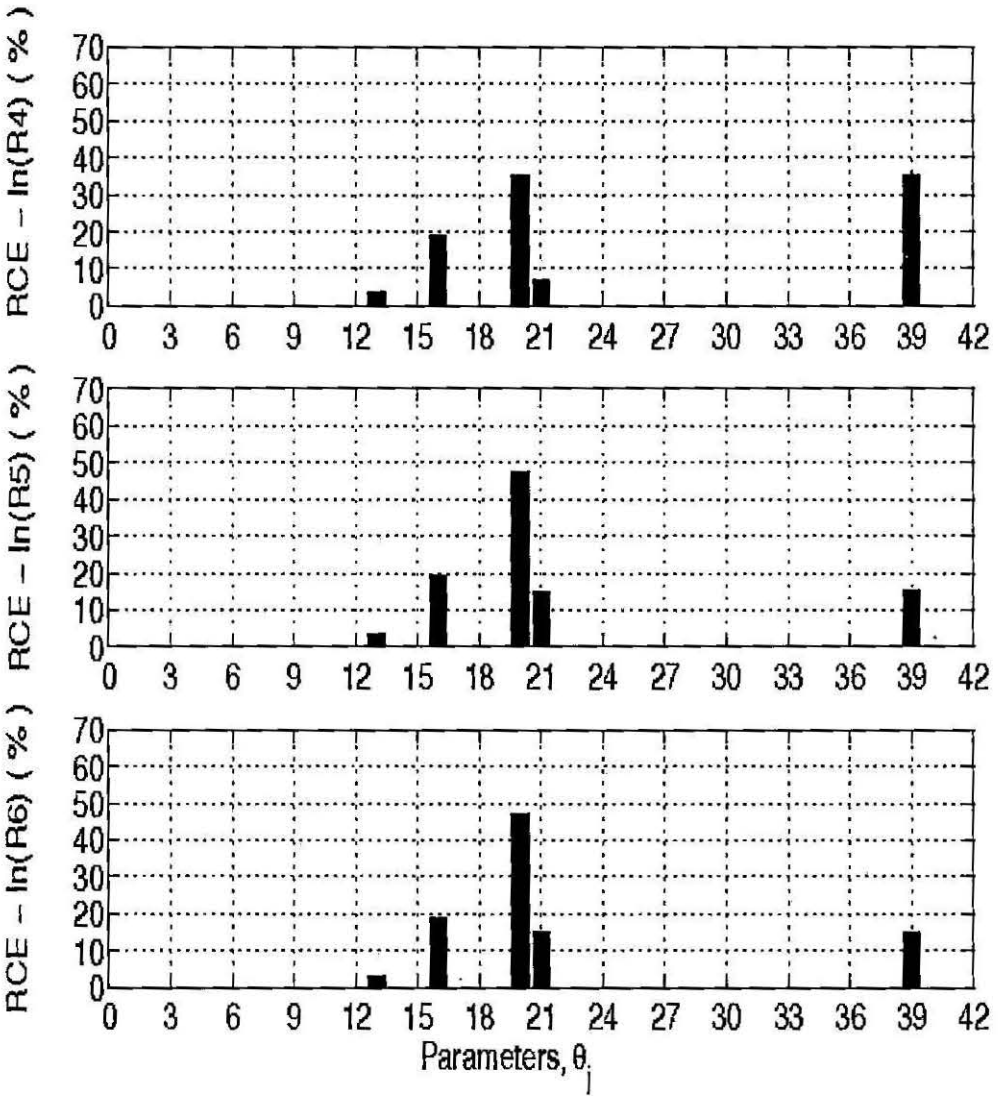

Figure 6.22: SAG Mill Breakage Rates ($ln(R4 - R6)$) Uncertainty

Therefore, the uncertainty in the inferential measurement of the SAG mill fresh feed is influenced by:

- the inferential model of the SAG mill ball charge level, J_b
- the estimate of the oversize crusher feed size distribution, $oscf$
- the inferential measurement of the SAG mill fresh feed itself via the eighty percent passing size, F_{80}

These points, particularly the latter point, represent a *recycling* of errors. Considering the inferential models behaved well in their validation and the comparative insignificance

of these parameters in the relative contribution to estimate error, RCE, in the inferential measurement model of the SAG mill feed size distribution, see Figure 6.19, further investigation of the effects of the *recycling* of errors was not pursued.

To minimise the uncertainty in the breakage rates (r_i) the uncertainty in the ball charge level (J_b), SAG mill fresh feed ($SMFF/smff$) and oversize crusher feed ($OSCF/oscf$) and product ($OSCP/oscp$) should be maintained at a low level which corresponds to:

- utilising the mill weight residual for charge estimates, utilising the best available mill weight measurement and periodic measurement of the mill diameter and mill length, see Section 6.2.
- ensuring the accuracy of the crusher and cyclone feed process measurements by regular calibration, ensuring the accuracy of the crusher gap setting by regular dipping and careful fitting of he SAG mill discharge grate parameters, see Section 6.4.
- model fitting the oversize crusher model (Section 3.3.3) with due care.

6.6 Primary Cyclone Underflow Split to the Ball Mill

The primary cyclone underflow split to the ball mill, PC_{split}, was considered as one of the parameters in the preceding analyses. It should be noted that it is possible to construct an inferential model of the split. Thorough detailing and analysis of such a model is considered beyond the scope of the present work. However, a general description of the model is presented here.

In a discrete time frame, a combination of:

- present estimates of the SAG mill discharge, oversize crusher feed and primary cyclone feed streams,
- the primary cyclone underflow split to the ball mill, and
- models of the oversize crusher and primary cylone,

allows the construction of a mass balance to estimate the current primary cyclone underflow split to ball mill.

Equations (6.17) to (6.18) express the model in mathematical terms.

$$PCUS_{tph\_sk} = SMDC_{tph\_sk} - OSCP_{tph\_sk} - SMFF_{tph\_sk} \tag{6.17}$$

$$PC_{split\,k} = 1 - \frac{PCUS_{tph\_sk}}{PCUF_{tph\_sk}} \tag{6.18}$$

where

$PCUS_{tph\_sk}$	=	the solids component of the primary cyclone underflow reporting to SAG mill feed chute
$PCUF_{tph\_sk}$	=	the primary cyclone underflow (obtained by the application of the primary cyclone model to the primary cyclone feed, $PCFD_k$)
$OSCP_{tph\_sk}$	=	the solids component arising from the application of the oversize crusher model
$OSCF_k$	=	the oversize crusher feed estimate
$SMDC_k$	=	the SAG mill discharge estimate
$SMFF_k$	=	the SAG mill fresh feed estimate
k	=	current time step

The estimation of the primary cyclone underflow split to the ball mill, PC_{split}, is important since it allows the primary grinding circuit mass balance to be fully defined. The full mass balance definition enhances the awareness of and the ability to optimise operating conditions.

6.7 Summary

Sensitivity and error analyses have been conducted on the inferential models described in Chapter 5. This Chapter has resulted in the following innovations (summarised in Table 6.19):

Mill Charge Levels : In Section 6.2, the analysis of the inferential mill inventory models concluded that the total (J_t) and ball charge (J_b) level estimates from the mill weight residual, Equation (6.6), are acceptable and contain less uncertainty than the estimates from the mill power draw residual, Equation (6.5). On account of the lower uncertainty, the mill weight residual is the recommended residual for charge level estimation. To ensure the low uncertainty level, it is recommended that the best available mill weight measurement, MV_{wt}, be utilised and mill diameter, D_{mill}, and mill length, L_{mill}, be measured at regular intervals to account for shell liner wear. The mill diameter, D_{mill}, measurements could be supplemented by and utilised to tune a dynamic mill liner model, *e.g.*, the model proposed in Chapter 5.

Mill Discharge : In Section 6.3, the discharge rate, density and size distribution estimates from SAG mill discharge inferential models were assessed as acceptable. On account of their influence on the estimate uncertainty, it is recommended that the oversize crusher and primary cyclone feed process measurements, the discharge screen aperture and the process water specific gravity be checked periodically.

Mill Feed : In Section 6.4, it was concluded that the inferential model of the SAG mill fresh feed provides satisfactory indication of fresh feed rate, density and size distribution. Due to their influence on the estimate uncertainties it is recommended to regularly check the oversize crusher feed conveyor calibration and gap setting and the primary cyclone feed density measurement. Diligent model fitting of the SAG mill discharge grate parameters is also recommended.

Breakage Rates : Due to model sensitivity to the SAG mill breakage rates encountered in the dynamic model development, the uncertainty in the breakage rates was also analysed, see Section 6.5. Mill speed, ball charge level, feed eighty percent passing size and oversize crusher feed size distribution were highlighted by the breakage rates analysis. The recommendations regarding the SAG mill fresh feed and inventory inferential models apply here and also the diligent model fitting of the oversize crusher model.

Cyclone Underflow Split : In Section 6.6, the inferential modelling of the primary cyclone underflow split to the ball mill was introduced. Considered as one of the parameters throughout this Chapter, the importance of the underflow split model was highlighted since it allows the primary grinding circuit mass balance to be fully defined, enhancing the awareness of and ability to optimise the operating conditions.

Table 6.19: Chapter 6 Innovation Summary

Section	Innovation
	The analysis and assessment of:
Section 6.2	• the inferential mill inventory models
Section 6.3	• the mill discharge rate, density and size distribution inferential models
Section 6.4	• the SAG mill fresh feed rate, density and size distribution inferential models
Section 6.5	• the SAG mill breakage rates model
Section 6.6	The introduction of the primary cyclone underflow split to the ball mill inferential model

Chapter 7

Combined State and Parameter Estimation Model

The inferential models of the SAG mill charge based on mill weight and power draw presented in Chapter 5 and analysed in Chapter 6 are not the only alternatives available for inferential charge measurement. As discussed in Chapter 2, a number of alternatives are available including the use of:

- conductivity probe measurements and energy balance
- acoustic spectral analysis and sound measurements
- state estimation

Comparative study of the former three is beyond the scope of this research. However, utilisation of the simulation models within a combined state and parameter estimation (CSPE) framework is a feasible extension of this work. Hence, a brief comparative study of two CSPE formulations follows. The purpose of this comparative investigation is to place the new inferential models into context by presenting their results alongside those of a method that has been utilised for some time and is gaining a degree of acceptance in industry. The purpose is not to recommend one method or model over another, since application selection would be expected to be on a case by case basis depending on the knowledge and expertise available and the process measurements available.

The formulation and context of the CSPE problem, along with details of Kalman filters, are discussed in Section 7.1. Intrinsic to the formulation are the measurement models which are presented in Section 7.2. The CSPE results are detailed in Section 7.3, including discussion on system observability and detectability and further measurement model development.

7.1 CSPE Model Formulation

Continuous-time nonlinear systems can be described as follows (Henson and Seborg, 1997):

$$\dot{x}(t) = \mathbf{f}(x, u, \theta, t) \tag{7.1}$$

$$\dot{\theta} = 0 \tag{7.2}$$

$$y(t) = \mathbf{g}(x, \theta, t) \tag{7.3}$$

where

x = the state of the system
u = the system input
y = the system output
t = time
θ = system model parameters to be estimated (assumed constant)
$\mathbf{f}$ = the system function
$\mathbf{g}$ = the measurement function

Equation (7.1) through Equation (7.3) is referred to as a combined state and parameter estimation (CSPE) model since it is utilised to estimate states (x) and parameters (θ), the latter are assumed to be constant. The problem formulation described here and the description of the measurement function for the SAG mill discharge stream, in Section 7.2, is based on material from the conference paper (Apelt *et al.*, 2001b).

In discrete-time, where measurements are only available at equally spaced intervals (sampling periods) Δt, Equation (7.1) through Equation (7.3) can be described as follows (Henson and Seborg, 1997):

$$x_{k+1} = \bar{\mathbf{f}}(x_k, u_k, \theta_k, k) \tag{7.4}$$

$$\theta_{k+1} = \theta_k \tag{7.5}$$

$$y_k = \bar{\mathbf{g}}(x_k, \theta_k, k) \tag{7.6}$$

where

k = discrete time index ($k\Delta t$)
$\bar{\mathbf{f}}$ = the discrete system function
$\bar{\mathbf{g}}$ = the discrete measurement function

One method of on-line state and parameter estimation achieved through the utilisation of an extended Kalman filter on the system, as described by Equation (7.7) through Equation (7.13) (Henson and Seborg, 1997).

$$\hat{x}_{k|k} = \hat{x}_{k|k-1} + L_k(y_k - \bar{\mathbf{g}}(\hat{x}_{k|k-1}, \hat{\theta}_{k|k-1}, k)) \tag{7.7}$$

$$L_k = \hat{P}_{k|k-1}\bar{G}_k^T(\bar{G}_k\hat{P}_{k|k-1}\bar{G}_k^T + R)^{-1} \tag{7.8}$$

$$\hat{P}_{k|k} = (I - L_k\bar{G}_k)\,\hat{P}_{k|k-1} \tag{7.9}$$

$$\hat{x}_{k+1|k} = \bar{\mathbf{f}}(\hat{x}_{k|k}, \hat{\theta}_{k|k}, u_k, k) \tag{7.10}$$

$$\hat{P}_{k+1|k} = \bar{F}_k\hat{P}_{k|k}\bar{F}_k^T + Q \tag{7.11}$$

$$\bar{G}_k = \left.\frac{\partial\bar{\mathbf{g}}(x,\theta,k)}{\partial x}\right|_{x=\hat{x}_{k|k-1},\,\theta=\hat{\theta}_{k|k-1}} \tag{7.12}$$

$$\bar{F}_k = \left.\frac{\partial\bar{\mathbf{f}}(x,\theta,u,k)}{\partial x}\right|_{x=\hat{x}_{k|k},\,\theta=\hat{\theta}_{k|k},\,u=u_k} \tag{7.13}$$

$\hat{x}_{k|k}$ = the filtered estimate of state x at time $k\Delta t$ (*correction*)

$\hat{x}_{k|k-1}$ = the prediction of state x at time $k\Delta t$ from the previous time step (*prediction*)

L_k = the Kalman filter gain at time $k\Delta t$

I = identity matrix

$\bar{G}_k$ = linearised, discrete-time measurement function

$\bar{F}_k$ = linearised, discrete-time system function

$\hat{P}_{k|k}$ = the *a posteriori* estimation error covariance matrix

$\hat{P}_{k+1|k}$ = the *a priori* estimation error covariance matrix

Q = the state covariance matrix

R = the process output (measurement) covariance matrix

The term "*extended* Kalman filter" is used when the measurement ($\bar{\mathbf{g}}$) and system ($\bar{\mathbf{f}}$) functions are linearised about a given operating point, see Equations (7.12) and (7.13), respectively (Henson and Seborg, 1997) as is the case here.

7.1.1 CSPE Model Context and Kalman Filter Discussion

The Kalman filter estimation procedure is presented in block diagram format in Figure 7.1. Here, the SAG mill process is the continuous-time nonlinear system described by Equations (7.1) to (7.3) and is the "Process" block in Figure 7.1. The behaviour of the SAG mill process is defined by the system function **f**. The prevailing operating conditions of the SAG mill process are defined by the states, x, and parameters, θ, of the system. How the SAG mill process reached the current operating conditions is a function of the system function **f**, the system the states, x, and parameters, θ, the system inputs, u, (control actions) and time, t.

There are two measurements of the SAG mill "Process", in this case, that indicate what is taking place in the SAG mill, namely, mill powerdraw and weight. These measurements constitute the measurement function **g** in Equation (7.3), which is also a function of the system states, x, and parameters, θ.

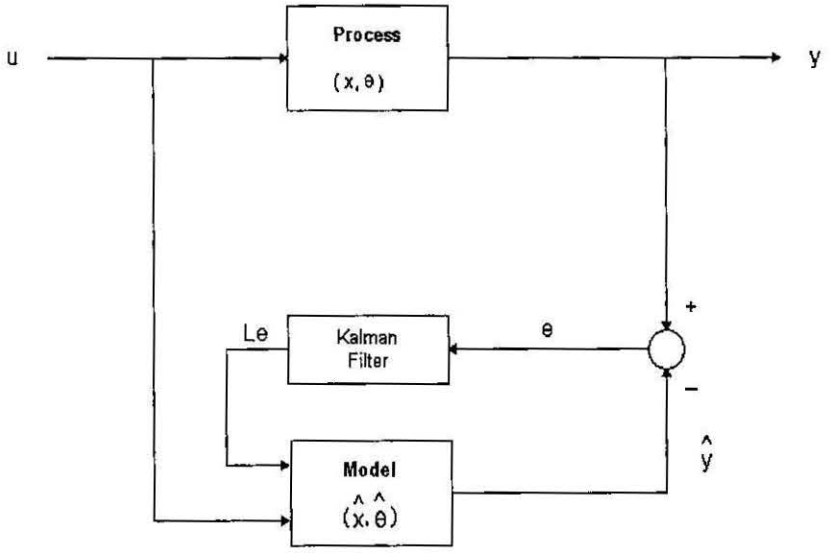

Figure 7.1: Kalman filter block diagram illustrating the Process and how the Kalman Filter adds corrections to the Model.

In the ideal case, all of the system states, x, and parameters, θ, and the discrete system function $\mathbf{f}$ are known. However, this is rarely the case and is not the case here. The states and parameters of the SAG mill process are not known or measured. Therefore, they must be estimated. Estimated states and parameters are distinguished from actual states and parameters by using the *hat* nomenclature, *e.g.*, the estimation of state x is $\hat{x}$.

The estimation of the "Process" is the "Model" block in Figure 7.1. Since the model is not a perfect estimate of the process, an error, e, is introduced, which is the difference between the actual system output, y, (the measurements) and the estimated system output, $\hat{y}$. The Kalman filter gain, L is applied to the error by the "Kalman Filter" to improve the state, parameter and system output estimates of the "Model". When the error is positive, the change in the state, $\hat{\dot{x}}$ is also positive. Figure 7.2 illustrates how an increase in the rate of change in a state, $\dot{x}$ translates to a more rapid increase in the state estimate, x.

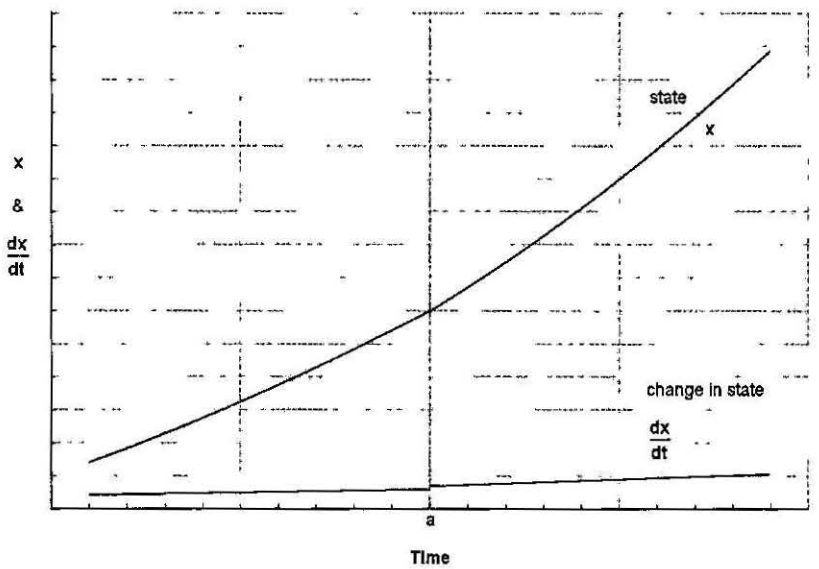

Figure 7.2: A linearly increasing Change in State $\left(\frac{dx}{dt}\right)$ translates to a quadratically increasing State x. The rate of change in the state changes at time = a, which translates to a more rapidly changing state.

The actual process defined by Equation (7.1) to (7.3) may now be restated as the model of the process in Equations (7.14) to (7.17).

$$\dot{\hat{x}}(t) = \mathbf{f}(\hat{x}, u, \hat{\theta}, t) + Le \tag{7.14}$$

$$\dot{\hat{\theta}} = 0 \tag{7.15}$$

$$\hat{y}(t) = \mathbf{g}(\hat{x}, \hat{\theta}, t) \tag{7.16}$$

$$e = y - \hat{y} \tag{7.17}$$

In discrete time, this system can be described by Equations (7.18) to (7.21).

$$\hat{x}_{k+1} = \bar{\mathbf{f}}(\hat{x}_k, u_k, \hat{\theta}_k, k) + L_k\, e_k \tag{7.18}$$

$$\hat{\theta}_{k+1} = \hat{\theta}_k \tag{7.19}$$

$$\hat{y}_k = \bar{\mathbf{g}}(\hat{x}_k, \hat{\theta}_k, k) \tag{7.20}$$

$$e_k = y_k - \hat{y}_k \tag{7.21}$$

where

e_k = error between the system output at time nstep k, y_k, and estimated system output at time step k, $\hat{y}_k$

$\bar{\mathbf{f}}$ = the discrete system function

$\bar{\mathbf{g}}$ = the discrete measurement function

k = discrete time index

L_k = Kalman filter gain

Another common way to describe the system is in terms of a state transition matrix, A, the control transition matrix, B, the measurement matrix, C and the direct connection matrix, D (usually zero). The system function $\mathbf{f}$ may be block-partitioned to form the state transition matrix, A, and the control transition matrix, B. The measurement function $\mathbf{g}$, may be partitioned to form the measurement matrix, C, and the direct connection matrix, D. Equations (7.22) to (7.25) presents the estimated system in discrete time and in terms of the transition and measurement matrices.

$$\hat{x}_{k+1} = \bar{\mathbf{A}}\left(\hat{x}_k, \hat{\theta}_k, k\right) + \bar{\mathbf{B}}\left(u_k, k\right) + L_k\, e_k \tag{7.22}$$

$$\hat{\theta}_{k+1} = \hat{\theta}_k \tag{7.23}$$

$$\hat{y}_k = \bar{\mathbf{C}}\left(\hat{x}_k, \hat{\theta}_k, k\right) \tag{7.24}$$

$$e_k = y_k - \hat{y}_k \tag{7.25}$$

where

$\bar{A}$ = discrete-time state transition matrix that defines the dynamic behaviour of the continuous-time nonlinear system

$\bar{B}$ = discrete-control transition matrix that relates the effects of control actions on the continuous-time nonlinear system

$\bar{C}$ = discrete-time measurement matrix that relates the system states to the process measurements

7.1.2 Kalman Filter: Predictor – Corrector

The Kalman filter can be considered a *predictor – corrector* algorithm (Welch and Bishop, 2001). In the prediction step, the Kalman filter predicts the states, $\hat{x}$, and the error covariance matrix, $\hat{P}$, one time-step into the future, see Equations (7.10) and (7.11), respectively.

One time-step later, the correction step takes place, which consists of calculating the Kalman filter gain, L (Equation (7.8)), adjusting the state estimates (Equation (7.7)), and adjusting the states covariance matrix (Equation (7.9)). The next prediction occurs immediately before the process moves one time-step forward, at which point the next correction is undertaken. Note that estimates of the intial states, $\hat{x}_0$, state covariance matrix, Q, and the measurement covariance matrix, R are required initially.

Assuming the correction has just taken place at time step k, the Kalman filter formulation predicts one time step into the future (time step = $k + 1$). The predictions are classified *a priori*, they are predicted before the time step takes place. Two predictions are made, firstly the future state, $\hat{x}_{k+1|k}$, is estimated, see Equation (7.26). Secondly, the *a priori* error covariance matrix, $\hat{P}_{k+1|k}$, is estimated, see Equation (7.27).

Time Step: k Prediction Step

$$\hat{x}_{k+1|k} = \bar{\mathrm{f}}(\hat{x}_{k|k}, \hat{\theta}_{k|k}, u_k, k) \tag{7.26}$$

$$\hat{P}_{k+1|k} = \bar{F}_k \hat{P}_{k|k} \bar{F}_k^T + Q \tag{7.27}$$

The time step transpires and the Kalman filter compares its prediction from the previous step with where it understands the process to be this time step and makes the appropriate corrections. The corrections are classified *a posteriori*, they are made after the system moves one time-step forward. The filter makes two corrections, firstly to the state estimates $\hat{x}_{k+1|k+1}$, see Equation (7.28). Secondly, a correction is made to the estimated error covariance matrix to give the *a posteriori* estimated error covariance matrix, $\hat{P}_{k+1|k+1}$, see Equation (7.30).

The state corrections are achieved via the residual (or "innovation") $(y_{k+1} - \bar{\mathbf{g}}(\hat{x}_{k+1|k}, \hat{\theta}_{k+1|k}, k+1))$ in Equation (7.28), weighted by the Kalman filter gain, L_{k+1}, which is calculated to minimise the *a posteriori* estimated error covariance, Equation (7.30). The residual has more impact on the corrected state estimate if the measurement covariance matrix, R, is small (larger Kalman filter gain) than if the *a priori* estimated error covariance matrix, $\hat{P}_{k+1|k}$, is small, refer to Equation (7.29). Therefore, the estimate will always weight in favour of dependable measurements. Further discussion of the selection and relative magnitudes of the element is contained in Section 7.3.2.

Time Step: $k+1$ Correction Step

$$\hat{x}_{k+1|k+1} = \hat{x}_{k+1|k} + L_{k+1}(y_{k+1} - \bar{\mathbf{g}}(\hat{x}_{k+1|k}, \hat{\theta}_{k+1|k}, k+1)) \tag{7.28}$$

$$L_{k+1} = \hat{P}_{k+1|k}\bar{G}_{k+1}^T(\bar{G}_{k+1}\hat{P}_{k+1|k}\bar{G}_{k+1}^T + R)^{-1} \tag{7.29}$$

$$\hat{P}_{k+1|k+1} = (I - L_{k+1}\bar{G}_{k+1})\,\hat{P}_{k+1|k} \tag{7.30}$$

Once the corrections are complete, the filter again enters a prediction phase and predicts one time step ahead (time step $= k+2$) into the future. The states are predicted and the error covariance matrix is predicted, see Equations (7.31) and (7.32), respectively. The correction–prediction cycle will then repeat when the time step transpires and the process is at time step $= k+3$. The prediction–correction cycle will continue henceforth.

Time Step: $k+1$ Prediction Step

$$\hat{x}_{k+2|k+1} = \bar{\mathbf{f}}(\hat{x}_{k+1|k+1}, \hat{\theta}_{k+1|k+1}, u_{k+1}, k+1) \tag{7.31}$$

$$\hat{P}_{k+2|k+1} = \bar{F}_{k+1}\hat{P}_{k+1|k+1}\bar{F}_{k+1}^T + Q \tag{7.32}$$

Further information on Kalman filter theory and Kalman filter application may be found in Henson and Seborg (1997), Welch and Bishop (2001) and Froisy et al. (1999).

7.1.3 Related Works

The utilisation of an extended Kalman filter in mineral processing and SAG milling is not a new idea. On-line estimation for SAG mills has constituted part of the work of Herbst and colleagues since the 1980's (Herbst et al., 1983; Hales et al., 1988). Recent examples of SAG mill soft sensors are described by Herbst and Pate (1996), Herbst and Pate (1999) and Schroder (2000).

The size of the systems utilised by Herbst are typically of the order five or seven (Herbst & Associates, 1996; Herbst and Pate, 1999). The states that feature in the system function, $\bar{\mathrm{f}}$, are:

- ore (considered as one or two size fractions, *e.g.*, $\pm$ 55 mm)
- water
- grinding media
- mill shell lining

These states are complemented by a number of parameters, θ. Two parameters are generally considered, *i.e.*, grindability and angle of repose. This brings the order of the system to seven or nine.

Two measurement models are utilised to model the process output, g, one for mill powerdraw and one for mill weight (load cell or bearing pressure). Typical examples are shown in Equation (7.33) and Equation (7.34), where three states are considered: rock, R, water, W, and, grinding media, B (Herbst and Pate, 1999). Both are functions of the states and the parameters which is a necessary feature of the measurement models, *i.e.*, the estimated variables "must be algebraically related to the variables which are measured"(Herbst and Gabardi, 1988). Detailed analysis of these two models and the equivalent Julius Kruttschnitt Mineral Research Centre models can be found elsewhere (Apelt *et al.*, 2001a).

$$Power = C1 \sin(\alpha)\,[R + W + B]\,(3.2 - 3\,V^*)\,\phi \tag{7.33}$$

$$Load\,Cell = C2\,(R + W + B + M_{mill}) + C3 \tag{7.34}$$

where

V^*	=	mill volumetric fraction occupied by the charge
ϕ	=	mill speed function
α	=	mill charge angle of repose
M_{mill}	=	mill weight (including liners)
C_i	=	constants

7.1.4 State Equations and Parameters

This research models the SAG milling process by the following thirty six (36) state equations and five (5) parameter equations:

1. **Solids.** The size by size solids mass balance developed by the Julius Kruttschnitt Mineral Research Centre (Napier-Munn *et al.*, 1996), (Valery Jnr., 1998) and presented in Section 4.2:

$$\begin{aligned} Accumulation &= In - Out + Generation - Consumption \\ \frac{ds_i}{dt} &= f_i - p_i + \sum_{j=1}^{i-1} r_j s_j a_{ij} - (1 - a_{ii}) r_i s_i \qquad (7.35) \\ p_i &= d_0 c_i s_i \qquad (7.36) \\ i &= 1 \ldots 27 \end{aligned}$$

2. **Water.** The water mass balance also developed by the Julius Kruttschnitt Mineral Research Centre (Napier-Munn *et al.*, 1996), (Valery Jnr., 1998) and presented in Chapter 3:

$$\begin{aligned} Accumulation &= In - Out \\ \frac{ds_w}{dt} &= f_w - p_w \qquad (7.37) \\ p_w &= d_0 s_w \qquad (7.38) \end{aligned}$$

3. **Grinding Balls.** The grinding ball mass balance proposed by this research in Section 4.1:

$$\begin{aligned} \text{Accumulation} &= \text{In - Out + Generation - Consumption} \\ \frac{dbc_i}{dt} &= bi_i - be_i + bw_{i-1} - bw_i \qquad (7.39) \\ i &= 1 \ldots 7 \end{aligned}$$

4. **Shell Lining.** The SAG mill liner weight mass balance proposed by this research in Section 4.3:

$$\begin{aligned} \text{Accumulation} &= \text{Wear} \\ \frac{dSMIW}{dt} &= -wearate \qquad (7.40) \end{aligned}$$

5. **Parameters.** These state equations are augmented by the following five (5) parameter equations:

$$\begin{aligned}
\dot{A} &= 0 \text{ (impact breakage ore parameter (in } a_{ij})) \\
\dot{b} &= 0 \text{ (impact breakage ore parameter (in } a_{ij})) \\
\dot{ta} &= 0 \text{ (abrasion breakage ore parameter (in } a_{ij})) \\
\dot{f_p} &= 0 \text{ (relative fraction pebble port open area (in } p_i)) \\
\dot{d_0} &= 0 \text{ (maximum mill discharge rate coefficient (in } p_i))
\end{aligned} \tag{7.41}$$

Ore breakage parameters A, b and ta are included in anticipation of an inferential measurement of ore grindability.

Mill discharge grate parameter f_p is included due to its close link to the pebble port diameter, x_p, which was found to be highly influential in the relative contribution to error in the feed passing sizes ($F_{80} \ldots F_{20}$) in Section 6.4.1.

Maximum discharge coefficient parameter, d_0, is included since it affects not only the mill discharge but also the rock and water charge remaining in the mill. A "mill discharge factor" parameter has also been used elsewhere (Schroder, 2000).

Tallying the number of states and parameters brings the order of the system function, $\mathbf{f}$, to forty one (41).

7.2 Measurement Models

The relevant process measurements present in the primary circuit, shown in Figure 7.3, are:

- SAG mill fresh (stockpile) feed (t/hr)
- SAG mill feed water addition (m^3/hr)
- SAG mill powerdraw (kW)
- SAG mill load cell (t)
- Primary cyclone feed water addition (m^3/hr)
- Primary cyclone feedrate (m^3/hr)
- Primary cyclone feed density (% solids w/w)
- Oversize crusher feedrate (t/hr)

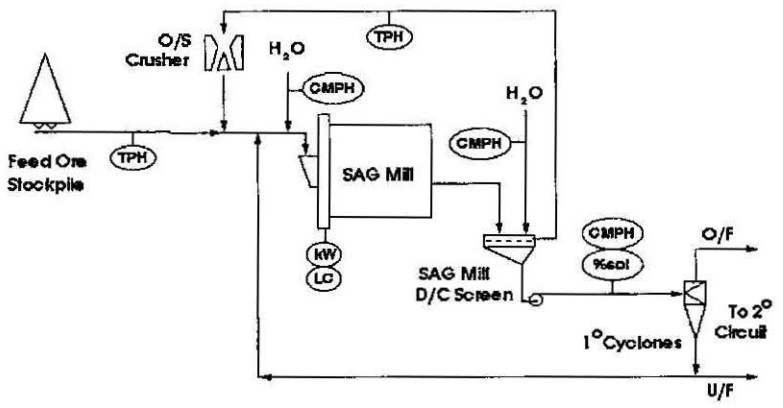

TPH	=	mass flowrate (t/hr)	kW	=	powerdraw (kW)
CMPH	=	volumetric flowrate (m^3/hr)	LC	=	load cell (t)
%sols	=	stream density (% solids w/w)			

Figure 7.3: Primary Grinding Circuit Process Measurements

The measurement (plant output) models typically utilised in CSPE are based on mill powerdraw, *e.g.*, Equation (7.33), and mill weight (by way of bearing pressure or load cell measurement), *e.g.*, Equation (7.34). The SAG mill discharge screen oversize conveyor measurement has also been utilised in a formulation that estimates a "mill discharge factor" parameter, (Schroder, 2000), which is assumed to be or related to d_0.

In this research, two plant measurement models are considered, namely:

1. SAG mill weight measurement model
2. SAG mill discharge measurement model

These models centre on two corresponding process outputs, $y_1(t)$ and $y_2(t)$. The SAG mill weight measurement model is similar to Equation (7.34) and is described in Section 7.2.1. The weight model is novel in that it utilises the shell weight model presented in Chapter 4. The SAG mill discharge measurement model is also a novel development of this research. The discharge model (Model 1) was presented to the *SAG* 2001 conference and is described in Section 7.2.2.

7.2.1 SAG mill weight measurement model

The SAG mill weight measurement model, $g_1(x, \theta, t)$, is a sum of the

- mass of ore particles, grinding balls and water in the mill charge kidney (the charge material that is not in free-fall from the charge shoulder to the charge toe), M_{kidney}
- mass of the mill shell discharge end lining and the discharge grate, $(lining_{DE} + D/C\ Grate)$, as presented in Section 4.3
- a calibration term, $tare$, that allows for the difference between the actual total mill weight and the load cell measurement (includes the mill shell weight and the feed end shell lining weight)

$$g_1(x, \theta, t) = M_{kidney} + (lining_{DE} + D/C\ Grate) - tare \tag{7.42}$$

The state functionality of the SAG mill weight measurement model, $g_1(x, \theta, t)$, is via the rock, ball and water charge components in the charge kidney and the discharge-end shell lining weight. The latter is, in fact, one of the states considered. The kidney mass is a state function, $M_{kidney}(x, \theta, t)$ - it is the sum of the rock, ball and water states in the charge kidney.

The SAG mill weight is measured in the plant by load cell. This measurement, $y_1(t)$, is the process output that corresponds to the mill weight model, $g_1(x, \theta, t)$.

7.2.2 SAG mill discharge measurement model (Model 1)

Referring to Figure 7.3, plant measurements are available for:

- oversize crusher mass feed rate
- primary cyclone feed volumetric flowrate (SAG discharge screen undersize plus discharge screen water addition)
- primary cyclone feed stream density
- SAG discharge screen water addition flowrate

The SAG mill discharge stream volumetric flowrate can be reconstructed from these four plant measurements. This reconstructed stream can then be utilised in the CSPE as the

second process output, $y_2(t)$:

$$\begin{aligned} y_2(t) &= \frac{MV_{OSCF}\,\%sols_{OSCF}}{100\,SG_s} \\ &+ \frac{MV_{PCFDm3}\,MV_{PCFD\%sols}\,SG_l}{MV_{PCFD\%sols}\,SG_l + (100 - MV_{PCFD\%sols})SG_s} \\ &+ \frac{MV_{PCFDm3}\,(100 - MV_{PCFD\%sols})\,SG_s}{MV_{PCFD\%sols}\,SG_l + (100 - MV_{PCFD\%sols})\,SG_s} \\ &+ \frac{MV_{OSCF}\,(100 - \%sols_{OSCF})}{100\,SG_l} - MV_{PCFWm3} \end{aligned} \tag{7.43}$$

where

MV_{OSCF}	=	oversize crusher total feedrate (t/hr)
MV_{PCFDm3}	=	primary cyclone feed flowrate (m^3/hr)
$MV_{PCFD\%sols}$	=	primary cyclone feed density (% solids w/w)
MV_{PCFWm3}	=	primary cyclone feed water addition flowrate (m^3/hr)
$\%sols_{OSCF}$	=	oversize crusher feed density (% solids w/w)

The corresponding measurement model, $g_2(x,\,\theta,\,t)$, is

$$g_2(x,\,\theta,\,t) = \frac{SMDC_s}{SG_s} + \frac{SMDC_l}{SG_l} \tag{7.44}$$

The state functionality of the SAG discharge measurement model, $g_2(x,\,\theta,\,t)$, is through the constituents of the terms in Equation (7.44). The solids mass flowrate, $SMDC_s$, is the summation of the size by size mill product stream and thus, is state dependent.

$$SMDC_s = \sum_{i=1}^{n} p_i = \sum_{i=1}^{n} d_0\,c_i\,s_i \tag{7.45}$$

The liquid mass flowrate, $SMDC_l$, is a function of $SMDC_s$ and thus is also state dependent:

$$SMDC_l = (k_g Q_m - \frac{SMDC_s}{SG_s})SG_l \tag{7.46}$$

On account of the SAG mill discharge grate characteristics, *i.e.*, high fractional open area ($foag$), high relative radial position of the open area (γ), and high relative radial position of the outermost aperture (r_n), the mill discharge flow is assumed to be only through the grinding media and that no slurry pool exists at the toe of the charge. Therefore, as per

Equation (3.6), the mill discharge flowrate may then be calculated as follows:

$$Q_m = 6100\, J_{pm}^2 \gamma^{2.5} A \phi^{-1.38} D^{0.5} \tag{7.47}$$

A = total discharge grate open area (m^2)

D = mill inside diameter (m)

γ = mean relative radial position of open area (fraction)

ϕ = fraction critical mill speed (fraction)

$$J_{pm} = \frac{\frac{\sum s_i}{SG_s}\Big|_{size<16mm} + \frac{s_w}{SG_l}}{V_{mill}} \tag{7.48}$$

= nett fractional holdup of slurry in mill that is contained within the grinding charge (live area) interstices

s_w = mill water charge (t)

V_{mill} = mill volume (m^3)

The parameter functionality of the SAG discharge measurement model, $g_2(x, \theta, t)$, is also through the constituents of the terms in Equation (7.44). The solids mass flowrate ($SMDC_s$), Equation (7.45), is a function of the maximum mill discharge rate constant (d_0), explicitly, and also the relative fraction pebble port open area (f_p), implicitly (via the grate classification function, c_i, described in Section 3.3.1). The maximum mill discharge rate constant (d_0) affects not only the mill discharge but also the rock and water charge remaining in the mill. The relative fraction pebble port open area (f_p) is linked by the classification function to the pebble port aperture size (x_p) which is an influential parameter in the feed passing size estimates, as described in Section 6.4.1. This reinforces the inclusion of the relative fraction pebble port open area (f_p) in the list of parameters in Equation (7.41).

The ore breakage parameters A, b and ta are implicit functions of the mill rock charge fractions (s_i) and are therefore present in the state equations, Equation (7.35) and(7.36), and the measurement model function, Equation (7.45). As mentioned, these parameters are included in the formulation in anticipation of an inferential measurement of ore grindability which influences mill performance.

7.3 CSPE Model Results

The state equations, Equations (7.35) to (7.40), the five parameter augmentation (7.41), and the measurement models, Equation (7.42) and (7.44), were coded into MATLAB-Simulink to form the discrete-time system, Equation (7.4) to (7.6).

The discrete-time system $\bar{f}$, and measurement, $\bar{g}$, functions are utilised by the state correction and prediction equations, Equation (7.7) and (7.10), of the extended Kalman filter. The linearised discrete-time system function $\bar{F}_k$, Equation (7.13), and measurement function $\bar{G}_k$, Equation (7.12), were obtained by a parallel coding conducted in Maple V Release 5.1, which has the symbolic manipulation capability to generate the required partial derivatives.

The outputs of the process simulation model of the circuit were utilised as the "plant measurements" $y_1(t)$ and $y_2(t)$. The mill weight measurement ($y_1(t)$) results directly from Equation (4.22). The mill mill discharge measurement ($y_2(t)$) is obtained through simulation model output manipulation, as per Equation (7.43).

7.3.1 Model Simplification

The mill rock charge and ball charge influence the breakage that occurs in the mill via the specific comminution energy, Ecs_i, the high energy, impact breakage parameter, $t_{HE_i} = t_{10_i}$, and the appearance function, a_{ij}. The latter dictates changes in the rock charge, *i.e.*, the rock mass balance, see Equation (7.35). This inter-relationship proved too complex for Maple in determining the partial derivatives in the linearised discrete-time system, $\bar{F}_k$, and measurement, $\bar{G}_k$, functions.

To simplify the problem, the state functionality of the specific comminution energy (by size), Ecs_i, was ignored. That is, calculated values of Ecs_i, Equation (3.34), were entered into the impact breakage parameter t_{10} calculation, Equation (3.33). This simplification reduced the dependence of the appearance function, a_{ij}, to the ore breakage parameters A, b and ta only.

7.3.2 Results and Discussion

The CSPE model was utilised to estimate the total (J_t) and ball (J_b) volumetric charge fractions. The simulation model was utilised to simulate the prevailing plant operating conditions. The CSPE model was able to estimate the mill inventories. Figure 7.4 illustrates the prevailing operating conditions and the initial results obtained.

The initial estimate results showed good agreement with the simulated conditions. However, the estimates diverged rapidly out of range as simulation time progressed. In the ensuing investigation Kalman filter tuning parameter selection proved to be the underlying cause for transient agreement. In arriving at this conclusion the investigation also tested for system observability and detectability, the findings of which are presented below.

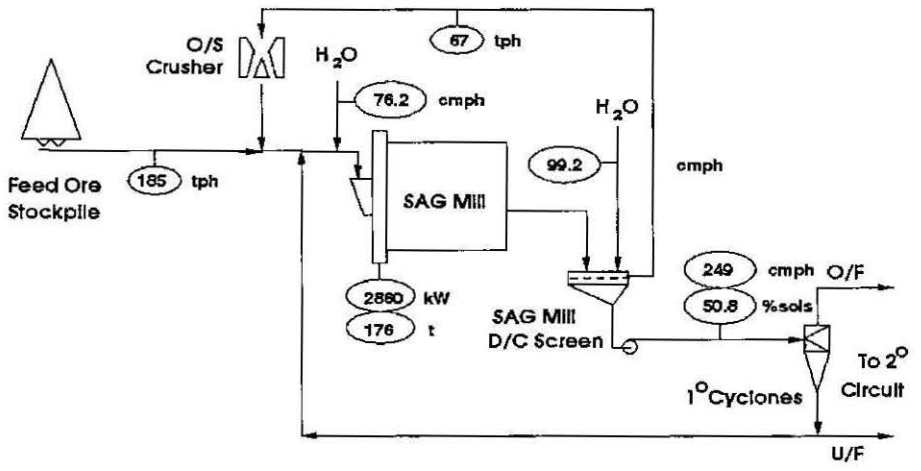

Figure 7.4: State Estimation Results Summary

System Observability and Detectability

During the investigation of the CSPE model performance, system observability and detectability were assessed. This was achieved by:

1. Linearising the CSPE at steady-state conditions to generate a state-space model of the form

$$\hat{x}(t) = Ax + Bu \tag{7.49}$$

$$y(t) = Cx \tag{7.50}$$

where

A, B, C = system matrices (ignoring the parameters)

x = system states (36 states without the 5 parameters)

u = process inputs

y = process outputs (measurements)

Equation (7.49) is a "set of equations that describe how the natural state of the given system changes with time" (Romagnoli, 1996).

2. Generating the "observability matrix", L_0, (Ray, 1981; Henson and Seborg, 1997)

$$L_0 = \left[C^T \mid A^T C^T \mid (A^T)^2 C^T \mid \ldots \mid (A^T)^{n-1} C^T\right] \tag{7.51}$$

Matrix A is $n \times n$ where n is the number of states and matrix C is $l \times n$ where l is the number of measurements. The observability matrix, L_0, has dimension $n \times nl$.

3. Determining the Rank of the observability matrix, L_0. If the Rank of L_0 is n then the system is completely observable and each initial state x_0 can be determined from knowledge of the process inputs, u, and process outputs, y over a finite time period.

   If the Rank of L_0 is less than n then the system is only partially observable. If the system modes that cannot be observed or reconstructed from the output measurements are stable then the system is detectable (Henson and Seborg, 1997) - "a weaker property" than observable (Ray, 1981). If "all of the eigenvalues of matrix A are negative, there are no unstable modes and the system is detectable" (Ray, 1981). For example, if in some system a measurement of the second state is available, *i.e.*, $y_1 = x_2$, and the second state, x_2, is dependent on itself and the first state, x_1, then the first state, x_1, is detectable. However, if instead the plant measurement was of the first state, *i.e.*, $y_1 = x_1$, the second state, x_2, is not detectable (Ray, 1981).

Results

The Rank of the observability matrix, L_0, was determined to be eight (8) which is less than the dimension of the system ($n = 36$). Therefore, the system is not completely observable.

To determine whether the states were all detectable, the system eigenvalues were determined as shown in Table 7.3.2. All eigenvalues are negative ($\lambda < 0$) except for the first ball charge fraction, $smbc_1$, and the SAG mill lining weight, $smiw$, which are either on or very near the zero cut-off for a detectable state.

CSPE Model 2

The Rank of the observability matrix, L_0, was determined to be significantly less than the dimension of the system and the system to be *not* completely observable. The eigenvalues of system matrix A, given in Table 7.3.2, suggest the system (Equation (7.35) to (7.40)) may *not* be fully detectable.

The results presented later in this Section show that the system *is* detectable in the combined state and parameter estimation formulation that utilises the mill discharge measurement model described by Equation (7.43) and (7.44), henceforth referred to as "Model 1". However, at this point in the analysis, appropriate selection of the tuning parameters had proven to be elusive and measures were undertaken to increase the Rank of the observability matrix.

The issue of primary concern was the low number of plant measurements and measurement models (2) relative to the number of states in the system (36). Two methods to address this difference are:

Table 7.1: System Eigenvalues

State	λ
$smrc_1$	-30.0
$smrc_2$	-31.4
$smrc_3$	-32.2
$smrc_4$	-31.6
$smrc_5$	-30.2
$smrc_6$	-30.7
$smrc_7$	-32.6
$smrc_8$	-36.2
$smrc_9$	-40.5
$smrc_{10}$	-45.5
$smrc_{11}$	-46.1
$smrc_{12}$	-51.4
$smrc_{13}$	-47.2
$smrc_{14}$	-52.5
$smrc_{15}$	-57.5
$smrc_{16}$	-62.5
$smrc_{17}$	-61.0
$smrc_{18}$	-53.5
$smrc_{19}$	-44.6
$smrc_{20}$	-23.7
$smrc_{21}$	-10.8
$smrc_{22}$	-5.0
$smrc_{23}$	-3.8
$smrc_{24}$	-4.9
$smrc_{25}$	-6.0
$smrc_{26}$	-6.1
$smrc_{27}$	-14.1
$smwc$	-38.9
$smbc_1$	0
$smbc_2$	-1
$smbc_3$	-0.003
$smbc_4$	-0.004
$smbc_5$	-0.002
$smbc_6$	-0.1
$smbc_7$	-1
$smiw$	0.0001

1. Reduce the number of states considered.

2. Increase the number of plant measurements.

A reduced number of states is a valid strategy and is an implicit part of the typical measurements presented in Equation (7.33) and (7.34) which utilise three states: rock, R, water, W, and, grinding media, B (Herbst and Pate, 1999). These two equations have also been utilised for five states: rock (larger than *grate size*), particles (less than or equal to the *grate size*), water, grinding media and mill shell lining (Herbst & Associates, 1996). Recent communications with one of the co-authors of Herbst and Pate (1999)[1] established that the formulation had been extended to cover three rock states (coarse, medium and fine).

Despite such success with utilising a reduced number of states, reducing the number of states here would require significant re-programming of the simulation model code (and the CSPE model code) and was deemed beyond the scope of this research. Therefore, the number of plant measurements was effectively increased through extension of the measurement and model pairings from one (1) SAG mill discharge flow measurement (Equation (7.43) and (7.44), see Section 7.2.2) to twenty eight (28) SAG mill discharge material (solids and liquid) tonnages.

The twenty eight (28) new plant measurements, $y_{2...29}(x, \theta, t)$, are generated by manipulation of the inferential models developed in Section 5.1.1 and are as follows:

$$y_{2...28}(x, \theta, t) = \left(\frac{oscf_i}{100}\right) OSCF_{tph\_s} + \left(\frac{pcfd_i}{100}\right) PCFD_{tph\_s} \quad i = 1...27 \quad (7.52)$$

$$y_{29}(x, \theta, t) = OSCF_{tph\_l} + PCFD_{tph\_s} - PCFW\,SG_l \quad (7.53)$$

[1]Discussion with WT Pate at *SAG* 2001 Conference, Vancouver, Sep 30 - Oct 3, 2001

where

$oscf_i$	=	oversize crusher feed % w/w retained in *size* i, seeEquation (5.4)
$pcfd_i$	=	primary cyclone feed % w/w retained in *size* i, see Equation (5.4)
$OSCF_{tph\_s}$	=	oversize crusher solids feedrate (tph), see Equation (5.1)
$OSCF_{tph\_l}$	=	oversize crusher liquid feedrate (tph), see Equation (5.2)
$PCFD_{tph\_s}$	=	primary cyclone solids feedrate (tph), see Equation (5.5)
$PCFD_{tph\_l}$	=	primary cyclone liquid feedrate (tph), see Equation (5.6)
$PCFW$	=	primary cyclone feedwater addition (m^3/hr) (Measured Variable)
SG_l	=	process water specific gravity (t/m^3)

The corresponding measurement models, $g_{2...29}(x, \theta, t)$, are the right hand sides of Equations (7.36) and (7.38), *i.e.*,

$$g_{2...28}(x, \theta, t) = d_0\, c_i\, s_i \quad i = 1 \ldots 27 \tag{7.54}$$

$$g_{29}(x, \theta, t) = d_0\, s_w \tag{7.55}$$

where

s_i	=	mill rock charge in *size* i (t)
s_w	=	mill water charge (t)
d_0	=	maximum discharge rate constant (hr^{-1})
c_i	=	discharge grate classification function (frac)

The system matrix A for Model 2 is the same as that for Model 1. Therefore the eigenvalues are (still) those presented in Table 7.3.2. Since the measurement (process output) matrix C has changed with the utilisation of twenty nine (29) measurements (instead of two (2)), the observability matrix, L_0, has changed accordingly.

The Rank of the observability matrix, L_0, for Model 2 is twenty (20) which, though a significant improvement on eight (8), is (still) less than the dimension of the system ($n = 36$). Therefore, the system remains not completely observable for the new CSPE formulation.

The system was shown to be detectible despite the incomplete observability of the system. This was the case for both CSPE formulations, *i.e.*, Model 1 and Model 2. Detectability was established not via rigorous proof but through achieving satisfactory results through the appropriate selection of Kalman filter tuning parameters. The results and the selection of tuning parameters are detailed in the following Section.

Kalman Filter Tuning

The Kalman filter has three (3) "tuning" parameters:

P_0 : estimate error covariance matrix

Q_0 : process noise covariance matrix

R_0 : measurement noise covariance matrix

The selection of each of these initial-value matrices was initially by trial-and-error. Cheng et al. (1997) make the following points regarding these matrices :

P_0 : the "magnitude of the P matrix is an indicator of the estimation quality and that "the matrix P inital value reflects the magnitude of the errors in initial conditions, and thus should be ... small when better intial conditions are available. The general assessment that "the initial value of P is not critical" is also given.

Q_0 : the "Q_k weights the measuring device errors" and that the "value of Q_k should be ... small in cases of small measurement errors." For a set of tray temperatures, considered relatively accurate, a diagonal matrix with all elements of the order of 10^{-10} (dimensionless) was utilised.

R_0 : the "selection of the R value reflects the degree of confidence in the model. Usually, the R value greatly influences the performance of the estimator, and thus [should be chosen] with caution." For the case considered, a symmetric matrix was generated with all elements of the order between 10^{-15} and 10^{-10}.

Selection of these tuning parameters is complicated by the following points (Cheng et al., 1997):

P_0 : "although the matrix $P(t)$ can be loosely associated to the uncertainty of the estimated state, it has no clear statistical meaning.

Q_0 & R_0 : "no general method is available" for their selection.

The matrices are also referred to as "weighting" matrices (Cheng et al., 1997):

Q_0: measurement error weighting matrix

R_0: model noise weighting matrix

This terminology indicates the effects the matrices have on the CSPE problem. Henson and Seborg (1997) detail the following behaviour which clarifies the use of the "weighting" terminology:

> $R_0 < Q_0$: measurements are more reliable than the model and the CSPE model adjusts the state estimates, $\hat{x}$, towards better agreement between the model and the measurements.
>
> $R_0 > Q_0$: measurements are less reliable than the model prevents the CSPE from adjusting the state estimates, $\hat{x}$, towards better agreement between the model and the measurements.

Welch and Bishop (2001) describe these effects as follows:

> $R_0 \rightarrow 0$: the Kalman gain, L_k, weights the residual $y_k - \bar{\mathbf{g}}(\hat{x}_{k|k-1}, \hat{\theta}_{k|k-1}, k)$ in Equation (7.7) more heavily.
>
> $P_0 \rightarrow 0$: the Kalman gain, L_k, weights the residual less heavily.

Welch and Bishop (2001) also state the following pertinent points about the tuning matrices P_0, Q_0 and R_0:

> P_0 : the choice of P_0 is not critical, as long as $P_0 \neq 0$ the filter will eventually converge.
>
> Q_0 : the determination of the process noise covariance is generally more difficult [compared to R_0] since direct observation of the process is not possible. If process uncertainty is introduced via Q_0, with reliable measurements, acceptable estimates are possible.
>
> R_0 : the measurement noise corvariance, R_0, is usually measured prior to operation of the filter and is generally practically possible via the analysis of the actual process measurements.

Accounting for these points of discussion and applying them to the two CSPE formulations under scrutiny, the initial values for the matrices were specified as follows:

> P_0 : since the process model within the CSPE formulation is equivalent to the simulation model, the simulated plant in this case, confidence in the initial conditions is high and the order of magnitude of P_0 small, nominally, 10^{-3} times the intial values of the states. P_0 was therefore specified as a diagonal matrix with the main diagonal equal to $10^{-3} \times x_0$ and all other elements equal to zero.

Q_0 : was specified as a diagonal matrix with the main diagonal equal to $10^{-10} \times x_0$ and all other elements equal to zero. Confidence in the measurements is high since they are generated from the simulation model. With Q_0 specified as such, the CSPE formulation considers the measurement errors to be small and as a result state estimates do not exhibit high fluctuation levels.

P_0 : since the measurements are simulated measurements containing no noise, the measurement noise corvariance, R_0, was set to zero[2].

The state and parameter estimates for both CSPE formulations are shown in Table 7.2 with the steady state information and the respective relative errors. Table 7.3 contains the corresponding volumetric total (J_t) and ball (J_b) charge estimates.

Model 1 The results show that good estimates are possible through the utilisation of this CSPE formulation ($2\times$ plant measurements). The relative error present in the state estimates is generally $< 5\%$. The relative error present in the parameter estimates is either exactly equal or approximately equal to zero.

The two state estimate results that stand out are the estimates of the twenty fifth and twenty seventh rock charge states, $smrc_{25}$ and $smrc_{27}$, respectively. These relatively high levels of error are due to the small amounts of rock in these size fractions. A small deviation from the steady state value represents a large relative error.

Model 2 Good estimates are also possible through the utilisation of this CSPE formulation ($29\times$ plant measurements). The extension of the SAG mill discharge volumetric flowrate measurement, Equations (7.43) and (7.44), to a size by size throughput measurement, Equations (7.52) to (7.55), improved the resulting state estimates. All state estimates displayed exact agreement with the steady state values. Exact agreement was also displayed in the estimates of the ore impact breakage and abrasion parameters (A, b and ta).

Relative error is present in the estimates of the mill discharge parameters (f_p and d_0). The high level of relative error in the notional fraction pebble port open area relative to total grate open area, f_p, is clearly evident. This is due to the CSPE model adjusting the mill discharge parameters (f_p and d_0) to achieve the exact agreement for the rock and water charge state estimates via Equations (7.54) and (7.55).

[2]Selected after discussion with Professor L. Kershenbaum, Imperial College, London, 19 September 2001.

Table 7.2: CSPE Model Results - States and Parameters

State	Unit	SS value	Model 1 Estimate	Error (%)	Model 2 Estimate	Error (%)
$smrc_1$	(t)	0	0	0	0	0
$smrc_2$	(t)	0.23	0.23	0.5	0.23	0
$smrc_3$	(t)	3.54	3.51	1.0	3.54	0
$smrc_4$	(t)	8.91	8.68	2.6	8.91	0
$smrc_5$	(t)	9.33	9.43	1.1	9.33	0
$smrc_6$	(t)	7.66	7.63	0.4	7.66	0
$smrc_7$	(t)	5.26	5.13	2.5	5.26	0
$smrc_8$	(t)	2.43	2.46	1.3	2.43	0
$smrc_9$	(t)	1.39	1.40	0.7	1.39	0
$smrc_{10}$	(t)	0.83	0.84	1.7	0.83	0
$smrc_{11}$	(t)	0.60	0.63	5.3	0.60	0
$smrc_{12}$	(t)	0.53	0.55	4.0	0.53	0
$smrc_{13}$	(t)	0.51	0.53	4.5	0.51	0
$smrc_{14}$	(t)	0.48	0.50	4.6	0.48	0
$smrc_{15}$	(t)	0.42	0.44	4.3	0.42	0
$smrc_{16}$	(t)	0.36	0.37	4.2	0.36	0
$smrc_{17}$	(t)	0.30	0.32	4.0	0.30	0
$smrc_{18}$	(t)	0.27	0.29	4.2	0.27	0
$smrc_{19}$	(t)	0.26	0.27	3.6	0.26	0
$smrc_{20}$	(t)	0.27	0.28	3.4	0.27	0
$smrc_{21}$	(t)	0.27	0.28	2.9	0.27	0
$smrc_{22}$	(t)	0.27	0.28	3.3	0.27	0
$smrc_{23}$	(t)	0.25	0.26	3.0	0.25	0
$smrc_{24}$	(t)	0.22	0.23	2.8	0.22	0
$smrc_{25}$	(t)	0.20	0.11	44.5	0.20	0
$smrc_{26}$	(t)	0.17	0.17	0.8	0.17	0
$smrc_{27}$	(t)	0.72	0.50	30.5	0.72	0
$smwc$	(t)	2.06	2.08	1.2	2.06	0
$smbc_1$	(t)	0	0	0	0	0
$smbc_2$	(t)	0.93	0.93	0	0.93	0
$smbc_3$	(t)	46.7	46.7	0.0	46.70	0
$smbc_4$	(t)	32.7	32.7	0.0	32.7	0
$smbc_5$	(t)	13.08	13.08	0.0	13.08	0
$smbc_6$	(t)	0	0	0	0	0
$smbc_7$	(t)	0	0	0	0	0
$smiw$	(t)	337.7	337.7	0.0	337.7	0
A	(-)	75.8	75.8	0	75.8	0
b	(-)	0.450	0.451	0.1	0.450	0
t_a	(-)	0.13	0.13	0	0.13	0
f_p	(fraction)	0.011	0.011	0	0.034	208
d_0	(hr^{-1})	29.85	29.85	0.0	28.79	3.6

The state estimates of Table 7.2 translate to the volumetric charge fraction estimates results in Table 7.3. Overall, all of the estimates show good agreement with the steady state conditions and reinforce that both CSPE formulations (Model 1 and 2) can be utilised for state estimation.

The volumetric ball charge (J_b) estimates from both CSPE formulations exhibit exact agreement with the steady state conditions. The total volumetric charge (J_t) estimates from both CSPE formulations exhibit good agreement with the steady state conditions (to within $\approx 0.6\%$). The exact agreement between the Model 2 formulation estimates of the mill charge levels (J_t and J_b) and the steady state conditions is expected following the analysis of Table 7.2 above. Said analysis also leads to the expectation of the relative error present in the Model 1 total volumetric charge (J_t) estimate.

Table 7.3: CSPE Model Results - Charge Fractions

Volumetric Fraction	SS value	Model 1 Estimate	Error (%)	Model 2 Estimate	Error (%)
Total Charge, J_t	0.230	0.228	0.6	0.230	0
Ball Charge, J_b	0.142	0.142	0	0.142	0

Although both CSPE formulations are capable of good estimates, the Model 2 formulation provides superior state estimates through adjustment (estimation) of the mill discharge parameters (f_p and d_0). On account of these two characteristics the Model 2 CSPE formulation is considered superior.

Referring to Table 6.3 (Section 6.2.2) the error in the charge estimates from the mill weight-based inferential model developed in Chapter 5 is 1.3% and 1.8% for the estimates of the total volumetric charge (J_t) and ball charge (J_b), respectively. Comparison of these figures with the results in Table 7.3 suggests that the CSPE formulations yield superior results. An uncertainty analysis of the CSPE results was considered beyond the scope of this research. However, uncertainty levels in the CSPE results would be expected to be at least comparable to the weight-based inferential model results.

A next step in the development of the CSPE formulations could be their validation against plant data: off-line and then on-line. Methods to estimate the covariances from process data as described by Romagnoli and Sanchez (2000) could be utilised here to calculate the measurement covariance matrix, R_0.

7.4 Summary

In this Chapter, two combined state and parameter estimation (CSPE) formulations for the SAG mill have been presented. Each model was programmed into the MATLAB-Simulink and Maple environments and validated against steady state industrial plant survey data, see Appendix C.

The CSPE results from the two formulations were compared to each other and also to the results from the inferential models developed in Chapter 5. The purpose of this comparative investigation into combined state and parameter estimation was not to recommend one method or model over another, since application selection would be expected to be on a case by case basis depending on the knowledge and expertise available and the process measurements available. The purpose was to place the new inferential models into context by presenting them alongside a method that has been utilised for some time and is gaining a degree of acceptance in industry. This objective has been achieved with the added benefit of presenting new information for CSPE model use and formulation.

The presentation of combined state and parameter estimation for SAG mills is not innovative in itself. However, the public presentation of a SAG mill application of this order (41) is novel, as is combination of models utilised by the CSPE formulations. Other innovations resulting from this work are:

- a mill weight model for utilisation in the CSPE formulation
- two mill discharge models for utilisation in the CSPE formulation
- system observability and detectability discussion and findings

A next step in the development of the CSPE formulations could be their validation against plant data: off-line and then on-line.

The innovations resulting from this Chapter are summarised in Table 7.4.

Table 7.4: Chapter 7 Innovation Summary

Section	Innovation
Section 7.1.4 to 7.3.2	Public presentation of the development and results of a high dimension (41×41) combined state and parameter estimation (CSPE) formulation.
Section 7.1.4 to 7.3.2	The CSPE formulation presented is novel in the combination of the models utilised, including those developed in the course of this research.
Section 7.2.1	SAG mill weight measurement model - Equation (7.42) (and Equation (4.22))
Section 7.2.2	SAG mill discharge measurement model (Model 1) - Equations (7.44) and (7.45)
Section 7.3.2	SAG mill discharge measurement model (Model 2) - Equations (7.54), (7.55), (7.52) & (7.53)
Section 7.3.2	Discussion and findings on system observability and detectability

Chapter 8

Case Studies

Further validation and analysis of the inferential models developed in Chapter 5 is presented here. Section 8.1 details the validation and assessment of the models on real Northparkes Mines plant data from October 1997. Section 8.2 describes the source of some unusual behaviour exhibited by the models. Further comment is made on model sensitivity, model characteristics, and a operative curve is constructed that may be utilised in a mill charge control strategy. In Section 8.3 the development and utilisation of the inferential models in a multi-variable controller is described.

8.1 Inferential Measurement Validation on Plant Data

Data collected during the execution of the *SAG Mill Control Project* (Romagnoli et al., 1997) on site at Northparkes Mines in late 1997 was utilised to validate the inferential measurement models. Appendix D contains the Module 1 Grinding Logsheets and Shift Communication Book Sheets for the period 8 - 16 October 1997. Data files for this period containing data for the tags on the SCADA system relevant to the Module 1 grinding circuit, were also obtained.

The MATLAB-Simulink files were configured to read in the plant data from a master data file, collated from the various files for this express purpose. The nine days' worth of data, recorded at 2-minute intervals, was read from the master data file spreadsheet and processed by the inferential measurement models developed in Chapter 5. The inferential models, as per the calculation sequence detailed in Section 5.1, generated results for:

1. Oversize crusher feed, primary cyclone feed, SAG mill discharge, including the transfer sizes ($T_{80} \ldots T_{20}$);
2. SAG mill rock charge;
3. SAG mill fractional total filling, J_t, fractional ball filling, J_b, and fractional rock charge filling, J_r, ($J_r = J_t - J_b$);
4. SAG mill total feed;
5. Oversize crusher product and primary cyclone underflow; and,
6. SAG mill fresh feed, including the feed sizes ($F_{80} \ldots F_{20}$).

These results were subsequently written from MATLAB-Simulink to a results spreadsheet. Obviously, there was a significant volume of results generated. Specific periods of the results were selected that highlight the performance of the key models. Section 8.1.1 discusses the mill charge estimates, including how the ball charge estimate captures SAG mill ball charging. Section 8.1.2 discusses the feedsize estimates, including how the F_{80} estimate captures increasing feedsize observed by the mill operators. In Section 8.1.3, model performance is shown to be strongly affected by unusual plant conditions.

8.1.1 Charge Estimates, Ball Charging and a Mill Inspection

The first set of results are shown in Figure 8.1 and Figure 8.2, which illustrate (referring also to the log sheet excerpt in Figure 8.3) the inferential model of the ball charge fraction, J_b, capturing the ball charging that occurs during the day shift. The model estimates the ball charge fraction firstly rising from 0.10 to 0.11 during day shift, while ball charging takes place. There is no further ball charging during afternoon shift, see Figure 8.3, and the model estimates fall back to the 0.10 level, plausibly due to ball charge wear and ball ejection (worn or broken balls).

The trends of the ball, rock and total charge estimates, J_b, J_r & J_t, respectively, and the feed size estimate, F_{80}, are five (5) sample averages. The noise prevalent in the charge estimates is due to the noise in the mill powerdraw signal. Recall that the total charge (J_t) and ball charge (J_b) estimates originate from a constrained minimisation problem. The powerdraw residual, Equation (5.17), and the weight residual, Equation (5.21) were solved subject to the constraint that the ball charge fraction is less than or equal to the total charge fraction ($J_b \leq J_t$). The powerdraw signal, even as a two (2) minute sample, contains significant noise. This noise translates to the noise in the estimates. Further model refinement should therefore incorporate a degree of signal filtering to eliminate most of this noise.

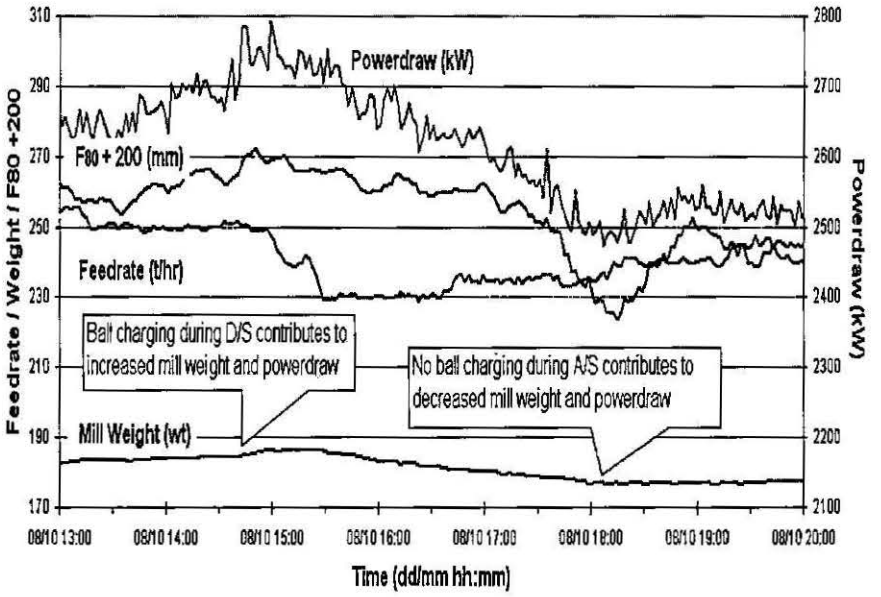

Figure 8.1: Results for 8 October 1997: Mill powerdraw and weight increase with ball charging and decrease when charging is ceased. (F_{80} results are shown also)

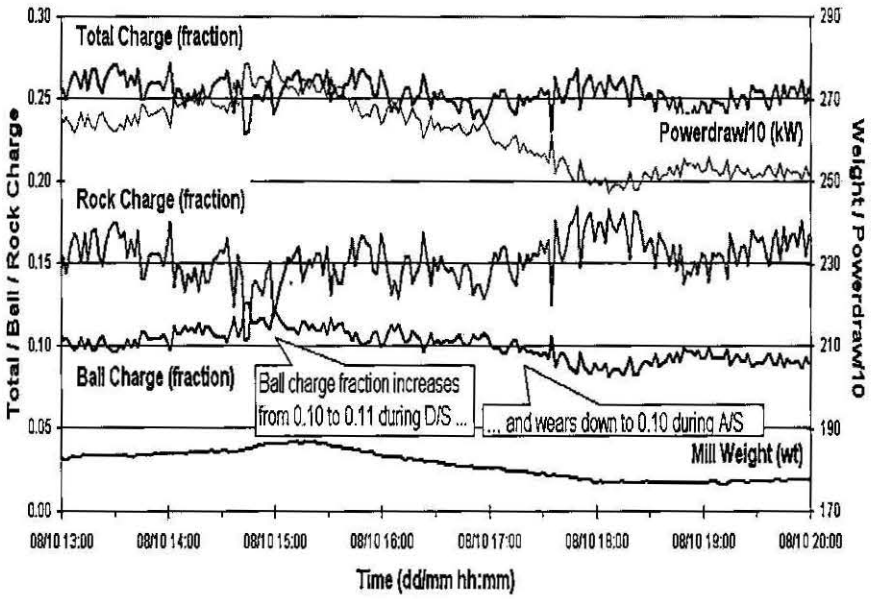

Figure 8.2: Results for 8 October 1997: Ball charge (J_b) increases during day shift and wears away in the absence of ball charging during afternoon shift.

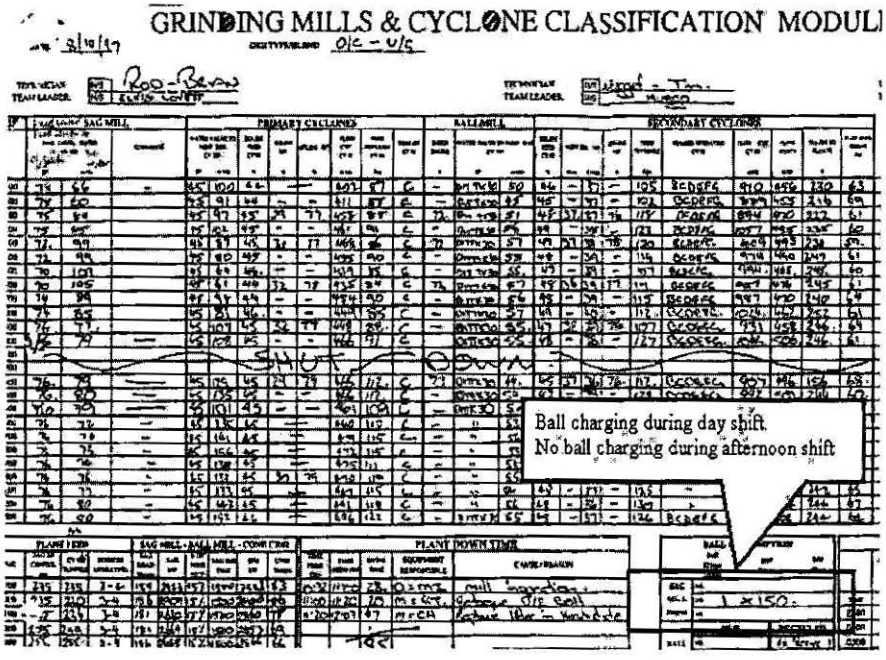

Figure 8.3: Module 1 Grinding Log Sheet, 8 October 1997: Ball charging occurs only during day shift

There is evidence of negative, proportional correlation between the ball charge estimate (J_b) and the estimates of total (J_t) and rock (J_r) charge in Figure 8.2. A degree of negative, proportional correlation is expected between the ball charge (J_b) and the rock charge (J_r) since increasing the ball charge generally causes more breakage to occur and thus, results in a decrease in the rock charge. Whether negative, proportional correlation should also be evident between the ball charge and the total charge is debatable. The cross-correlation of these estimates are analysed in further detail in Section 8.1.1.

A mill inspection was conducted on 14 October 1997 as part of the data collection phase of the *SAG Control Project* (Romagnoli et al., 1997). The excerpt from the Shift Communication Book from the date in question, see Figure 8.4, contains the results of the mill inspection. The author participated in this inspection and, visually, the total charge fraction (J_t) was 0.17 (17%) and the ball charge fraction (J_b) was 0.12 (12%).

The prevailing conditions, at the time of the mill inspection, and the inferential charge measurement model results are shown in Figure 8.5 and Figure 8.6, respectively. The inferential measurement model results of $J_t = 0.25$ and $J_b = 0.08$, although in the ball-park, do not exhibit excellent agreement with the mill inspection results. The total charge estimate, J_t, is some 50% above and the ball charge estimate is approximately 33% below the mill inspection results.

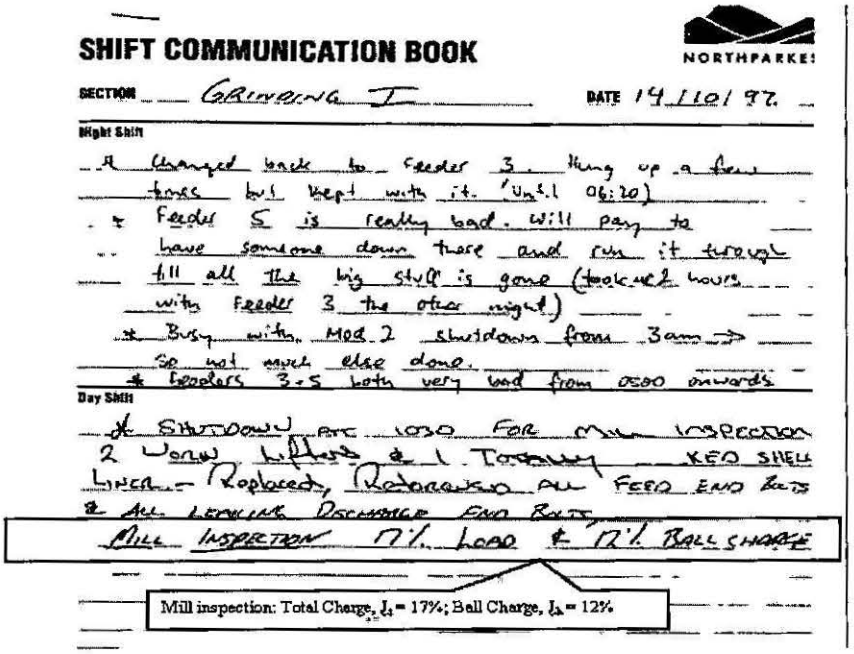

Figure 8.4: Module 1 Shift Communication Book 14 October 1997: Mill inspection - Total charge (J_t): 17%, Ball charge ()J_b): 12%

Although the mill inspection was conducted on a purely visual-basis, and, as such, is subject to a degree of error, measurements errors of 30 to 50% are not expected. Therefore, the mill charge measurement models contain significant error. Although significant, this level of error is not considered a major concern in this instance. The estimates, as mentioned above, arise from the mill powerdraw and weight residuals, Equations (5.17) and (5.21), respectively. These equations have parameters that can be adjusted to better fit the data.

These parameters, such as M_{shell} for the mill weight residual and and k for the powerdraw residual, were not adjusted from the values utilised in the earlier analysis conducted in Chapters 3 and 4, which correspond to data from January 1997, some nine (9) months earlier and undoubtedly out of date. Detailed model fitting was not conducted due to time constraints and the perceived low-priority of the task. The aspect considered most important, in this instance, is the ball-park agreement and the ability of the model results to trend in a sensible manner, which was demonstrated in the analysis of the 8 October 1997 results above. In any case, in controlling a variable, the nature in which it trends is equally, and often more, important as its absolute value.

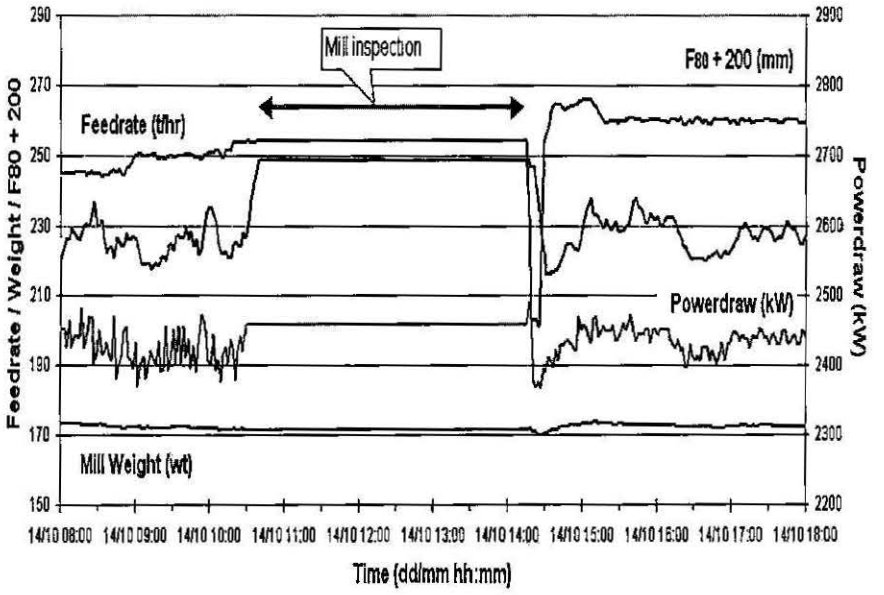

Figure 8.5: Results for 14 October 1997: Mill powerdraw and weight prevailing at the time of the mill inspection.

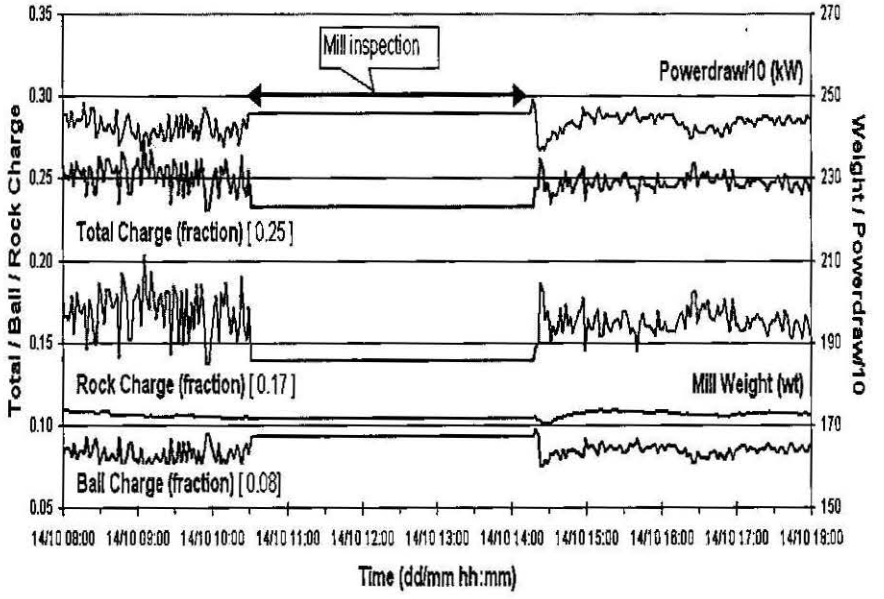

Figure 8.6: Results for 14 October 1997: Mill charge estimates for the time of the mill inspection. Total charge (J_t): 0.25, Ball charge (J_b): 0.08.

Charge Estimate Cross-Correlation

As mentioned above, there is evidence in the inferential measurement model results of negative, proportional correlation between the ball charge estimate (J_b) and the estimates of total (J_t) and rock (J_r) charge. The results were plotted on X-Y plots to determine the level of cross-correlation and ascertain whether it was of concern.

Figure 8.7 shows the correlation between the total charge (J_t) estimates and the ball charge (J_b) estimates. The linear regression of the data exhibits a moderate degree of correlation only, $\approx$ 53%. Visual inspection suggest that the data could possibly be classified into three or more bands that exhibit linear behaviour with a slope close to negative two(-2). It is beyond the scope of this research to investigate this possibility in further detail but it could be hypothesised that the apparent bands could correspond to different ore hardness levels. That is, for a given ball charge level, say 0.10, for periods of softer ore feed, lower rock and total charge levels would prevail, say 0.13 & 0.23, respectively. For periods of harder ore feed, rock and total charge levels of 0.17 & 0.27, respectively, could prevail. Further investigation of this proposed phenomenon could be the focus of future work.

Figure 8.8 shows the correlation between the rock charge (J_r) estimates and the ball charge (J_b) estimates. Although there is a hint of the striations that seem evident in Figure 8.7, the linear regression shows there is a strong correlation, $\approx$ 84%, between rock charge and ball charge. As mentioned above, a strong correlation is expected in this case since increasing the ball charge will generally cause more breakage thus a reduced rock charge.

This analysis was deemed sufficient to conclude that there was no undesirable correlation present in the charge estimate results.

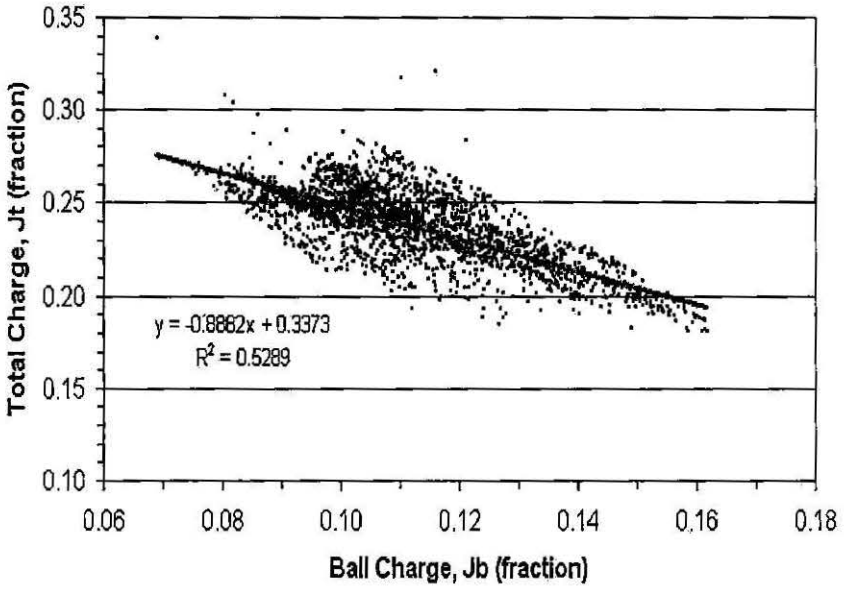

Figure 8.7: X-Y plot of Total charge (J_t) *versus* Ball charge (J_b). Moderate correlation ($\approx$ 53%) only.

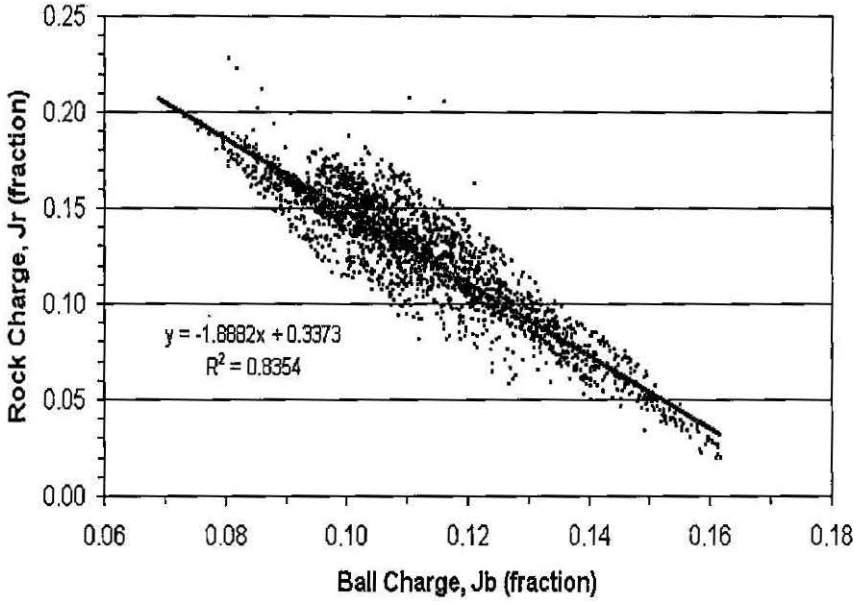

Figure 8.8: X-Y plot of Rock charge (J_r) *versus* Ball charge (J_b). High correlation ($\approx$ 84%) as expected.

8.1.2 Increasing Feed Size and Feed F_{80} Estimate

During the afternoon shift of 9 October 1997, the mill control room operator noted that the feed size was increasing, see Figure 8.9.

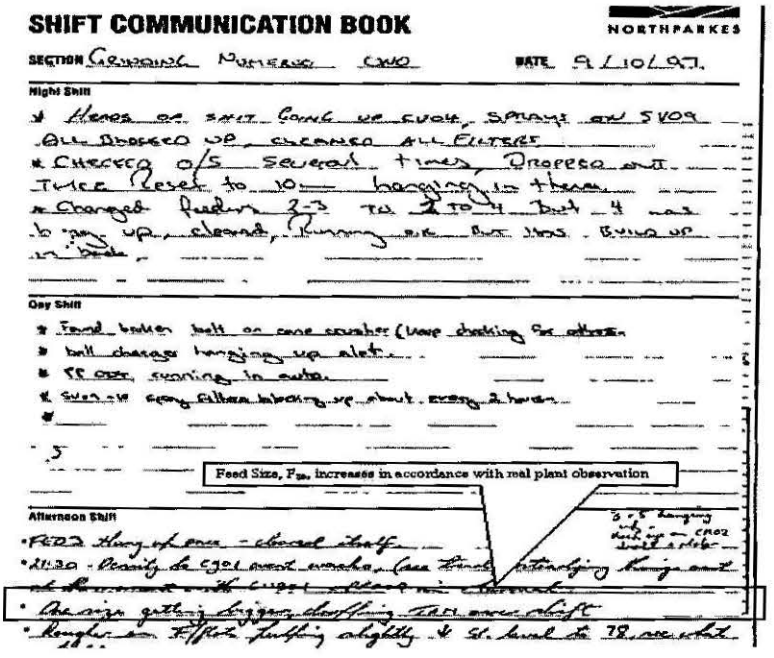

Figure 8.9: Module 1 Shift Communication Book 9 October 1997: Feed size increasing during afternoon shift

This observation is captured well by the inferential measurement model of the feed size - by way of theF_{80} measurement, see Figure 8.10. The increasing mill powerdraw corresponds to the increasing feed size. To accommodate this feed size increase (presumably due to increasing hardness), the operator decreases the feedrate.

The absolute value of the actual F_{80} trend on 9 October 1997 is not known. However, the utilisation of the F_{80} inferential measurement model within a controller structure would still be possible, since the way the model measurement trends is the key characteristic here. Suitable high and low limits may be set nominally or via a calibration procedure to accommodate any offset between model prediction and plant reality.

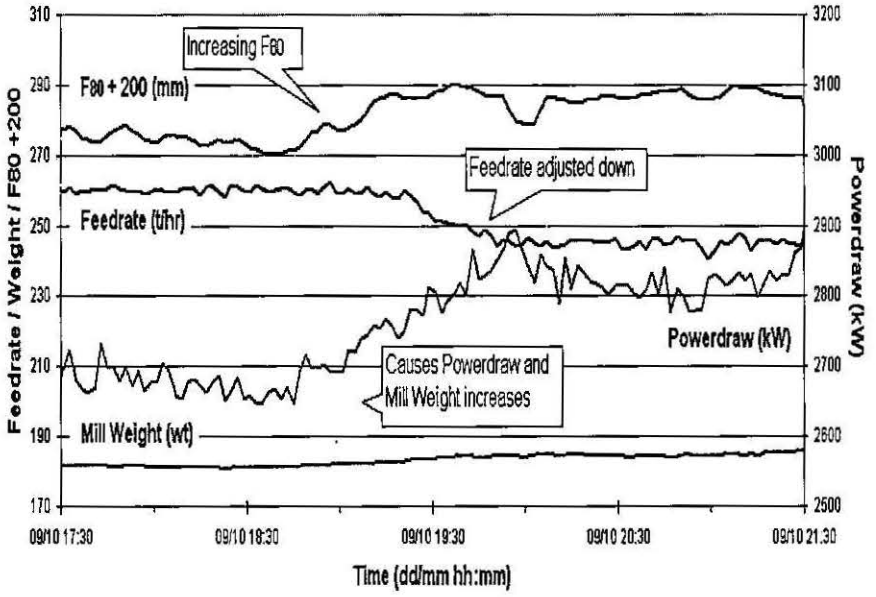

Figure 8.10: Results for 9 October 1997: F_{80} model increases as observed by the Control Room Operator.

8.1.3 Mill Density Increase and Oversize Crusher Off-line

Although the results produced by the inferential measurement models were most encouraging overall, two situations dramatically affected model performance, namely:

1. the oversize crusher going off-line
2. a sudden increase in the SAG mill feed density

In the first case, as detailed on day shift in the Shift Communication Book, see Figure 8.11, the problems are experienced with the oversize crusher.

The problems with the oversize crusher are reflected in the feed size (F_{80}) estimate, see Figure 8.12. When the oversize crusher is off-line, the F_{80} estimate increases markedly. When the oversize crusher is off-line, the SAG mill *scats* (oversize crusher feed) are recycled directly causing a build up of critically-sized within the mill and an increase in mill powerdraw and weight.

The oversize crusher outage also affects the mill charge estimates, see Figure 8.13. While the oversize crusher is off-line, the charge inferential measurement model estimates an elevated ball charge (J_b) and depressed total (J_t) and rock (J_r) charges. In reality, the ball charge level would have remained constant and the rock and total charges would have increased.

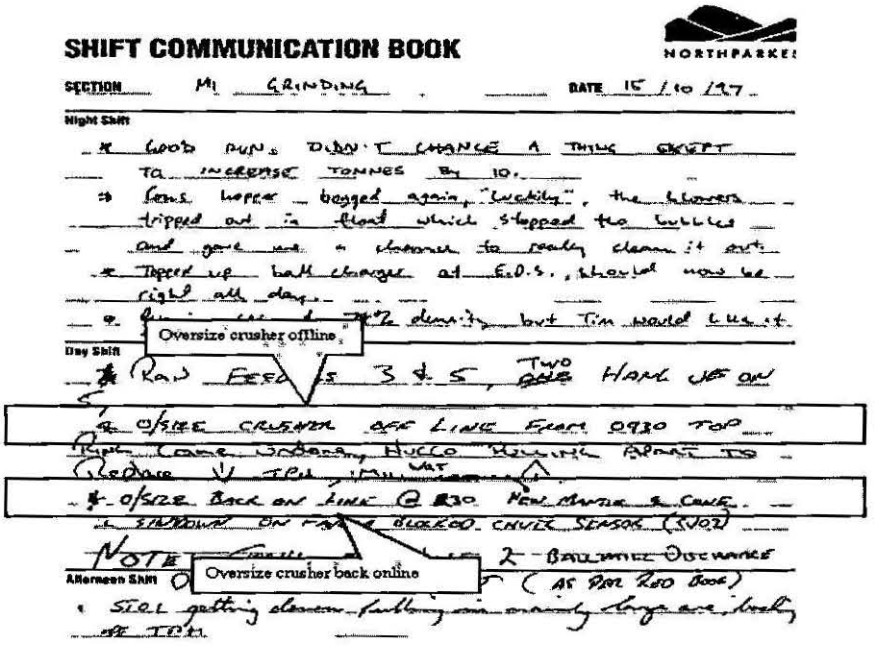

Figure 8.11: Module 1 Shift Communication Book 15 October 1997: Oversize crusher taken off-line and returned on-line later.

If the models were part of a controller at the time, normal plant operating status checks would have switched the controller off, thus avoiding any undue control action. Additionally, this model feature could potentially be utilised as a process monitoring and diagnostic tool to alert the process operators of the advent of unusual process conditions.

Further analysis of the source of this model behaviour is discussed in the next Section 8.2. The possible utilisation of the model as a process diagnostic tool is considered beyond the scope of this research. Potential future work could further investigate this area of research.

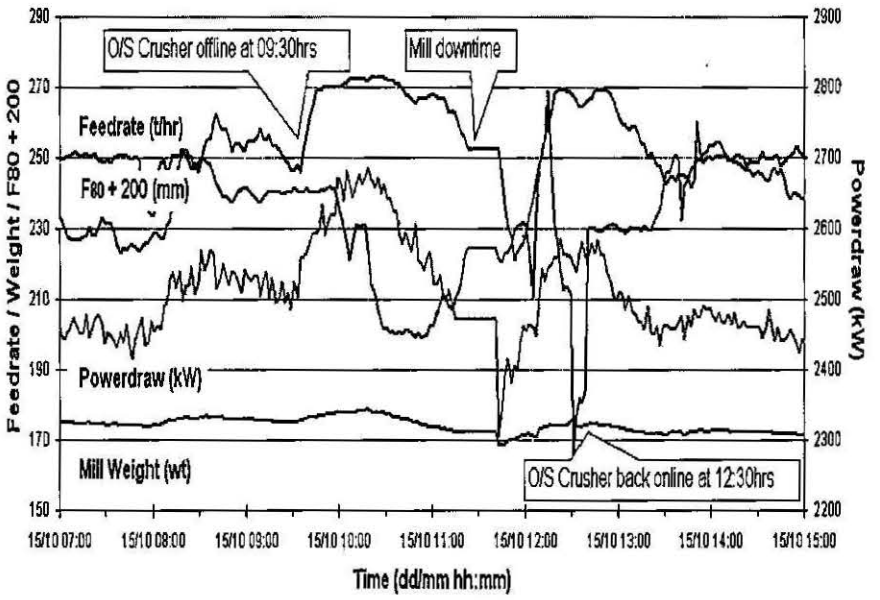

Figure 8.12: Results for 15 October 1997: Oversize crusher going off-line affects feed size (F_{80}) estimate.

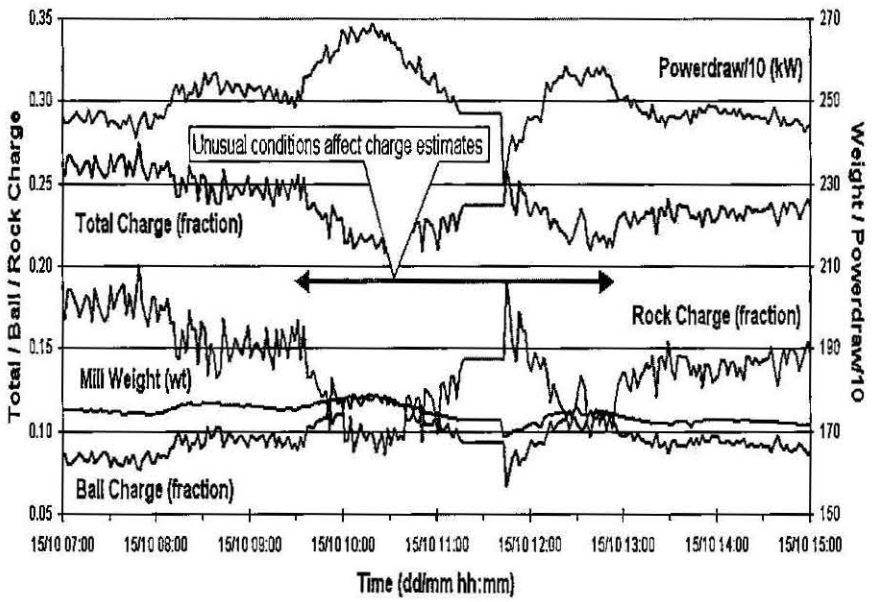

Figure 8.13: Results for 15 October 1997: Oversize crusher going off-line also affects the mill charge estimates.

In the second case, during afternoon shift on 9 October 1997, the mill feed density was increased two percent to stop shell-bolts leaking, refer to Figure 8.14. This change was made at approximately 19:00 hrs. Now referring to Figure 8.15, one observes that at 19:00 hrs, the increased feed density causes an increase in mill powerdraw and mill weight. These increases in the plant measurements cause ball charge estimate increases and the rock and total charge estimate decreases.

The analysis conducted in Chapter 6 did not capture the sensitivity of the mill charge estimates to feed or mill charge density. The further analysis presented in Section 8.2 encompasses feed density changes. Although mill density changes have not been captured as explicitly, the forcing of the mill weight measurement could conceivably be seen as incorporating mill density. Further, future work could expand this research area.

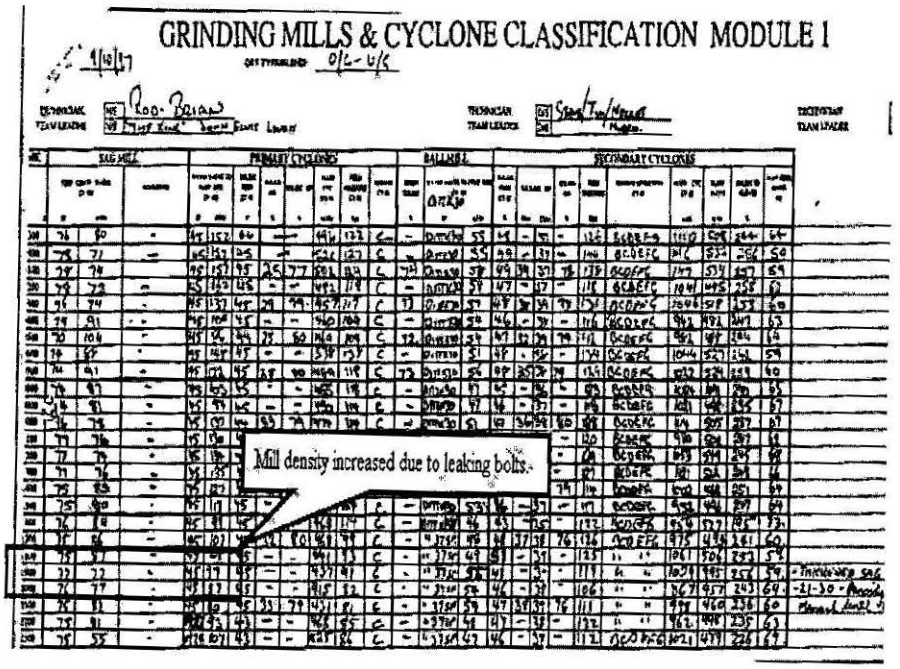

Figure 8.14: Module 1 Grinding Log Sheet, 9 October 1997: Mill density is increased to stop shell-bolts leaking.

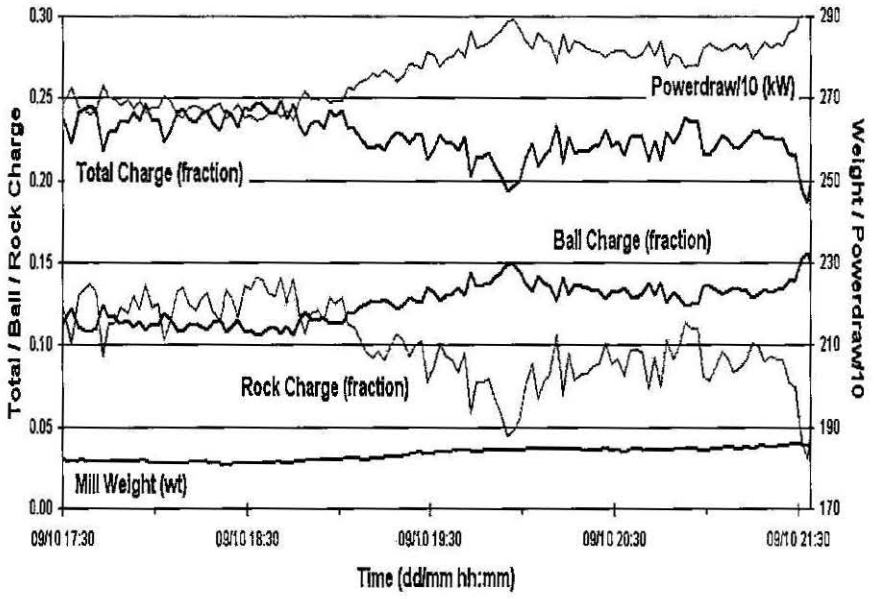

Figure 8.15: Results for 9 October 1997: Increase in mill density is thickened causes increases in mill powerdraw and weight, which affects the mill charge estimates.

The preceding discussion has illustrated that the inferential measurement models developed in Chapter 5 are able to produce results consistent with plant observations and thus are considered to be valid. Further research into model behaviour during abnormal plant operating conditions and sensitivity to operating conditions, such as feed slurry density, are possible avenues to progress research in this area. The next Section progresses the research in this topic area as it investigates model behaviour, sensitivity and characteristics.

8.2 Mill Charge and Feed Size Sensitivity Analysis

Here we investigate the discrepancy between the expected and witnessed behaviour of the inferential models. In Section 8.2.1, the models are artificially excited and the cause, effect and sensitivity are described. In Section 8.2.2, the source of the unusual behaviour of the feedsize estimate is investigated and the nature of the mill charge estimates and their relative uncertainties are examined. In Section 8.2.3, the nature of the mill charge estimates is utilised to generate a SAG mill operating curve, which is discussed in the context of mill charge control.

In Section 8.1.3, unusual behaviour was noted in the charge and feed size inferential model estimates that occurred when the oversize crusher went off-line. Specifically, when the crusher went off-line:

- the ball charge (J_b) increased
- the total charge (J_t) and rock charge, (J_r) decreased
- the feedsize estimate (F_{80}) increased

In reality, the ball charge level would have remained constant and the rock and total charges would have increased, with the build up of critically sized material, and there would have been no effect on the feedsize.

Also noted in Section 8.1.3, was the effect of feed density on the estimates. When the mill density increased:

- the mill powerdraw and mill weight increased
- the ball charge (J_b) increased
- the total charge (J_t) and rock charge, (J_r) decreased
- the feedsize estimate (F_{80})

In reality, the ball charge level would have remained constant and the rock and total charges would have increased, with the reduced breakage resulting from increased pulp viscosity and cushioning. Again, there would have been no effect on the feedsize.

Additional data was required to analyse the source of this behaviour. The additional information required to further analyse the models was obtained by subjecting the SAG mill charge and feedsize models to artificial stimulation.

Each of the key model inputs were ramped up and down by $\pm$ 10%. The nominal conditions are those prevailing at 10:27 a.m. on 14 October 1997. The key model inputs, with their nominal starting values in parentheses, are:

1. SAG mill powerdraw (2422 kW);
2. SAG mill weight (172 t);
3. Oversize crusher feedrate (scats) (55 t/hr);
4. SAG mill feedrate (252 t/hr);
5. SAG mill feed water (90 m^3/hr).

The corresponding mill charge and feed size estimates for these conditions are:

J_t = 25% - SAG mill total charge

J_b = 8% - SAG mill ball charge

J_r = 17% - SAG mill rock charge

F_{80} = 27 mm - SAG mill fresh feed 80% passing size

8.2.1 Artificial Stimulation: Cause, Effect & Sensitivity

In this Section, the models are artificially excited and the cause, effect and sensitivity are described. The key model inputs were perturbed sequentially as per the order above. The cause and effect of the artificial disturbance to powerdraw are shown in Figures 8.16 and 8.17, respectively. Note that the time series is generated from the starting time. As described, four of the model inputs are held constant while the fifth input is varied. The time series is only a framework to support the generated results (rather than a reference to the actual date and time).

The cause and effect of the artificial disturbance to mill weight are shown in Figures 8.18 and 8.19, respectively.

The cause and effect of the artificial oversize crusher feedrate (scats), SAG mill feedrate and SAG mill feedwater addition disturbances are shown in Figures 8.20 and 8.21, respectively.

Addressing two anomalies from the outset:

1. F_{80} behaviour: Observing Figures 8.17, 8.19 and 8.21, it is clear that the behaviour of the feedsize, F_{80}, inferential model is irregular. The cause of this behaviour is

discussed further in the next Section. Suffice to say, model assumptions and structure strongly influence the behaviour of this estimate.

2. Cause – Effect capping: In Figure 8.19, the model estimates are capped. (The rock charge estimate (J_r) has also ventured into the sub-zero region.) The capping was enforced when the mill weight was forced below approximately 160 t. Beyond this point, the constrained optimisation problem became infeasible. Recall that the optimisation problem estimates the total charge (J_t) and ball charge (J_b) from the powerdraw residual (Equation (5.17)) and the weight residual (Equation (5.21)) subject to the physical constraint that the ball charge can never be greater than the total charge ($J_b \leq J_t$). The rock charge (J_r) and feedsize (F_{80}) estimates depend on the ball and total charge estimates. Therefore, calculation of these estimates also became infeasible.

Generally, holding four of the input variables steady while ramping the fifth has highlighted that movement in the inputs translates to movement in the estimates. This will also apply to measurement noise translating to noise in the estimates. For example, moving the powerdraw value, see Figure 8.16, results in movement in total, ball and rock charge estimates and feedsize estimate, see Figure 8.17.

A further general comment is that since rock charge fraction (J_r) is calculated by subtracting ball charge fraction (J_b) from the total charge fraction (J_t), it follows then that behaviour evident in either of the total or ball charge fraction estimates appears also in the rock charge fraction estimate.

More specific observations on the sensitivity of the estimates to the model inputs are as follow (by model input):

- **Powerdraw**: Referring to Figures 8.16 and 8.17, the movement of the total charge fraction (J_t) and rock charge fraction (J_r) estimates is negatively proportional to changes in powerdraw. The movement of the ball charge fraction (J_b) estimate is proportional. Table 8.1 contains the "sensitivities" of the estimates to powerdraw and the other model inputs. The sensitivities are calculated by dividing the range of the estimate by the range of the input. For example, for the total charge and powerdraw case, the input range of ± 10% equates to 484 kW. The resulting range in the total charge estimate (nominal value of 25%) of −19% (shown here in *per cent volume* rather than volumetric fraction). The sensitivity of the total charge fraction estimate to an increase of 100 kW in powerdraw is there will be a **decrease** in the total charge of 4% volume.

The sensitivities of the ball and rock charge fraction estimates to a 100 kW change in powerdraw are 2% and −6% volume, respectively.

Taken in isolation, the magnitudes of the sensitivities appear near-credible. However, perhaps half of these figures is more realistic. The ranges exhibited in the estimates are of the same order of magnitude as their nominal values. The large sensitivities suggest the inferential models may be highly sensitive to changes in powerdraw, which was found to be the case in Section 6.2.3. Reinforcing this finding is that all of the changes take place concurrently. That is, a 100 kW increase in powerdraw represents a 2% increase in ball charge volume and a 4% decrease in total charge volume (these in turn represent a 6% decrease in rock charge volume). Once again, figures half this magnitude would be more realistic, *i.e.*, an increase in powerdraw of 100 kW could be expected to result from a 1% increase in ball charge volume and a 3% decrease in rock charge volume (2% increase in total charge volume).

This degree of sensitivity adds to the case for measurement filtering. The noise inherent in the measuring device plus the noise of the tumbling charge within the mill warrants significant filtering, *e.g.*, a 5-minute moving average. The fact that the operating point does not move in large sudden steps has an attenuating effect on the sensitivities also.

It should also be noted that an increase in powerdraw is likely to be accompanied by an increase in mill weight in the real plant. Therefore, changes in the charge estimates due to powerdraw changes would be tempered by changes in the mill weight. The sensitivities of the charge estimates to changes in mill weight are discussed below.

The feedsize (F_{80}) estimate also exhibits a high degree of sensitivity to changes in powerdraw: a 100 kW change in powerdraw will result in a 20 mm change in feedsize estimate. A change in the feedsize estimate of between 2 - 10 mm (10 - 50%) would be more realistic.

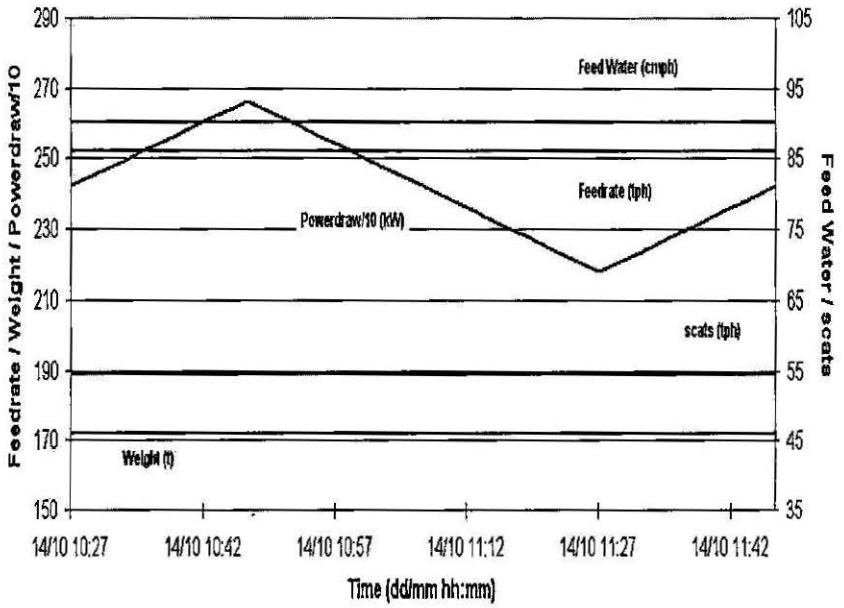

Figure 8.16: Cause: Artificial disturbance of the SAG mill powerdraw. Four model inputs held constant with powerdraw ramping up and down.

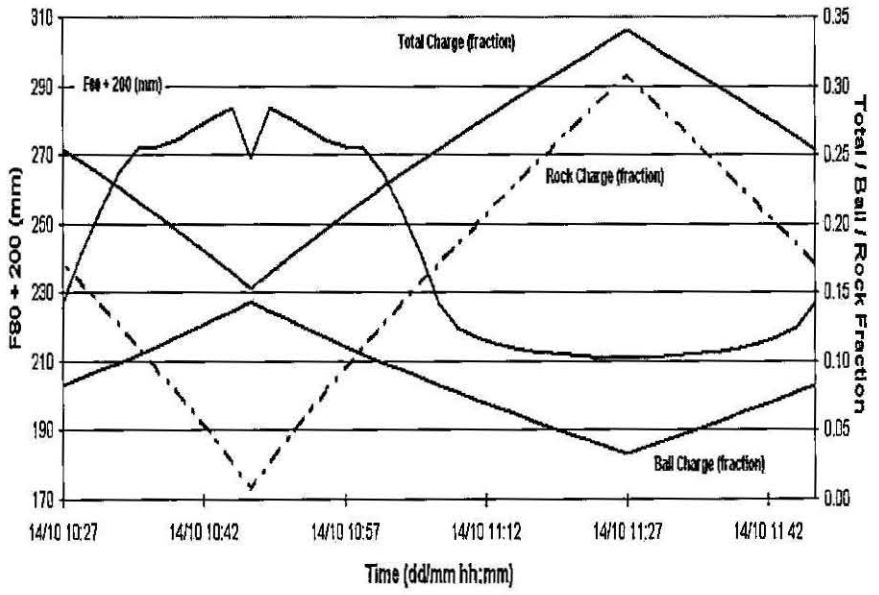

Figure 8.17: Effect: Artificial disturbance of the SAG mill powerdraw. Total charge and rock charge move negatively-proportional to powerdraw. Ball charge moves proportionally. Feedsize moves non-uniformly but generally proportionally.

Table 8.1: SAG Mill Charge and Feedsize Model Sensitivities

		Total Charge, J_t		Ball Charge, J_b		Rock Charge, J_r	
Input	Range	Range (25%)	$\frac{\Delta J_t}{\Delta Input}$	Range (8%)	$\frac{\Delta J_b}{\Delta Input}$	Range (17%)	$\frac{\Delta J_r}{\Delta Input}$
Powerdraw	484 kW	-19%	-4%	11%	2%	-30%	-6%
Weight	31 t	35%	1%	-12%	-0.4%	48%	2%
scats	11 t/hr	0.2%	0.1%	0.0%	0.0%	0.0%	0.0%
feedrate	50 t/hr	0	0	0	0	0	0
H_2O addition	18 m^3/hr	0	0	0	0	0	0

		Feedsize, F_{80}	
Input	Range	Range (27 mm)	$\frac{\Delta F_{80}}{\Delta Input}$
Powerdraw	484 kW	72.9	0.2
Weight	31 t	-68.9	-2.2
scats	11 t/hr	8.5	0.8
feedrate	50 t/hr	0	0
H_2O addition	18 m^3/hr	0	0

- **Weight**: Referring to Figures 8.18 and 8.19, the movement of the total charge fraction (J_t) and rock charge fraction (J_r) estimates is near-linearly proportional to changes in mill weight. The movement of the ball charge fraction (J_b) estimate is near-linearly, negatively, proportional. Table 8.1 contains the "sensitivities" of the estimates to mill weight. The input range of $\pm$ 10% equates to 31 t. The sensitivity of the total charge fraction estimate to an increase of 1 tonne in mill weight is an increase in the total charge of 1% volume. The sensitivities of the ball and rock charge fraction estimates to a 1 tonne change in mill weight are -0.4% and 2% volume, respectively.

These sensitivities to weight changes are more credible than those for powerdraw changes. Filtering the mill weight measurement to remove measurement noise and noise due to the tumbling charge is still warranted. A five-minute moving average could be applicable here. Further research could investigate the appropriate filtering for both the weight and powerdraw signals.

The feedsize (F_{80}) estimate exhibits an unusual degree of sensitivity to changes in mill weight: a 1 tonne increase in mill weight will result in a -2 mm change in feedsize estimate. A decrease in feedsize generally accompanies a decrease in feed ore hardness. A decrease in mill weight would be expected as the rock charge would decrease since the rock breaks more easily. The behaviour of the estimate is unusual also and this will be discussed further in the next Section.

- **Scats**: Referring to the left-hand-side of Figures 8.20 and 8.21, the mill charge estimates are affected only slightly by changes in the oversize crusher feedrate (*scats*). One would expect increased "scats" could reflect an increase in the rock charge, a decrease in the ball charge (by increased wear) and an increase in the total charge fraction overall, as is the case here. However, the "sensitivities" here, see Table 8.1, are not attributed to such processing conditions. Here it it due to the nature of the models. The "scats" tonnage and an assumed particle size distribution are used in the estimate of the SAG mill discharge stream. The discharge stream affects the mill rock charge, which in turn, affects and feed estimates. Hence, changes in the "scats" cascade upstream through the mill charge inferential models to the feedsize inferential model.

  There is near-linear proportionality in the movement of the feedsize model estimate with respect to "scats" movement. A 10 t/hr increase in *scats* will result in an 8 mm increase in the feed F_{80} estimate. In the real plant an increase in "scats" would be expected with an increase in feedsize (and ore hardness). The model captures this to degree in that with an increased "scats" tonnage, the SAG mill discharge stream, the mill rock charge and total feed and fresh feed estimates are all more coarse. However, the feedsize estimate is also influenced by the subtraction of the oversize crusher product from the total mill feed stream. The assumptions made for the oversize crusher product size distribution may result in a fine, closely-sized stream being subtracted from the total mill feed stream. Thus, rendering the fresh feed more coarse. Further research could investigate how the oversize product size distribution changes with "scate" tonnage to check the validity of the crusher product size distribution assumptions.

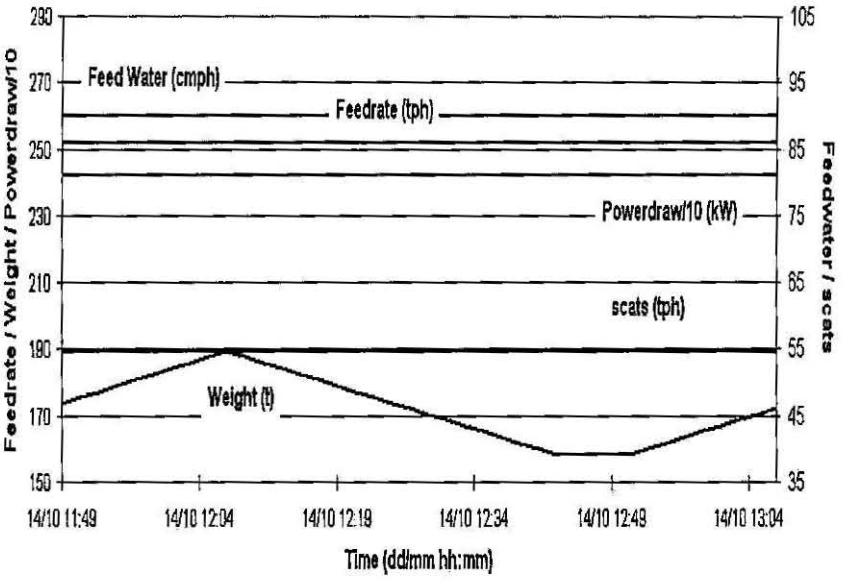

Figure 8.18: Cause: Artificial disturbance of the SAG mill weight. Four model inputs held constant with mill weight ramping up and down (with capping at low mill weight).

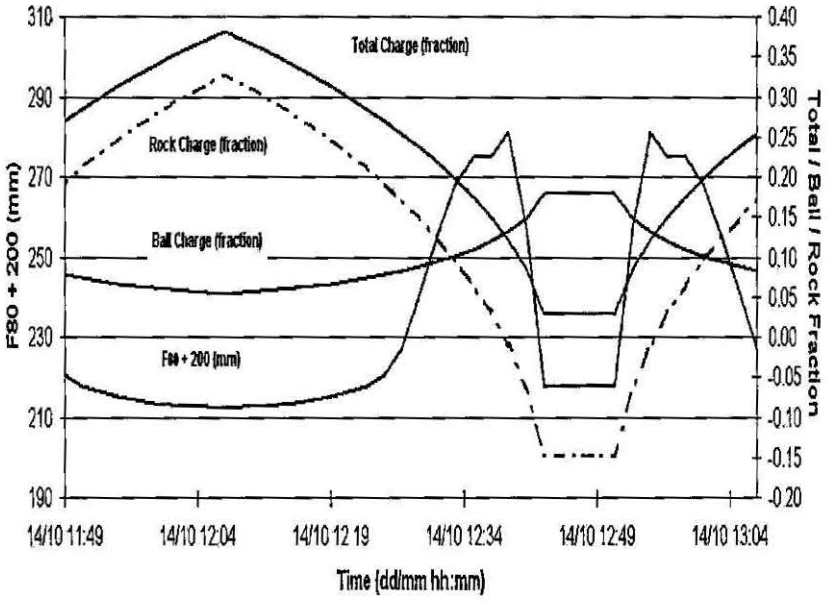

Figure 8.19: Effect: Artificial disturbance of the SAG mill weight. Total charge and rock charge move proportionally to mill weight. Ball charge moves negatively-proportionally. Feedsize moves non-uniformly but generally negatively-proportionally.

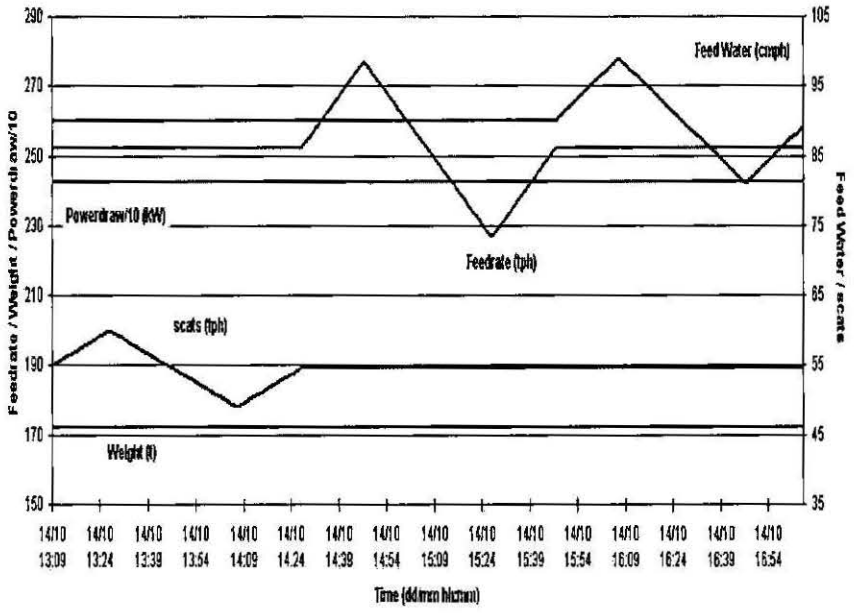

Figure 8.20: Cause: Artificial disturbance of the oversize crusher feedrate, SAG mill feedrate and SAG mill water addition. Four model inputs held constant with the ramping up and down of oversize crusher feedrate, SAG mill feedrate and SAG mill water addition sequentially.

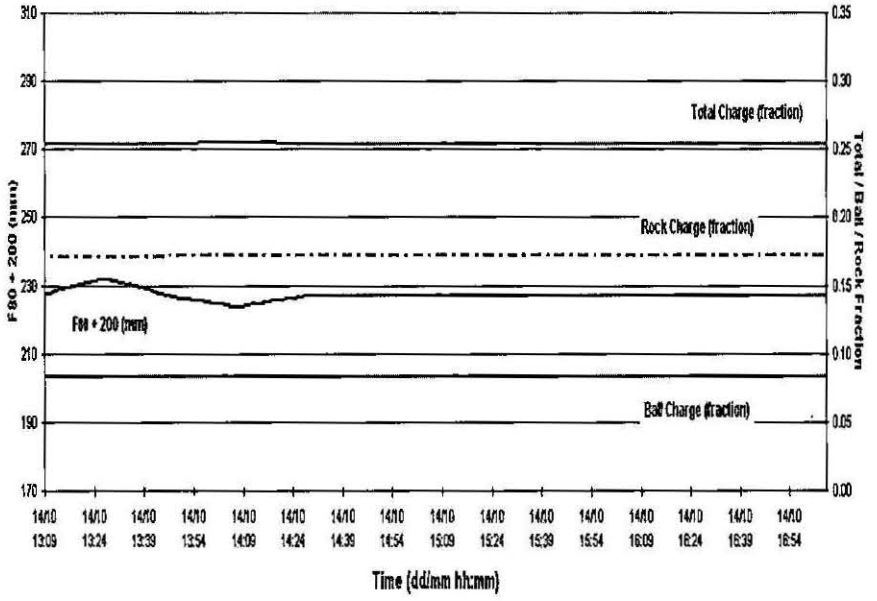

Figure 8.21: Effect: Artificial disturbance of the oversize crusher feedrate, SAG mill feedrate and SAG mill water addition. Minimal effect except for proportional feedsize movement with "scats".

The construction of the feedsize model and the resulting propagation of "scat" and mill discharge and charge model results through to the feedsize estimate is a limitation and should be noted. However, in the absence of an online size measuring device, the feedsize model estimate could be utilised, particularly since changes in "scats" do not generally happen in isolation. The surrounding process condition changes would possibly attenuate this limitation. Further research could investigate this.

- **Feedrate**: Referring to the central third of Figures 8.20 and 8.21, one can see that the feedrate has no effect on the mill charge or feedsize estimates. In practice, an increase in feedrate would result in an increase in mill weight and powerdraw, which would affect the mill ball, rock and total charges estimates.

- **Water addition**: Referring to the right-hand-side of Figures 8.20 and 8.21, it is also evident that SAG mill water addition does not affect on the mill charge and feedsize estimates. In practice, a decrease in water addition would result in an increase in mill weight and powerdraw, which would affect the mill ball, rock and total charges estimates.

  These latter two points appear to be at odds with the observations described in Section 8.1.3. The apparent conflict in findings can be explained by looking at the real plant situation. The increased mill feed density in the real plant was accompanied by increases in mill weight and powerdraw, which do have an impact on the inferential model estimates, as described above. In contrast, the changes made to the inputs in this Section were made in isolation. Hence, these changes do not reflect real changes in operating conditions.

In this Section, the models were artificially excited and the cause, effect and sensitivity are described. In isolation, without an associated change in mill weight or powerdraw, the feedrate and water addition were found to have no affect on the mill charge and feedsize estimates. The oversize crusher feedrate (*scats*) was found to affect the mill charge and feedsize estimates but not as a reflection of process conditions. Rather, the nature of the construction of the model was found to be the cause of these relationships. This is considered a model limitation, which should be noted when dealing with the results. The mill weight and powerdraw were found to affect the mill charge and feedsize estimates. Filtering of these measurements was suggested to diminish the effect of noise. It was noted that the model sensitivity would be tempered by real process behaviour, where powerdraw changes are accompanied by mill weight changes.

8.2.2 Further Inferential Model Behaviour Analysis

The behaviour of the inferential models observed in the previous Section, particularly during the artificial stimulation of the mill weight input, warranted further analysis. In this Section, the source of the unusual behaviour of the feedsize estimate is investigated. The nature of the mill charge estimates is examined and highlights the behaviour of the total charge estimate (J_t) in relation to the ball charge estimate (J_b).

Feedsize inferential model

As noted previously, the behaviour of the feedsize, F_{80}, inferential model is somewhat irregular. The feedsize estimate is at the end of a chain of calculations. The results of the calculations in the chain and assumptions made in them affect the feedsize estimate.

Recalling from Chapter 5, that estimates of the primary cyclone feed and oversize crusher feed are added together to estimate the SAG mill discharge stream, see Section 5.1.1. The discharge stream is passed through the grate classification function to estimate the bottom of the SAG mill rock charge size distribution, the coarser size fractions estimated from extrapolation of a Rosin-Rammler size distribution, Section 5.1.2.

The total, ball and rock charge fractions are estimated from the mill powerdraw and weight measurements in Section 5.1.3. From the rock and ball charge estimates, the breakage parameters are estimated. The SAG mill total feed is estimated using these parameters, the rock charge fraction and size distribution estimates and the SAG mill discharge stream estimate, see Section 5.1.4.

Finally, an estimate of the SAG mill fresh feed is obtained by subtracting estimates of the oversize crusher product and primary cyclone underflow from the SAG mill total feed estimate, see Sections 5.1.5 and 5.1.6.

All of these steps contain model inaccuracy and errors introduced by simplifying assumptions. Although the primary cyclones are several unit operations removed from the feed stockpile, the nature of the feedsize estimate model means that the primary cyclone streams (and all other streams between) influence the feedsize estimate.

Considering this, the behaviour of the model variables during the weight excitation was further investigated. The specific comminution energy (E_{cs_i}), high energy impact parameter (t_{10_i}) and the breakage rates (r_i) were plotted over the period that the mill models were undergoing weight excitation.

Figures 8.22 and 8.23 show how the specific communition energy and high impact breakage parameter vary during the period of excitation of the mill weight. Apart from the capped

area, there is no real highlight to the curves. They both seem to exhibit fairly ordered behaviour.

It is not until the plot of the breakage rates over this period is observed that something more striking is evident, see Figure 8.24. At the point when the mill weight was capped (prevented from going lower than approximately 160 t), the breakage rates were undergoing an order-of-magnitude change.

Graphing the SAG mill discharge and SAG mill rock charge size distributions for reference (10:29 a.m.), high-powerdraw (10:47 a.m.) and low mill weight (12:47 p.m.) conditions, see Figures 8.25 and 8.26, respectively, illustrated that these streams were not actually changing during the mill weight and powerdraw excitations. Therefore, these streams were not contributing to the changes in the feedsize estimate.

We see from Equation (5.22) that the feed estimate is a function of the appearance function (a_{ij}) and the breakage rate function (r_i). The appearance function is dependent on the specific comminution energy (E_{cs}) and the impact breakage parameter (t_{10}). These were plotted for the reference (10:29 a.m.), high-powerdraw (10:47 a.m.) and low mill weight (12:47 p.m.) conditions, see Figures 8.27 and 8.28, respectively.

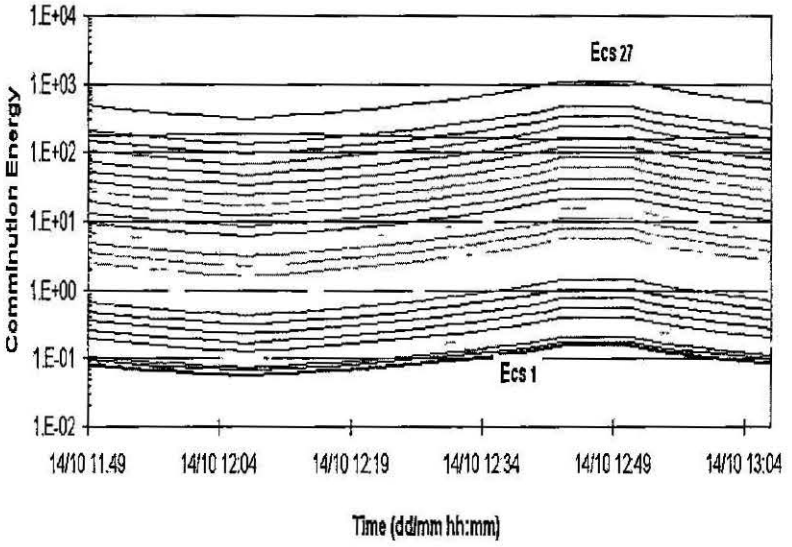

Figure 8.22: Specific comminution energy (E_{cs_i}) during weight excitation. Ordered behaviour. No remarkable features.

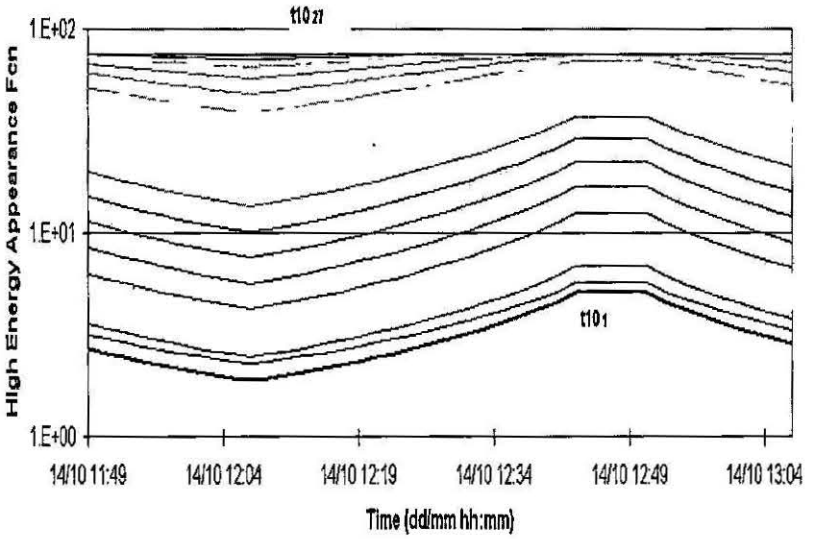

Figure 8.23: High impact breakage parameter (t_{10_i}) during weight excitation. Ordered behaviour. Effect of mill weight capping evident at right.

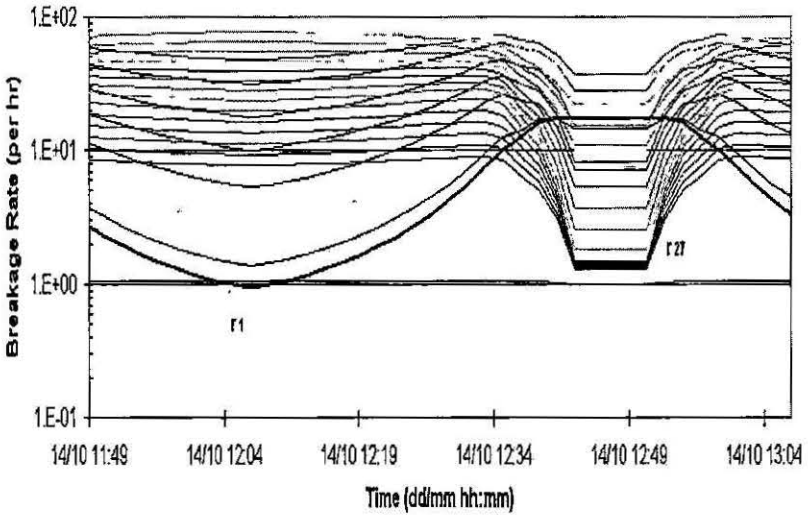

Figure 8.24: Breakage rates (r_i) during weight excitation. Order of magnitude changes occurring around weight capping at right.

For the extreme conditions, both the specific comminution energy and the impact breakage parameter are higher than for the reference conditions. The resulting appearance function would have smaller elements near the diagonal (the appearance function is a lower triangular matrix), which translates to more breakage and a finer product. Applied in reverse, as is the case here, this translates to a coarser total SAG mill feed. Clearly there is an impact on the feed size estimate here. However, the changes in the specific comminution energy and impact breakage parameter do not appear to be major. The feedsize estimate behaved quite orderly when the ball charge estimate was less than the reference (starting point), see the periods of low mill powerdraw and high weight, see Figures 8.17 and 8.19, respectively.

In Section 3.3.1, we note that the breakage rate equations (Equations 3.22 to 3.26) are all functions of mill ball charge fraction, J_b. As the ball charge estimate increases with mill weight, the breakage rates increase in an exponential manner. This suggests that the feedsize estimate will be strongly affected by the ball charge estimate. The breakage rates were plotted for the reference (10:29 a.m.), high-powerdraw (10:47 a.m.) and low mill weight (12:47 p.m.) conditions, see Figure 8.29. It is immediately clear that the breakage rates for the extreme conditions are markedly different to the reference case.

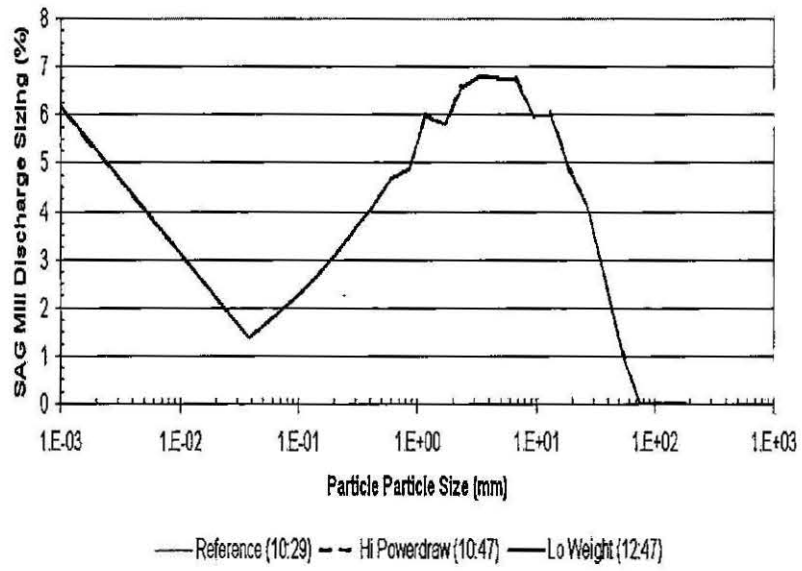

Figure 8.25: SAG mill discharge size distribution for reference, high-powerdraw and low mill weight conditions. Estimates are co-linear.

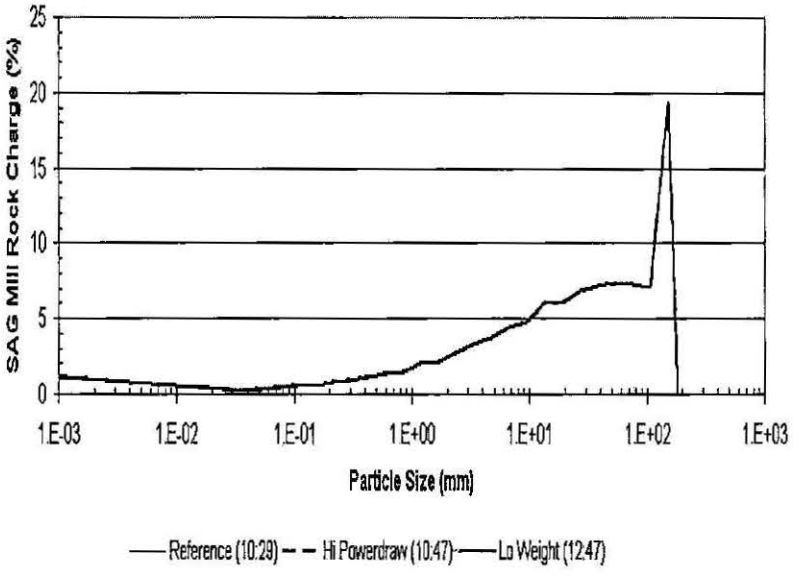

Figure 8.26: SAG mill rock charge size distribution for reference, high-powerdraw and low mill weight conditions. Estimates are co-linear.

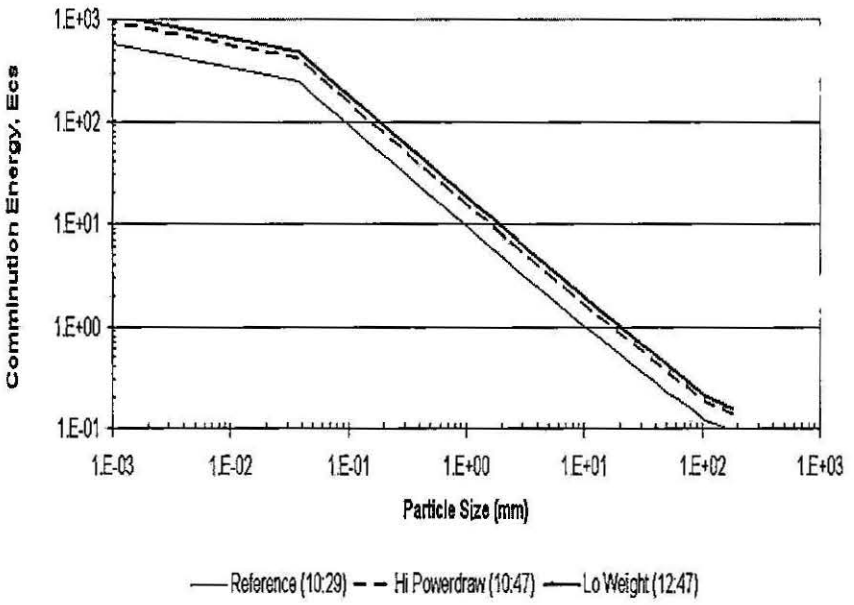

Figure 8.27: Specific comminution energy (E_{cs}) by size for reference, high-powerdraw and low mill weight conditions. Ordered behaviour. No remarkable features.

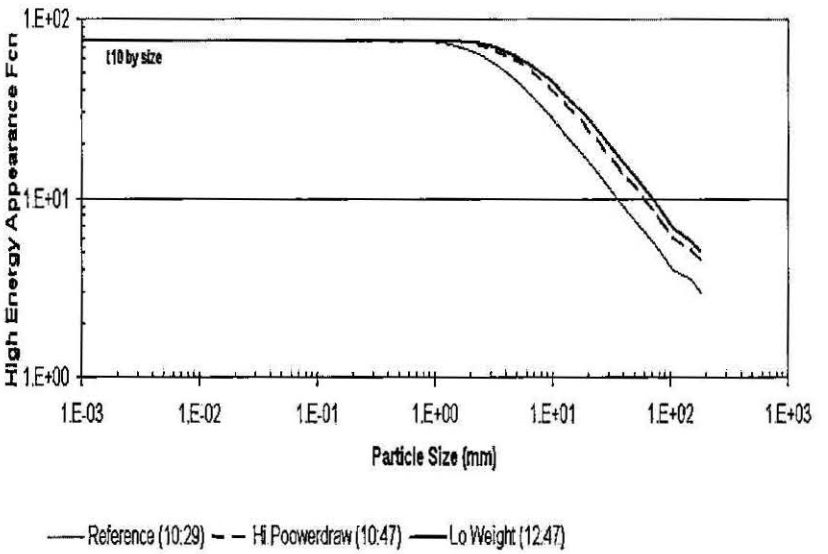

Figure 8.28: Impact breakage parameter (t_{10}) by size for reference, high-powerdraw and low mill weight conditions. Ordered behaviour. No remarkable features.

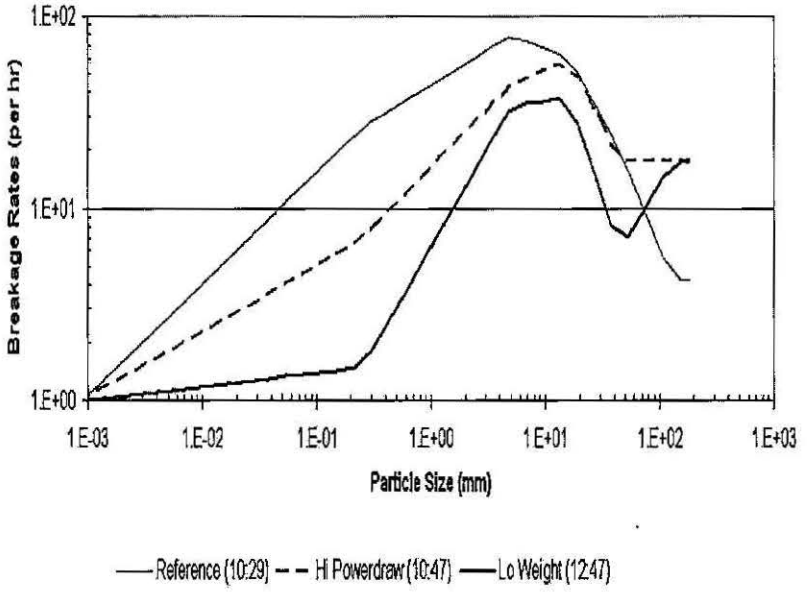

Figure 8.29: Breakage rate (r_i) by size for reference, high-powerdraw and low mill weight conditions. Large differences between estimates. Order of magnitude differences in places.

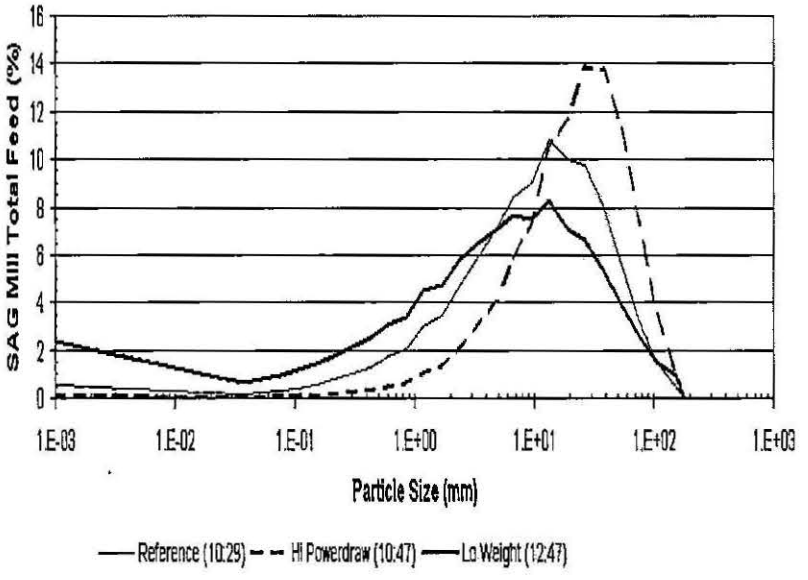

Figure 8.30: SAG mill total feed size distribution for reference, high-powerdraw and low mill weight conditions. Significant differences between estimates - as a result of the differing breakage rates.

The effect of the different breakage rates on the SAG mill total feed is evident in Figure 8.30. The reference feedsize F_{80} estimate is 27 mm. If the estimate had held its level for the low mill weight conditions, see Figure 8.19, then for both extreme conditions, the feedsize F_{80} estimate is approximately 80 mm - a significant increase in estimate size.

The source of the unusual behaviour of the feedsize F_{80} estimate is now evident. The high sensitivity to the SAG mill breakage rates is a concern and should be noted duely. This finding is consistent with the discussion of sensitivity of the dynamic SAG mill rock charge model to the breakage rates in Sections 4.2.3 and 6.5. Filtering the mill powerdraw and weight signals specifically for the feedsize estimate could reduce the impact of measurement and process noise. A 15-minute rolling average could be utilised here. Feedsize changes typically occur over a longer time period, *e.g.*, 15-30 minutes. Therefore, valuable information will not be lost whilst achieving a more reliable estimate.

Mill charge inferential model

In this Section, the nature of the mill charge estimates is examined and highlights the behaviour of the total charge estimate (J_t) in relation to the ball charge estimate (J_b) and the behaviour of the comparative uncertainties in the estimates.

Four other reference operating points were selected arbitrarily from the plant data to encompass high and low mill powerdraw and mill weight, see Table 8.2. From each of these reference points, the mill powerdraw and weight were ramped up and down 10% to obtain powerdraw contours and weight contours in the total charge (J_t) – ball charge (J_b) space. Figure 8.31 shows the contours for the reference conditions discussed in the previous Section, *i.e.*, Powerdraw = 2422 kW and Weight = 172 t (14/10/97 11:47 a.m.). Figure 8.32 shows the contours for all of the conditions listed in Table 8.2.

The contours for constant weight are isolated in Figure 8.33, with the direction of increasing weight indicated. The contours of constant powerdraw are isolated in Figure 8.34, with the direction of increasing powerdraw indicated.

The weight contours appear linear. However, the powerdraw contours are non-linear. The essential nature of the contours were explored using the symbolic manipulation capabilities of MATLAB. The mill weight residual (Equation (5.21)) and powerdraw residual (Equation (5.17)) were reduced to functions of only ball charge (J_b) and total charge (J_t).

The weight contours were found to be linear as expected, see Equation (8.1). The proportionality constant is between -1.7 and -1.6. This slope is consistent with the slope proposed for Figure 8.7 in Section 8.1.1. The different "bands" could correspond in some way to the weight contours. As such, the contours could, therefore, correspond to different

ore hardness levels. Further investigation of this hypothesis could be the focus of future work. However, such research is beyond the scope of this work.

Table 8.2: Mill Operating Conditions for Mill Charge Model Analysis

Date	Time	Weight (t)	Powerdraw (kW)	Total Charge J_t (fraction)	Ball Charge J_b (fraction)	Rock Charge J_r (fraction)
09/10/97	00:23	175	2415	0.27	0.07	0.20
14/10/97	11:47	172	2422	0.25	0.08	0.17
11/10/97	11:41	171	2461	0.21	0.10	0.11
08/10/97	10:29	182	2666	0.25	0.11	0.14
10/10/97	19:25	186	2974	0.19	0.16	0.03

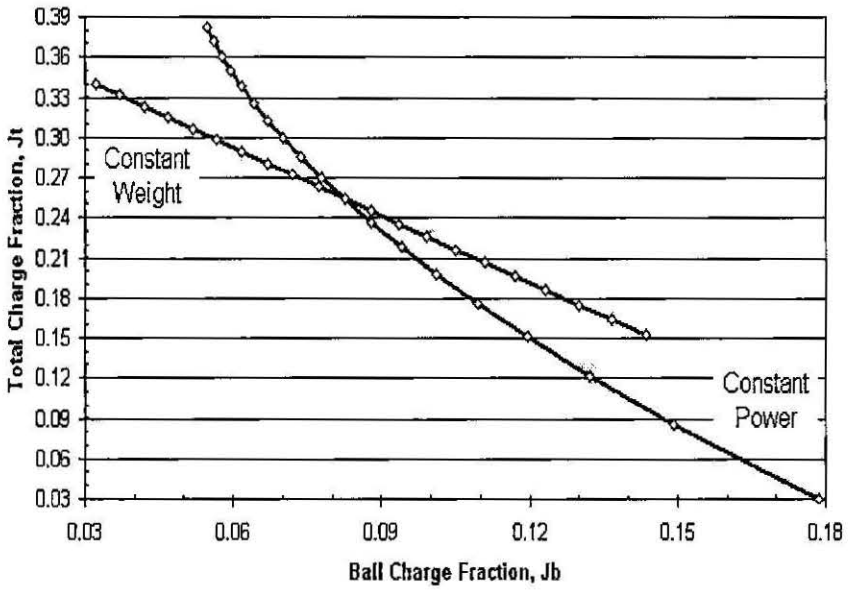

Figure 8.31: Powerdraw and weight contours (mill powerdraw and weight ramped up and down 10%) for reference point 14/10/97 11:47 a.m.: 2422 kW, 172 t

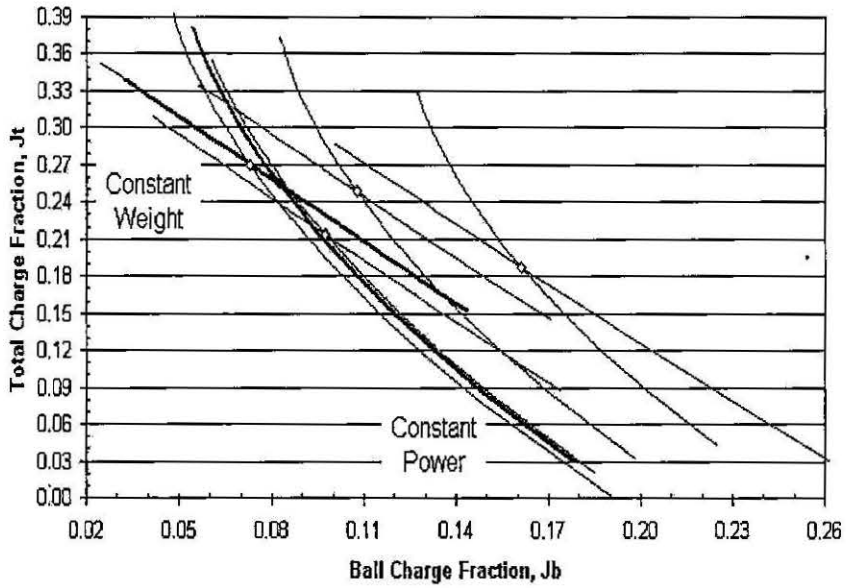

Figure 8.32: Powerdraw and weight contours (mill powerdraw and weight ramped up and down 10%) for the conditions listed in Table 8.2

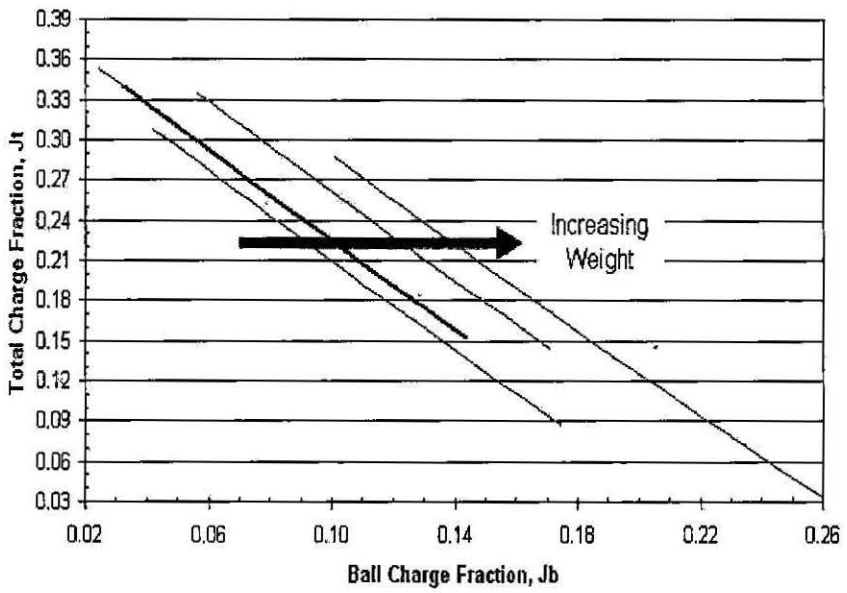

Figure 8.33: Weight contours isolated from Figure 8.32 (mill powerdraw ramped up and down 10%). Mill weight increasing left to right.

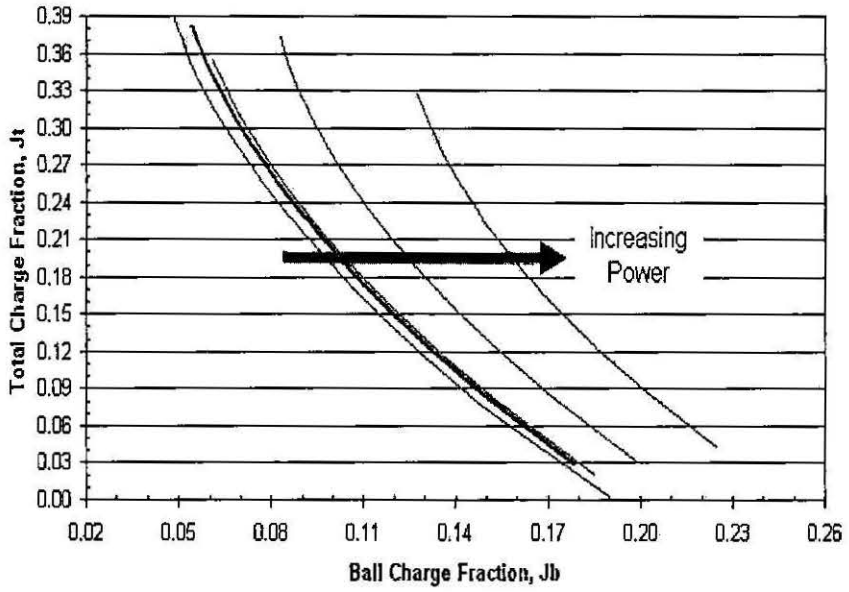

Figure 8.34: Powerdraw contours isolated from Figure 8.32 (mill weight ramped up and down 10%). Mill powerdraw increasing left to right.

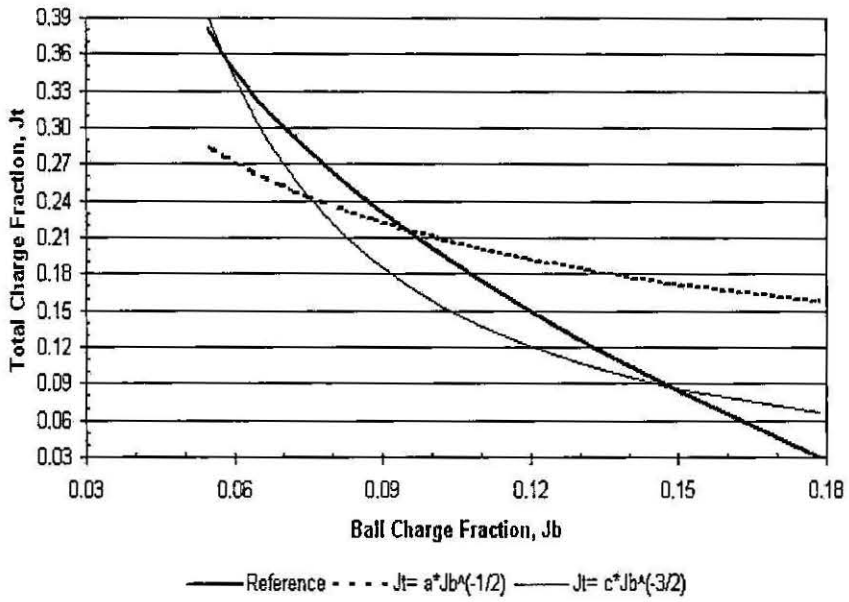

Figure 8.35: Essential nature of the powerdraw contour. Plots of $J_t = a\, J_b^{-0.5}$ and $J_t = c\, J_b^{-1.5}$ superimposed on the reference powerdraw contour.

The powerdraw contours are distinctly non-linear, see Equation (8.2). The polynomial in the numerator on the right-hand-side is a detailed function in J_b, e^{J_b} and the *sine* of these in various combinations. The plots of $J_t = a\,J_b^{-0.5}$ and $J_t = a\,J_b^{-1.5}$ were superimposed on the reference powerdraw contour, see Figure 8.35. (The values of the constants a and c were selected here to align the plots in the ball charge – total charge space and are not relevant in this discussion.) Of these two simplifications, the latter captures much of the curvature of the contour. For the powerdraw contour, total charge (J_t) can, therefore, be considered proportional to $J_b^{-1.5}$.

$$\textit{Weight Contour}: \quad J_t \propto -J_b \tag{8.1}$$

$$\textit{Powerdraw Contour}: \quad J_t \propto \frac{1}{\sqrt{J_b}} \cdot \frac{\textit{polynomial in } J_b,\ e^{J_b} \ \&\ \textit{sin}(J_b,\ e^{J_b})}{J_b} \tag{8.2}$$

$$J_t \approx\propto \frac{1}{\sqrt{J_b}} \cdot \frac{1}{J_b} \tag{8.3}$$

Recalling from Section 6.2.3 that the slope of the contours reflects the relative uncertainties in the estimates, see Equation (6.16). Therefore, for the weight contour, the uncertainty in the total charge estimate (δJ_t) remains constant in relation to the uncertainty in the ball charge estimate (δJ_b), see Equation (8.4). The uncertainty in the total charge estimate is between 1.6 and 1.7 times large than the uncertainty in the ball charge estimate.

For the powerdraw contour, the uncertainty in the total charge estimate (δJ_t) varies in relation to the uncertainty in the ball charge estimate (δJ_b). The uncertainty in the total charge estimate (δJ_t) increases with respect to the the uncertainty in the ball charge estimate (δJ_b) the higher the total charge is above the the ball charge, *i.e.*, increasing slope. Differentiating the approximate relationship between the charge estimates described by Equation (8.3), yields an approximate, quantitative measure of how the comparative uncertainties change with ball charge fraction, see Equation (8.5).

$$\textit{Weight Contour}: \quad \frac{\delta J_t}{\delta J_b} = \textit{constant}\ (-1.7\ \textit{to}\ -1.6) \tag{8.4}$$

$$\textit{Powerdraw Contour}: \quad \frac{\delta J_t}{\delta J_b} \propto J_b^{-2.5} \tag{8.5}$$

The reference powerdraw contour is plotted in Figure 8.36 with the approximation of the contour ($J_t = a\,J_b^{-1.5}$) and the derivative of the approximation ($dJ_t\,/\,dJ_b = c\,J_b^{-2.5}$). The values of the constants a and c are now relevant to the discussion. The value of a ($1/200 = 0.005$) was selected, non-rigorously, by trial-and-error to obtain a reasonable fit (by eye). Through differentiation the absolute value of constant c is, therefore, equal to $3/400 = 0.0075$. The relative uncertainty in the total charge to the uncertainty in

the ball charge may now be easily calculated. (The derivative of the approximation in Figure 8.36 has been scaled to fit in to the ball charge – total charge space.) Table 8.3 contains a selection of calculated comparative uncertainties. For a low ball charge estimate (J_b) of 0.08, the relative uncertainty of the total charge estimate (J_t) is eight ($8 = 4/0.5$) times higher than the relative uncertainty of the total charge estimate for a high ball charge estimate of 0.18. The uncertainties in the estimates are approximately equal for ball charge estimates around 0.14.

Further research could include a more formal model fitting of the approximation of the contour, to improve the estimate of the relative uncertainties in the estimates.

The nature of the mill charge estimates has been examined. As has the behaviour of the relative uncertainty in the estimates. For the weight contour (varying powerdraw):

- the total charge estimate (J_t) has been found to be directly proportional to the ball charge estimate (J_b)
- the uncertainty in the total charge estimate (δJ_t) remains constant with respect to the uncertainty in the ball charge estimate (δJ_b)

For the mill powerdraw contour (varying weight):

- the total charge estimate (J_t) has been found to be approximately proportional to the inverse of the ball charge estimate to the power of 1.5 ($J_b^{-1.5}$)
- the uncertainty in the total charge estimate (δJ_t) varies with respect to the uncertainty in the ball charge estimate (δJ_b according, approximately, to the function $cJ_b^{-2.5}$

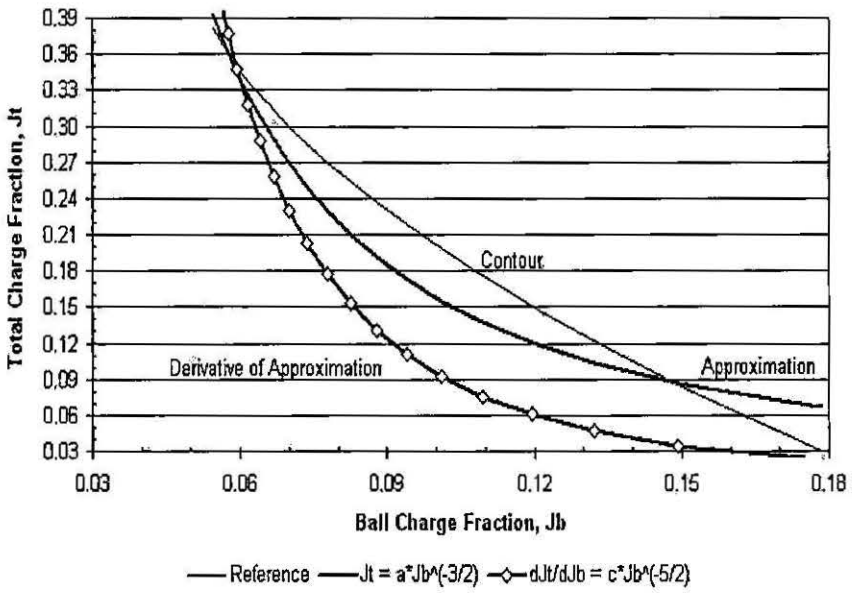

Figure 8.36: Powerdraw contour, Contour approximation ($J_t = a\, J_b^{-1.5}$) and Derivative of approximation ($dJ_t / dJ_b = c\, J_b^{-2.5}$).

Table 8.3: Comparative Uncertainty in Total Charge

Ball Charge J_b (fraction)	Relative Uncertainty $\frac{\delta J_t}{\delta J_b}$ (-)
0.08	4.1
0.09	3.1
0.10	2.4
0.14	1.0
0.15	0.9
0.18	0.5

8.2.3 Model Characteristics in a MVC context

In this Section, the nature of the mill charge estimates is utilised to generate a SAG mill operating curve, which is discussed in the context of mill charge control. The powerdraw and weight contours have been useful in examining the nature of the inferential charge models (and the behaviour of the relative uncertainty in the estimates). They also have utility in relation to a multiple variable (MVC) controller. The development of a MVC controller is discussed in Section 8.3. The controller rate-of-change (ROC) coefficients are listed in Table 8.8. For ease of reference, the relevant ROC coefficients are shown here in Table 8.4. Since the total charge is the addition of the rock and ball charges, the ROC coefficient for a given manipulated variable is calculated from the addition of the ROC coefficients for ball charge and rock charge.

Table 8.4: Rate of Change Coefficients and Control Action Contour Slopes

Manipulated Variable	Control Variables			Contour Slope $\frac{\Delta J_t}{\Delta J_b}$
	Ball Charge J_b	Rock Charge J_r	Total Charge $J_t\ (=\ J_b\ +\ J_r\ )$	
Feedrate, $SMFF$	-8E-06	0.037	0.037	-4906
Ball Addition, $SMBA$	0.013	-0.312	-0.299	-23.5

The feedrate and ball addition are the two manipulated variables (MVs) that affect the mill charge fractions. Control-action contours for each of the MVs can be calculated from the ROC coefficients. For feedrate, if we assume the ball addition remains constant, then the slope of control-action contours for feedrate in the total charge - ball charge space is calculated by dividing the total charge ROC coefficient by that of the ball charge, see Table 8.4. As long as the units for the ROC coefficients are consistent, the actual units are not crucial because they cancel out. By assuming feedrate remains constant, the control-action contour slopes for ball addition may be calculated similarly.

The control-action contours may be super-imposed on the total charge fraction versus ball charge fraction plots, see Figure 8.37. The near-vertical (slope: -4906) line is a feedrate contour. Feedrate changes have little effect on ball charge but a large effect on rock charge and, therefore, total charge.

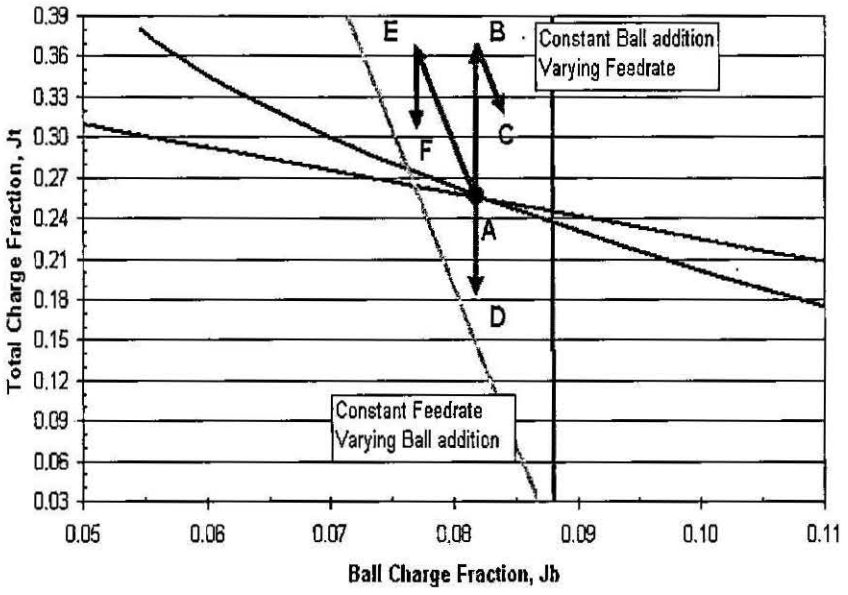

Figure 8.37: Control-Action Contours super-imposed on the reference mill powerdraw and weight contours. Feedrate control-action contour near-vertical (slope: −4906). Ball addition control-action contour has slope −23.5. Movements A – F explained in Table 8.5.

Table 8.5: Controller Moves in $J_t - J_b$for Figure 8.37

A → B → C	**Objective**: Increase ball charge and total charge **Controller moves**: Increase feedrate (A → B) and Increase ball addition (B → C) **Powerdraw–weight**: Increased powerdraw – Increased weight
A → D	**Objective**: Decrease total charge (rock charge) while maintaining ball charge **Controller moves**: Decrease feedrate **Powerdraw–weight**: Decreased powerdraw – Decreased weight
A → E → F	**Objective**: Increase total charge and decrease ball charge **Controller moves**: Decrease ball addition (A → E) and Decrease feedrate (E → F) **Powerdraw–weight**: Increased powerdraw – Increased weight

The other steep line (slope: −23.5) in Figure 8.37 is a ball addition contour. Ball addition changes clearly affect the ball charge. They also affect the total charge because the ball charge affects the rock charge. For example, increasing the ball addition, increases the ball charge, which decreases the total charge because it decreases the rock charge through breakage. Note that this contour has been placed to show the slope of the contour on the plot. The contour should not extend below the $J_t = J_b$ line (not shown) as it does in this diagram.

Also shown in Figure 8.37 is a number of arrows connecting points labeled A − F. These can be considered as controller moves, as detailed in Table 8.5. For example, increasing the ball charge and total charge (moving from A − C), is achieved through two control moves. Firstly, an increase in feedrate increases the total charge (by increasing the rock charge) with a near-zero decrease in ball charge (moving from A − B). Secondly, an increase in ball addition increases the ball charge with a decrease in total charge due to increased breakage of the rock charge (moving from B − C). The overall result is an increased ball charge and and an increased rock charge (with an increase in mill weight and an increase in powerdraw).

Plotting the control moves in the two-dimensional charge fraction space (J_b, J_t) and describing what is happening to the powerdraw and weight is not ideal for visualisation of what is occurring. The four-dimensional space may be reduced to a three-dimensional space by multiplying the prevalent powerdraw and weight signals together for each ball charge fraction, total charge fraction pairing (J_b, J_t). The powerdraw and weight contours may be expanded into the three-dimensional space by mutiplying these by the prevailing weight or powerdraw.

Three sets of operating conditions were selected from Table 8.2 - the first and last two rows. These conditions were selected because they are close together in time and display a trend, which is beneficial for clarity of plotting and is consistent with the proposal that they are for a constant ore hardness. The complement of this proposal is that the other conditions in Table 8.2 are for situations of different ore hardness. To fully investigate this hypothesis is not feasible here, nor is it in the scope of this research. However, it could be the topic of future research. The Logsheet and Shift Communication Book entries for Afternoon Shift 11 October 1997 onwards certainly support an ore hardness change, as the feed tonnage is backed off by 35 t/hr and feeders start "hanging up", see Appendix D.

The three sets of operating conditions are plotted on Figure 8.38 and form an operating curve in the (J_b, J_t, $Powerdraw \cdot Weight$) space. The powerdraw and weight contours are plotted in this space also and now form intersecting powerdraw and weight surfaces, respectively.

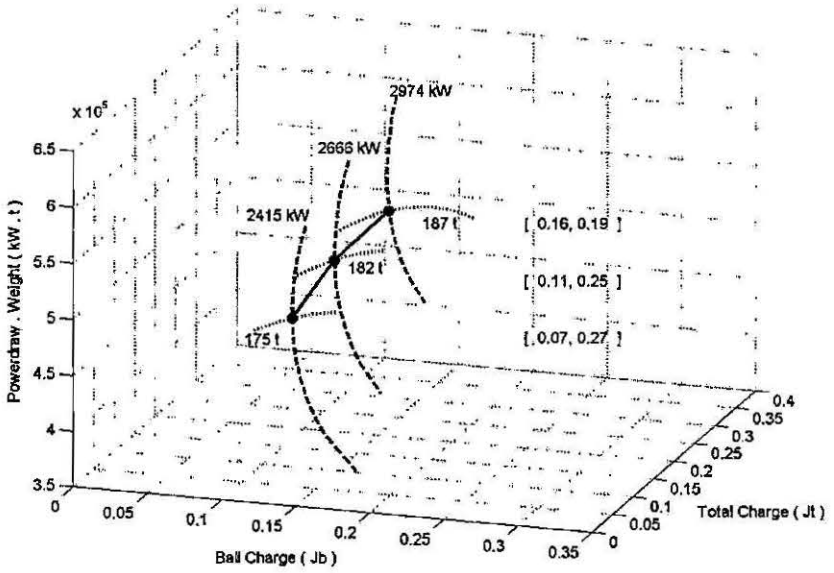

Figure 8.38: SAG mill operating curve, Powerdraw contours & Weight contours in the $J_b - J_t - Powerdraw \cdot Weight$ space

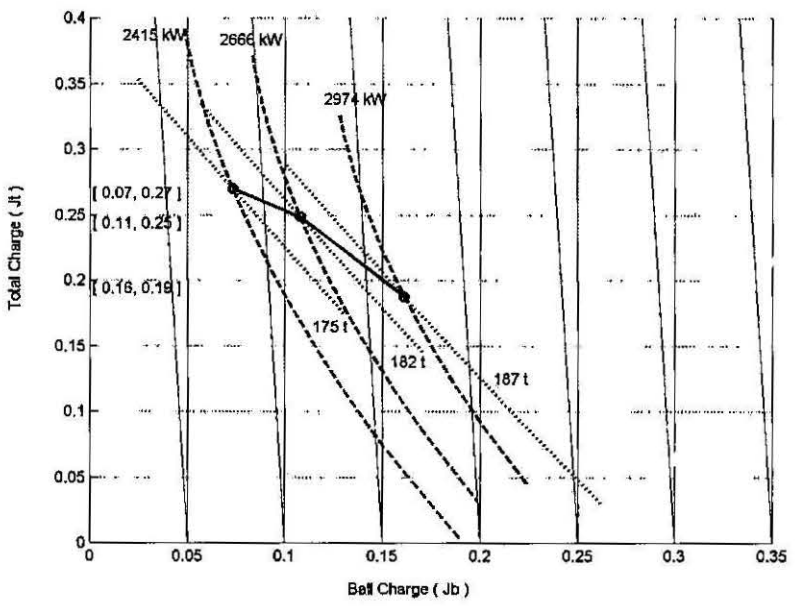

Figure 8.39: SAG mill operating curve, Powerdraw contours, Weight contours and Control-Action contours in the $J_b - J_t$ space

Taking a position normal to the ball charge fraction – total charge fraction plane and plotting the control-action contours results in Figure 8.39, which is another version of Figure 8.32. The three operating conditions that make the operating curve did not occur in a left-to-right sequence. The central point is the first set of conditions in time, the left point is the second and the right point is the third.

Moving from the central point to the left point would require decreases in feedrate and ball addition. The time between these two conditions is approximately 14 hours. To achieve the second set of conditions, the controller would have made multiple moves in feedrate and ball addition (in contrast to one large decrease in feedrate and one large decrease in ball addition rate). One can imagine these moves as a saw-tooth profile moving right-to-left, above the operating curve from the central point to the left point. The segments that make up the "saw-tooth" would be parallel to the control-action contours.

Moving the operating conditions from the left point to the right point, the controller moves would make a saw-tooth profile moving left-to-right, below the operating curve (increases in ball addition and increases in feedrate). The time between these two conditions is approximately 43 hours.

It is not possible to validate the proposed controller moves against the actual process since:

1. The controller and process it controls are simulations.
2. The controller assumes the SAG mill is a purely integrating vessel. Whilst this is true overall, there is also some first-order plus dead time behaviour exhibited by the real plant, particularly for the rock (and total) charge, that this simplification does not capture.
3. The simulation occurs over a time frame of minutes rather than hours
4. The MV of SAG mill ball addition ($SMBA$) does not exist in the real plant. Grinding balls are batch-fed to the mill as dictated by the operator.

However, the following points illustrate that overall the controller moves would have been consistent with what actually took place in the plant:

Central-to-Left Point: During the 14-hour period there was no ball charging (effectively a ball addition decrease) and the weighted-average of the nine (9) feedrate changes is – 25 t/hr (a feedrate decrease).

Left-to-Right Point: During the 43-hour period three batches of grinding balls were charged to the mill (a ball addition increase) and the weighted-average of the forty (40) feedrate changes is + 95 t/hr (a feedrate increase).

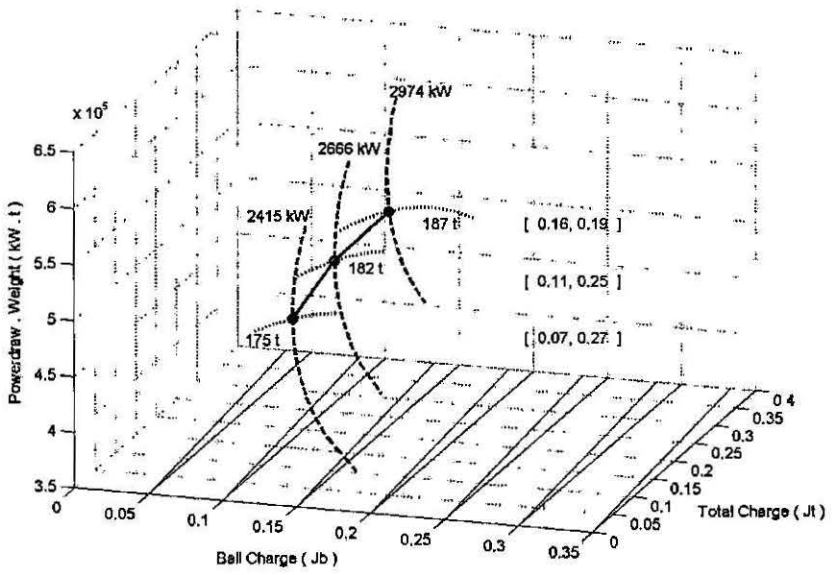

Figure 8.40: SAG mill operating curve, Powerdraw contours, Weight contours and Control-Action contours in the $J_b - J_t - Powerdraw \cdot Weight$ space - View 1

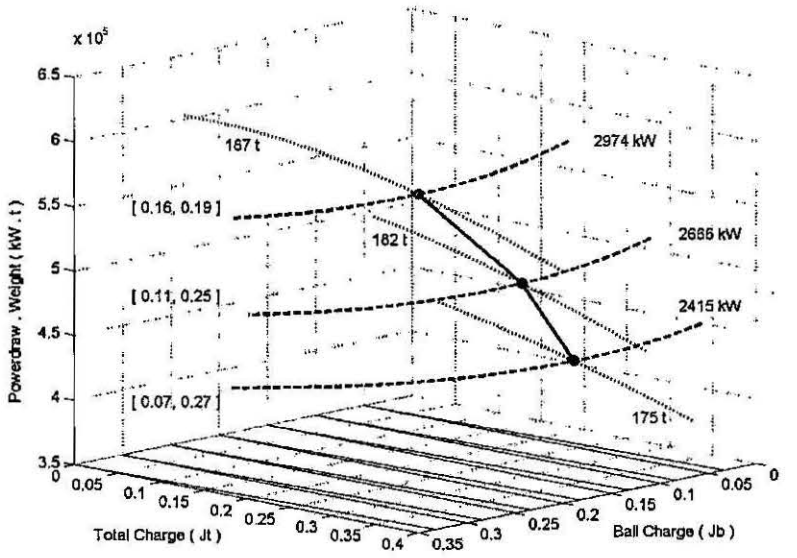

Figure 8.41: SAG mill operating curve, Powerdraw contours, Weight contours and Control-Action contours in the $J_b - J_t - Powerdraw \cdot Weight$ space - View 2

Further research could investigate control actions of a real controller in relation to the operating curve. Figures 8.40 and 8.41 are alternative views of operating curve in the (J_b, J_t, $Powerdraw \cdot Weight$) space with the control-action contours also shown on the $J_b - J_t$ plane.

In this Sub-section a SAG mill operating curve, along with the mill weight and powerdraw contours, has been projected into the (J_b, J_t, $Powerdraw \cdot Weight$) space. This has eased visualisation of the interrelations of the mill charge fractions and powerdraw and weight measurements. Control-action contours, of the MVC controller developed in the next Section, were superimposed, which has furthered the understanding of how control actions could move the process along the operating curve.

The preceding discussion has illustrated the cause of the unusual behaviour exhibited by the inferential measurement models, developed in Chapter 5, first noted when the oversize crusher went off-line and the mill charge density was increased.

Further sensitivity analysis highlighted the behaviour of the charge estimates in relation to the mill powerdraw and weight measurements. The oversize crusher feedrate (*scats*) was found to affect the mill charge and feedsize estimates due to the nature of model construction. This is considered a model limitation, which should be noted when dealing with the results. Additionally, the feedsize F_{80} estimate was found to be highly sensitivity to the breakage rates used in the SAG mill total feed estimate. Furthermore, the breakage rates are dependent on the ball charge estimate, which is dependent on the mill powerdraw and weight measurements.

The nature of the mill charge estimates and the behaviour of the relative uncertainty in the estimates has been examined. For the weight contour (varying powerdraw), the total charge estimate (J_t) has been found to be directly proportional to the ball charge estimate (J_b). This translates to the uncertainty in the total charge estimate (δJ_t) remaining constant with respect to the uncertainty in the ball charge estimate (δJ_b). For the mill powerdraw contour (varying weight), the total charge estimate (J_t) has been found to be approximately proportional to the inverse of the ball charge estimate to the power of 1.5 ($J_b^{-1.5}$). This translates to the uncertainty in the total charge estimate (δJ_t) varying with respect to the uncertainty in the ball charge estimate (δJ_b according, approximately, to the function $cJ_b^{-2.5}$.

Placement of the operating curve in the (J_b, J_t, $Powerdraw \cdot Weight$) space eased visualisation of the interrelations of the mill charge fractions and powerdraw and weight measurements. Superimposing control-action contours of the MVC controller developed in the next Section furthered the understanding of how control actions could move the process along the operating curve.

The fitting of the approximation of the mill powerdraw contour (for improved estimation of the relative uncertainties in the charge estimates), investigating the dependence of the operating curve on ore hardness, and, investigation of control actions of a real controller in relation to the operating curve are possible avenues to progress research in this area.

The next Section discusses how the inferential measurement models developed in Chapter 5 can be incorporated in an advanced process control structure for setpoint and constraint-control.

8.3 Inferential Measurement Model Implementation: A simulation

To place the utilisation of the inferential measurement models into context, the development of a multi-variable controller simulation was embarked upon. The simulation was conducted using *Connoisseur*, the multi-variable, model-predictive control package of the process control hardware and software company *Invensys*.

Table 8.6: Plant Transfer Functions A

	Manipulated & Feedforward Variables	(1) SAG Mill Feedrate $SMFF_{tphs}$ [225 (t/hr)]	(2) SAG Mill Water Addition $SMFW$ [75 (m^3/hr)]	(3) Primary Cyclone Water Addition $PCFW$ [90 (m^3/hr)]
	Controlled Variables			
(1)	Mill Weight, SM_{wt} [185 (t)]	$\frac{0.30\ e^{-5s}}{50s+1}$	–	–
(2)	Mill Power, SM_{kW} [2,825 (kW)]	$\frac{9.0\ e^{-5s}}{50s+1}$	–	–
(3)	Rock Charge, J_r [12 (%)]	$\frac{0.21\ e^{-5s}}{30s+1}$	–	–
(4)	Ball Charge, J_b [12 (%)]	$\frac{-0.022\ e^{-5s}}{40s+1}$	–	–
(5)	Scats, $OSCF_{tphs}$ [80 (t/hr)]	$\frac{1.66\ e^{-7s}}{64s+1}$	–	–
(6)	1° Cyclone Flowrate, $PCFD_{m3ph}$ [440 (m^3/hr)]	$\frac{3.86\ e^{-10s}}{42s+1}$	$\frac{4.11\ e^{-2s}}{8s+1}$	$\frac{1.25\ e^{-4s}}{2s+1}$
(7)	1° Cyclone Density, $PCFD_{\%s\_w/w}$ [45 (% solids w/w)]	$\frac{0.10\ e^{-10s}}{42s+1}$	$\frac{-0.012\ e^{-2s}}{8s+1}$	$\frac{-0.13\ e^{-2s}}{2s+1}$
(8)	SAG Discharge Transfer Size, T_{80} [13 (mm)]	$\frac{0.09\ e^{-8s}}{62s+1}$	–	–
(9)	SAG Feed Density, $SMTF_{\%s\_w/w}$ [72 (% solids w/w)]	$\frac{0.08\ e^{-5s}}{2s+1}$	$\frac{-0.23\ e^{-2s}}{2s+1}$	–
(10)	Total Circuit Water, H_2O_{Total} [165 (m^3/hr)]	–	$\frac{1.0\ e^{-2s}}{2s+1}$	$\frac{1.0\ e^{-2s}}{2s+1}$

Table 8.7: Plant Transfer Functions B

	Manipulated & Feedforward Variables	(4) SAG Mill Ball Ball Addition $SMBA$ [2.5 (t/hr)]	(5) Feed Size F_{80} [65 (mm)]
	Controlled Variables		
(1)	Mill Weight, SM_{wt} [185 (t)]	$\frac{1.81\ e^{-2s}}{13s+1}$	$\frac{0.016\ e^{-15s}}{7s+1}$
(2)	Mill Power, SM_{kW} [2,825 (kW)]	$\frac{84.4\ e^{-2s}}{13s+1}$	$\frac{0.67\ e^{-2s}}{12s+1}$
(3)	Rock Charge, J_r [12 (%)]	$\frac{-1.96\ e^{-2s}}{13s+1}$	$\frac{0.046\ e^{-2s}}{15s+1}$
(4)	Ball Charge, J_b [12 (%)]	$\frac{1.21\ e^{-2s}}{13s+1}$	$\frac{-0.022\ e^{-5s}}{40s+1}$
(5)	Scats, $OSCF_{tphs}$ [80 (t/hr)]	$\frac{3.01\ e^{-5s}}{13s+1}$	$\frac{-0.13\ e^{-5s}}{2s+1}$
(6)	1° Cyclone Flowrate, $PCFD_{m3ph}$ [440 (m^3/hr)]	$\frac{-38.7\ e^{-5s}}{13s+1}$	$\frac{-1.77\ e^{-7s}}{2s+1}$
(7)	1° Cyclone Density, $PCFD_{\%s\_w/w}$ [45 (% solids w/w)]	$\frac{0.41\ e^{-5s}}{13s+1}$	$\frac{-0.041\ e^{-2s}}{7s+1}$
(8)	SAG Discharge Transfer Size, T_{80} [13 (mm)]	$\frac{1.50\ e^{-5s}}{13s+1}$	$\frac{0.024\ e^{-11s}}{19s+1}$
(9)	SAG Feed Density, $SMTF_{\%s\_w/w}$ [72 (% solids w/w)]	—	—
(10)	Total Circuit Water, H_2O_{Total} [165 (m^3/hr)]	—	—

The interactions between variables in primary and secondary milling circuits, real and simulated, may be characterised by transfer functions (Radhakrishnan, 1999; Freeman et al., 2000a; Ivezić and Petrović, 2003; Apelt, 2004; Ramasamy et al., 2005). The plant data and inferential measurement model results discussed in Section 8.1 were analysed to determine estimates for the interactions between key variables. A matrix of ten (10) controlled variables (CVs) by five (5) manipulated variables (MVs) and Feed-forward variables (FVs), *i.e.*, 10 × 5, defines the controller structure. The results of the analysis of the plant interactions are contained in Tables 8.6 and 8.7.

Each process interaction was approximated by a first-order plus time-delay transfer (FOPTD) function. Such an approximation is satisfactory for process variables that are not integrating by nature, such as tank levels. The approximation can successfully be applied in real-plant situation, as seen in Freeman et al. (2000).

Experimenting with a simulation based on FOPTD models gave unsatisfactory (unrealistic) results. The simulation was predicting the asymptotic approach to a new steady-state process value (characteristic of a $FOPTD$ model) for the rock charge, regardless of the starting conditions. For certain conditions this would occur but not across the full range of possible conditions. For example, for high rock (and total) charge levels and a constant moderate ball charge level, an increase in feedrate would cause the mill to overload (from rock charge integration). The $FOPTD$ transfer function does not capture changing breakage rates (for the rock contents) and changing wear rates (for the grinding charge contents) for different operating conditions. Therefore, since the different operating conditions cause different behavior in the SAG mill charge levels, the $FOPTD$ approximation is not satisfactory.

Therefore, the SAG mill was modelled as an integrator for rock and grinding media. The in-flows are the mill ore feed and the ball addition rate. The out-flows are the rock charge breakage and the ball charge wear. An isolated increase in either the feedrate or the ball addition rate will cause either the rock charge or ball charge, respectively, to increase monotonically until mill over-load. (This is effectively true for the ball charge but only an approximation for the rock charge.) The asymptotic approach to a new steady-state process value, characteristic of a $FOPTD$ transfer function, will not eventuate for the ball charge and rarely for the rock charge.

To address this issue, the CVs in Tables 8.6 and 8.7 that relate to the integrating nature of the SAG mill, namely the mill weight, powerdraw, rock charge and ball charge, were modelled as integrators. In the *Connoisseur* environment, integrators are modelled by way of rate-of-change (ROC) models. The ROC coefficients are calculated using Equation (8.6).

$$ROC_{CV} = \frac{Range_{CV}}{Volume_{Vessel}} * \frac{PI}{Time\ Conversion} * \Delta MV \tag{8.6}$$

where

ROC_{CV}	=	Rate of change of the CV (CV units per PI)
PI	=	Prediction Interval (time units)
$Range_{CV}$	=	CV range over the vessel volume (CV units)
$Time\ Conversion$	=	Conversion factor for MV time units to PI units (time over time)
CV	=	Controlled Variable (−)
MV	=	Manipulated Variables (−)
ΔMV	=	The change in the MV that causes the change in CV (−)

Table 8.8 contains the ROC coefficients utilised in this simulation. The coefficients were either calculated from first principles or from the plant data and results presented in Section 8.1. For example, ball addition, $SMBA$ (t/hr) can be translated into a volumetric rate based on ball specific gravity and voidage, which can in turn be translated into a ball charge change based on the mill dimensions. A first principles determination.

The ROC coefficient for ball addition ($SMBA$) to rock charge (J_r), on the other hand, is derived from the data. An increase in the ball charge level causes a decrease in the rock charge level, observed from the data. The increase in ball charge level may be translated to a ball addition rate, by the reverse procedure of the previous example.

Further elaboration about the determination of the ROC coefficients is both somewhat tedious and outside the focus of this research. Therefore, it will not be undertaken here.

Table 8.8: Rate of Change Model Coefficients

	Relationship	*ROC*	Notes
(a)	$SMFF \rightarrow SM_{wt}$	0.025 (t/min)	Accumulating rock charge increases mill weight
(b)	$SMFF \rightarrow SM_{kW}$	0.782 (kW/min)	Accumulating rock charge increases mill powerdraw
(c)	$SMFF \rightarrow J_r$	0.037 (%/min)	Extra feedrate increases rock charge
(d)	$SMFF \rightarrow J_b$	-8e-6 (%/min)	Ball charge wear caused by extra feedrate
(e)	$SMBA \rightarrow SM_{wt}$	0.024 (t/min)	Extra ball addition increases mill weight (increased ball charge *and* rock charge reduction)
(f)	$SMBA \rightarrow SM_{kW}$	2.606 (kW/min)	Accumulating ball charge increases powerdraw
(g)	$SMBA \rightarrow J_r$	-0.312 (%/min)	Rock charge breakage due to Increasing ball charge
(h)	$SMBA \rightarrow J_b$	0.013 (%/min)	Extra ball addition increases ball charge
(i)	$F_{80} \rightarrow SM_{wt}$	0.025 (t/min)	Larger (harder) feed rocks increase rock charge and mill weight
(j)	$F_{80} \rightarrow SM_{kW}$	0.719 (kW/min)	Increased rock charge causes powerdraw increases
(k)	$F_{80} \rightarrow J_r$	0.037 (%/min)	Larger (harder) feed rocks increase rock charge
(l)	$F_{80} \rightarrow J_b$	-8e-6 (%/min)	Ball charge wear caused by increased rock charge

With the transfer functions and *ROC* coefficients in hand, development of a model predictive controller (MPC) progressed according to the structure shown in Figure 8.42.

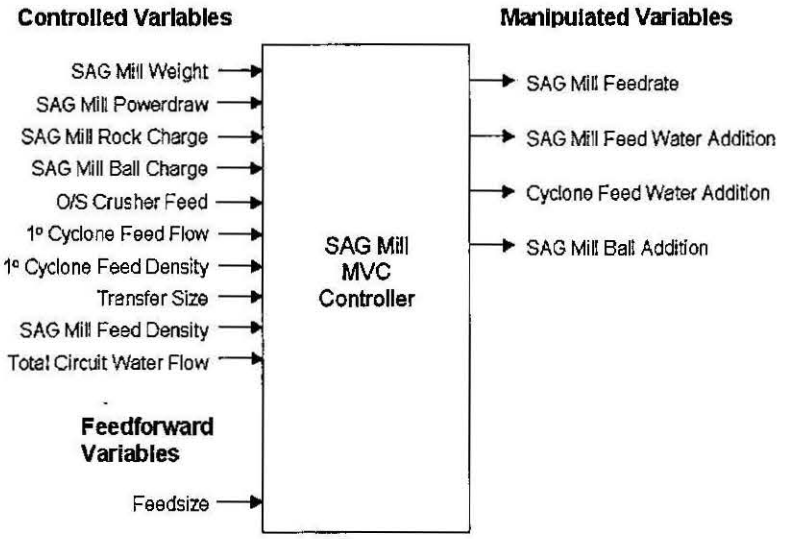

Figure 8.42: Model predictive controller structure.

For the purpose of MPC performance assessment, a simulation PID controller was also developed. The structure of the PID controller is shown in Figure 8.43. The PID controller manipulates the SAG mill feedrate to control the mill powerdraw.

Figure 8.43: Simulation PID controller structure.

The simulation study comprised the introduction of a disturbance in the feed size (F_{80}), which can occur in its own right but is usually associated with a disturbance in the ore hardness. Generally, the harder the ore, the more coarse the feed ore and thus, the larger the F_{80}.

The FV is stepped up ten (10) times from 65 mm to 70 mm. The elevated F_{80} is held for a period before the disturbance is reversed, returning the F_{80} to its original level.

The model predictive controller was configured to utilise the inferential measurement models developed in this research. The ball charge (J_b) and rock charge (J_r) were specified to be setpoint controlled CVs. The transfer size (T_{80}) was specified as a constraint-controlled CV. That is, the MPC would let its value take whatever value it took as long as it was between specified high and low limits. The remaining CVs were also specified as constraint-controlled CVs with various priority levels. This configuration ensured that the controller was not over-specified and had the flexibility to achieve the control objectives. Due to obvious impact the violation of the high constraint would have, the constraint-control of the powerdraw was given the highest priority. Adherence to the ball charge setpoint was given the same priority. The rock charge setpoint and the other constraint-controlled variables were assigned lower priorities.

Figure 8.44 shows the open-loop and closed-loop behaviour of the rock charge. A close-up of the closed-loop behaviour is given in Figure 8.45, which show that rock charge is maintained between $\approx \pm 0.2\%$ from setpoint. The PID controller is actually controlling powerdraw not weight. However, as both variables are highly correlated, control of powerdraw brings mill weight under a degree of control.

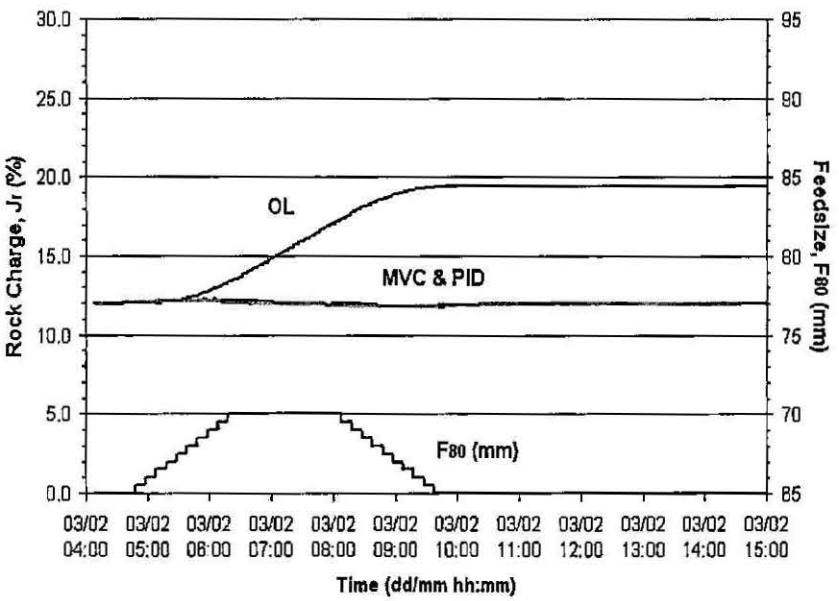

Figure 8.44: Simulated Plant Results: Open and Closed-loop rock charge behaviour.

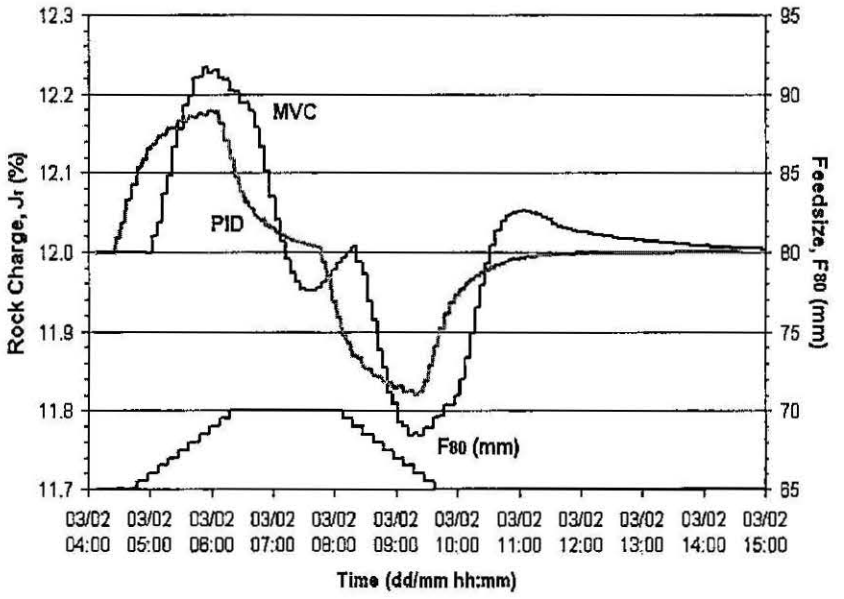

Figure 8.45: Simulated Plant Results: Closed-loop rock charge behaviour.

The movements made to the feedrate MV is shown in Figure 8.46. The behaviour of the MPC and PID controllers are not markedly different. The predominant difference in behaviour is in the PID controller moving the feedrate before the the MPC moves the feedrate, and that the PID movement follows an overshoot-with-trim type of shape.

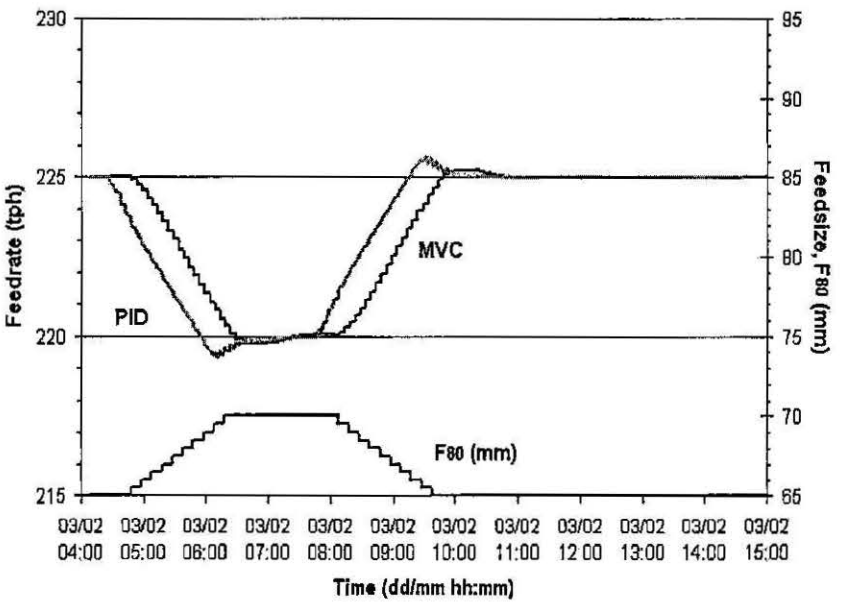

Figure 8.46: Simulated Plant Results: Closed-loop feedrate behaviour.

Figure 8.47 illustrates the open and closed-loop behaviour of the SAG mill ball charge. The PID response is essentially constant, lying virtually concurrent with the 12.0% grid-line. The high level of setpoint control achieved by the MPC here $\approx \pm 0.005\%$, compared to the setpoint control of the rock charge, is on account of the higher priority placed on the ball charge setpoint control. The open and closed-loop manipulation of the ball addition rate is shown in Figure 8.48. Since, there is no manipulation of the ball addition rate in the PID and Open-loop scenarios, the ball addition rate is a constant 2.5 t/hr in these cases.

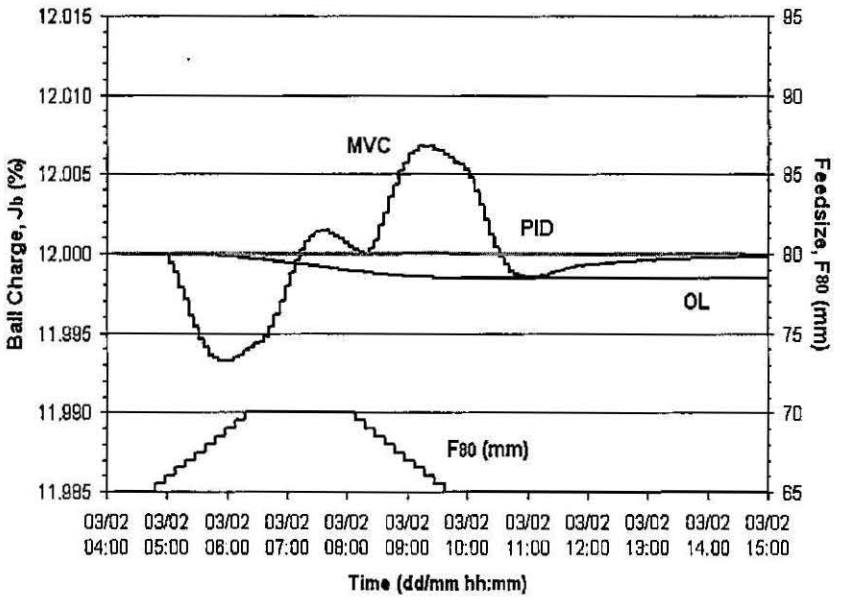

Figure 8.47: Simulated Plant Results: Open and Closed-loop ball charge behaviour.

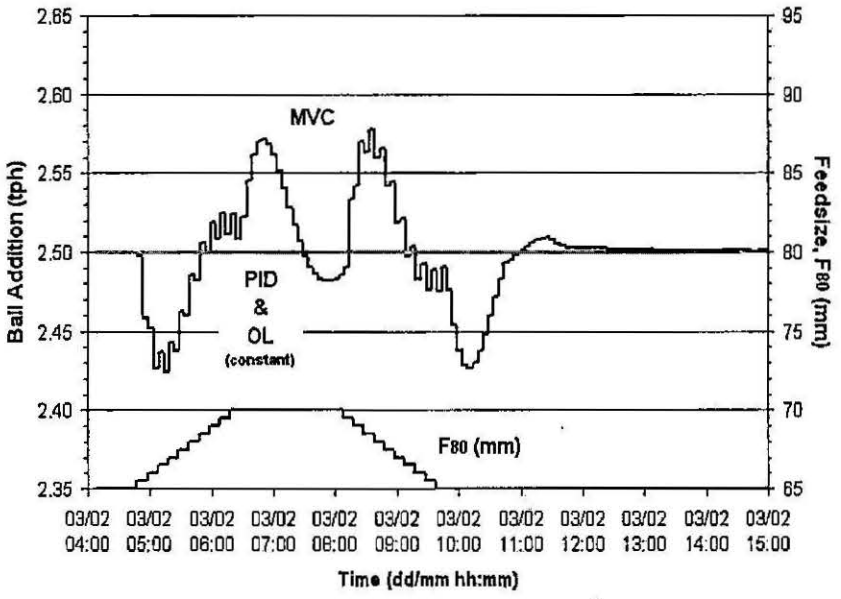

Figure 8.48: Simulated Plant Results: Open and Closed-loop ball addition behaviour.

Powerdraw is a constraint-controlled variable in the MPC, while it is the *CV* for the PID loop. The open loop behaviour of the powerdraw is shown in Figure 8.49. The closed-loop behaviour is shown in Figure 8.50. In these results is the most obvious difference in the behaviour of the close-loop controllers. The PID controller does not hold the powerdraw tightly to the setpoint of 2,825 kW. In contrast, the model predictive controller holds the powerdraw firmly at 2,825 kW. Since the powerdraw is a constraint-controlled *CV* in the MPC, the fact that the powerdraw is held at 2,825 kW is a consequence of the high priority placed on the observance of the powerdraw constraints and the controller trying to achieve the other control objectives, such as ball charge setpoint control.

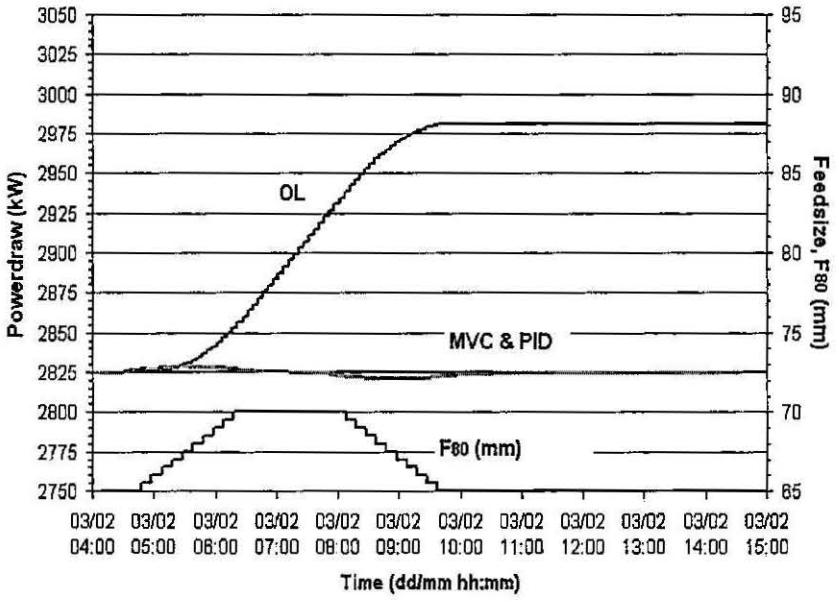

Figure 8.49: Simulated Plant Results: Open-loop powerdraw behaviour.

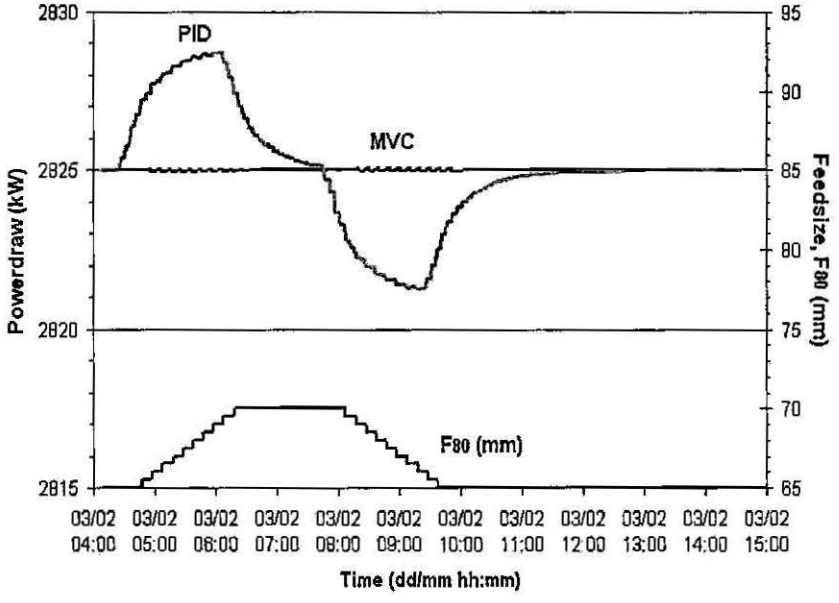

Figure 8.50: Simulated Plant Results: Closed-loop powerdraw behaviour.

Figure 8.51 shows the open-loop behaviour of the mill weight.Mill weight is a constraint-controlled variable in the MPC. Since, weight is closely correlated to mill powerdraw,

control of the latter results in good control of the former also. Figure 8.52 illustrates the closed-loop behaviour of the mill weight.

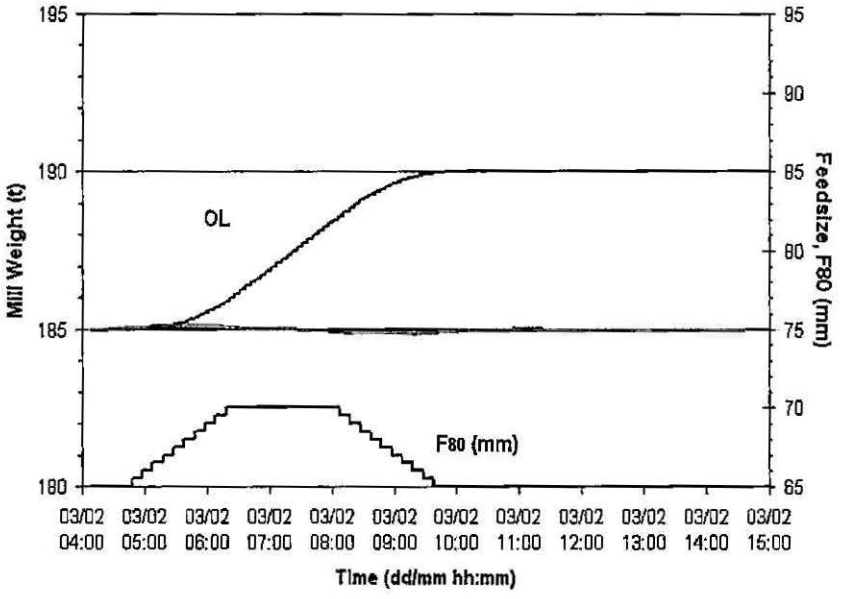

Figure 8.51: Simulated Plant Results: Open-loop weight behaviour.

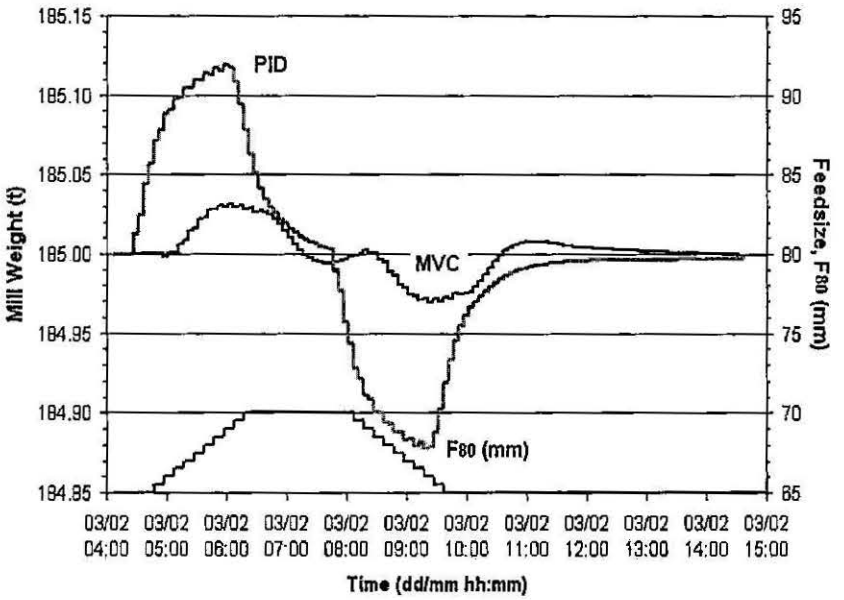

Figure 8.52: Simulated Plant Results: Closed-loop weight behaviour.

Figure 8.53 shows the open and closed-loop behaviour of the transfer size, T_{80}. Neither of the closed-loop controllers attempt to control the transfer size to a setpoint. The multi-variable controller (MVC) does, however, control the transfer size within the low (11 mm) and high (13 mm) constraints.

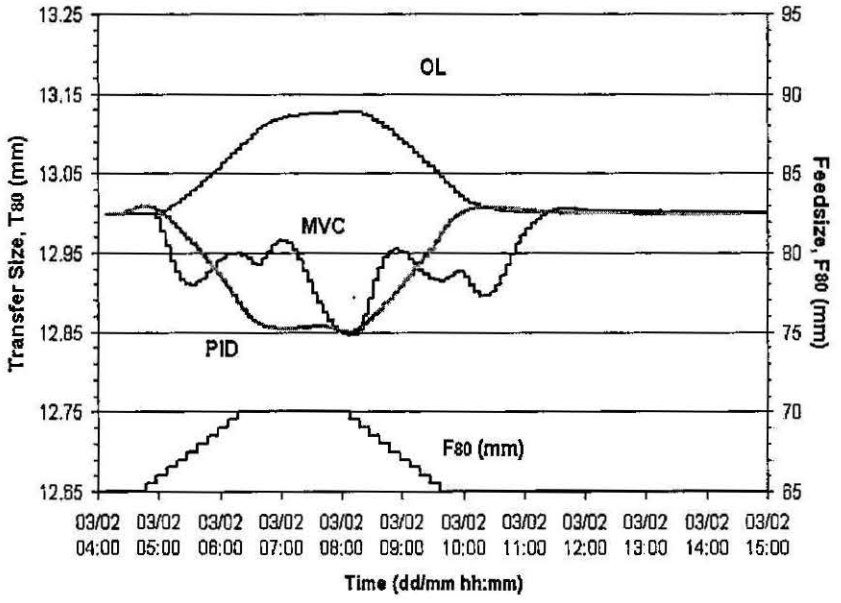

Figure 8.53: Simulated Plant Results: Open and Closed-loop T_{80} behaviour.

Overall, the performance of model-predictive (multi-variable) controller is superior to that of the PID controller. The superiority in this simulation study is only slight however. This marginal difference is attributable to the fact that the PID controller is the "perfect" PID controller in that it was modelled, tuned and implemented in *Connoisseur*. The difference in performance would be greatly magnified in a real-plant application.

The marginal difference in the manipulation of the SAG mill fresh feed ($SMFF$) in Figure 8.46, for example, represents a 0.1% increase in production achieved by MPC. Based on a nominal copper price of US$920 *per tonne* and assumptions on mill availability and copper recovery, this equates to $\approx$ US$18,500 *per annum*. Typical production increases from MPC implemented at well instrumented and controlled operations, such as Northparkes Mines , are 1 - 2%. Increased yearly revenue of between US$180,000 and US$250,000 *per annum* makes it somewhat easier to make the economic case for the implementation of advanced process control.

The preceding discussion has illustrated that the inferential measurement models developed in Chapter 5 can be incorporated in an advanced process control structure for setpoint or constraint-control. Research in this area could be progress through the further investigation of the use of the proposed model-predictive controller in conjunction with an optimiser, which would set the process setpoints based on certain economic criteria. Investigation of other controller configurations could also be undertaken.

8.4 Summary

In this Chapter, the inferential measurement models developed in Chapter 5 were further validated and analysed against Northparkes Mines plant data from October 1997. The model results exhibited good agreement with the plant data and observations. The novel inferential models developed by this research were thus deemed valid. Unusual operating conditions produced unusual results from the models. However, this characteristic could potentially be utilised in a plant monitoring/diagnostic capacity.

The unusual behaviour was investigated with the artificial stimulation of the models and further sensitivity analysis. The mathematical construction of the model means the oversize crusher feedrate (*scats*) affects the mill charge and feedsize estimates. This is considered a model limitation, which should be noted when dealing with the results.

The feedsize F_{80} estimate was found to be highly sensitivity to the breakage rates, which are dependent on the ball charge estimate, which, in turn, is dependent on the mill powerdraw and weight measurements.

The nature of the mill charge estimates was investigated and utilised to generate contours for the mill weight and powerdraw and a SAG mill operating curve. Sensitivity analysis of the contours was also presented. The SAG mill operating curve was discussed in the context of mill charge control.

Possible areas for further research include: the fitting of the approximation of the mill powerdraw contour (for improved estimation of the relative uncertainties in the charge estimates), investigation of the dependence of the operating curve on ore hardness, and, investigation of control actions of a real controller in relation to the operating curve.

The inferential measurement model results were utilised to generate an advanced process control simulation environment within *Connoisseur*. Controller performance was assessed against a the base performance of a PID controller. Further investigation of the use of the advanced controller in conjunction with an optimiser and other controller structures are avenues for potential future work.

The generation of a simulation test-bed for SAG mills from transfer functions is not innovative in itself. However, the use of the novel inferential measurement models developed in this research is innovative. Other innovations resulting from this work are:

- the use of integrating models for the SAG mill rock and ball charges, weight and powerdraw in the controller development modelling
- the 10 $\times$ 5 controller structure utilised

The innovations resulting from this Chapter are summarised in Table 8.9.

Table 8.9: Chapter 8 Innovation Summary

Section	Innovation
Section 8.1	The generation, presentation and discussion of the validation results for the novel inferential measurement models developed in this research.
Section 8.2	The sensitivity analysis of the charge and feedsize inferential models and the description of nature of the models.
Section 8.2	The construction of the mill weight and powerdraw contours and the development and presentation of the SAG mill operating curve in a mill charge fraction - kilowatt·tonne space.
Section 8.2	The discussion of the contours and operating curve in the context of mill charge control.
Section 8.3	The formulation of a model predictive controller that utilises the novel inferential measurement models developed in this research.
Section 8.3	The integrating models for the SAG mill weight, powerdraw and rock and ball charges in the controller development modelling.
Section 8.3	The 10 $\times$ 5 controller structure utilised in testing a potential implementation configuration.

Chapter 9

Conclusion

This Chapter provides a summary of the Thesis. A synopsis of the preceding Chapters is provided in Section 9.1. The accomplishments of this research is given in Section 9.2, where a summary of the contribution this research makes is also provided. In Section 9.3 the thesis is brought to a close with some discussion of future work and recommendations.

9.1 Synopsis

Chapter 1: The influence of ball charge, rock charge and feed properties on SAG mill performance and the difficulty in their direct measurement were introduced in Chapter 1. The Northparkes Mines Module 1 grinding circuit was described with mention of the various difficulties associated with circuit operation and control. Northparkes Mines personnel were consulted regarding grinding process bottlenecks which were aligned with research capabilities. The focus that stemmed from this interaction was the inferential measurement modelling of the following SAG mill parameters:

- ball charge (J_b) and total charge (J_t) levels,
- mill feed rate and size distribution, and,
- mill discharge rate and size distribution.

Chapter 2: Chapter 2 presented a summary of the literature relevant to delineating the current state-of-the-art for SAG mill parameter measurement and establishing the context and focus of this research. Whilst the significant extent and progress of research and technological development in this area is acknowledged, the scope for further advances is outlined, namely,

- estimates of ball charge (J_b) and total charge (J_t) levels may be determined simultaneously from either mill weight or power draw measurements,
- estimates of the mill feed rate and size distribution may be obtained via model based approaches,
- estimates of SAG mill discharge rate and size distribution may be obtained using cyclone and oversize crusher feed process measurements and mill discharge screen specifications,
- state estimation for SAG mills is a significantly developed method, the wider adoption of which may be influenced by further contribution, analysis and discussion.

Chapter 3: Pursuant to the development of suitable inferential models to address the scope for further development, steady state models of the SAG mill and the other comminution circuit unit operations were presented in Chapter 3. These models were programmed into MATLAB-Simulink and validated against reference data. The source of the reference data was detailed. The reference data comprised the results of a comprehensive grinding circuit survey conducted by Julius Kruttschnitt Mineral Research Centre and Northparkes Mines personnel in early 1997 (David, 1997), see Appendix B. The models were validated individually and as the as-surveyed circuit. Supplementary steady state model validation against published data was also conducted. Model validation at the simulation model level was considered sufficient toward the achievement of the objectives of the research (inferential model development) and also leaves the simulation models in a state of readiness for further research and development.

Chapter 4: Due to the focus on the SAG mill and in anticipation of the model requirements of state estimation, Chapter 4 detailed dynamic models of SAG mill:

1. ball charge
2. protective shell lining wear
3. rock and water charges

Whilst the development of dynamic rock and water charge models can be attributed to the Julius Kruttschnitt Mineral Research Centre, the dynamic ball charge and shell lining models are original to this research. All dynamic models were validated against the steady state Reference Data of the circuit survey (David, 1997). A high degree of sensitivity was encountered during the model fitting stage of the rock charge model. Small shifts in the

breakage rates, r_i, caused divergent changes in the mill rock charge. Research personnel recognise this area as one with "room for improvement" (Morrell *et al.*, 2001). Further validation is recommended at or prior to an implementation stage.

Chapter 5: Chapter 5 detailed the inferential model development, a summary of which follows:

1. The SAG mill discharge rate and size distribution and recirculating load may be estimated simultaneously using plant measurements of oversize crusher feed rate, primary cyclone feed flowrate and pulp density, SAG mill discharge water addition rate and SAG mill feedrate, the specifications of the mill discharge grate and screen and by assuming the cyclone and crusher feed streams have Rosin-Rammler size distributions.

2. The SAG mill rock and water charges may be estimated from mill discharge stream properties, the discharge grate specifications and classification function, c_i, and by assuming a Rosin-Rammler size distribution.

3. Mill ball charge (J_b) and total charge (J_t) levels may be estimated from model-measurement pairings of either mill weight or power draw.

4. SAG mill total feed may be estimated using rock, water and ball charge estimate, the mill discharge estimate and the perfect mixing mill model.

5. Primary cyclone underflow and oversize crusher product streams may be estimated by the application of the hydrocylone model and crusher model to the primary cyclone and oversize crusher feed streams, respectively.

6. SAG mill fresh feed rate and size distribution may be estimated from the SAG mill total feed *less* the SAG mill feed water addition and the oversize crusher product, primary cyclone underflow recycle estimates.

Like the steady state and dynamic models, the inferential models were validated against the steady state Reference Data of the circuit survey (David, 1997), see Appendices B and C. The inferential models were also validated against the Simulation Model results - the steady state MATLAB-Simlink simulation results, Appendix C. Further model validation is recommmended at or prior to an implementation stage.

Chapter 6: Sensitivity and uncertainty analyses were conducted on the SAG mill charge level estimates, the SAG mill discharge rate and size distribution estimates, the SAG

mill fresh feed rate and size distribution estimates, and the SAG mill breakage rates, r_i. Chapter 6 presents the results of these analyses and introduces an inferential model of the primary cyclone underflow split to the ball mill, PC_{split}. The main conclusions arising from Chapter 6 are:

Charge Level.

1. Good ball and total charge level estimates (J_b & J_t) may be obtained from mill weight or power draw measurements. Despite relatively good agreement amongst the estimates, the underlying uncertainty is somewhat larger.

2. The mill charge level estimates obtained from the mill weight measurement contain the least uncertainty and are therefore the recommended choice for charge level estimation.

3. The ball charge level (J_b) estimate from the power draw model showed good agreement and reasonable certainty. However, the total charge level (J_t) estimate from the power draw model whilst showing good agreement, displayed high uncertainty. This is attributed to large inferential model sensitivity to the total charge level, compensating errors, inferential model non-linearity and the concave nature of the power draw curve.

Mill Discharge.

4. Good estimates of SAG mill discharge rate and size distribution are possible. To minimise uncertainty in these estimates the accuracy of the oversize crusher and primary cyclone feed instrumentation should be maintained through regular calibration. Error in the transfer size estimates increased from the eighty percent passing size (T_{80}) to the twenty percent passing size (T_{20}). This trend is attributed to interpolation errors, minor model approximations and error compounding effects of the cummulative percent passing format. These errors may be minimised through the monitoring of the SAG mill discharge screen aperture size and the appropriate adjustment of the corrected fifty percent passing size, $SMD50_c$, ensuring the accuracy of the oversize crusher and primary cyclone process measurements via periodic calibration and the periodic verification of the process water specific gravity, SG_l.

Mill Feed.

5. Good estimates of SAG mill fresh feed rate and size distribution are possible. The errors in the estimates may be minimised by ensuring the accuracy of the oversize crusher and primary cyclone feed instrumentation, through regular calibration, and

the crusher gap setting, via regular lead-bob gap checking. The SAG mill discharge grate parameters: pebble port size, x_p; and relative open area fraction of the pebble ports, f_p; also strongly influence the size estimates and hence, should be fitted with due care.

Breakage Rates.

6. The breakage rates, r_i, are most influenced by mill speed (RPM), ball charge level (J_b) and the feed eighty percent passing size (F_{80}). The recommendations regarding the SAG mill fresh feed and inventory inferential models apply here and also the diligent model fitting of the oversize crusher model.

Cyclone Underflow Split.

7. The primary cyclone underflow split to the ball mill (PC_{split}) was considered as one of the parameters in this research. The inferential model of PC_{split} was introduced due to the important role it plays in defining the primary grinding mass balance. A fully defined mass balance enhances the awareness of and ability to optimise the operating conditions.

Chapter 7: Due to its relatively near proximity, the inferential modelling suite was extended to combined state and parameter estimation (CSPE) in Chapter 7. The CSPE formulation utilised the dynamic models presented in Chapter 4. Two novel measurement models of the SAG mill discharge were presented for utilisation in the CSPE problem along with the novel mill weight measurement model. Initial tuning difficulties with the Kalman filter (within the CSPE problem) dictated the assessment of system observability and detectability and was the motivation for the development of the second SAG mill discharge measurement model. Both of the CSPE formulations, whilst not completely observable, are detectable. The appropriate selection of filter tuning parameters yielded good state and parameter estimates in both CSPE formulations. The main conclusions arising from Chapter 7 are:

1. The CSPE formulation incorporating the size-by-size SAG mill discharge measurement model is deemed the favourable formulation based on its superior state estimate results and its sensitivity and capacity to adust the important discharge parameters (f_p and d_0).

2. The successful presentation of the CSPE formulations provide a suitable, positively supportive context for the inferential models presented in Chapter 5. The CSPE

presentation also adds to the information available on the comminution application of CSPE which may further the acceptance that CSPE is gaining in industry.

Chapter 8: Chapter 8 detailed the validation of the inferential models developed in Chapter 5 on real plant data. The investigation of the nature of the models and further sensitivity analysis was also presented. A SAG mill operating curve was developed and discussed in terms of potential use in mill charge control. A simulation environment was constructed to test an advanced controller structure that incorporated the inferential measurement models. The controller structure could be implemented at plant level. The advanced controller incorporating the novel inferential measurement models is an innovative development. The use of integrator models for the SAG mill powerdraw, weight and rock and ball charges in the controller development is novel also. Other findings arising from this Chapter are:

1. The inferential measurement models are deemed valid after data from October 1997 was processed and the results analysed.
2. The inferential measurement models could potentially be utilised in a process monitoring/diagnostic capacity as unusual model results arose during unusual process conditions.
3. Due to model construction, the feedsize estimate is sensitive to the SAG mill breakage rates estimates, which are in turn, dependent on the mill charge estimates. The oversize crusher feedrate also affects the feedsize estimate. This is considered a model limitation, which should be noted when dealing with the results.
4. A SAG mill operating curve may be developed and visualised, with mill weight and powerdraw contours, in the (J_b, J_t, $Powerdraw \cdot Weight$) space.
5. The operating curve may potentially be utilised in a mill charge control strategy and may be dependent on ore hardness.
6. In a simulation environment, the advanced process controller performed well against a PID loop reference controller

9.2 Accomplishment and Contribution Summary

9.2.1 Research Accomplishments

The accomplishments of this research are as follows:

1. Steady state models of comminution circuit unit operations.
2. Steady state model of a full grinding circuit.
3. Dynamic models of:
   (a) SAG mill rock and water charges
   (b) SAG mill ball charge
   (c) SAG mill protective shell lining
4. Inferential models of the SAG mill:
   (a) discharge rate and size distribution (including size indicators: $T_{80} \ldots T_{20}$)
   (b) recirculating load (RCL)
   (c) total charge (J_t) and ball charge (J_b) levels
   (d) rock charge and size distribution
   (e) total feed rate and size distribution
   (f) fresh feed rate and size distribution (including size indicators: $F_{80} \ldots F_{20}$)
5. Inferential model of the primary cyclone underflow split to the ball mill (PC_{split}).
6. Sensitivity and uncertainty analyses of the inferential models.
7. A combined state and parameter estimation (CSPE) formulation of the SAG mill.
8. One measurement model of SAG mill weight for the CSPE formulation.
9. Two measurement models of SAG mill discharge for the CSPE formulation.
10. Comparative assessment of the CSPE formulations.
11. Process data validated inferential measurement models of mill ball, rock and total charges and feed size.
12. An advanced controller structure that utilises the novel inferential measurement models.
13. A selection of papers and reports:
    (a) Romagnoli, J. A., Galan, O. and Apelt, T. A., (1997) "Preliminary Study of SAG Mill Control at Northparkes Mines", Technical Report. ICI Laboratory for Process Systems Engineering. Dept of Chemical Eng, University of Sydney NSW Australia.

(b) Apelt, T. A., Galan, O. and Romagnoli, J. A. (1998) "Dynamic Environment for Comminution Circuit Operation and Control" In: CHEMECA '98, 26th Australasian Chemical Engineering Conference. CHEMECA. Port Douglas QLD Australia.

(c) Apelt, T. A. (1998) "Dynamic environment for comminution circuit control, simulation and training", ME(Research) to PhD Upgrade Report, Dept of Chemical Engineering, University of Sydney NSW Australia, 13 November1998.

(d) Apelt, T.A., Thornhill, N.F. and Romagnoli, J.A., (2000) "Mineral Grinding Process Modelling in Simulink" In: The Process Applications of MATLAB, Simulink and Stateflow Conference, Cambridge Control Ltd / Mathworks, April 5^{th}, Pope Lecture Theatre, School of Chemical, Environmental and Mining Engineering, University of Nottingham.

(e) Apelt, T.A., Asprey, S.P. and Thornhill, N.F (2001) "Inferential measurement of SAG mill parameters", Minerals Engineering, Vol. 14, No. 6, 575-591.

(f) Apelt, T.A., Asprey, S.P. and Thornhill, N.F. (2001) "SAG mill discharge measurement model for combined state and parameter estimation" In: SAG 2001, Vol. IV. pp. 138-149, UBC. Vancouver, B.C., Canada, Third international conference on: Autogenous and Semiautogenous Grinding Technology, Sep 30 - Oct 3, 2001.

(g) Apelt, T.A., Asprey, S.P. and Thornhill, N.F (2002) "Inferential measurement of SAG mill parameters II: state estimation", Minerals Engineering, Vol. 15, No. 12, 1043-1053.

(h) Apelt, T.A., Asprey, S.P. and Thornhill, N.F (2002) "Inferential measurement of SAG mill parameters III: inferential models", Minerals Engineering, Vol. 15, No. 12, 1055-1071.

(i) Apelt, T.A. and Thornhill, N.F (In Press) "Inferential measurement of SAG mill parameters IV: inferential model case study application", Minerals Engineering.

9.2.2 Research Contributions

The key contributions of this research are as follows:

1. Inferential model of the SAG mill discharge rate and size distribution (including size indicators: $T_{80} \ldots T_{20}$).

2. Inferential model of the SAG mill recirculating load.

3. Inferential model of the SAG mill rock charge and size distribution.

4. Inferential models of the SAG mill total charge and ball charge levels.
5. Inferential model of the SAG mill total feed rate and size distribution.
6. Inferential model of the SAG mill fresh feed rate and size distribution (including size indicators: F_{80}... F_{20}).
7. Inferential model of the primary cyclone underflow split to the ball mill.
8. Sensitivity and uncertainty analyses and assessment of mill discharge, charge levels and fresh feed inferential models.
9. Sensitivity and uncertainty analyses and assessment of mill breakage rates.
10. Dynamic model of the SAG mill ball charge.
11. Dynamic model of the SAG mill protective shell.
12. One SAG mill weight model.
13. Two SAG mill discharge models.
14. Two combined state and parameter estimation (CSPE) model formulations for the estimation of thirty six (36) SAG mill states and five (5) parameters, incorporating the SAG mill weight model and both of the SAG mill discharge models.
15. Observability and detectability analysis of the two CSPE formulations.
16. Assessment of the two CSPE formulations.
17. Validation of the inferential measurement models against real plant data.
18. Investigation and further analysis of the sensitivity, nature and unusual behaviour of the SAG mill charge and feed size models.
19. Development and construction of a SAG mill operating curve and discussion of its possible utilisation in a mill charge control strategy.
20. Construction of an advanced controller structure that utilises the the inferential measurement models in a simulation environment.
21. Assessment of the advanced controller performance.

9.3 Future Work and Recommendations

This research has studied several aspects of the inferential modelling of SAG mill parameters. There is scope for further work in this area that is a consequence of the research findings, problem boundaries and time constraints. The scope may be considered in terms of research and application. Further model validation is an integral part of each consideration.

9.3.1 Research

There is scope for further research in this area, including:

1. Further simulation model validation against industrial data, particularly of the dynamic models of the SAG mill rock charge, ball charge and protective shell lining.

2. Investigation of measures to improve the determination of SAG mill breakage rates in order to achieve "stable" breakage rate and dynamic mill rock charge models.

3. Further model validation of the inferential models of the SAG mill total and ball charge levels, discharge rate and size distribution, and fresh feed rate and size distribution against a larger set of industrial data.

4. Further sensitivity and uncertainty analysis of the inferential models to include the effects of model parameters not included in this research.

5. The symbolic sensitivity and uncertainty analyses conducted here for the SAG mill inferential models in Maple, could be conducted on the SAG mill simulation model itself to determine the influence of parameters on the model outputs. Similarly, symbolic analyses could be conducted on other comminution unit operation models, *e.g.*, ball mill, hydrocyclone, screen, and crusher.

6. Investigation of the reduction of the dimension of the combined state and parameter estimation (CSPE) formulation to improve the system observability, *e.g.*, by a simplification of the SAG mill rock charge model.

7. Investigation of the utilisation of the inferential models and CSPE formulations in control strategy simulation, including the utilisation of SAG mill discharge stream throughput and/or size distribution as a controlled variable.

8. Investigation of the utilisation of the inferential measurement models in a process monitoring/diagnostic capacity.

9. Investigation of the sensitivity of the inferential measurement models to other process variables not as yet assessed.

10. The fitting of the approximation of the mill powerdraw contour (for improved estimation of the relative uncertainties in the charge estimates)

11. Investigation of the dependence of the SAG mill operating curve on ore hardness

12. Investigation of the other configurations of the model predictive controller.

13. Investigation of the utilisation of the advanced controller in conjunction with an optimiser.

9.3.2 Application

During model development, the potential for implementation has always been a consideration. Consequently, the scope for the application of the findings of this research, particularly with respect to the Northparkes Mines grinding process, ranges from immediately implementable to further into the future and includes:

1. Inferential measurement of the SAG mill discharge rate and size.

2. Inferential measurement of recirculating load.

3. Inferential measurement of the SAG mill total and ball charge levels.

   These three cases are considered immediately implementable. The requirements for implementation are coding of the appropriate (relatively simple) models into a site spreadsheet[1] and linking the models to the current SCADA[2] system for model input and output. Minor model validation may be required until satisfactory confidence is attained.

4. The utilisation of the above inferential measurements for process control may then be investigated. The discharge and recirculating load may be utilised as measurement of SAG mill performance and balance between primary-secondary circuits.

5. Inferential measurement of the primary cyclone underflow split to the ball mill (PC_{split}), thus, definition of the primary grinding circuit mass balance, is implementable with the spreadsheet coding of the hydrocyclone model (more detailed than the first three models although relatively straight forward). Initial and periodic hydrocyclone model tuning to the prevailing cyclone conditions would be required.

[1] *e.g.*, Microsoft Excel

[2] Supervisory control and data acquisition

The PC_{split} measurement could then be utilised in process control.

6. Inferential measurement of SAG mill feed size distribution could also be implemented utilising current site spreadsheet and SCADA system capacity. Significant levels of spreadsheet programming would be required to achieve this particularly due to the detailed nature of the SAG mill rock charge model. The increased number of parameters involved in the required system of models would necessitate significant levels of model validation and parameter fitting (initially and periodically). The utilisation of proprietary software, *e.g.*, MATLAB, (instead of the use of spreadsheets) could also be considered here for its increased solver capabilities. These issues complicate implementation and hence medium-term implementation only is considered practically possible.

   The SAG mill fresh feed size distribution measurement could then be utilised in process control.

7. The implementation of combined state and parameter estimation (off-line and on-line) is also considered a medium-term possibility considering the complexity of the problem formulation and mathematical software requirements. In the case of Northparkes Mines, utilisation of the JA Herbst and Associates state estimation formulation, NorthEst, should be considered and pursued as the first option for state estimation.

   The incorporation of the state estimation formulations into an advanced process control strategy would be the next logical step.

8. The implementation of a model predictive controller, which utilises the inferential measurement models, at plant level. On a controller-only basis initially. Followed by a in-conjunction-with-an-optimiser phase.

9. Investigation of control actions of a real controller in relation to the SAG mill operating curve.

   Any findings from research furthered in this area should be incorporated where possible and as appropriate.

Whilst these recommendations are particularly relevant to Northparkes Mines, they are also relevant to any operation with similar circuit topography. Specific recommendations are expected to be relevant in cases where the circuit flowsheet differs, *i.e.*, the wider minerals processing community.

9.4 Closing Remarks

The primary research objectives of developing and assessing inferential models of the SAG mill inventories, discharge and fresh feed and the comparative development of a combined state estimation formulation have been met. Developments and assessments beyond the primary objectives have also been achieved.

Increasing the number of inferential measurement models available to industry and the body of knowledge supporting them adds further impetus to the transition taking the control methods of autogenous grinding circuit supervisory control and the on-line use of phenomenological models from the "active" or "emerging" phase to the "mature" phase.

References

Aldrich, C. and D.A. Theron (2000). Acoustic estimation of the particle size distributions of sulphide ores in a laboratory ball mill. The Journal of the South African Institute of Mining and Metallurgy pp. 243–248.

Alonso, M. and E.J. Finn (1969). Physics. Addison-Wesley.

Apelt, T. (2004). SAG Mill Grinding Circuit Case Study. Invensys Performance Solutions, UK. Highbank House, Exchange Street, Stockport Cheshire SK3 0ET, UK. Fundamentals of Connoisseur training course material.

Apelt, T. A. (1998). Dynamic environment for comminution circuit control, simulation and training. Technical report. Dept of Chemical Engineering. University of Sydney NSW Australia. ME(Research) to PhD Upgrade Report.

Apelt, T. A., O. Galan and J. A. Romagnoli (1998). Dynamic Environment for Comminution Circuit Operation and Control. In: CHEMECA '98. 26th Australasian Chemical Engineering Conference. CHEMECA. Port Douglas QLD Australia.

Apelt, T.A. and N.F Thornhill (In Press). Inferential measurement of SAG mill parameters IV: inferential model case study application. Minerals Engineering.

Apelt, T.A., S.P. Asprey and N.F Thornhill (2001a). Inferential measurement of SAG mill parameters. Minerals Engineering **14**(6), 575 – 591.

Apelt, T.A., S.P. Asprey and N.F. Thornhill (2001b). SAG mill discharge measurement model for combined state and parameter estimation. In: SAG 2001. Vol. IV. UBC. Vancouver, B.C., Canada. pp. 138–149. Third international conference on: Autogenous and Semiautogenous Grinding Technology.

Apelt, T.A., S.P. Asprey and N.F Thornhill (2002a). Inferential measurement of SAG mill parameters II: state estimation. Minerals Engineering **15**(12), 1043 – 1053.

Apelt, T.A., S.P. Asprey and N.F Thornhill (2002b). Inferential measurement of SAG mill parameters III: inferential models. Minerals Engineering **15**(12), 1055 – 1071.

Austin, L.G. and H. Cho (2002). An alternative method for programming mill models. Powder Technology **122**, 96–100.

Austin, L.G., J.M. Menacho and J. Pearcy (1987). A General Model for Semi-autogenous and Autogenous Milling. In: APCOM 87 (K.P. King and I.J. Barker, Eds.). Vol. 2 of Twentieth International Symposium on the Application of Computers and Mathematics in the Mineral Industries. SAIMM. Johannesburg, South Africa. pp. 107–126.

Banisi, S., G. Langari-Zadeh, M. Pourkani, M. Kargar and A.R. Laplante (2000). Measurement fo ball size distribution and wear kinetics in an 8 m by 5 m primary mill of Sarcheshmeh copper mine. CIM Bulletin.

Barratt, D.J. and M. Brodie (2001). The "Tent" Diagram, What It Means. In: SAG 2001. Vol. IV. UBC. Vancouver, B.C., Canada. pp. 368–379. Third international conference on: Autogenous and Semiautogenous Grinding Technology.

Bond, F.C. (1961). Crushing & Grinding Calculations Part I & II. British Chemical Engineering **6**, 378–385;543–548.

Borell, M., P-O. Bacstrom and L. Soderberg (1996). Supervisory control of autogenous grinding circuits. International Journal of Mineral Processing **44-45**, 337–348.

Boulvin, M., C. Renotte, A. Vande Wouwer, M. Remy, S. Tarsiewicz and P. Cesar (1999). Modelling, Simulation and Evaluation of Control Loops for a Cement Grinding Process. European Journal of Control **5**, 10–18.

Broussaud, A., O. Guyot, J. McKay and R. Hope (2001). Advanced Control of SAG and FAG Mills with Comprehensive or Limitedd Instrumentation. In: SAG 2001. Vol. II. UBC. Vancouver, B.C., Canada. pp. 358–372. Third international conference on: Autogenous and Semiautogenous Grinding Technology.

Bwalya, M.M. and M.H. Moys (2001). The use of DEM in modeling and scaling-up of (S)AG mills. In: SAG 2001. Vol. IV. UBC. Vancouver, B.C., Canada. pp. 180–190. Third international conference on: Autogenous and Semiautogenous Grinding Technology.

Campbell, J., D. Spencer, S. amd Sutherland, T. Rowlands, K. Weller, P. Cleary and A. Hinde (2001). SAG Mill Monitoring Using Surface Vibrations. In: SAG 2001. Vol. II. UBC. Vancouver, B.C., Canada. pp. 373–385. Third international conference on: Autogenous and Semiautogenous Grinding Technology.

Cheng, Y.S., T. Mongkhonsi and L.S. Kershenbaum (1997). Sequential estimation fo rnonlinear differential and algebraic systems - theoretical development and application. Computers in Chemical Engineering **21**(9), 1051–1067.

Cleary, P.W., R. Morrison and S. Morrell (2001). DEM validation for a scale model SAG mill. In: SAG 2001. Vol. IV. UBC. Vancouver, B.C., Canada. pp. 191–206. Third international conference on: Autogenous and Semiautogenous Grinding Technology.

Craig, I. K. and I. M. MacLeod (1995). Specification Framework for robust control of run-of-mine ore milling circuit. Control Engineering Practice **3**(5), 621–630.

Craig, I. K. and I. M. MacLeod (1996). Robust controller design and implementation for a run-of-mine ore milling circuit. Control Engineering Practice **4**(1), 1–12.

Craig, I. K., D. G. Hulbert, G. Metzner and S. P. Moult (1992a). Extended particle-size control of an industrial run-of-mine milling circuit. Powder Technology **73**, 203–210.

Craig, I. K., D. G. Hulbert, G. Metzner and S. P. Moult (1992b). Optimized multivariable control of an industrial run-of-mine milling circuit. Journal of the South African Intitute of Mining and Metallurgy **92**(6), 169–176.

David, D. (1997). Simulations of Northparkes Grinding Circuits, 1997. Technical report. JKTech - JKMRC Commercial Division. Julius Kruttschnitt Mineral Reseach Centre, University of Queensland, Australia. Job No 96259.

Davies, G., L. Crew and S. Jackson (2000). Evaluation of the Laser Online Ore Sizer at the WMC Leinster Nickel Operation. In: Seventh Mill Operators' Conference. pp. 27–31. Kalgoorlie, WA.

Davis, Jim (1999). SAG Mill Loops. Personal correspondance from Northparkes Mines process operator.

Desbiens, A., F. Flament and A. Pomerleau (1997). Distributed control at Kidd Creek grinding plant. Part II: Implementation. CIM Bulletin pp. 145–150.

Erickson, M.T. (1989). SAG Mill Ball Charge Determination. In: SAG 1989. Vol. 2. UBC. Vancouver, B.C., Canada. pp. 449–460. First international conference on: Autogenous and Semiautogenous Grinding Technology.

Evans, G. (2001). A New Method for Determining Charge Mass in AG/SAG Mills. In: SAG 2001. Vol. II. UBC. Vancouver, B.C., Canada. pp. 331–345. Third international conference on: Autogenous and Semiautogenous Grinding Technology.

Fimeri, M. (1997). Computer based vision for ore sizing. PACE.

Flament, F., A. Desbiens and R. del Villar (1997). Distributed control at Kidd Creek grinding plant. Part I: Control strategy design. CIM Bulletin pp. 139–144.

Freeman, N., P. Feltoe and D. Nicoli (2000a). The Improvements in Control of the Mill 3 Circuit at Alcoa's Wagerup Refinery. In: Seventh Mill Operators' Conference. Australasian Institute of Mining and Metallurgy. Kalgoorlie, WA, Australia. pp. 303–310.

Freeman, N., W. Keenan, S. Hancock and G. LePage (1994). Grinding Circuit Control - Techniques and Experiences. In: Fifth Mill Operators Conference. Olympic Dam, Australia. pp. 193–199.

Freeman, W.A., R. Newell and K.B. Quast (2000b). Effect of grinding media and NaHS on copper recovery at Northparkes Mine. Minerals Engineering **13**(13), 1395–1403.

Froisy, B., C. Hart, S. Lingard, S. Papastratos, D. Dixon and P. McGrath (1999). Industrial Application of On-line First Principle Dynamic Models using State Estimation. prepared for presentation at aiche'99 annual meeting, friday november 5th 1999 ed.. AspenTech and Equistar Chemicals. (http://www.aspentech.com/publication_files/TA27.pdf).

Fuenzalida, R., E. Cubillos and J. Sepulveda (1996). Plant Experiences on Expert Supervisor Control of Semiautogenous Grinding Circuits. In: SAG 1996. Vol. 2. UBC. Vancouver, B.C., Canada. pp. 642–656. Second international conference on: Autogenous and Semiautogenous Grinding Technology.

Gault, G.A. (1975). Modelling and Control of Autogenous Grinding Circuits. PhD thesis. Julius Kruttschnitt Mineral Research Centre, Department of Mining and Metallurgical Engineering, University of Queensland, Australia. December 1975.

Girdner, K., J. Handy and J Kemeny (2001). Improvements in Fragmentation Measurement Software for SAG Mill Process Control. In: SAG 2001. Vol. II. UBC. Vancouver, B.C., Canada. pp. 270–281. Third international conference on: Autogenous and Semiautogenous Grinding Technology.

Hales, Lynn B., James L. Vanderbeek and John A. Herbst (1988). Supervisory Control of a Semi-Autogenous Grinding Circuit. International Journal of Minerals Processing **22**, 297–312.

Hart, J. R. and C. L. E. Swartz (1997). An Optimising Control Strategy For Milling Circuit Operation. Proceedings of the South African Institue of Mining and Metallurgy.

Henson, Michael A. and Seborg, Dale E., Eds.) (1997). Nonlinear Process Control. Prentice Hall PTR.

Herbst & Associates, J.A. (1996). Semi Autogenous Mill Filling Using a Model-Based Methodology. Proposal submitted to North Limited - Northparkes Mines.

Herbst, J. A. and W. T. Pate (1999). Object components for comminution system softsensor design. Powder Technology **105**, 424–429.

Herbst, J. A., W. T. Pate and A. E. Oblad (1992). Model-based control of mineral processing operations. Powder Technology **69**, 21–32.

Herbst, J. A., W. T. Pate and Y. C. Lo (1993). A Model-Based Methodology for Steady State and Dynamic Optimisation of Autogenous and Semiautogenous Grinding Mills. In: XVIII International Mineral Processing Congress. Sydney. pp. 519–527.

Herbst, J.A. (2000). Model-Based Decision Making for Mineral Processing - A Maturing Technology. In: CONTROL 2000 (J.A. Herbst, Ed.). Mineral and Metallurgical Processing. SME. Littleton, Colorado, USA. pp. 187–200.

Herbst, J.A. and F. Alba J. (1985). An approach to adaptve optimal control of mineral processing operations. In: XV International Mineral Processing Congress. Vol. 3. France. pp. 75–87.

Herbst, J.A. and S.L. Blust (2000). Video Sampling for Mine-to-Mill Performance Evaluation: Model Calibration and Simulation. In: CONTROL 2000 (J.A. Herbst, Ed.). Mineral and Metallurgical Processing. SME. Littleton, Colorado, USA. pp. 157–166.

Herbst, J.A. and T. Gabardi (1988). Closed Loop Media Charging of Mills Based on a Smart Sensor System. In: IFAC Applied Measurements in Mineral and Metallurgical Processing (G. Sommer, Ed.). IFAC. Pergamon Press. Transvaal, South Africa. pp. 17–21.

Herbst, J.A. and W.T Pate (1996). On-line estimation of charge volumes in semiautogenous and autogenous grinding mills. In: SAG 1996. Vol. 2. Vancouver, B.C., Canada. pp. 817–827. Second international conference on: Autogenous and Semiautogenous Grinding Technology.

Herbst, J.A. and W.T. Pate (2001). Dynamic Modeling and Simulation of SAG/AG Circuits With MinOOcad: Off-line and On-line Applications. In: SAG 2001. Vol. IV. UBC. Vancouver, B.C., Canada. pp. 58–70. Third international conference on: Autogenous and Semiautogenous Grinding Technology.

Herbst, J.A., W.T. Pate and A.E. Oblad (1989). Experience inthe use of Model Based Expert Control Systems in Autogenous and Semi Autogenous Grinding Circuits. In: SAG 1989. UBC. Vancouver, B.C., Canada. pp. 669–686. First international conference on: Autogenous and Semiautogenous Grinding Technology.

Herbst, J.A., W.T. Pate, J.L. Vanderbeek and L.B. Hales (1983). Real-time estimation of unmeasured variables in a semiautogenous grinding circuit. In: SME-AIME Fall Meeting. Salt Lake City, Utah.

Hodouin, D., S.-L. Jamsa-Jounela, M.T. Carvalho and L. Bergh (2001). State of the art and challenges in mineral processing control. Control Engineering Practice **9**(9), 995–1005.

Hulbert, D. G. (1989). The State of the Art in the Control of Milling Circuits. In: IFAC Automation in Mining, Mineral and Metal Processing. IFAC. Pergamon Press, Oxford. pp. 1–10.

Hulbert, D.C. (2001). Review Papers on Automation in Mineral and Metal Processing. Control Engineering Practice **9**(9), 993.

Ivezić, D.D. and T.B. Petrović (2003). New approach to milling circuit control - robust inverse Nyquist array design. International Journal of Mineral Processing **70**, 171–182.

Jamsa-Jounela, S.-L. (2001). Current status and future trends in automation of mineral and metal processing. Control Engineering Practice **9**(9), 1021–1035.

JKTech (1994). JK SimMet steady state mineral processing simulator: User Manual Version 4. JKTech - JKMRC Commercial Division. Julius Kruttschnitt Mineral Research Centre, University of Queensland, Australia.

Jones Jnr, S.M. (2001). Autogenous and Semiautogenous Mills 2000 Update. In: SAG 2001. Vol. IV. UBC. Vancouver, B.C., Canada. pp. 362–400. Third international conference on: Autogenous and Semiautogenous Grinding Technology.

Koivistoinen, P. and J. Miettunen (1989). The Effect of Mill Lining on the Power Draw of a Grinding Mill and its Utilisation in Grinding Control. In: SAG 1989. Vol. 2. UBC. Vancouver, B.C., Canada. pp. 687–695. First international conference on: Autogenous and Semiautogenous Grinding Technology.

Kojovic, T., J.R. Pyecha and J.R. Corbin (2001). Use of Online Mill Charge Simulators at the Red Dog Grinding Circuit. In: SAG 2001. Vol. IV. UBC. Vancouver, B.C., Canada. pp. 11–23. Third international conference on: Autogenous and Semiautogenous Grinding Technology.

Lange, T.B. (1988). Real-time measurement of the size distribution of rocks on a conveyor belt. In: IFAC Applied Measurements in Mineral and Metallurgical Processing (G. Sommer, Ed.). IFAC. Pergamon Press. Transvaal, South Africa. pp. 25–34.

Lynch, A.J. (1977). Mineral Crushing and Grinding Circuits: Their Simulation, Optimisation, Design and Control. Vol. 1 of Developments in Mineral Processing. Elsevier.

Lynch, A.J. and R.D. Morrison (1999). Simulation in mineral processing: history, present status and possibilities. The Journal of the South African Institute of Mining and Metallurgy pp. 283–288.

Lyon, G.Q. (1988). Discussion on papers presented during the 1st Session Technical Summary and Comments on papers submitted by Moys, Vermeulen, Herbst and Lange. In: IFAC Applied Measurements in Mineral and Metallurgical Processing (G. Sommer, Ed.). IFAC. Pergamon Press. Transvaal, South Africa. pp. 35–36.

MacPherson, A.R. (1989). The Development of AUtogenous Grinding and Semi-Autogenous Grinding. In: SAG 1989. Vol. 1. UBC. Vancouver, B.C., Canada. pp. 5–7. First international conference on: Autogenous and Semiautogenous Grinding Technology.

Maerz, N.H. (2001). Automated Online Optical Sizing Analysis. In: SAG 2001. Vol. IV. UBC. Vancouver, B.C., Canada. Third international conference on: Autogenous and Semiautogenous Grinding Technology.

Maerz, N.H. and T.C. Palangio (2000). On-Line Fragmentation Analysis for Grinding and Crushing Control. In: CONTROL 2000 (J.A. Herbst, Ed.). Mineral and Metallurgical Processing. SME. Littleton, Colorado, USA. pp. 109–116.

Marklund, U. and J. Oja (1996). Grinding Control Aitik: Optimisatin of an Autogeous Grinding Circuit through Mill Filling Measurement and Multivariate Statistical Analysis. In: SAG 1996. Vol. 2. UBC. Vancouver, B.C., Canada. pp. 617–631. Second international conference on: Autogenous and Semiautogenous Grinding Technology.

McKen, A., H. Raabe and J. Mosher (2001). Application of Operating Work Indices to Evaluate Individual Sections in Autogenous-Semiautogenous/Ball Mill Circuits. In: SAG 2001. Vol. III. UBC. Vancouver, B.C., Canada. pp. 151–164. Third international conference on: Autogenous and Semiautogenous Grinding Technology.

Morrell, S. (1994). Powerdraw Draw of Grinding Mills - Its Measurement and Prediction. In: Fifth Mill Operators Conference. Olympic Dam, Australia. pp. 109–114.

Morrell, S. (2004). A new autogenous and semi-autogenous mill model for scale-up, design and optimisation. Minerals Engineering **17**, 437–445.

Morrell, S. and H. Delboni Jnr (1996). The modelling of autogenous and semi-autogenous mills. In: SAG 1996. Vol. 2. UBC. Vancouver, B.C., Canada. pp. 713–728. Second international conference on: Autogenous and Semiautogenous Grinding Technology.

Morrell, S. and R.D. Morrison (1989). Ore Charge, Ball Charge amd Material Flow Effects on an Energy Based SAG Mill Model. In: SAG 1989. Vol. 2. UBC. Vancouver, B.C., Canada. pp. 697–711. First international conference on: Autogenous and Semiautogenous Grinding Technology.

Morrell, S. and R.D. Morrison (1996). AG and SAG Mill Circuit Selection and Design by Simulation. In: SAG 1996. UBC. Vancouver, B.C., Canada. pp. 769–790. Second international conference on: Autogenous and Semiautogenous Grinding Technology.

Morrell, S. and W. Valery (2001). Influence of Feed Size on AG/SAG Mill Performance. In: SAG 2001. Vol. I. UBC. Vancouver, B.C., Canada. pp. 204–214. Third international conference on: Autogenous and Semiautogenous Grinding Technology.

Morrell, S., W. Valery, G. Banini and S. Latchireddi (2001). Developments in AG/SAG Mill Modelling. In: SAG 2001. Vol. IV. UBC. Vancouver, B.C., Canada. pp. 71–84. Third international conference on: Autogenous and Semiautogenous Grinding Technology.

Morrison, R. D. (n.d.). Concentrator Optimisation. In: XVIII International Mineral Processing Congress.

Morrison, R.D. (2000). Applying Image Analysis to Process Control - From Blasting to Flotation. In: CONTROL 2000 (J.A. Herbst, Ed.). Mineral and Metallurgical Processing. SME. Littleton, Colorado, USA. pp. 51–58.

Moys, M.H. (1985). The Measurement of Parameters Describing the Dynamic Behaviour of the Load in a Grinding Mill. In: Proceedings of MINTEK 50. Vol. 1 of International Conference on Mineral Science and Technology. The Council for Mineral Technology. South Africa.

Moys, M.H. (1988). Measurement of Slurry Properties and Load Behaviour in Grinding Mills. In: IFAC Applied Measurements in Mineral and Metallurgical Processing (G. Sommer, Ed.). IFAC. Pergamon Press. Transvaal, South Africa. pp. 3–10.

Moys, M.H. (1989). Slurry Rheology - The Key to a Further Advance in Grinding Mill Control. In: SAG 1989. UBC. Vancouver, B.C., Canada. pp. 713–727. First international conference on: Autogenous and Semiautogenous Grinding Technology.

Moys, M.H. (1993). A model of mill power as affected by mill speed, load volume, and liner design. Journal of The South African Institute of Mining and Metallurgy **93**(6), 135–141.

Moys, M.H., J. De Souza, S. Tshabalala and M. Giddy (1987). Use of an Energy Balance around the Mill Sump to Estimate Mill Discharge Density. In: APCOM 87 (K.P. King and I.J. Barker, Eds.). Vol. 2 of Twentieth International Symposium on the Application

of Computers and Mathematics in the Mineral Industries. SAIMM. Johannesburg, South Africa. pp. 15–26.

Mular, A.L. and A. Burkert (1989). Automatic Control of Semiautogenous Grinding (SAG) Circuits. In: SAG 1989. Vol. 2. UBC. Vancouver, B.C., Canada. pp. 651–668. First international conference on: Autogenous and Semiautogenous Grinding Technology..

Napier-Munn, T. J., S. Morrell, R. D. Morrison and T. Kojovic (1996). Mineral Comminution Circuits - Their Operation and Operation. Julius Kruttschnitt Mineral Research Centre, Australia.

Niemi, A. J., L. Tian and R. Ylinen (1997). Model Predictive Control For Grinding Systems. Control Engineering Practice **5**(2), 271–278.

Niemi, A. J., R. Ylinen and V. Rasanen (1992). Control of grinding circuits using phenomenological models. Powder Technology **69**, 47–52.

Pax, R. (2001). Non-Contact acoustic measurement of in-mill variables of SAG mills. In: SAG 2001. UBC. Vancouver, B.C., Canada. pp. 386–393. Third international conference on: Autogenous and Semiautogenous Grinding Technology.

Perry, R. and L. Anderson (1996). Development of Grinding Circuit Control at P.T.Freeport Indonesia's New SAG Concentrator. In: SAG 1996. Vol. 2. UBC. Vancouver, B.C., Canada. pp. 671–699. Second international conference on: Autogenous and Semiautogenous Grinding Technology.

Perry, T.H., Green, D.W. and Maloney, J.O., Eds.) (1984). Perry's Chemical Engineers' Handbbok. 6th ed.. McGraw-Hill.

Petersen, K.R.P., C. Aldrich and J.S.J.. van Deventer (1998). Analysis of Ore Particles Based on Textural Pattern Recognition. Minerals Engineering **11**(10), 959–977.

Pontt, J. (2004). MONSAG: A new monitoring system for measuring the load filling of a SAG mill. Minerals Engineering **17**, 1143–1148.

Radhakrishnan, V.R. (1999). Model based supervisory control of a ball mill grinding circuit. Journal of Process Control **9**, 194–211.

Rajamani, R. and B.K. Mishra (2001). Three dimensional simulation of charge motion in plant size SAG mills. In: SAG 2001. Vol. IV. UBC. Vancouver, B.C., Canada. pp. 48–57. Third international conference on: Autogenous and Semiautogenous Grinding Technology.

Ramasamy, M., S. Narayanan and Ch.H.P. Rao (2005). Control of ball mill grinding circuit using model predictive control scheme. Journal of Process Control **15**, 273–283.

Ranamani, R.K. and B.K. Mishra (1996). Dynamics of Ball and Rock Charge in SAG Mills. In: SAG 1996. Vol. 2. UBC. Vancouver, B.C., Canada. pp. 700–712. Second international conference on: Autogenous and Semiautogenous Grinding Technology.

Ray, W.H. (1981). Advanced Process Control. McGraw-Hill Book Company.

Romagnoli, J. A. (1996). Advanced Process Control. Dept of Chemical Eng, University of Sydney NSW Australia. course notes.

Romagnoli, J. A., O. Galan and T. A. Apelt (1997). Preliminary Study of SAG Mill Control at Northparkes Mines. Technical report. ICI Laboratory for Process Systems Engineering. Dept of Chemical Eng, University of Sydney NSW Australia.

Romagnoli, J.A. and M.C. Sanchez (2000). Data Processing and Reconciliation for Chemical Process Operations. Vol. 2 of Process Systems Engineering. Academic Press.

Samskog, P.O., P. Soderman, U. Storeng, J. Bjorkman, O. Guyot and A. Broussaud (1996). Model-based Control of Autogenous and Pebble Mills at LKAB Kiruna KA2 Concentrator (Sweden). In: SAG 1996. Vol. 2. UBC. Vancouver, B.C., Canada. pp. 599–616. Second international conference on: Autogenous and Semiautogenous Grinding Technology.

Schroder, A.J. (2000). Towards Automated Control of Milling Operations. IIR Conference - Crushing and Grinding Technologies for Mineral Extraction. Perth, Australia.

Sherman, M. (2001). Optimization of the Alumbrera SAG Mills. In: SAG 2001. Vol. I. UBC. Vancouver, B.C., Canada. Third international conference on: Autogenous and Semiautogenous Grinding Technology.

Smith, V.C. and C.L.E. Swartz (1999). Development of a Hydrocyclone Product Size Soft-Sensor. In: International Symposium on Solid/Liquid Separation (G.B. Harris and S.J. Omelon, Eds.). 38th Annual Conference of Metallurgist. Canadian Institute of Mining, Metallurgy and Petroleum. Quebec City, Canada.

Sotelo, R.R., L.M. Gordon and C. Jewart (1996). Implementing advanced control on a copper ore grinding circuit. unknown source.

Spencer, S.J., J.J. Campbell, K.R. Weller and Y. Liu (2000). Monitoring of SAG Mill Performance Using Acoustic Emissions. In: Proceedings of the XXI International Mineral Processing Congress. Vol. 1. Elsevier. Amsterdam. pp. A4–13–A4–20.

Strohmayr, S. and W. Valery (2001). SAG Mill Circuit Optimisation at Ernest Henry Mining. In: SAG 2001. Vol. III. UBC. Vancouver, B.C., Canada. pp. 11–42. Third international conference on: Autogenous and Semiautogenous Grinding Technology.

Taylor, J.R (1982). An Introduction to Error Analysis: The Study of Uncertainties in Physical Measurements. University Science Books.

Thornton, A.J., T. Pethybridge, T. Rivett and R. Dunn (2005). SAG Mill Control at Northparkes Mines (Not So Hard After All). www.mipac.com.au.

Valenzuela, J., K. Najim, R. del Villar and M. Bourassa (1993). Learning control of an autogenous grinding circuit. International Journal of Mineral Processing **40**, 45–56.

Valenzuela, J., M. Bourassa, K. Najim and R. del Villar (1994). Technical Note: Dynamic Matrix Control of an Autogenous Grinding Circuit. Minerals Engineering **7**(1), 105–114.

Valery Jnr., Walter (1998). A model for dynamic and steady-state simulation of autogenous and semi-autogenous mills. PhD thesis. University of Queensland (Dept of Mining, Minerals and Materials Engineering). Publ St Lucia, Qld. 1997.

Valery Jnr, Walter and Steve. Morrell (1995). The Development of a Dyamic Model for Autogenous and Semi-Autogenous Grinding. In: Minerals Engineering Conference, St. Ives, England.

Van Drunick, W.I. and M.H. Moys (2001). The Use of an Energy Balance to Measure and Control the Rheology of Mill Discharge Slurry. In: SAG 2001. Vol. II. UBC. Vancouver, B.C., Canada. pp. 304–316. Third international conference on: Autogenous and Semiautogenous Grinding Technology.

van Nierop, M.A. and M.H. Moys (1996). Measurement of Load Behaviour in an Industrial Mill. In: SAG 1996. Vol. 2. UBC. Vancouver, B.C., Canada. pp. 657–670. Second international conference on: Autogenous and Semiautogenous Grinding Technology.

van Nierop, M.A. and M.H. Moys (1997a). The effect of overloading and premature centrifuging on the power of an autogenous mill. Journal of The South African Institute of Mining and Metallurgy **97**(7), 313–317.

van Nierop, M.A. and M.H. Moys (1997b). Measurement of Load Behaviour in an Industrial Grinding Mill. Control Engineering Practice **5**(2), 257–262.

Vermeulen, L.A. and F.A. Schakowski (1988). Estimation, by use if a conductivity bolt, of the charge volume and other milling parameters in an operating mill. In: IFAC Applied Measurements in Mineral and Metallurgical Processing (G. Sommer, Ed.). IFAC. Pergamon Press. Transvaal, South Africa. pp. 11–15.

Wardell-Johnson, L., S. Green, G. McKernan and J. Skrypniuk (1997). Expert Control at Boddington Gold Mine. In: Sixth Mill Operators Conference. Madang. pp. 73–78.

Welch, G. and G. Bishop (2001). An Introduction to the Kalman Filter. (http://www.cs.unc.edu/ welch/media/pdf/kalman_intro.pdf). Department of Computer Science, University of North Carolina at Chapel Hill.

Whiten, W.J. (1972). The Simulation of Crushing Plants with Models Developed using Multiple Spline Regression. In: Proceedings of the Tenth International Symposium on the Application of Computer Methods in the Mineral Industry (M.D.G. Salamon and F.H. Lancaster, Eds.). SAIMM. Johannesburg, South Africa. pp. 317–323.

Whiten, W.J. (1974). A Matrix Theory of Comminution Machines. Chemical ENgineering Science **29**, 589–599.

Wills, B.A. (1989). Mineral Processing Technology: An Introduction to the Practical Aspects of Ore Treatment and Mineral Recovery. Vol. 41 of International Series on Material Science and Technology. 4th ed.. Pergamon Press.

Appendix A

Northparkes Mines Communications Summary

M E M O R A N D U M

TO: RICK M DUNN TEAM LEADERS

FROM: THOMAS APELT

COPIES: NINA THORNHILL JOSE ROMAGNOLI
JIM DAVIS JEFF SMITH

SUBJECT: GRINDING CIRCUIT MODELLING PROGRESS UPDATE

DATE: 28 FEBRUARY 2000

Executive Summary

The ongoing research work is focused on the modelling of the Module 1 grinding circuit in the Matlab-Simulink environment. A full steady state circuit model has been constructed. Following communications with NPM in late 1999 the research focus shifted to the primary circuit and the SAG mill. This memorandum has the following aims:

1. To summarise the communications of late 1999
2. To provide an update on the research work
3. To discuss the future direction of the work
4. To instigate further NPM feedback

Control of the conditions within the SAG mill was one of the recurring themes in the responses received from NPM personnel. The model has been developed such that it is capable of estimating the SAG mill rock and ball charge and new feed F_{80} from prevailing operating conditions. Future work direction will focus the refinement of the estimations and proving their accuracy on plant data. Feedback is now required from NPM personnel on their interest in the model and the work completed thus far. Comment on the direction the future work is also requested. Other comments and questions are welcome.

Communications Summary

In late September 1999 the major milestone of a complete steady state circuit in Matlab-Simulink was reached. The next task was to decide how to utilise the model. Meetings to address the situation were commenced with Dr Nina Thornhill. In October and November NPM was contacted with the intent to determine a practically useful application of the model. The question:

> "What is stopping NPM making more money?"

was put to the Ore Processing Department staff. The question was kept general so that it was not a leading question. The only guidance was that it was in relation to the grinding circuits. Table A.1 contains the responses which were received with much appreciation. The suggestions marked with a star ($\star$) are those thought to have potential for model application.

The potential applications were assessed to have the following common underlying themes:

1 throughput (more)
2 product size (finer)
3 feed ore characteristics
- hardness
- size

4 SAG mill parameters
- ball charge
- rock charge

Table A.1: Ore Processing Money Bottlenecks

	No.	SUGGESTIONS
	1	Limited, low grade ore sources
	2	External factors such as low metal price etc
⋆	3	Coarse grind size - imperfect liberation hence loss of metal recovery
	4	Under designed grinding circuit - insufficient consideration/knowledge of ore characteristics
	5	Limited access to capital investment
⋆	6	Process variation due to varying ore types, feed grade, process parameters etc
	7	Insufficient understanding of process inefficiencies (eg losses of metal in fine size fractions, relative difference between gold and copper recovery etc)
	8	A constant feed ore size to the mills for steady throughput. (an underground issue really)
	9	Constant ore type i.e. feed grade through the plant enabling fine tuning for that type of ore. (planning ahead)
⋆	10	Grinding bottlenecks, pump capacity limited for ore which recirculates a lot due to its hard grinding nature.
⋆	11	Oversize crusher capacity, affected when there is increased wear in the discharge grates of the mill, and having to cope with sizes up to 70mm. Huge costs involved in the rebuilds of the crushers, only lasting about 5 weeks.
⋆	12	Sag mill optimum ball charge, power consumption and internals wear rate, these factors contribute to the most expenses incurred in the plant, and if the optimum rates and balance between these 3 factors could be found then there would be significant savings in running costs. This isn't to say we are far off the mark now, but we always seem to be moving the line of best performance all in the name of throughput.
⋆	13	Grindsize is another issue directly related to recovery and dollars at the end of the day. With success of a regrind circuit on one of the modules, it would seem a good idea to have one on both circuits to optimise recovery when the larger tonnes are being put through.
⋆	14	Determination of volumetric / ball charge
⋆	15	Using all of the available installed power
⋆	16	Consistent media charging
	17	Reliability and consistency of recycle circuit
⋆	18	Determination of control parameters to mimic mill conditions e.g. sound monitoring
	19	Cone crusher availability.
⋆	20	Mill feed top size.
⋆	21	Liberation in final grind. (ie: not enough) or (need more tertiary mills)
	22	Copper prices.
	23	The value of the Australian dollar on the international market.
⋆	24	The most obvious one is that the mills aren't big enough to handle the size, abrasiveness and hardness of the ore that we treat
	25	Probably the only things that can be done are to pretreat the ore down further to a smaller size or add some tertiary mills, both of which are very costly and in these economic times unrealistic
	26	Another option that may that could be considered is to close the aperture of our vibrating screen to almost nothing and putting more emphasis on the oversize circuit to achieve the oresize that you require, but this would also be costly

To choose an application that would interest NPM and satisfy research requirements the themes were correlated with the five main research areas at the Centre for Process Systems Engineering, namely:

1. Dynamic modelling
2. Optimisation
3. Advanced process control
4. Inferential methods
5. Plant scheduling

The outcome of the assessment was the selection of an application in the inferential methods: SAG mill parameter estimation.

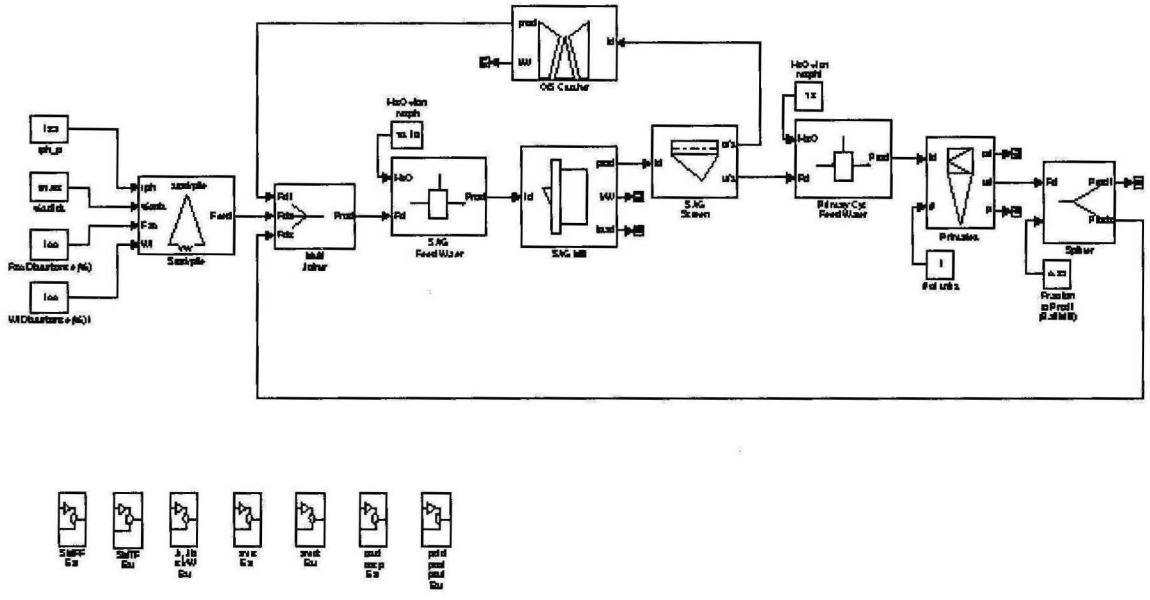

Figure A.1: Primary Circuit Model

Abbreviations		*Stream Properties*	
SMFF	SAG mill fresh feed	tph_s	solids tph
SMTF	SAG mill total feed	tph_l	water tph
SMRC	SAG mill rock charge	tph_p	total (pulp) tph
SMBC	SAG mill ball charge	%s w/w	%solids by weight
SMDC	SAG mill discharge	%l w/w	%water by weight
PCFD	Primary cyclone feed	m3ph_s	volumetric flow of solids
PCUF	Primary cyclone underflow	m3ph_l	volumetric flow of water
PCUS	Primary cyclone underflow to SAG mill	m3ph_p	total (pulp) volumetric flow
OSCF	Oversize crusher feed	%s v/v	%solids by volume
OSCP	Oversize crusher product	%l v/v	%water by volume
	uppercase = stream properties	SGp	pulp specific gravity
	lowercase = size distribution	P80	80% passing size (mm)

Work Update

Primary Circuit Model

The primary circuit model is shown in Figure A.1. The model equations behind the blocks are essentially those used by JKSimMet. The Stockpile block is structured to allow variations in feed ore throughput (tph_p), moisture (%solids), size (F_{80}) and hardness (Work Index). The model calculates the stream characteristics and size distribution of each stream which is passed from one block to the next. Table A lists the abbreviations used for stream names and the information corresponding to "stream properties". The model also calculates:

- SAG mill power draw
- SAG mill load
- O/S crusher power draw
- 1° cyclone pressure

SAG Mill Parameter Estimation

The seven blocks in the lower left corner of Figure A.1 have the main function of calculating:

- SAG mill rock charge
- SAG mill ball charge
- Stockpile feed F_{80}

The calculation sequence is as follows:

1. OSCF and PCFD streams are calculated based on scats tph, primary cyclone feed flowrate and %solids data and assumptions about the size distributions (based on SAG mill grate size and D/C screen aperture size).
2. SMRC is calculated by applying the SAG mill discharge function in reverse.
3. Fractional total filling, J_t, and ball filling, J_b, are determined by applying the powerdraw equations in reverse, utilising mill power draw and weight data as inputs.
4. SMTF is then calculated by the reverse application of the mill model after making assumptions about the ball charge size distribution.
5. OSCP and PCUF are calculated by the direct application of the crusher and cyclone models.
6. SMFF is calculated by subtracting the OSCP and PCUS from the SMTF stream. SMFF F_{80} is calculated in the process.

In each case the stream properties and size distributions of the streams are calculated. The basis of the calculations can be either the simulated plant data or operating data.

Future Work and Feedback

Work Projection

The immediate work schedule involves:

- completion of a paper for a conference on *Process Applications of MATLAB, Simulink and Stateflow* at the University of Nottingham. Attached is a copy of the abstract submitted to and accepted by the conference organisers.
- model validation and results generation using NPM operating data

Following on from the immediate tasks are:

- closer study of the estimation of the mill parameters J_t and J_b
- assessment of the possible r benefits of incorporating a dynamic model of the SAG mill rock and ball charge
- a paper for the Minerals Engineering 2000 conference

Request for Feedback

In its current state the model has two main capabilities:

1. steady state simulation of operating conditions
2. prediction of SAG mill and feed ore parameters

These capabilities could be utilised off-line following minimal model validation. The Matlab-Simulink environment allows for the variation of inputs during the simulation. The effects of variations can be graphed quickly and easily in the course of *"what if?"* scenario investigations or sensitivity analyses. Matlab also possesses sophisticated mathematical capability. This capability includes a range of process control functions which make the practical implementation at NPM a definite option in the longer term.

NPM feedback is now requested on the following topics:

1. Value/interest of the work completed thus far to NPM
2. Appropriateness of the future work direction
3. Other comments or questions

Thomas Apelt

Appendix B

Northparkes Mines Grinding Circuit Survey Data

(David, 1997)

Table 4: Measured and Simulated Performance - Survey 1 (Table 29 in first report)

SAG Circuit	Measured	Simulated	% Difference
Feed Rate	185	185	0.0%
Feed F_{80}	91.9	91.9	0.0%
Scats tph	65.3	67.1	2.8%
Scats P_{80} (mm)	42.8	41.5	-3.0%
Crusher Product P_{80} (mm)	33.1	33.1	0.0%
SAG Load %	21.8	21.8	0.0%
SAG Power (kW)	2810	2863	1.9%
Primary Cyclone Feed % Solids	50.5	50.8	0.6%
Primary Cyclone Feed F_{80} (mm)	1.93	2.6	34%
Primary Cyclone Feed %-75µm	24.7	22.8	-7.7%
Primary Cyclone Pressure (kPa)	59	57	-3.4%
Prim. Cyc o/f % Solids	21.5	22.7	5.6%
Prim. Cyc o/f tph		34	
Prim. Cyc o/f P_{80}	52.7	62	17.6%
Prim. Cyc u/f % Solids	70.1	70.7	0.9%
Prim. Cyc u/f tph		151	
Prim. Cyc u/f P_{80} (mm)	2.72	3.22	86%
Ball Mill Circuit			
Ball Mill Discharge tph		1069	
Ball Mill Discharge % solids		76.9	
Ball Mill Scats tph	2.76	3.41	24%
Trommel u/s tph		1066	
Secondary Cyc Feed % Sol	66.1	66.1	0.0%
Secondary Cyc Feed tph		1100	
Secondary Cyc Feed P_{80} (µm)	360	420	16.7%
Secondary Cyc Pressure (kPa)	152	150	-1.3%
Secondary Cyc u/f % Sol	78.3	78.0	-0.4%
Secondary Cyc u/f tph		918	
Secondary Cyc u/f P_{80} (µm)	460	488	6.1%
Secondary Cyc o/f % Sol	36.8	37.3	1.4%
Secondary Cyc o/f tph	182	182	0%
Secondary Cyc o/f P_{80} (µm)	87.6	86.3	-1.5%

Figure B.1: Module 1 Survey Summary

Module 1 Simulations — SAG Streams — As Surveyed

As Surveyed

	New Mill Feed	SAG Discharge	Scats	Crusher Product	Screen U/S	Load	Prim Cyc Feed	Prim Cyc U/F	PrCyU/F to BM	PrCyU/F to SAG
TPH Solids	165.00	252.06	87.06	87.06	165.00	45.87	165.00	150.67	150.67	0
Solids S.G.	2.70	2.70	2.70	2.70	2.70	2.70	2.70	2.70	2.7	2.7
TPH Water	3.81	60.03	0.05	0.05	84.97	2.05	179.32	62.36	62.36	0
% Solids	97.68	75.90	99.92	99.92	66.08	95.89	50.78	70.73	70.73	100
Pulp S.G.	2.61	1.92	2.70	2.70	1.71	2.52	1.47	1.80	1.8	0
V. Flowrate	72.33	173.39	24.90	24.90	163.49	18.27	247.84	116.16	118.16	0
% Passing 75micron	1.29	16.75	0.03	0.12	22.81	2.37	22.81	8.35	8.35	100
80% passes(mm)	91.88	16.38	41.52	33.08	2.80	84.43	2.80	3.21	3.21	0
SIZINGS										
175 mm										
152 mm	0.75	0.00	0.00	0.00	0.00	0.50	0.00	0.00		
106 mm	11.25	0.00	0.00	0.00	0.00	7.75	0.00	0.00		
75 mm	21.38	0.00	0.00	0.00	0.00	19.51	0.00	0.00		
53 mm	14.12	1.99	7.47	0.00	0.00	20.43	0.00	0.00		
37.5 mm	12.58	5.13	19.27	11.71	0.00	16.77	0.00	0.00		
26.5 mm	12.41	5.92	22.25	26.27	0.00	11.51	0.00	0.00		
19 mm	4.39	5.11	19.20	22.50	0.00	5.32	0.00	0.00		
13.2 mm	5.97	4.67	17.46	18.82	0.03	3.06	0.03	0.04		
9.5 mm	4.26	3.80	11.20	12.70	1.12	1.81	1.12	1.38		
6.7 mm	3.30	3.49	2.49	3.57	3.85	1.31	3.85	4.73		
4.75 mm	1.90	3.71	0.41	1.14	4.80	1.15	4.80	6.02		
3.35 mm	1.17	4.20	0.10	0.61	5.69	1.11	5.69	6.89		
2.36 mm	0.91	4.54	0.04	0.39	6.17	1.04	6.17	7.58		
1.7 mm	0.87	4.50	0.02	0.25	6.13	0.92	6.13	7.53		
1.18 mm	0.53	4.28	0.01	0.20	5.83	0.78	5.83	7.16		
0.85 mm	0.40	4.01	0.01	0.14	5.46	0.66	5.46	6.71		
0.6 mm	0.35	3.98	0.01	0.12	5.42	0.60	5.42	6.65		
0.425 mm	0.27	4.10	0.01	0.10	5.58	0.58	5.58	6.86		
0.3 mm	0.26	4.14	0.01	0.08	5.64	0.59	5.64	6.92		
0.212 mm	0.21	4.22	0.01	0.08	5.74	0.60	5.74	7.02		
0.15 mm	0.20	4.13	0.01	0.05	5.63	0.59	5.63	6.69		
0.106 mm	0.16	3.85	0.01	0.04	5.25	0.55	5.25	5.54		
0.075 mm	0.16	3.48	0.01	0.03	4.74	0.49	4.74	3.65		
0.053 mm	0.15	3.04	0.01	0.03	4.15	0.43	4.15	2.30		
0.038 mm	0.11	2.56	0.01	0.02	3.52	0.37	3.52	1.37		
-0.038 mm	1.03	11.12	0.02	0.08	15.15	1.58	15.15	4.69		

Figure B.2: Module 1 Primary Grinding Circuit Stream Simulation Data

Module : Simulations — SAG Units — As Surveyed

AUTOGENOUS MILL

Unit	SAG Mill				
Model	SAG Mill (Variable Rates)				
Controlled by:	Water Addition				
Required % solids	75.9 %	Solids flow	252.00 tph	% solids	75.9 %
New water addition	76.19 m3/h	Water flow	80.00 tph	Volume	173.39 m3/h
Number of mills in parallel As Surveyed	1				
New Feed F80 mm	91.9	Recycle Streams			
New Feed tph	185	Crusher Product			
Fixed Recycle (-20+4mm) tph	0	PrCyLiff to SAG			
Recycle (-20+4mm) tph	27.76				
Recycle ratio (-20+4mm)	0.1308				
Diameter (inside liners)	7.12 metres				
Belly length (inside liners)	3.53 metres				
Feed trunnion diameter	1.6 metres				
Feed end Cone Angle (flat=0)	15				
Discharge end Cone Angle (flat=0)	15				
Grate Size (xg)	26.3 mm				
Fine Size (xm)	0.5427 mm				
Grate Open Area fraction	0.129				
Pebble Port fraction of total Oper. Area	0.0829				
Pebble Port Size (xp)	74.11 mm				
Vesm re. radial pos. of the grate aperture	0.8035				
Ball Load	14.9 %ag vol.				
Calculated Load	110.02 tonnes				
Ball Top Size	125 mm				
SIZE 1 = Top Size ÷ √2	50 %				
SIZE 2 = Top Size ÷ 2	35 %				
SIZE 3 = Top Size ÷ 2√2	15 %				
SIZE 4 = Top Size ÷ 4	0 %				
Calc Sub Size					

Knot	Size	Const	Breakage Rate	Disch. Coeff.	0.150
				m1	0.2819
1	0.25	0.3365	1.79	m2	0.5
2	4	-1.15	3.66	Coarse Factor	1.2
3	16	0.0458	3.83	Max Mill Capacity	1152 (m3/h)
4	44.8	0.04445	2.63	User design tot. l	25 (%)
5	128	-2.96	2.7	Max design flow	1398.5 (m3/h)

Impact Breakage			
Parameter A	75.8	Attrition ta	0.13
Parameter B	0.45	Calculated Ecs	0.000086
Fraction critical speed	0.758	Tot. charge den.	4.15
Ball specific gravity	7.8	Void fill fr.	0.3258
Ball and "rock" charge porosity	0.4	No load power	363.56
Net power adjustment factor	1.26	Gross power	2862.99
%Volumetric total loss	22.96		

SAG MILL TROMMEL

Model	Efficiency Curve
	Discharge Scrn
Operating conditions	
% Water to Fines	99.94
Efficiency curve parameters	
Effcy. Curve Steep.	6.24
Efficiency Curve Dip	0.003663
Corrected D50	9.82

RECYCLE CRUSHER

Model	Anderson/Whiten
	Swing Crusher
Number of Crushers	1
Operating data	
Closed side set (mm)	15
Cr Feed Rate (TPH)	57.06
Cr Feed F80 (mm)	61.52
Cr Prod P80 (mm)	33.06
Classification equation data	67.08
Parameter K1	44.5
Parameter K2	49.81
Parameter K3	2.3
Reduction Parameter equation	
Parameter T10	12.18
Power equation	
Calc. Power (kW)	427.8
+ no load power	45

PRIMARY CYCLONE

Model	Nageswararao
	Primary Cyclone
Operating Variables	
Number of Cyclones	1
Cyclone Diameter (m)	0.66
Inlet Diameter (m)	0.215
Vortex Finder Dia(m)	0.28
Spigot (Apex) Dia(m)	0.14
Cylinder Length (m)	0.448
Cone Angle (degrees)	20
Model Constants	
KD0 (D50)	0.000081
KQ0 (Capacity)	378.15
KV1 (Volume Split)	10.90
KW1 (Water Split)	16.56
alpha (Effcy. Curve)	1.61
beta (Effcy. Curve)	1.02
Calculated Data	
Water split to O/F %	65.23
Corrected D50 (mm)	0.06229
Operat. Press. (Kpa)	57.28

Figure B.3: Module 1 Primary Grinding Circuit Equipment Simulation Data

Module 1 Simulations — Ball Mill Streams — As Surveyed

BALL MILL SIZINGS

	Prim Cyc O/F	Ball Mill Disch	BM Trommel U	BM Scats	Sec Cyc Fee	Sec Cyc U	Flotation Feed
TPH Solids	34.33	1068.50	1065.10	3.41	1099.43	917.91	181.51
Solids S.G.	2.70	2.70	2.70	2.70	2.70	2.70	2.70
TPH Water	116.96	321.21	336.19	0.02	563.85	258.85	305.00
% Solids	22.69	76.89	76.01	99.30	66.10	78.00	37.31
Pulp S.G.	1.17	1.94	1.92	2.67	1.71	1.97	1.31
V. Flowrate	129.68	716.95	730.67	1.29	971.05	598.82	372.23
% Passing 75micron	86.24	22.84	22.91	0.00	24.89	14.91	75.33
80% passes(mm)	0.06	0.44	0.43	10.86	0.42	0.49	0.09
SIZINGS							
175 mm							
152 mm	0.00	0.00	0.00	0.00	0.00	0.00	0.00
106 mm	0.00	0.00	0.00	0.00	0.00	0.00	0.00
75 mm	0.00	0.00	0.00	0.00	0.00	0.00	0.00
53 mm	0.00	0.00	0.00	0.00	0.00	0.00	0.00
37.5 mm	0.00	0.00	0.00	0.00	0.00	0.00	0.00
26.5 mm	0.00	0.00	0.00	0.00	0.00	0.00	0.00
19 mm	0.00	0.00	0.00	0.01	0.00	0.00	0.00
13.2 mm	0.00	0.01	0.00	1.60	0.00	0.00	0.00
9.5 mm	0.00	0.32	0.19	41.55	0.18	0.22	0.00
6.7 mm	0.00	1.28	1.13	49.01	1.09	1.31	0.00
4.75 mm	0.00	1.17	1.15	7.84	1.11	1.33	0.00
3.35 mm	0.00	0.94	0.94	0.00	0.91	1.09	0.00
2.36 mm	0.00	0.85	0.86	0.00	0.83	0.99	0.00
1.7 mm	0.00	0.97	0.98	0.00	0.95	1.13	0.00
1.18 mm	0.00	1.38	1.39	0.00	1.35	1.61	0.00
0.85 mm	0.00	2.29	2.30	0.00	2.23	2.67	0.00
0.6 mm	0.00	4.09	4.10	0.00	3.97	4.76	0.00
0.425 mm	0.00	7.26	7.28	0.00	7.05	8.46	0.00
0.3 mm	0.00	11.30	11.34	0.00	10.99	13.15	0.06
0.212 mm	0.12	14.73	14.78	0.00	14.32	16.98	0.87
0.15 mm	1.02	14.19	14.24	0.00	13.83	15.72	4.24
0.106 mm	3.96	9.98	10.02	0.00	9.83	10.06	8.68
0.075 mm	8.65	6.39	6.41	0.00	5.46	5.62	10.83
0.053 mm	12.24	4.33	4.34	0.00	4.59	3.34	10.88
0.038 mm	12.96	3.20	3.21	0.00	3.51	2.24	9.94
-0.038 mm	61.04	15.31	15.36	0.00	16.79	9.33	54.51

Figure B.4: Module 1 Secondary Grinding Circuit Stream Simulation Data

Module 1 Simulations — Ball Mill Units — As Surveyed

BALL MILL		HYDROCYCLONE		SINGLE DECK SCREEN	
Model	Perfect Mixing	Model:	Nageswararao	Model:	
	Ball Mill		Sec Cyclone		
Number of Ball Mills	1	Operating Variables		Operating conditions	
		Number of Cyclones	7	% Water to Fines	
Data for Simulated Mill		Cyclone Diameter (m)	0.362		
Int. Mill Dia. (m)	4.8	Inlet Diameter (m)	0.103	Efficiency curve parameters	
Int. Mill Length (m)	7.6	Vortex Finder Dia(m)	0.14	Effcy. Curve Sharp.	
Fr. Critical Speed	0.751	Spigot (Apex) Dia(m)	0.09	Efficiency Curve Dip	
Load Fraction	0.336	Cylinder Length (m)	0.243	Corrected D50	
Ore Work Index	20	Cone Angle (degrees)	10		
Data from Original Mill		Model Constants			
Int. Mill Dia. (m)	4.8	KD0 (D50)	0.000046		
Fr. Critical Speed	0.751	KQ0 (Capacity)	467.71		
Load Fraction	0.336	KV1 (Volume Split)	12.06		
Ore Work Index	20	KW1 (Water Split)	18.89		
		alpha (Effcy. Curve)	1.48		
Rate/discharge function data		beta (Effcy. Curve)	0.5259		
Active spline knots	4				
Knot #1 Size (mm)	0.09	Calculated Data			
Ln R/D* meas	0.827	Water split to O/F %	64.09		
Ln R/D* calc	0.827	Corrected D50 (mm)	0.09179		
Knot #2 Size (mm)	0.45	Operat. Press. (Kpa)	150.17		
Ln R/D* meas	1.55				
Ln R/D* calc	1.55	SINGLE DECK SCREEN			
Knot #3 Size (mm)	2.5	Model:	Efficiency Curve		
Ln R/D* meas	3.41				
Ln R/D* calc	3.41		Ball Mill Trom!		
Knot #4 Size (mm)	12				
Ln R/D* meas	1	Operating conditions			
Ln R/D* calc	1	% Water to Fines	99.99		
Ball size scaling		Efficiency curve parameters			
Ball top size (sim)	58.91	Effcy. Curve Sharp.	4.68		
Breakage rate fact.	0.00044	Efficiency Curve Dip	0.1269		
Ball top size (org)	58.91	Corrected D50	12.13		

Figure B.5: Module 1 Secondary Grinding Circuit Equipment Simulation Data

Appendix C

NPM Grinding Circuit Data: Survey Data, Simulation Model and Inferential Model Results

Table C.1: Reference Data: 1° Circuit - SAG mill

Stream Properties	SMFF	OSCP	SMTF	SMRC	SMDC
tph_s	185.0	67.1	252.1	45.7	252.1
tph_l	3.8	0.1	80.0	2.1	80.0
tph_p	188.8	67.1	332.1	47.7	332.1
%s w/w	98.0	99.9	75.9	95.7	75.9
%l w/w	2.0	0.1	24.1	4.3	24.1
m3ph_s	69.8	25.3	95.1	17.2	95.1
m3ph_l	3.8	0.1	80.0	2.1	80.0
m3ph_p	73.6	25.4	175.2	19.3	175.2
%s v/v	94.8	99.8	54.3	89.3	54.3
%l v/v	5.2	0.2	45.7	10.7	45.7
SGp	2.56	2.65	1.90	2.47	1.90
P_{80}	94.5	34.0	84.0	87.3	16.7
Power				2863	(kW)
Pressure					
Size (mm)	wt rtd (%)	wt rtd (%)	wt rtd (%)	wt rtd (%)	wt rtd (%)
181	0	0	0	0	0
152	0.8	0	0.6	0.5	0
106	11.4	0	8.3	7.8	0
75.0	21.4	0	15.7	19.5	0
53.0	14.1	0	10.4	20.4	2.0
37.5	12.6	11.7	12.3	16.8	5.1
26.5	12.4	26.3	16.1	11.5	5.9
19.0	4.4	22.5	9.2	5.3	5.1
13.2	7.0	19.9	10.4	3.0	4.7
9.5	4.3	12.7	6.5	1.8	3.8
6.7	3.3	3.6	3.4	1.3	3.5
4.75	1.9	1.1	1.7	1.2	3.7
3.35	1.2	0.6	1.0	1.1	4.2
2.36	0.9	0.4	0.8	1.0	4.5
1.70	0.7	0.25	0.6	0.9	4.5
1.18	0.53	0.2	0.4	0.8	4.3
0.850	0.4	0.1	0.3	0.7	4.0
0.600	0.4	0.1	0.3	0.6	4.0
0.425	0.3	0.1	0.2	0.6	4.1
0.300	0.3	0.1	0.2	0.6	4.1
0.212	0.2	0.1	0.2	0.6	4.2
0.150	0.2	0.1	0.2	0.6	4.1
0.106	0.2	0.0	0.1	0.6	3.9
0.075	0.2	0.0	0.1	0.5	3.5
0.053	0.2	0.0	0.1	0.4	3.0
0.038	0.1	0.0	0.1	0.4	2.6
0.001	1.0	0.1	0.8	1.6	11.1

Table C.2: Reference Data: 1^o Circuit - Screen/Crusher/Cyclones

Stream Properties	SMDC	OSCF	OSCP	PCFD	PCUF	PCOF
tph_s	252.1	67.1	67.1	185.0	150.7	34.3
tph_l	80.0	0.1	0.1	179.3	62.4	117.0
tph_p	332.1	67.1	67.1	364.3	213.0	151.3
%s w/w	75.9	99.9	99.9	50.8	70.7	22.7
%l w/w	24.1	0.1	0.1	49.2	29.3	77.3
m3ph_s	95.1	25.3	25.3	69.8	56.9	13.0
m3ph_l	80.0	0.1	0.1	179.3	62.4	117.0
m3ph_p	175.2	25.4	25.4	249.1	119.2	129.9
%s v/v	54.3	99.8	99.8	28.0	47.7	10.0
%l v/v	45.7	0.2	0.2	72.0	52.3	90.0
SGp	1.90	2.65	2.65	1.46	1.79	1.16
P_{80}	16.7	42.9	34.0	2.6	3.2	0.1
Power			43	(kW)		
Pressure				57.3	(kPa)	
Size (mm)	wt rtd (%)	wt rtd (%)	wt rtd (%)	wt rtd (%)	wt rtd (%)	wt rtd (%)
181	0	0	0	0	0	0
152	0	0	0	0	0	0
106	0	0	0	0	0	0
75.0	0	0	0	0	0	0
53.0	2.0	7.5	0	0	0	0
37.5	5.1	19.3	11.7	0	0	0
26.5	5.9	22.2	26.3	0	0	0
19.0	5.1	19.2	22.5	0	0	0
13.2	4.7	17.5	19.9	0.0	0.0	0
9.50	3.8	11.2	12.7	1.1	1.4	0
6.70	3.5	2.5	3.6	3.8	4.7	0
4.75	3.7	0.4	1.1	4.9	6.0	0
3.35	4.2	0.1	0.6	5.7	7.0	0
2.36	4.5	0.0	0.4	6.2	7.6	0
1.70	4.5	0.0	0.2	6.1	7.5	0
1.18	4.3	0.0	0.2	5.8	7.2	0
0.850	4.0	0.0	0.1	5.5	6.7	0
0.600	3.9	0.0	0.1	5.4	6.6	0
0.425	4.1	0.0	0.1	5.6	6.9	0
0.300	4.1	0.0	0.1	5.6	6.9	0
0.212	4.2	0.0	0.1	5.7	7.0	0.1
0.150	4.1	0.0	0.0	5.6	6.7	1.0
0.106	3.9	0.0	0.0	5.2	5.5	4.0
0.075	3.5	0.0	0.0	4.7	3.8	8.7
0.053	3.0	0.0	0.0	4.2	2.3	12.2
0.038	2.6	0.0	0.0	3.5	1.4	13.0
0.001	11.1	0.0	0.1	15.2	4.7	61.0

Table C.3: Reference Data: 2º Circuit - Ball mill/Screen

Stream Properties	PCUF	SCUF	BMFD	BMDC	BSOS	BSUS
tph_s	150.7	918	1067	1068	3.4	1065
tph_l	62.4	258.9	321.2	321.1	0.0	336.2
tph_p	213.0	1177	1390	1390	3.4	1401
%s w/w	70.7	78.0	76.9	76.9	99.3	76.0
%l w/w	29.3	22.0	23.1	23.1	0.7	24.0
m3ph_s	56.9	346.4	403.2	403.2	1.3	401.9
m3ph_l	62.4	258.9	321.2	321.1	0.0	336.2
m3ph_p	119.2	605.3	724.5	724.4	1.3	738.1
%s v/v	47.7	57.2	55.7	55.7	98.2	54.5
%l v/v	52.3	42.8	44.3	44.3	1.8	45.5
SGp	1.79	1.94	1.92	1.92	2.62	1.90
P_{80}	3.2	0.5	0.6	0.4	11.6	0.4
Power				≈ 2850	(kW)	
Pressure						
Size (mm)	wt rtd (%)	wt rtd (%)	wt rtd (%)	wt rtd (%)	wt rtd (%)	wt rtd (%)
181	0	0	0	0	0	0
152	0	0	0	0	0	0
106	0	0	0	0	0	0
75.0	0	0	0	0	0	0
53.0	0	0	0	0	0	0
37.5	0	0	0	0	0	0
26.5	0	0	0	0	0	0
19.0	0	0	0	0	0.0100	0
13.2	0.0	0	0.0	0.0	1.6	0
9.50	1.4	0.2	0.4	0.3	41.5	0.2
6.70	4.7	1.3	1.8	1.3	49.0	1.1
4.75	6.0	1.3	2.0	1.2	7.8	1.1
3.35	7.0	1.1	1.9	0.9	0	0.9
2.36	7.6	1.0	1.9	0.8	0	0.9
1.70	7.5	1.1	2.0	1.0	0	1.0
1.18	7.2	1.6	2.4	1.4	0	1.4
0.850	6.7	2.7	3.2	2.3	0	2.3
0.600	6.6	4.8	5.0	4.1	0	4.1
0.425	6.9	8.4	8.2	7.3	0	7.3
0.300	6.9	13.2	12.3	11.3	0	11.3
0.212	7.0	17.0	15.6	14.7	0	14.8
0.150	6.7	15.7	14.4	14.2	0	14.2
0.106	5.5	10.1	9.4	10.0	0	10.0
0.075	3.8	5.6	5.4	6.4	0	6.4
0.053	2.3	3.3	3.2	4.3	0	4.3
0.038	1.4	2.2	2.1	3.2	0	3.2
0.001	4.7	9.3	8.7	15.3	0	15.4

Table C.4: Reference Data: 2^o Circuit - Cyclones

Stream Properties	BSUS	PCOF	SCFD	SCUF	SCOF
tph_s	1065	34.3	1099	918	181.5
tph_l	336.2	117.0	564	258.9	305.0
tph_p	1401	151.3	1663	1177	486.5
%s w/w	76.0	22.7	66.1	78.0	37.3
%l w/w	24.0	77.3	33.9	22.0	62.7
m3ph_s	401.9	13.0	414.9	346.4	68.5
m3ph_l	336.2	117.0	564	258.9	305.0
m3ph_p	738	129.9	979	605	373.5
%s v/v	54.5	10.0	42.4	57.2	18.3
%l v/v	45.5	90.0	57.6	42.8	81.7
SGp	1.90	1.16	1.70	1.94	1.30
P_{80}	0.4	0.1	0.4	0.5	0.1
Power					
Pressure			150	(kPa)	
Size (mm)	wt rtd (%)	wt rtd (%)	wt rtd (%)	wt rtd (%)	wt rtd (%)
181	0	0	0	0	0
152	0	0	0	0	0
106	0	0	0	0	0
75.0	0	0	0	0	0
53.0	0	0	0	0	0
37.5	0	0	0	0	0
26.5	0	0	0	0	0
19.0	0	0	0	0	0
13.2	0	0	0	0	0
9.50	0.2	0	0.2	0.2	0
6.70	1.1	0	1.1	1.3	0
4.75	1.1	0	1.1	1.3	0
3.35	0.9	0	0.9	1.1	0
2.36	0.9	0	0.8	1.0	0
1.70	1.0	0	0.9	1.1	0
1.18	1.4	0	1.3	1.6	0
0.850	2.3	0	2.2	2.7	0
0.600	4.1	0	4.0	4.8	0
0.425	7.3	0	7.0	8.4	0
0.300	11.3	0	11.0	13.2	0.1
0.212	14.8	0.1	14.3	17.0	0.9
0.150	14.2	1.0	13.8	15.7	4.2
0.106	10.0	4.0	9.8	10.1	8.7
0.075	6.4	8.7	6.5	5.6	10.8
0.053	4.3	12.2	4.6	3.3	10.9
0.038	3.2	13.0	3.5	2.2	9.9
0.001	15.4	61.0	16.8	9.3	54.5

Table C.5: Simulation Model: 1º Circuit - SAG mill

Stream Properties	SMFF	OSCP	SMTF	SMRC	SMDC
tph_s	185.0	67.1	252.2	45.7	252.1
tph_l	3.8	0.1	80.1	2.1	80.0
tph_p	188.8	67.2	332.3	47.7	332.1
%s w/w	98.0	99.9	75.9	95.7	75.9
%l w/w	2.0	0.1	24.1	4.3	24.1
m3ph_s	69.8	25.3	95.2	17.2	95.1
m3ph_l	3.8	0.1	80.1	2.1	80.0
m3ph_p	73.6	25.4	175.2	19.3	175.1
%s v/v	94.8	99.8	54.3	89.3	54.3
%l v/v	5.2	0.2	45.7	10.7	45.7
SGp	2.56	2.65	1.90	2.47	1.90
P_{80}	94.5	27.2	84.0	87.3	16.4
Power				2800	(kW)
Pressure					
Size (mm)	wt rtd (%)	wt rtd (%)	wt rtd (%)	wt rtd (%)	wt rtd (%)
181	0	0	0	0	0
152	0.8	0	0.6	0.5	0
106	11.4	0	8.3	7.8	0
75.0	21.4	0	15.7	19.5	0
53.0	14.1	0	10.4	20.4	0.6
37.5	12.6	3.4	10.1	16.8	0.8
26.5	12.4	17.8	13.8	11.5	4.7
19.0	4.4	37.2	13.1	5.3	9.8
13.2	7.0	31.3	13.4	3.0	9.1
9.50	4.3	9.6	5.7	1.8	6.7
6.70	3.3	0.2	2.5	1.3	5.5
4.75	1.9	0.1	1.4	1.2	5.3
3.35	1.2	0.1	0.9	1.1	5.4
2.36	0.9	0.1	0.7	1.0	5.3
1.70	0.7	0.0	0.5	0.9	4.8
1.18	0.5	0.0	0.4	0.8	4.1
0.850	0.4	0.0	0.3	0.7	3.5
0.600	0.4	0.0	0.3	0.6	3.2
0.425	0.3	0.0	0.2	0.6	3.1
0.300	0.3	0.0	0.2	0.6	3.2
0.212	0.2	0.0	0.2	0.6	3.2
0.150	0.2	0.0	0.2	0.6	3.2
0.106	0.2	0.0	0.1	0.6	3.0
0.075	0.2	0.0	0.1	0.5	2.6
0.053	0.2	0.0	0.1	0.4	2.3
0.038	0.1	0.0	0.1	0.4	2.0
0.001	1.0	0.0	0.8	1.6	8.5

Table C.6: Simulation Model: 1^o Circuit - Screen/Crusher/Cyclones

Stream Properties	SMDC	OSCF	OSCP	PCFD	PCUF	PCOF
tph_s	252.1	67.1240	67.1	185.0	150.7	34.3
tph_l	80.0	0.1	0.1	179.2	62.3	116.9
tph_p	332.1	67.2	67.2	364.2	213.0	151.1
%s w/w	75.9	99.9	99.9	50.8	70.7	22.7
%l w/w	24.1	0.1	0.1	49.2	29.3	77.3
m3ph_s	95.1	25.3	25.3	69.8	56.9	12.9
m3ph_l	80.0	0.1	0.1	179.2	62.3	116.9
m3ph_p	175.1	25.4	25.4	249.0	119.2	129.8
%s v/v	54.3	99.8	99.8	28.0	47.7	10.0
%l v/v	45.7	0.2	0.2	72.0	52.3	90.0
SGp	1.90	2.65	2.65	1.46	1.79	1.16
P_{80}	16.4	28.2	27.2	5.2	6.2	0.1
Power			41	(kW)		
Pressure				57.1	(kPa)	
Size (mm)	wt rtd (%)	wt rtd (%)	wt rtd (%)	wt rtd (%)	wt rtd (%)	wt rtd (%)
181	0	0	0	0	0	0
152	0	0	0	0	0	0
106	0	0	0	0	0	0
75.0	0	0	0	0	0	0
53.0	0.6	2.1	0	0	0	0
37.5	0.8	3.0	3.4	0	0	0
26.5	4.7	17.6	17.8	0	0	0
19.0	9.8	36.9	37.3	0.0	0.0	0
13.2	9.1	31.0	31.3	1.1	1.3	0
9.50	6.7	9.4	9.6	5.7	7.0	0
6.70	5.5	0	0.2	7.5	9.3	0
4.75	5.3	0	0.1	7.2	8.8	0
3.35	5.4	0	0.1	7.4	9.0	0
2.36	5.3	0	0.1	7.2	8.8	0
1.70	4.8	0	0.0	6.5	8.0	0
1.18	4.1	0	0.0	5.6	6.9	0
0.850	3.5	0	0.0	4.8	5.9	0
0.600	3.2	0	0.0	4.4	5.4	0
0.425	3.1	0	0.0	4.3	5.2	0
0.300	3.2	0	0.0	4.3	5.3	0
0.212	3.2	0	0.0	4.4	5.4	0
0.150	3.2	0	0.0	4.3	5.3	0.1
0.106	3.0	0	0.0	4.1	3.2	7.8
0.075	2.6	0	0.0	3.6	0	19.5
0.053	2.3	0	0.0	3.2	0	17.1
0.038	2.0	0	0.0	2.7	0.1	14.1
0.001	8.5	0.0	0.0	11.6	4.9	41.5

Table C.7: Simulation Model: 2° Circuit - Ball mill/Screen

Stream Properties	PCUF	SCUF	BMFD	BMDC	BSOS	BSUS
tph_s	150.7	919	1069	1069	3.3	1066
tph_l	62.3	374.6	436.9	436.9	0.0	451.9
tph_p	213.0	1294	1506	1506	3.3	1518
%s w/w	70.7	71.0	71.0	71.0	99.0	70.2
%l w/w	29.3	29.0	29.0	29.0	1.0	29.8
m3ph_s	56.9	346.8	403.6	403.6	1.2	402.3
m3ph_l	62.3	374.6	436.9	436.9	0.0	451.9
m3ph_p	119.2	721	840	840	1.3	854
%s v/v	47.7	48.1	48.0	48.0	97.5	47.1
%l v/v	52.3	51.9	52.0	52.0	2.5	52.9
SGp	1.79	1.95	1.92	1.92	2.62	1.90
P_{80}	6.2	0.3	0.4	0.3	17.1	0.3
Power				2994	(kW)	
Pressure						
Size (mm)	wt rtd (%)	wt rtd (%)	wt rtd (%)	wt rtd (%)	wt rtd (%)	wt rtd (%)
181	0	0	0	0	0	0
152	0	0	0	0	0	0
106	0	0	0	0	0	0
75.0	0	0	0	0	0	0
53.0	0	0	0	0	0	0
37.5	0	0	0	0	0	0
26.5	0	0	0	0	0	0
19.0	0.0	0	0.0	0.0	1.9	0
13.2	1.3	0.0	0.2	0.2	56.2	0.0
9.50	7.0	0.6	1.5	0.6	41.9	0.5
6.70	9.3	0.5	1.8	0.5	0	0.5
4.75	8.8	0.4	1.6	0.3	0	0.3
3.35	9.0	0.2	1.5	0.2	0	0.2
2.36	8.8	0.2	1.4	0.2	0	0.2
1.70	8.0	0.3	1.4	0.3	0	0.3
1.18	6.9	0.4	1.3	0.4	0	0.4
0.850	5.9	0.6	1.3	0.5	0	0.5
0.600	5.4	1.1	1.7	1.0	0	1.0
0.425	5.2	4.0	4.2	3.4	0	3.4
0.300	5.3	7.9	7.5	6.8	0	6.8
0.212	5.4	57.1	49.8	49.1	0	49.2
0.150	5.3	13.1	12.0	13.7	0	13.7
0.106	3.2	0.6	0.9	2.6	0	2.7
0.075	0	0.8	0.7	2.1	0	2.1
0.053	0	1.0	0.9	2.0	0	2.0
0.038	0.1	1.1	1.0	1.9	0	1.9
0.001	4.9	9.9	9.2	14.2	0	14.3

Table C.8: Simulation Model: 2^o Circuit - Cyclones

Stream Properties	BSUS	PCOF	SCFD	SCUF	SCOF
tph_s	1066	34.3	1100	919	181.6
tph_l	451.9	116.9	680	374.6	304.8
tph_p	1518	151.1	1780	1294	486.4
%s w/w	70.2	22.7	61.8	71.0	37.3
%l w/w	29.8	77.3	38.2	29.0	62.7
m3ph_s	402.3	12.9	415.3	346.8	68.5
m3ph_l	451.9	116.9	680	374.6	304.8
m3ph_p	854	129.8	1095	721	373.3
%s v/v	47.1	10.0	37.9	48.1	18.4
%l v/v	52.9	90.0	62.1	51.9	81.6
SGp	1.90	1.16	1.70	1.95	1.30
P_{80}	0.3	0.1	0.3	0.3	0.1
Power					
Pressure			151.2	(kPa)	
Size (mm)	wt rtd (%)	wt rtd (%)	wt rtd (%)	wt rtd (%)	wt rtd (%)
181	0	0	0	0	0
152	0	0	0	0	0
106	0	0	0	0	0
75.0	0	0	0	0	0
53.0	0	0	0	0	0
37.5	0	0	0	0	0
26.5	0	0	0	0	0
19.0	0	0	0	0	0
13.2	0.0	0	0.0	0.0	0
9.50	0.5	0	0.5	0.6	0
6.70	0.5	0	0.5	0.5	0
4.75	0.3	0	0.3	0.4	0
3.35	0.2	0	0.2	0.2	0
2.36	0.2	0	0.2	0.2	0
1.70	0.3	0	0.3	0.3	0
1.18	0.4	0	0.3	0.4	0
0.850	0.5	0	0.5	0.6	0
0.600	1.0	0	1.0	1.1	0
0.425	3.4	0	3.3	4.0	0
0.300	6.8	0	6.6	7.9	0
0.212	49.2	0	47.7	57.1	0.1
0.150	13.7	0.1	13.3	13.1	14.1
0.106	2.7	7.8	2.8	0.6	14.1
0.075	2.1	19.5	2.6	0.8	11.8
0.053	2.0	17.1	2.5	1.0	10.0
0.038	1.9	14.1	2.3	1.1	8.4
0.001	14.2	41.5	15.1	9.9	41.4

Table C.9: Inferential Model: 1° Circuit - SAG mill

Stream Properties	SMFF	OSCP	SMTF	SMRC	SMDC
tph_s	184.9	67.1	252.1	48.0	252.1
tph_l	3.7	0.1	79.9	2.7	79.9
tph_p	188.5	67.2	332.0	50.7	332.0
%s w/w	98.1	99.9	75.9	94.7	75.9
%l w/w	1.9	0.1	24.1	5.3	24.1
m3ph_s	69.8	25.3	95.1	18.1	95.1
m3ph_l	3.7	0.1	79.9	2.7	79.9
m3ph_p	73.4	25.4	175.0	20.8	175.1
%s v/v	95.0	99.7	54.3	87.2	54.3
%l v/v	5.0	0.3	45.7	12.8	45.7
SGp	2.57	2.65	1.90	2.45	1.90
P_{80}	70.7	37.7	61.2	144.3	16.9
Power				2800	(kW)
Pressure					
Size (mm)	wt rtd (%)	wt rtd (%)	wt rtd (%)	wt rtd (%)	wt rtd (%)
180	0	0	0	0	0
152	1.2	0	0.9	18.8	0
106	4.8	0	3.5	7.3	0
75.0	10.8	0	7.9	7.6	0
53.0	16.4	0	12.2	7.8	1.4
37.5	14.2	20.3	14.4	7.5	3.7
26.5	7.2	24.4	14.2	7.1	5.7
19.0	6.7	20.1	11.8	6.3	6.4
13.2	8.7	14.8	10.3	6.2	7.5
9.50	7.5	8.3	7.0	4.9	7.0
6.70	6.5	5.1	5.5	4.5	7.3
4.75	4.8	2.9	3.8	3.8	6.9
3.35	3.5	1.6	2.7	3.2	6.5
2.36	2.5	0.9	1.9	2.7	6.0
1.70	1.6	0.5	1.2	2.1	5.1
1.18	1.2	0.3	0.9	2.0	5.1
0.850	0.7	0.2	0.5	1.4	4.1
0.600	0.5	0.2	0.4	1.3	3.9
0.425	0.4	0.1	0.3	1.0	3.4
0.300	0.2	0.1	0.2	0.9	3.1
0.212	0.2	0.1	0.1	0.7	2.7
0.150	0.1	0.0	0.1	0.6	2.3
0.106	0.1	0.0	0.1	0.5	2.0
0.075	0.0	0.0	0.0	0.4	1.7
0.053	0.0	0.0	0.0	0.3	1.4
0.038	0.0	0.0	0.0	0.2	1.2
0.001	0.0	0.0	0.0	1.0	5.5

Table C.10: Inferential Model: 1° Circuit - Screen/Crusher/Cyclones

Stream Properties	SMDC	OSCF	OSCP	PCFD	PCUF	PCOF
tph_s	252.1	67.1	67.1	185.0	146.1	38.9
tph_l	79.9	0.1	0.1	179.2	62.3218	116.9
tph_p	332.0	67.2	67.2	364.2	208.4	155.7
%s w/w	75.9	99.9	99.9	50.8	70.1	25.0
%l w/w	24.1	0.1	0.1	49.2	29.9	75.0
m3ph_s	95.1	25.3	25.3	69.8	55.1	14.7
m3ph_l	79.9	0.1	0.1	179.2	62.3	116.9
m3ph_p	175.1	25.4	25.4	249.0	117.5	131.5
%s v/v	54.3	99.7	99.7	28.0	46.9	11.2
%l v/v	45.7	0.3	0.3	72.0	53.1	88.8
SGp	1.90	2.65	2.65	1.46	1.77	1.18
P_{80}	16.9	43.5	37.7	2.6	3.3	0.1
Power			42.1	(kW)		
Pressure				57.1	(kPa)	
Size (mm)	wt rtd (%)	wt rtd (%)	wt rtd (%)	wt rtd (%)	wt rtd (%)	wt rtd (%)
181	0	0	0	0	0	0
152	0	0.0000	0	0.0	0.0	0
106	0	0.0	0	0.0	0.0	0
75.0	0	0.9	0	0.0	0.0	0
53.0	1.4177	7.5405	0	0.0215	0.0272	0
37.5	3.7	18.8	20.3	0.1	0.1	0
26.5	5.7	23.3	24.4	0.2	0.3	0
19.0	6.4	18.7	20.1	0.5	0.7	0
13.2	7.5	13.7	14.8	1.1	1.4	0
9.50	7.0	7.4	8.3	1.8	2.2	0
6.70	7.3	4.5	5.1	2.8	3.6	0
4.75	6.9	2.4	2.9	3.8	4.8	0
3.35	6.5	1.3	1.6	4.9	6.2	0
2.36	6.0	0.7	0.9	5.8	7.4	0
1.70	5.1	0.3	0.5	6.1	7.7	0
1.18	5.2	0.2	0.3	7.2	9.1	0
0.850	4.1	0.1	0.2	6.6	8.3	0
0.600	3.9	0.1	0.2	6.9	8.7	0
0.425	3.4	0.0	0.1	6.5	8.3	0
0.300	3.1	0.0	0.1	6.2	7.8	0
0.212	2.7	0.0	0.1	5.6	7.1	0
0.150	2.3	0.0	0.0	5.1	6.4	0.1
0.106	2.0	0.0	0.0	4.5	3.7	7.6
0.075	1.7	0.0	0.0	4.0	0.0	18.8
0.053	1.4	0.0	0.0	3.5	0.0	16.5
0.038	1.2	0.0	0.0	2.9	0.2	13.1
0.001	5.5	0.0	0.0	14.0	6.0	43.9

Table C.11: Inferential Model: 2^o Circuit - Ball mill/Screen

Stream Properties	PCUF	SCUF	BMFD	BMDC	BSOS	BSUS
tph_s	146.1	905	1051	1051	3.9	1047
tph_l	62.3	374.3	436.6	436.6	0.0	451.6
tph_p	208.4	1280	1488	1488	4.0	1499
%s w/w	70.1	70.7	70.7	70.7	99.2	69.9
%l w/w	29.9	29.3	29.3	29.3	0.8	30.1
m3ph_s	55.1	341.6	396.7	396.7	1.5	395.2
m3ph_l	62.3	374.3	436.6	436.6	0.0	451.6
m3ph_p	117.5	715.9	833.3	833.3	1.5	846.8
%s v/v	46.9	47.7	47.6	47.6	97.9	46.7
%l v/v	53.1	52.3	52.4	52.4	2.1	53.3
SGp	1.77	1.94	1.91	1.91	2.62	1.89
P_{80}	3.27	0.29	0.36	0.29	25.21	0.29
Power				2993	(kW)	
Pressure						
Size (mm)	wt rtd (%)	wt rtd (%)	wt rtd (%)	wt rtd (%)	wt rtd (%)	wt rtd (%)
181	0	0	0	0	0	0
152	0.0	0	0.0	0.0	0.0	0
106	0.0	0	0.0	0.0	0.0	0
75.0	0.0	0	0.0	0.0	0.2	0
53.0	0.0	0	0.0	0.0	1.0	0
37.5	0.1	0	0.0	0.0	3.7	0
26.5	0.3	0	0.0	0.0	10.9	0
19.0	0.6	0	0.1	0.1	24.2	0
13.2	1.4	0.0	0.2	0.2	49.2	0.0
9.5	2.2	0.2	0.5	0.2	10.8	0.2
6.70	3.6	0.2	0.7	0.2	0	0.2
4.75	4.8	0.2	0.8	0.2	0	0.2
3.35	6.2	0.1	0	0.1	0	0.1
2.36	7.4	0.2	1.2	0.1	0	0.1
1.70	7.7	0.2	1.3	0.2	0	0.2
1.18	9.1	0.4	1.6	0.3	0	0.3
0.850	8.3	0.6	1.6	0.5	0	0.5
0.600	8.7	1.2	2.2	1.0	0	1.0
0.425	8.3	4.1	4.7	3.5	0	3.6
0.300	7.8	8.1	8.1	7.0	0	7.0
0.212	7.1	57.7	50.7	49.7	0	49.9
0.150	6.4	13.2	12.2	13.8	0	13.8
0.106	3.7	0.6	1.0	2.6	0	2.6
0.075	0.0	0.8	0.7	2.0	0	2.0
0.053	0.0	1.0	0.9	2.0	0	2.0
0.038	0.1	1.1	1.0	1.9	0	1.9
0.001	6.0	10.2	9.6	14.4	0	14.5

Table C.12: Inferential Model: 2^o Circuit - Cyclones

Stream Properties	BSUS	PCOF	SCFD	SCUF	SCOF
tph_s	1047	38.9	1086	905	181.0
tph_l	451.6	116.9	679	374.3	304.8
tph_p	1499	155.7	1765	1280	485.8
%s w/w	69.9	25.0	61.5	70.7	37.3
%l w/w	30.1	75.0	38.5	29.3	62.7
m3ph_s	0.4	0.0	0.4	0.3	0.1
m3ph_l	451.6	116.9	679	374.3	304.8
m3ph_p	847	131.5	1089	716	373.1
%s v/v	46.7	11.2	37.6	47.7	18.3
%l v/v	53.3	88.8	62.4	52.3	81.7
SGp	1.89	1.18	1.69	1.94	1.30
P_{80}	0.3	0.1	0.3	0.3	0.1
Power					
Pressure			149.3	(kPa)	
Size (mm)	wt rtd (%)	wt rtd (%)	wt rtd (%)	wt rtd (%)	wt rtd (%)
181	0	0	0	0	0
152	0	0	0	0	0
106	0	0	0	0	0
75.0	0	0	0	0	0
53.0	0	0	0	0	0
37.5	0	0	0	0	0
26.5	0	0	0	0	0
19.0	0	0	0	0	0
13.2	0.0	0	0.0	0.0	0
9.50	0.2	0	0.2	0.2	0
6.70	0.2	0	0.2	0.2	0
4.75	0.2	0	0.2	0.2	0
3.35	0.1	0	0.1	0.1	0
2.36	0.1	0	0.1	0.2	0
1.70	0.2	0	0.2	0.2	0
1.18	0.3	0	0.3	0.4	0
0.850	0.5	0	0.5	0.6	0
0.600	1.0	0	1.0	1.2	0
0.425	3.6	0	3.4	4.1	0
0.300	7.0	0	6.7	8.1	0
0.212	49.9	0	48.1	57.7	0.1
0.150	13.8	0.1	13.3	13.2	14.0
0.106	2.6	7.6	2.8	0.6	14.0
0.075	2.0	18.8	2.6	0.8	11.7
0.053	2.0	16.5	2.5	1.0	9.8
0.038	1.9	13.1	2.3	1.1	8.2
0.001	14.5	43.9	15.5	10.2	42.2

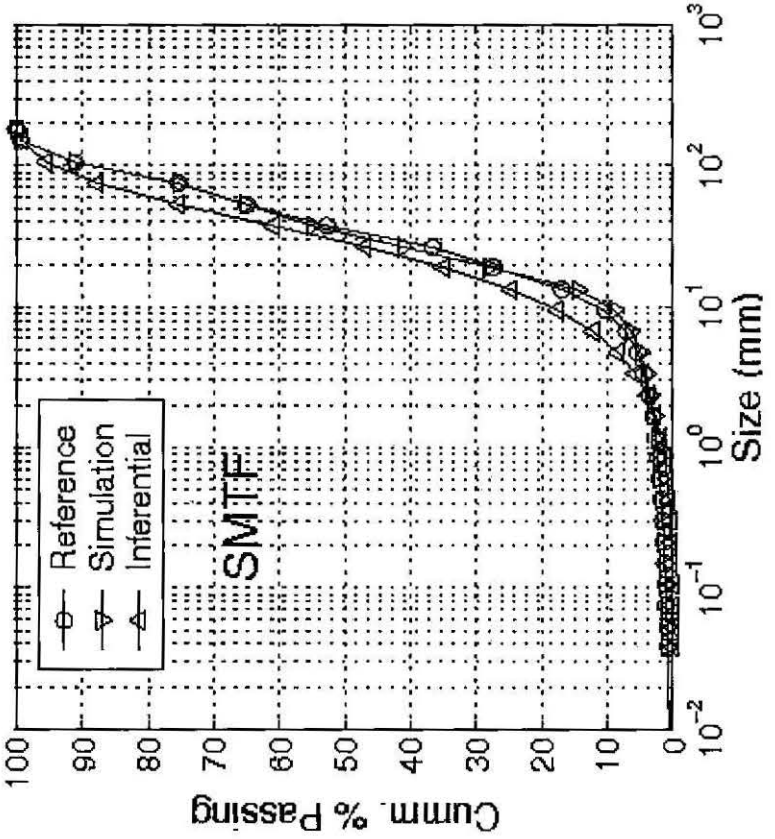

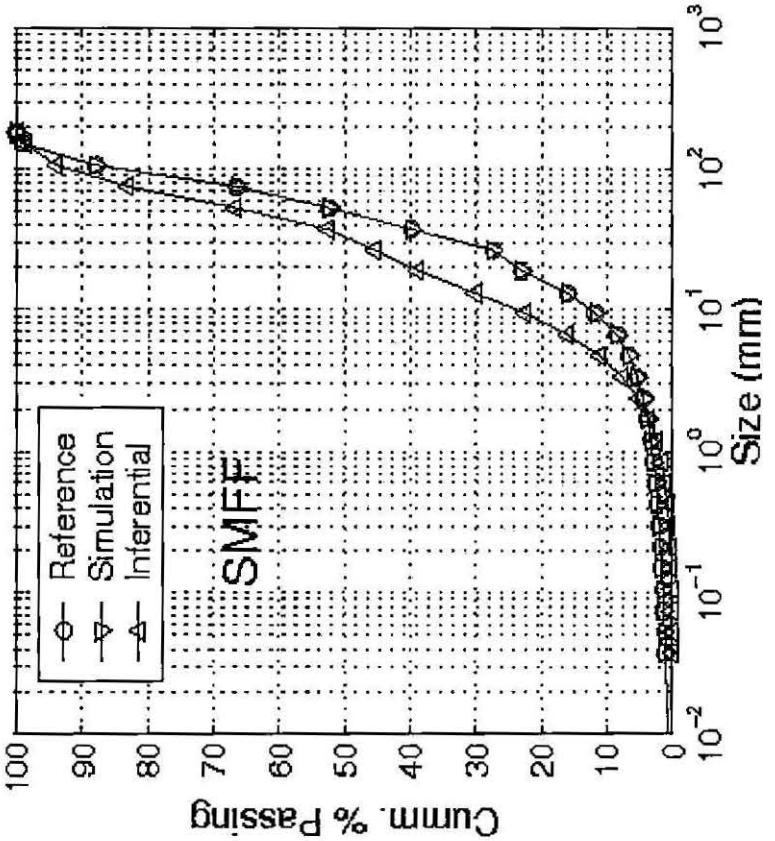

Figure C.1: Size Distribution Results: SMFF & SMTF

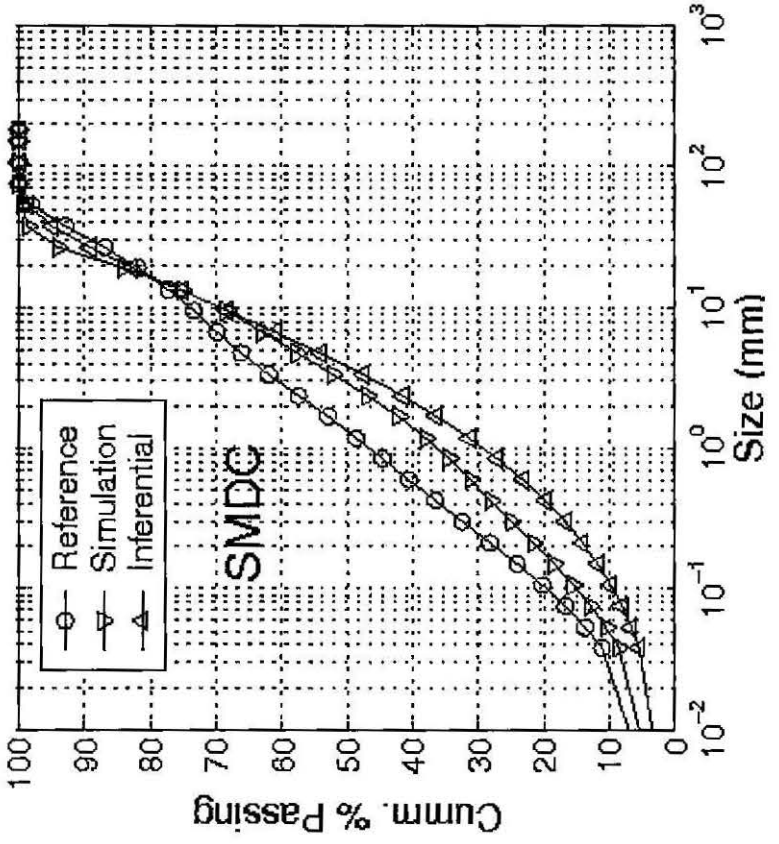

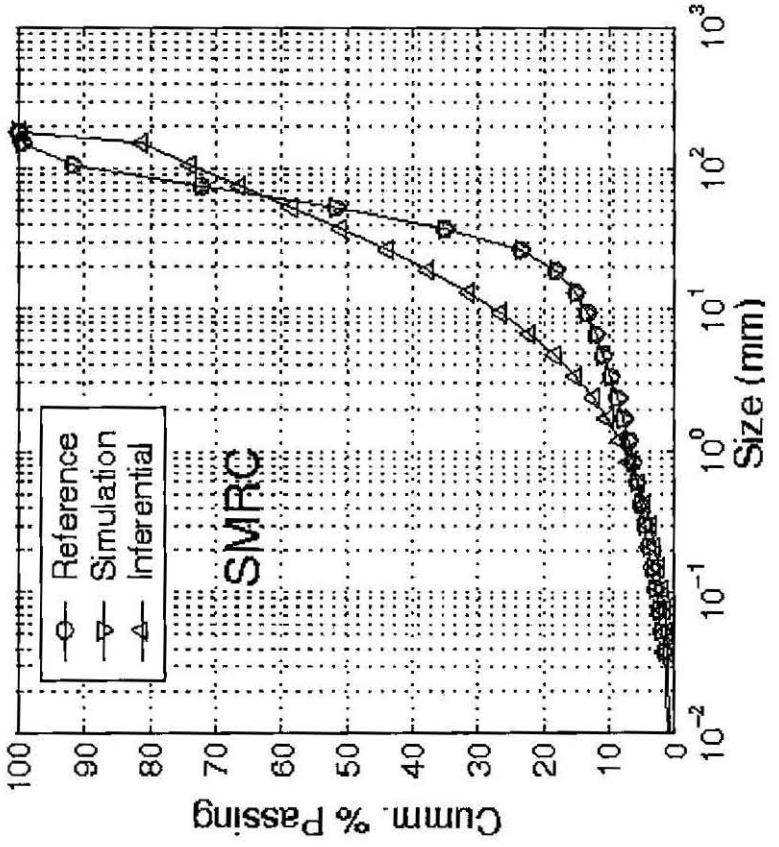

Figure C.2: Size Distribution Results: SMRC & SMDC

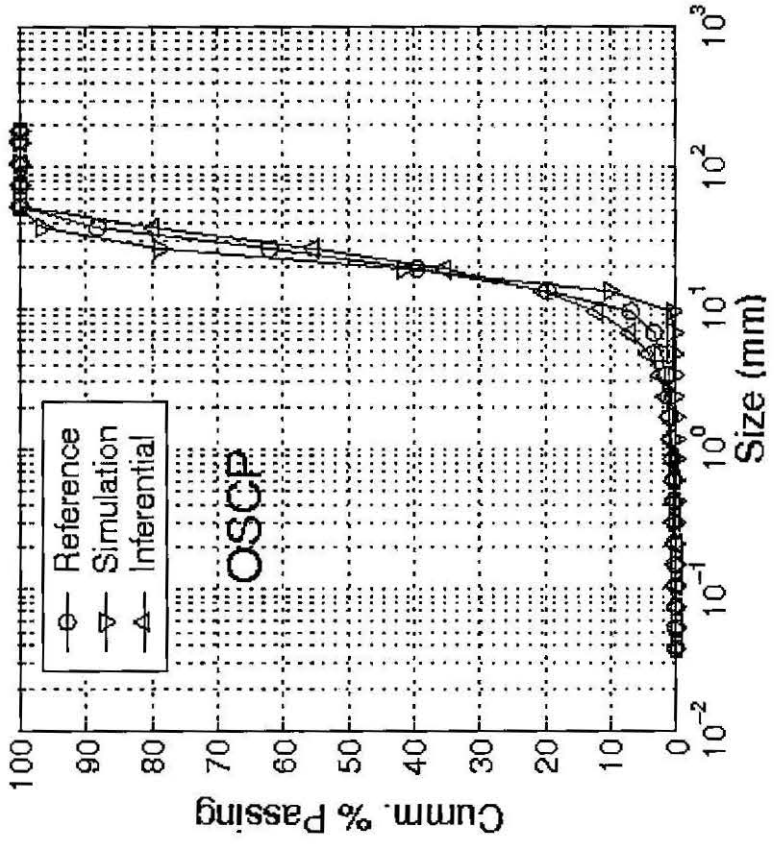

Figure C.3: Size Distribution Results: OSCF & OSCP

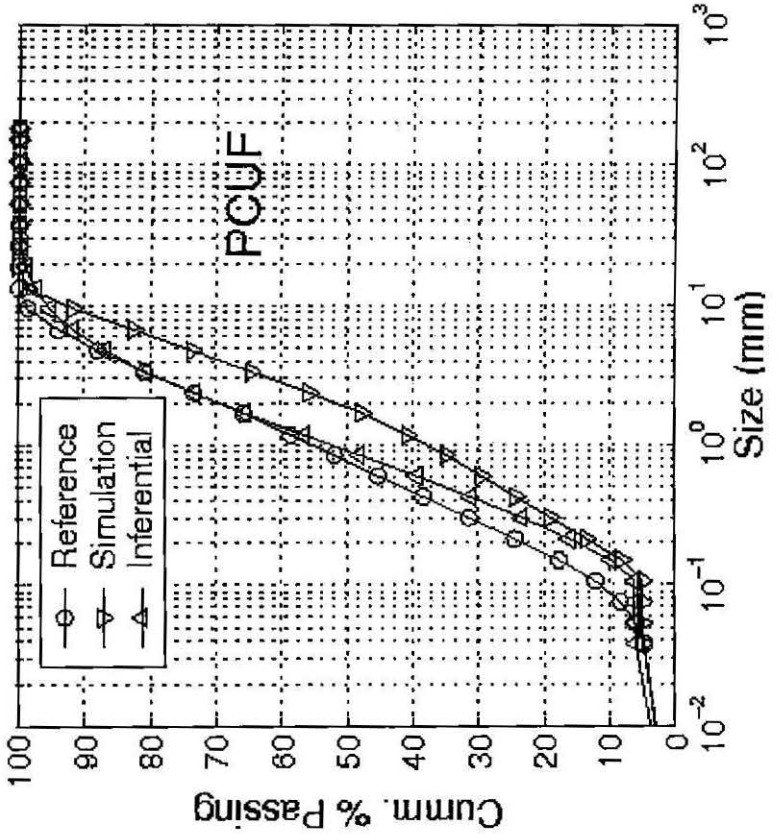

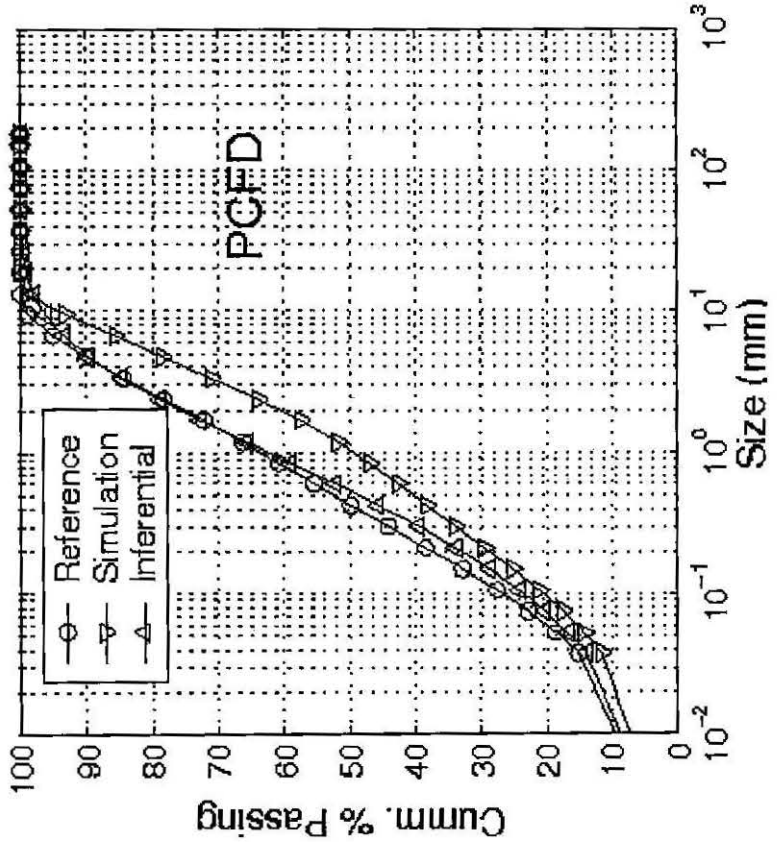

Figure C.4: Size Distribution Results: PCFD & PCUF

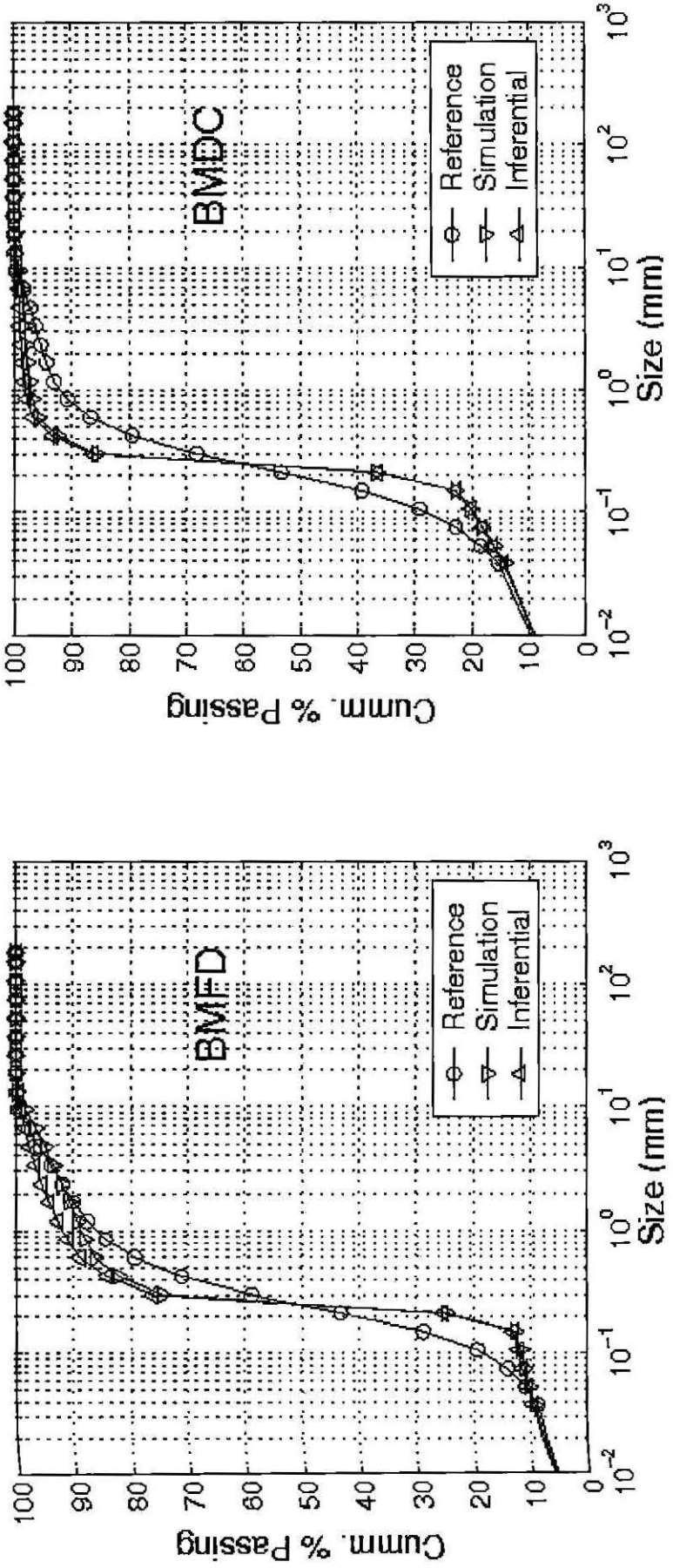

Figure C.5: Size Distribution Results: BMFD & BMDC

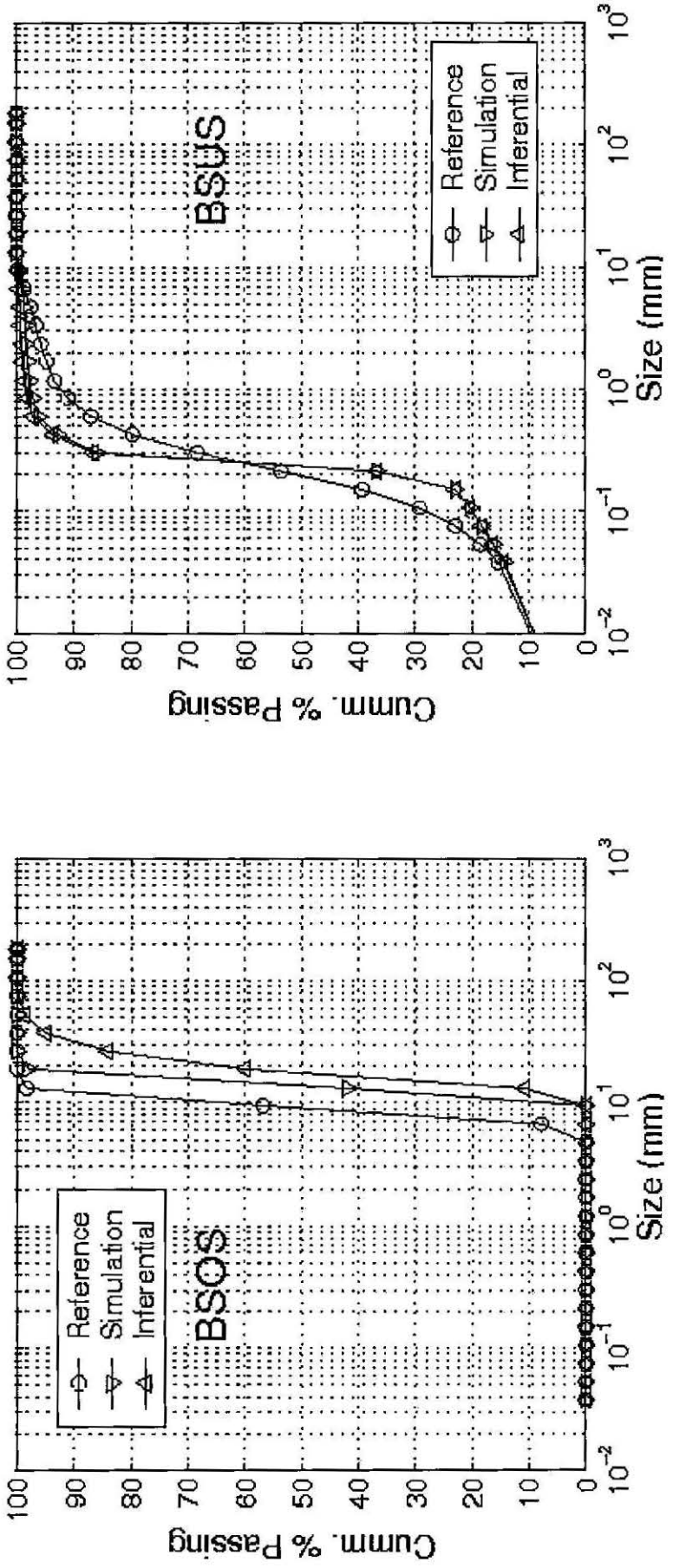

Figure C.6: Size Distribution Results: BSOS & BSUS

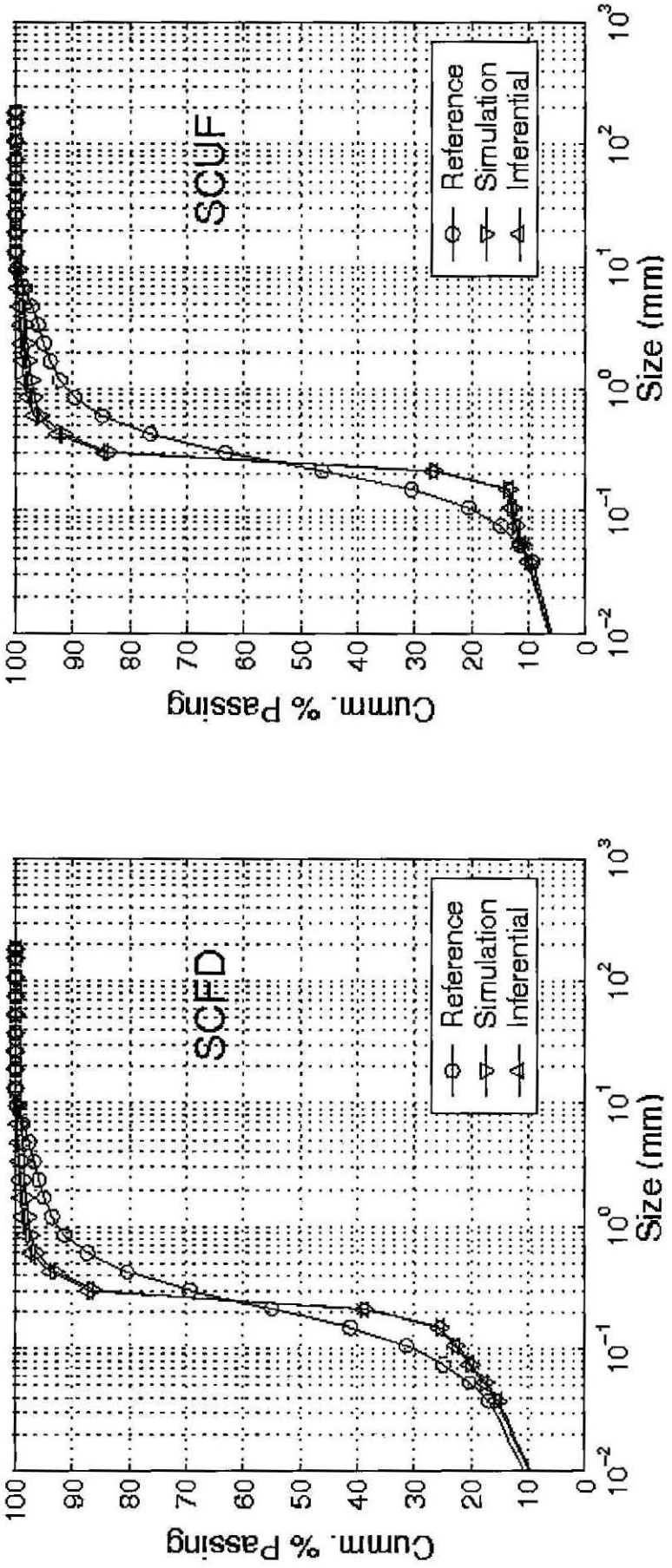

Figure C.7: Size Distribution Results: SCFD & SCUF

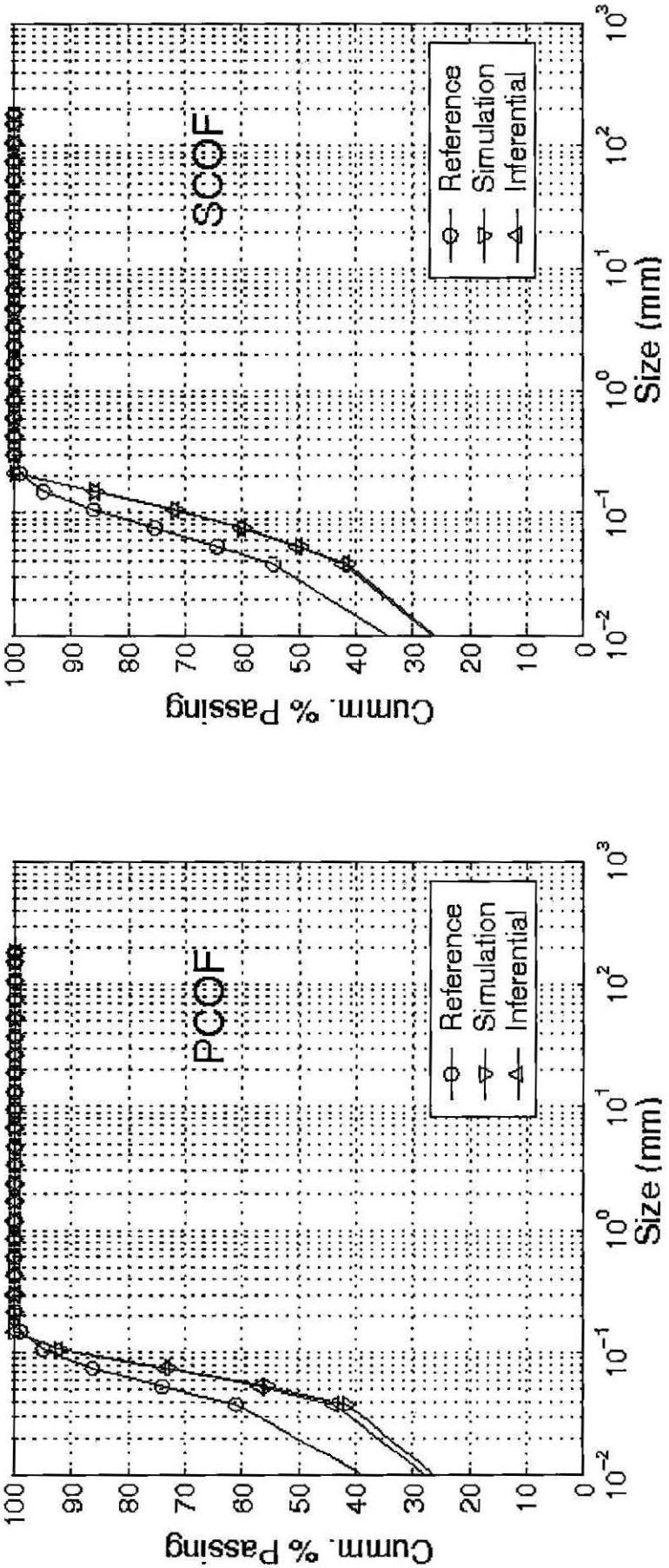

Figure C.8: Size Distribution Results: PCOF & SCOF

Appendix D

Northparkes Mines Grinding Circuit Logsheets and Shift Communication Book Sheets

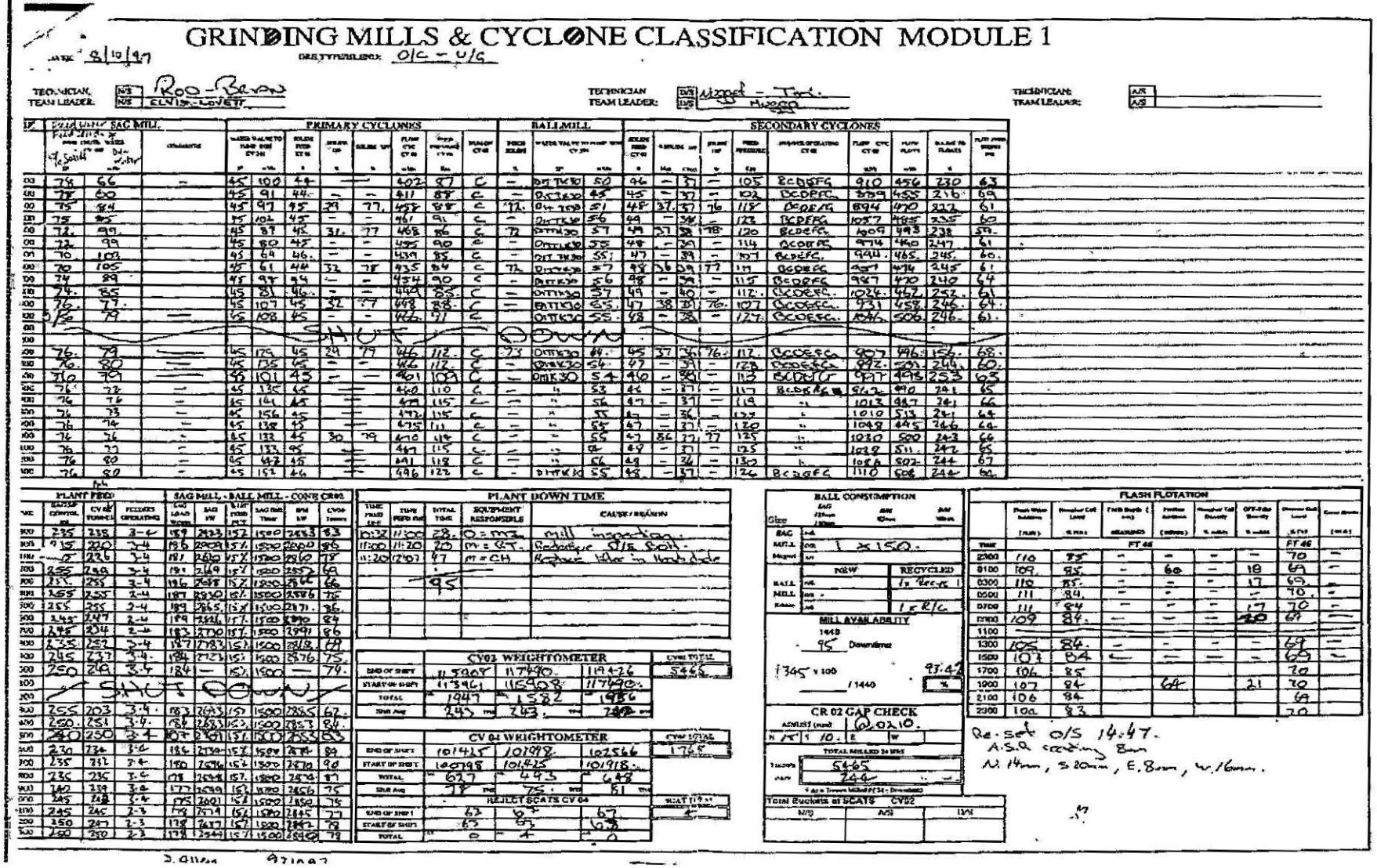

GRINDING MILLS & CYCLONE CLASSIFICATION MODULE 1

DATE 8/10/97 — DRILLTYPE/BLENDS: O/C - U/G

TECHNICIAN, N/S: Roo-Bevan — TEAM LEADER, N/S: ELVIS - LOVETT

TECHNICIAN, D/S: Nisbet - Tait — TEAM LEADER, D/S: Hugo

TECHNICIAN, A/S: — TEAM LEADER, A/S:

	SAG MILL			PRIMARY CYCLONES							BALL MILL		SECONDARY CYCLONES						
	Feed Water SAG Mill																		
	% Solids	DA m³/hr	COMMENTS	WATER VALVE TO HEAD BOX CV201	SOLIDS FEED CV15	SPIGOT DP	SOLIDS SP	FLOW CYC CV08	PRESS CYCLONE CV06	PUMP CV18	FEED SOLIDS	WATER VALVE TO PUMP BOX CV301	SOLIDS FEED CV09	% SOLIDS SP	SPIGOT DP	FEED PRESSURE	UNDERFLOW CV10	FLOW CYC CV10	FLOW FLOW	SLURRY TO FLOATS
	%	m³/hr		%	t/hr	kPa	%	m³/hr	kPa	%	t/hr	%	t/hr	%	kPa	kPa	%	m³/hr	m³/hr	t/hr
03	78	66	—	45	100	49	—	402	87	C	—	DIT TK30 50	96	—	37	—	105	BCDEFG	910	456	730	63
02	78	60	—	45	91	44	—	411	88	C	—	DIT TK30 45	45	—	37	—	103	BCDEFG	389	455	216	69
01	75	84	—	45	97	45	39	77	457	88	C	—	DIT TK30 51	48	37	37	76	115	BCDEFG	894	470	232	61
00	75	85	—	45	102	43	—	—	461	91	C	—	DIT TK30 56	49	—	36	—	123	BCDEFG	1087	485	235	60
29	72	99	—	45	87	45	31	77	468	86	C	72	DIT TK30 57	49	37	38	118	120	BCDEFG	1009	493	238	59
28	72	99	—	45	80	45	—	—	495	90	C	—	DIT TK30 55	48	—	36	—	114	BCDEFG	974	490	247	61
27	70	103	—	45	64	46	—	—	439	85	C	—	DIT TK30 55	47	—	39	—	107	BCDEFG	994	485	245	60
26	70	105	—	45	61	44	32	78	435	84	C	72	DIT TK30 57	48	36	39	77	119	BCDEFG	987	494	245	61
25	74	89	—	45	98	44	—	—	454	90	C	—	DIT TK30 56	48	—	39	—	115	BCDEFG	987	490	240	64
24	74	85	—	45	81	46	—	—	449	88	C	—	DIT TK30 57	49	—	40	—	117	BCDEFG	1026	462	252	61
23	76	77	—	45	107	45	32	77	448	88	C	—	DIT TK30 55	47	38	39	76	107	BCDEFG	931	458	246	64
22	5/6	79	—	45	108	45	—	—	446	91	C	—	DIT TK30 55	48	—	38	—	127	BCDEFG	836	506	246	61
21						SHUT						DOWN										
20																						
19	76	79	—	45	179	45	29	77	446	112	C	73	DIT TK30	49	45	37	36	76	117	BCDEFG	907	496	154	68
18	76	80	—	45	135	45	—	—	446	112	C	—	DIT TK30	54	47	—	39	—	128	BCDEFG	892	500	246	60
17	710	79	—	45	101	43	—	—	461	109	C	—	DIT TK30	54	46	—	38	—	113	BCDEFG	987	493	253	63
16	76	72	—	45	135	45	—	—	460	110	C	—	〃	53	46	—	37	—	117	BCDEFG	942	490	241	65
15	74	76	—	45	141	45	—	—	471	115	C	—	〃	56	47	—	37	—	119	〃	1013	487	241	66
14	74	73	—	45	156	45	—	—	492	115	C	—	〃	55	47	—	36	—	127	〃	1010	513	241	64
13	76	74	—	45	138	45	—	—	475	111	C	—	〃	55	47	—	37	—	120	〃	1048	445	246	64
12	76	76	—	45	133	45	30	79	470	118	C	—	〃	55	47	36	77	77	125	〃	1030	500	243	66
11	76	77	—	45	133	45	—	—	469	115	C	—	〃	54	49	—	37	—	125	〃	1039	511	242	65
10	76	80	—	45	142	45	—	—	491	118	C	—	〃	56	49	—	36	—	130	〃	1084	502	244	67
09	76	80	—	45	152	46	—	—	496	122	C	—	DIT TK30	55	48	—	37	—	124	BCDEFG	1110	508	244	66

	PLANT FEED			SAG MILL - BALL MILL - CONE CRUS					
	ROM/SP Control t/hr	CV 07 TONNES	FEEDERS OPERATING	SAG LOAD Tonnes	SAG kW	SAG FEED Tonnes/hr	SAG Bm Time	SAG RPM kW	CV09 Tonnes
00	235	238	3-4	189	2933	152	1500	2653	83
05	235	240	3-4	186	2909	154	1500	2900	86
04	225	226	3-4	181	2860	154	1500	2860	78
03	255	249	3-4	191	2969	154	1500	2852	68
02	235	255	3-4	196	2988	152	1500	2866	66
01	265	255	3-4	187	2890	154	1500	2896	75
00	255	255	3-4	189	2865	153	1500	2871	86
29	245	247	3-4	189	2886	153	1500	2890	84
28	245	234	3-4	183	2790	153	1500	2791	86
27	245	252	3-4	187	2783	151	1500	2818	88
26	245	237	3-4	184	2723	151	1500	2676	75
25	250	249	3-4	184	—	152	1500	—	79
24			SHUT		DOWN				
23									
22	255	203	3-4	183	2693	151	1500	2855	67
21	250	251	3-4	184	2783	152	1500	2853	84
20	240	250	3-4	187	2791	151	1500	2855	85
19	230	234	3-4	184	2730	151	1500	2814	89
18	235	232	3-4	180	2696	152	1500	2870	90
17	235	235	3-4	178	2648	151	1500	2854	87
16	240	239	3-4	177	2699	151	1500	2856	75
15	245	248	3-4	175	2601	151	1500	2850	75
14	245	246	3-4	179	2674	151	1500	2845	77
13	250	247	3-4	178	2617	152	1500	2842	78
12	260	250	3-4	178	2644	151	1500	2850	79

	PLANT DOWN TIME				
	TIME STARTED LOST	TIME FEED LOST	TOTAL TIME	EQUIPMENT RESPONSIBLE	CAUSE / REASON
1	10:30	11:00	28.	O = MS	Mill inspection.
2	11:00	11:20	20	M = ST.	Reduce size SAG.
3	11:20	17:07	47	M = CH	Replace liner in Hydrocone
4					
5					
6					
7					
8					
9					
10			95		

CV02 WEIGHTOMETER				CV04 TOTAL
END OF SHIFT	11:5905	11:7490	11:9426	5465
START OF SHIFT	11:3961	11:5908	11:7490	
TOTAL	1947	1582	1936	
TONS/HR	243 TPH	243 TPH	242 TPH	

CV 04 WEIGHTOMETER				CV04 TOTAL
END OF SHIFT	101425	101998	102566	1768
START OF SHIFT	100998	101425	101918	
TOTAL	427	573	648	
TONS/HR	78 TPH	75 TPH	81 TPH	

REJECT SCATS CV 04				REJECT TOTAL
END OF SHIFT	63	84	67	4
START OF SHIFT	63	84	67	
TOTAL	0	0	0	

BALL CONSUMPTION

Size	SAG	MILL	BALL
SAG			
MILL	1 x 150.		
Magnet			

	NEW	RECYCLED
BALLS		To Recycle
MILLS		
Rubber		1 L R/C

MILL AVAILABILITY

1440 − 95 Downtime = 1345 x 100 / 1440 = 93.4 %

CR 02 GAP CHECK

ADJUST (mm): 6.02 10.

N	15	10.	E	W

TOTAL MILLED 24 HRS: 5465 + 244 = 5709

Total Buckets at SCATS CV02

N/S	A/S	D/S

FLASH FLOTATION

	Flash Water Addition (%w/w)	Flash Cell Level (% max)	FMB Starch (g/t) ADJUSTED	Frother Addition (g/t)	Flash Cell Froth Density (% solids)	OFF-Gas Density (% solids)	Flash Cell Froth (t/hr)	Cleaner Froth (t/hr)
TIME			FT 46				FT 46	
2200	110	95	—	—	—	—	70	—
0100	109	95	—	60	—	18	69	—
0300	110	85	—	—	—	17	69	—
0500	111	84	—	—	—	—	70	—
0700	111	84	—	—	—	17	70	—
0900	109	84	—	—	—	20	69	—
1100								
1300	105	84	—	—	—	—	69	—
1500	103	84	—	—	—	—	69	—
1700	106	85					70	
1900	107	84		64		21	70	
2100	106	84					69	
2300	106	83					70	

Re-set O/S 14.47.
A.S.O cooking 8mm
N. 14mm, S 20mm, E. 8mm, W. 16mm.

Figure D.1: Module 1 Grinding Logsheet - 08 October 1997

SHIFT COMMUNICATION BOOK

NORTHPARKES

SECTION GRINDING ONE DATE 8/10/97

Night Shift

* PUT A.S.R INTO AUTO AT 0100 hrs & SET AT 12mm. - DIDN'T TRIP OUT, So Lowered to 10mm at 0200.
* DISCHARGE & SHELL BOLTS (2) WEEPING KEEP A EYE ON, A.S.R, set back to 12mm. Gear holding better and a bit longer on A.S.R to Do it Later, will let come up towards end of shift dropped tons, Reset o/size.

Day Shift

* Shutdown at 10:30 for mill inspection, Re-torqued bolts on O/E, Potted screen decking on SW09 and Replaced liners in feed chute & Heat chute.
* A.S.R set at 12mm will not go to 10 as someone has changed some settings in the A.S.R
* Re calibrate CROC.

Afternoon Shift

* ASR sitting on 12mm. Hitting metal - metal at 10 - 8 mm
* Cleared FEOS but FEOA still gummed up with fines.

Figure D.2: Module 1 Shift Communication Book Sheet - 08 October 1997

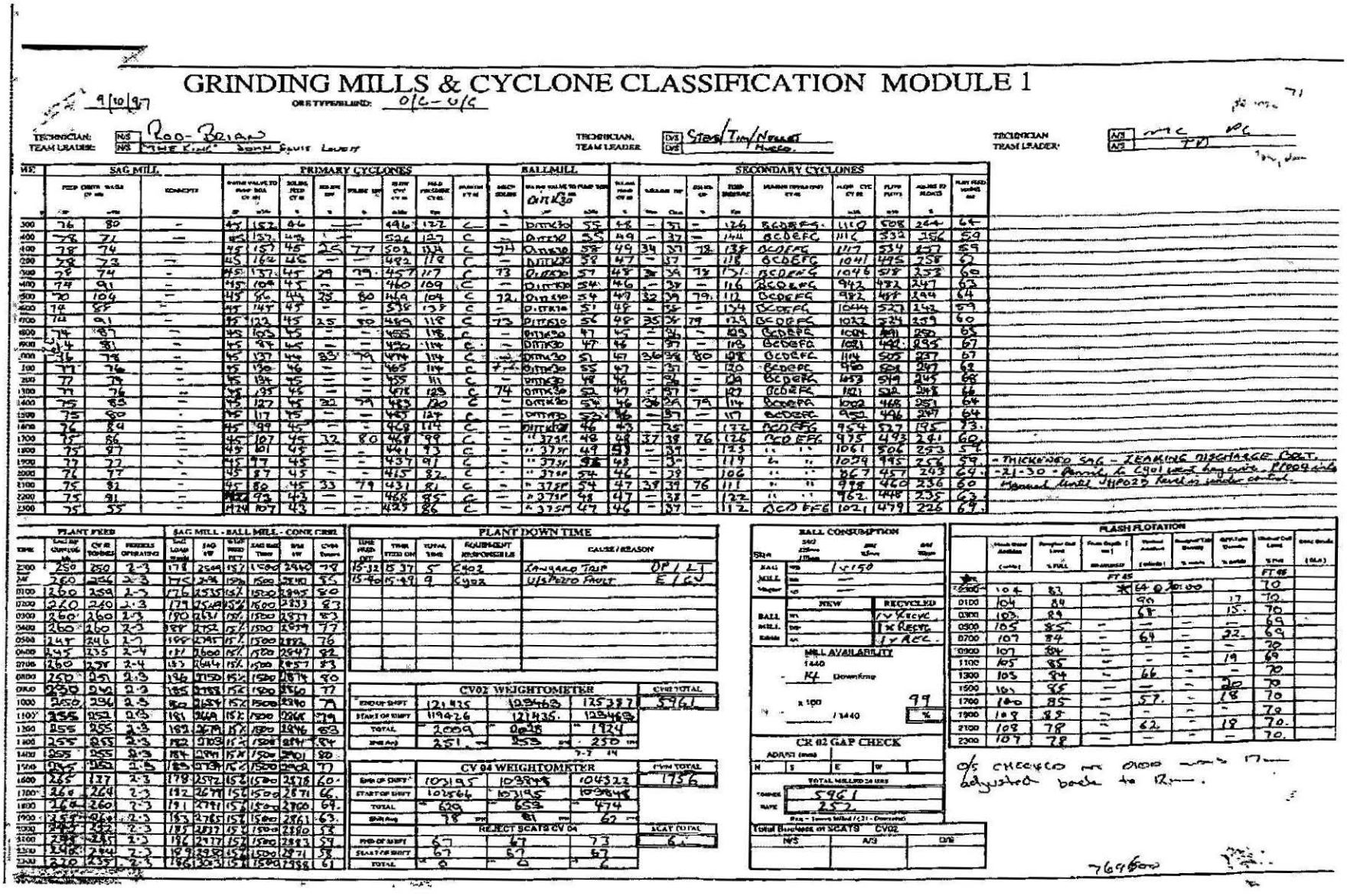

GRINDING MILLS & CYCLONE CLASSIFICATION MODULE 1

9/10/97

ORE TYPE/BLEND: O/C-U/G

TECHNICIAN: NS Roo-Brian
TEAM LEADER: NS Mike Kidd / John Squire Lauren

TECHNICIAN: D/S Steve/Tim/Norman
TEAM LEADER: D/S Hugo

TECHNICIAN: N/S mic RPC
TEAM LEADER: A/S TM

SAG MILL | PRIMARY CYCLONES | BALL MILL | SECONDARY CYCLONES

TIME	SAG MILL			PRIMARY CYCLONES							BALL MILL			SECONDARY CYCLONES								
0300	76	80	-	45	152	46	-	-	496	122	C	-	DITCH 10	55	48	-	51	-	126	BCDEFG	1110	508	244	66
0400	78	71	-	45	153	45	-	-	504	120	C	-	DITCH	55	49	-	37	-	144	BCDEFG	1116	532	256	50
0500	78	74	-	45	157	45	25	77	502	118	C	74	Ditch	58	49	34	37	78	138	BCDEFG	1117	534	257	59
0600	78	73	-	45	162	46	-	-	492	119	C	-	DITCH	58	47	-	37	-	118	BCDEFG	1041	495	258	62
0700	78	74	-	45	157	45	29	79	457	117	C	73	DITCH	57	48	36	36	78	121	BCDEFG	1046	518	253	60
0800	74	91	-	45	108	45	-	-	460	109	C	-	DITCH	54	46	-	37	-	116	BCDEFG	942	482	247	62
0900	70	104	-	45	96	45	28	80	449	104	C	72	DITCH	54	49	32	39	79	112	BCDEFG	982	488	244	64
1000	74	85	-	45	147	45	-	-	538	138	C	-	DITCH	51	48	-	35	-	134	BCDEFG	1044	527	243	59
1100	74	91	-	45	122	45	25	80	469	118	C	73	DITCH	56	48	35	36	79	123	BCDEFG	1032	534	239	60
1200	74	87	-	45	105	45	-	-	465	118	C	-	DITCH	57	45	-	36	-	103	BCDEFG	1004	1011	230	65
1300	74	81	-	45	94	45	-	-	430	114	C	-	DITCH	57	46	-	37	-	103	BCDEFG	1081	490	235	67
1400	76	78	-	45	137	44	25	79	494	114	C	-	DITCH	51	47	36	36	80	108	BCDEFG	1114	505	237	67
1500	77	76	-	45	130	46	-	-	465	114	C	-	DITCH	55	47	-	37	-	120	BCDEFG	980	504	247	68
1600	77	79	-	45	134	45	-	-	455	111	C	-	DITCH	58	46	-	36	-	104	BCDEFG	1053	519	245	68
1700	77	76	-	45	135	45	-	-	476	123	C	74	DITCH	52	47	-	37	-	127	BCDEFG	1101	528	248	66
1800	75	85	-	45	127	45	32	79	463	120	C	-	DITCH	54	46	38	38	79	114	BCDEFG	1002	468	251	64
1900	75	80	-	45	117	45	-	-	465	127	C	-	DITCH	52	46	-	37	-	117	BCDEFG	952	496	249	64
2000	76	84	-	45	99	45	-	-	468	114	C	-	DITCH	46	43	-	35	-	122	BCDEFG	954	527	195	73
2100	75	86	-	45	107	45	32	80	468	99	C	-	" 3735	48	44	37	38	76	126	BCDEFG	935	493	241	60
2200	75	87	-	45	101	45	-	-	441	93	C	-	" 3735	49	43	-	37	-	123	" "	1061	506	253	59
2300	77	77	-	45	97	45	-	-	437	91	C	-	" 3735	48	48	-	35	-	119	" "	1039	495	256	59
2000	76	77	-	45	87	45	-	-	415	82	C	-	" 3735	54	46	-	39	-	106	" "	867	457	243	64
2100	75	81	-	45	80	45	33	79	431	81	C	-	" 3735	54	47	39	39	76	111	" "	918	460	236	60
2200	75	91	-	44	93	43	-	-	468	85	C	-	" 3735	58	47	-	38	-	122	" "	962	448	235	63
2300	75	55	-	44	107	43	-	-	429	86	C	-	" 3735	47	46	-	37	-	112	ACDEFG	1021	479	226	64

- THICKENED SAG - LEAKING DISCHARGE CONE.
-21-30 - Pump & CYCL west hog ends. Flood and Manual Mill JH0025 Rock in feeder control.

TIME	PLANT FEED: SAG MILL FEED RATE (tph)	CV 01 TONNES	FEEDERS OPERATING	SAG MILL - BALL MILL - CONE CRUSHER: BALL MILL LOAD (%)	SAG kW	MILL SPEED (%)	BALL MILL FEED RATE (tph)	BALL MILL Time	BALL MILL kW	CONE CRUSHER Power
0200	250	250	2-3	178	2565	157	1500	2440	2440	78
0300	260	254	2-3	175	2498	159	1500	2430	2430	55
0400	260	258	2-3	176	2535	157	1500	2395	2395	80
0500	260	260	2-3	179	2554	157	1500	2433	2433	83
0600	260	260	2-3	170	2451	157	1500	2377	2377	83
0700	260	260	2-3	168	2452	157	1500	2379	2379	77
0800	245	246	2-3	169	2495	157	1500	2382	2382	76
0900	245	235	2-3	171	2600	157	1500	2547	2547	82
1000	260	258	2-3	183	2644	157	1500	2557	2557	83
1100	250	251	2-3	176	2550	157	1500	2574	2574	80
1200	250	245	2-3	185	2688	157	1500	2560	2560	77
1300	250	256	2-3	180	2587	157	1500	2590	2590	71
1400	255	251	2-3	181	2618	157	1500	2566	2566	79
1500	255	255	2-3	182	2671	157	1500	2596	2596	83
1600	255	255	2-3	184	2696	157	1500	2601	2601	80
1700	245	250	2-3	180	2638	157	1500	2608	2608	77
1800	265	237	2-3	178	2592	157	1500	2578	2578	60
1900	260	264	2-3	192	2671	157	1500	2871	2871	66
2000	260	260	2-3	191	2791	157	1500	2700	2700	69
2100	255	260	2-3	183	2765	157	1500	2761	2761	63
2200	245	252	2-3	185	2837	157	1500	2880	2880	58
2300	238	245	2-3	196	2917	157	1500	2883	2883	59
2000	248	244	2-3	189	2858	157	1500	2871	2871	58
2100	220	235	2-3	186	2823	157	1500	2758	2758	61

PLANT DOWN TIME

TIME FEED OFF	TIME FEED ON	TOTAL TIME	EQUIPMENT RESPONSIBLE	CAUSE / REASON
15:32	15:37	5	C402	Kangaroo Trip OP / LT
15:40	15:49	9	C402	U/S Pebble Feed E / CV

CV02 WEIGHTOMETER

			CV02 TOTAL
END OF SHIFT	121435	123688	125387
START OF SHIFT	119426	121436	123468
TOTAL	2009	2252	1924
RATE (tph)	251	253	250

7-7-14

CV 04 WEIGHTOMETER

			CV04 TOTAL
END OF SHIFT	101395	103898	104323
START OF SHIFT	101566	103195	103848
TOTAL	629	653	474
RATE (tph)	78	81	62

REJECT SCATS CV 04

			SCAT TOTAL
END OF SHIFT	67	67	73
START OF SHIFT	67	67	67
TOTAL	0	0	6

BALL CONSUMPTION

Size	3x2	4x4	5x5
BALL	14150		
MILL	—		
Weight			

	NEW	RECYCLED
BALL		1 x Recyc
MILL		1 x Recyc
Rods		1 x Recyc

MILL AVAILABILITY
1440
- 14 Downtime
x 100 = 99 %
/ 1440

CR 02 GAP CHECK
ADJUST (mm)
N | S | E | W

TOTAL MILLED 24 HRS
TONNES 5961
RATE 252

Total Breakage on SCATS CV02

N/S	A/3	D/S

FLASH FLOTATION

	Flash Feed Addition (cm/min)	Flash Cell Level % FULL	Flash Depth (mm)	Flash Froth Level (cm/min)	Flash Froth Density % solids	Flash Cell Level % FULL	Flash Cell Level FT 65
							FT 65
2300	104	83	*	64 @ 01:00			70
0100	104	84		90		17	70
0300	103	89		68		15	70
0500	105	85	—	—	—	—	69
0700	107	84	—	69	—	32	69
0900	107	84	—	—	—	—	70
1100	105	85	—	—	—	19	69
1300	105	84	—	66	—	—	70
1500	101	85	—	—	—	20	70
1700	100	85	—	57	—	18	70
1900	108	85	—	—	—	—	70
2100	109	78	—	62	—	18	70
2300	107	78	—	—	—	—	70

o/s checked on 0100 — was 17 — adjusted back to 12.

7678 ton

Figure D.3: Module 1 Grinding Logsheet - 09 October 1997

SHIFT COMMUNICATION BOOK

NORTHPARKES

SECTION Grinding Numeroo CNO DATE 9/10/97

Night Shift

* Heads of shit going up CV04, sprays on SV09 all blocked up, cleaned all filters.
* Checked o/s several times, dropped out twice Reset to 10— hanging in there.
* Changed feeders 2-3 to 2½ to 4 but 4 was hanging up, cleared, running o.k but has build up in 'back'.

Day Shift

* Found broken bolt on cone crusher (keep checking for others).
* ball charger hanging up alot.
* PP 004 running in auto.
* SV09 + 10 spray filters blocking up about every 2 hours.
*
*

Afternoon Shift

3 + 5 hanging up Keep eye on CV02 dribble chute

- FE03 Hung up once - cleared itself.
- 21:30 - Density to CV01 event wacko, (see trend) steadying things out at the moment with CV301 + PR004 in Manual.
- Ore size getting bigger, dropping TPH over shift
- Danger on F/Feeds pulling slightly ↓ SL level to 78, see what happens
- Possible hole in SV09 screen, Ball Mill ejecting out small ♦ reato.

Figure D.4: Module 1 Shift Communication Book Sheet - 09 October 1997

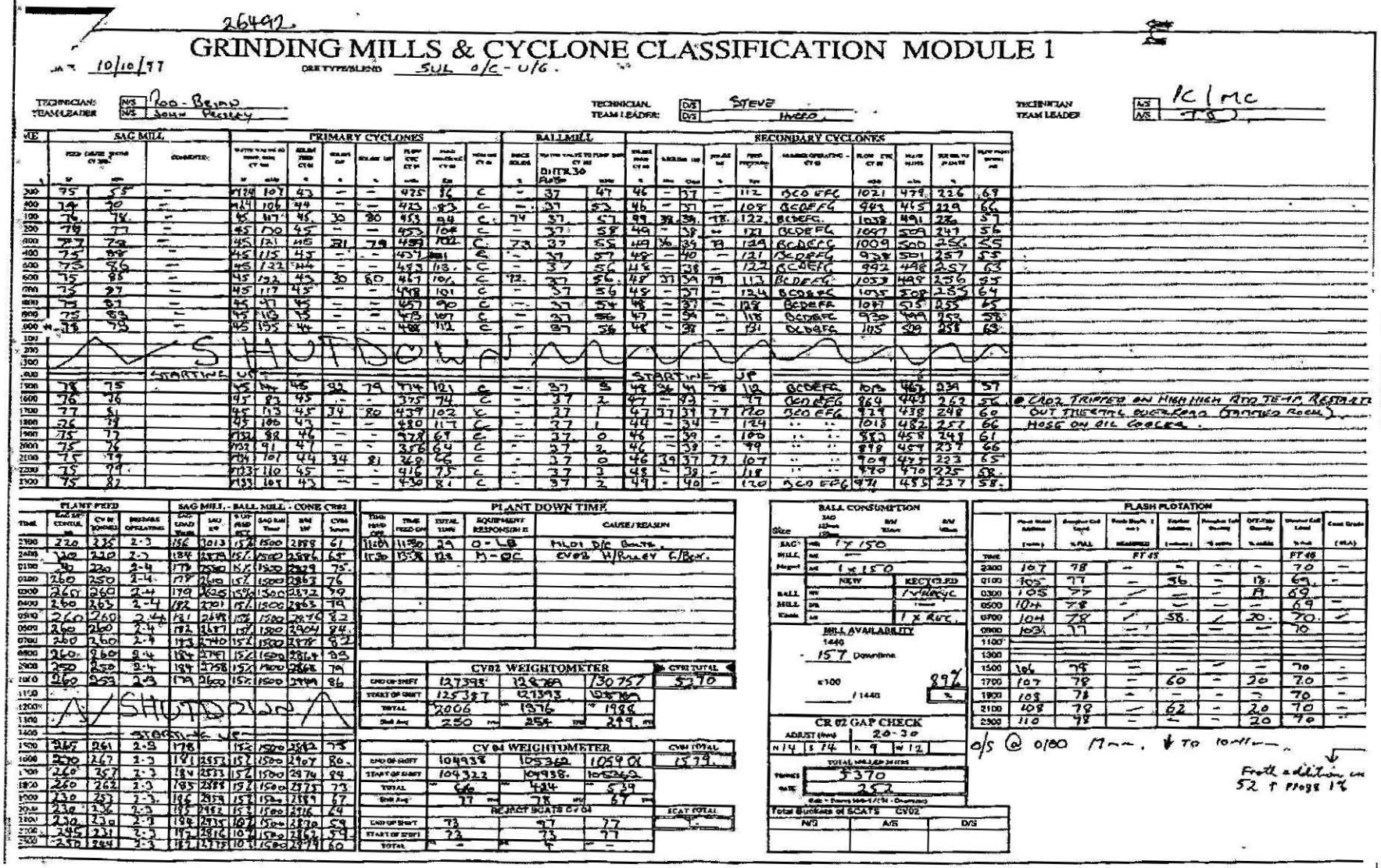

26492

GRINDING MILLS & CYCLONE CLASSIFICATION MODULE 1

DATE 10/10/97 ORE TYPE/BLEND SUL O/C - U/G.

TECHNICIAN / TEAM LEADER: N/S Rod - Brad; N/S Sean - Peggy

TECHNICIAN / TEAM LEADER: D/S STEVE; D/S HUGO

TECHNICIAN / TEAM LEADER: N/S RC / MC; N/S TB

TIME	SAG MILL: FEED RATE (TPH)	SAG MILL: SPEED (% OF MAX)	SAG MILL: COMMENTS	PRIMARY CYCLONES: WATER TO SAG MILL (M³/H)	PRIMARY CYCLONES: SAG MILL DISCH. CYC. FEED (TPH)	PRIMARY CYCLONES: SAG MILL DISCH. CYC. FEED (%)	PRIMARY CYCLONES: BALL MILL DISCH. CYC. FEED (TPH)	PRIMARY CYCLONES: BALL MILL DISCH. CYC. FEED (%)	PRIMARY CYCLONES: WATER TO BALL MILL (M³/H)	BALL MILL: BALL MILL SPEED (%)	BALL MILL: DIFFR 36 PULSE (TPH)	BALL MILL: DIFFR 36 PULSE (%)	SECONDARY CYCLONES: WATER TO CYC (M³/H)	SECONDARY CYCLONES: DISCH. PRESSURE (KPA)	SECONDARY CYCLONES: NUMBER OPERATING - CYC	SECONDARY CYCLONES: FLOW TO CYC (M³/H)	SECONDARY CYCLONES: FEED TO CYC (TPH)	SECONDARY CYCLONES: SIZE TO CYC (% PASSING 75 µm)	SECONDARY CYCLONES: FEED PERCENT SOLIDS (%)
0000	75	58	-	4128	107	43	-	-	475	86	C	-	37	47	46	-	37	-	112	BCDEFG	1021	479	226	69
0100	74	70	-	4124	106	44	-	-	473	83	C	-	37	52	46	-	37	-	108	BCDEFG	983	415	229	66
0200	76	74	-	45	117	45	30	80	453	94	C	74	37	57	99	38	38	78	122	BCDEFG	1038	491	280	57
0300	79	77	-	45	120	45	-	-	453	104	C	-	37	58	49	-	38	-	121	BCDEFG	1047	509	247	56
0400	77	79	-	45	121	46	21	79	489	102	C	73	37	55	49	36	39	79	129	BCDEFG	1009	500	256	55
0500	75	88	-	45	115	43	-	-	457	-	C	-	37	57	48	-	40	-	121	BCDEFG	938	501	257	55
0600	73	56	-	45	122	44	-	-	493	113	C	-	37	56	46	-	38	-	122	BCDEFG	992	498	257	63
0700	75	85	-	45	122	45	30	80	467	100	C	72	37	56	48	33	39	79	113	BCDEFG	1053	489	256	55
0800	73	87	-	45	117	45	-	-	448	101	C	-	37	56	48	-	37	-	134	BCDEFG	1035	508	285	64
0900	74	81	-	45	117	45	-	-	457	90	C	-	37	54	48	-	37	-	128	BCDEFG	1047	515	255	65
1000	73	89	-	45	119	43	-	-	473	107	C	-	37	56	47	-	39	-	118	BCDEFG	930	499	262	58
1100	76	93	-	45	125	44	-	-	488	112	C	-	37	56	48	-	38	-	131	BCDEFG	1115	509	258	63
1200	SHUTDOWN																		
1300																			
1400	STARTING UP														STARTING UP				
1500	78	75	-	45	114	42	29	79	434	101	C	-	37	5	48	26	41	78	118	BCDEFG	1015	463	239	57
1600	76	76	-	45	83	45	-	-	375	74	C	-	37	2	47	-	83	-	79	BCDEFG	864	443	262	56
1700	77	81	-	45	113	45	34	80	439	102	C	-	37	1	47	37	37	77	120	BCDEFG	939	438	248	60
1800	76	79	-	43	100	43	-	-	480	117	C	-	37	1	44	-	34	-	124	" " "	1018	482	257	66
1900	75	77	-	1132	98	46	-	-	378	69	C	-	37	0	46	-	39	-	100	" " "	880	458	248	61
2000	75	76	-	1137	91	47	-	-	356	64	C	-	37	2	46	-	38	-	99	" " "	898	459	237	66
2100	75	79	-	1134	101	44	34	81	369	66	C	-	37	0	46	39	37	77	107	" " "	909	493	223	65
2200	75	79	-	1133	110	45	-	-	416	75	C	-	37	3	48	-	38	-	118	" " "	990	470	225	58
2300	75	82	-	1133	103	43	-	-	430	81	C	-	37	2	49	-	40	-	120	BCD EFG	994	455	237	58

@ CAD2 TRIPPED ON HIGH HIGH RTD TEMP. RESTARTED OUT THE STAY SUCCESSFUL (CONTROL ROOM).
HOSE ON OIL COOLER.

TIME	PLANT FEED: SAG MILL FEED RATE CONTROL	PLANT FEED: CV 01 TONNES	PLANT FEED: PERCENT OPERATING	SAG MILL - BALL MILL - CONE CR02: SAG MILL SPEED (% OF MAX)	SAG MILL - BALL MILL - CONE CR02: SAG MILL SPEED (RPM)	SAG MILL - BALL MILL - CONE CR02: MILL POWER (KW)	SAG MILL - BALL MILL - CONE CR02: % OF MAX SAG MILL SPEED	SAG MILL - BALL MILL - CONE CR02: SAG MILL POWER (KW)	SAG MILL - BALL MILL - CONE CR02: BALL MILL POWER (KW)	SAG MILL - BALL MILL - CONE CR02: CYC1 SPRAY WATER
0000	220	235	2.3	166	3013	152	1500	2888	6	61
0100	220	230	2.3	164	2975	151	1500	2886	6	65
0200	230	220	2.4	179	2580	156	1500	2829	7	75
0300	260	250	2.4	179	2610	157	1500	2963	7	76
0400	260	260	2.4	179	2625	158	1500	2872	7	79
0500	260	263	2.4	182	2701	157	1500	2963	7	79
0510	260	260	2.4	181	2698	157	1500	2870	7	82
0600	260	260	2.4	182	2687	157	1500	2904	7	84
0700	260	260	2.4	183	2740	154	1500	2878	6	82
0800	260	260	2.4	184	2791	152	1500	2814	6	85
0900	250	250	2.4	184	2758	152	1500	2865	7	79
1000	260	253	2.3	179	2600	152	1500	2799	6	86
1100	SHUTDOWN									
1200										
1300										
1400	STARTING UP									
1500	245	241	2.3	178		152	1500	2842	7	75
1600	230	247	2.3	181	2557	152	1500	2907	8	86
1700	240	257	2.3	184	2573	152	1500	2974	9	94
1800	260	262	2.3	185	2588	152	1500	2975	7	73
1900	230	253	2.3	186	2658	152	1500	2989	7	87
2000	230	236	2.3	185	2982	152	1500	2716	6	64
2100	230	230	2.3	184	2935	107	1500	2870	5	59
2200	245	231	2.3	182	2816	104	1500	2862	5	59
2300	250	244	2.3	182	2775	104	1500	2779	5	60

PLANT DOWN TIME

TIME FEED OFF	TIME FEED ON	TOTAL TIME	EQUIPMENT RESPONSIBLE	CAUSE/REASON
1140h	1130	29	O-LB	MLO1 D/F Boots.
1230	1358	128	M-OC	CV02 W/Pulley C/Bolt.

CV02 WEIGHTOMETER

				CV02 TOTAL
END OF SHIFT	127395	129368	130757	5370
START OF SHIFT	125387	127393	128787	
TOTAL	2006	1976	1988	
Dmt/hr	250	256	249	

CV04 WEIGHTOMETER

				CV04 TOTAL
END OF SHIFT	104935	105362	105901	1579
START OF SHIFT	104322	104938	105260	
TOTAL	613	424	539	
Dmt/hr	77	78	67	

REJECT SCATS CV04

				SCAT TOTAL
END OF SHIFT	73	77	77	
START OF SHIFT	73	73	77	
TOTAL	-	4	-	

BALL CONSUMPTION

Size	SAG	BM	BM
SAG	1"	1" x 150	
MILL			
Magnet		1 x 150	

	NEW	RECYCLED
BALL	1"	1" x RECYC
MILL		
Blank		

1 x RUC

MILL AVAILABILITY

1440

- 157 Downtime

1283 / 1440 = 89%

CR 02 GAP CHECK

ADJUST (mm) 20-30

N 14 | S 14 | N 9 | W 12

TOTAL MILLED HOURS: 5370 / 252

Total Buckets of SCATS CV02

N/S	A/S	D/S

FLASH FLOTATION

TIME	Flash Water Addition (mm)	Flash Cell Depth (%FULL)	Flash Depth 1 (%FULL)	Flash Depth 2 (%FULL)	Flash Cell Aeration (mm)	Flash Froth Cell Density (%)	Flash Froth Cell Density (%)	Flash Cell Level (%FULL)	Flash Grade (g/t)
		FLASH						FLASH	
2200	107	78	-	-	-	-	-	70	-
0100	105	77	-	36	-	13	6	69	-
0300	105	77	-	/	-	8	6	69	-
0500	104	78	/	/	-	-	-	69	-
0700	104	78	/	58	/	20	7	70	/
0900	103	77	/	/	/	-	-	70	
1100									
1300									
1500	104	78	-	-	/	-	7	70	-
1700	107	78	-	60	-	20	7	70	-
1900	108	78	-	-	-	-	7	70	-
2100	108	78	-	62	-	20	7	70	-
2300	110	78	-	-	-	20	7	70	-

o/s @ 0100 17mm. ↓ TO 10mm.
↓
From addition on 52 T Prods 17

Figure D.5: Module 1 Grinding Logsheet - 10 October 1997

SHIFT COMMUNICATION BOOK

NORTHPARKES

SECTION GRINDING ONE DATE 10/10/97.

Night Shift LOTS OF CHUNKY ROCK.

* CHANGED FEEDERS FROM 3 TO 4, CV04 BELT LIFTING ABOUT 2 (PATCHES) INCHES ROUND, CONSISTENTLY ALONG THE FULL LENGTH OF BELT
* O/SIZE HANGING AROUND 10-11 m.
* IF SHUTDOWN OCCURS COULD SOMEONE CHECK SV09.
* STILL ONLY ONE BOLT BROKEN ON O/SIZE.
* GOOD RUN ALL SHIFT.
* RUNNING CV301 & PP004 BACK IN AUTO, SEEMS OK.
* FILTERS BLOCKING UP REGULAR ON SPRAYS (SV09)

Day Shift

* CHANGED FROM FEEDER 4 to 3 as CV03 was tracking realy badly.
* shutdown to repair leaking bolt on discharge end of sag, checked SV09 + cut loose pieces of rubber off CV04.
* CV 03 & head pulley gearbox shit itself on start up, replaced g/box + head scrapers.

10

Afternoon Shift

- 21:09 - 15% Now has come to a 20%, 10% in to try something different, maybe get M/weight change?
- Auto Level (Sag) went stupid again, back to manual (limit + CV301)
- ↑ FROTHER to F/Bots ¾ to 60 m/m.
- Same shit in filters.
- Keep eye out on CR02 Bolts.
- Ball charger hangs up occasionally.

NPM24

Figure D.6: Module 1 Shift Communication Book Sheet - 10 October 1997

GRINDING MILLS & CYCLONE CLASSIFICATION MODULE 1

Date: 11/10/97. ORE TYPE/BLEND: SUL o/c

TECHNICIAN: NS — TEAM LEADER: NS — TECHNICIAN: NS — TEAM LEADER: NS

Hr	SAG MILL			PRIMARY CYCLONES						BALLMILL			SECONDARY CYCLONES							
08	75	82		M33	109	43	—	—	430	81	C	—	27	2	49	—	40	—	170	ACDEFG	971	455	227	58
09	75	83		M33	109	45	—	—	412	74	C	—	DM=90	3	89	—	39	—	164	BCDEFG	980	470	297	59
10	75	83		M35	66	47	—	—	396	90	C	—	"	0	50	—	44	—	128	"	1022	490	245	62
11	75	86		M34	110	43	—	—	439	84	C	—	"	5	49	—	40	—	116	"	1077	492	251	61
12	75	81		M34	110	43	31	79	439	84	C	—	"	6	50	40	40	79	119	"	1015	479	260	57
13	75	81		M34	110	43	—	—	450	82	C	—	"	5	50	—	40	—	120	"	1097	483	262	56
14	75	82		M34	110	43	—	—	449	90	C	—	"	5	51	—	41	—	126	"	1096	538	258	59
15	75	79		M34	110	43	—	—	447	78	C	—	"	4	50	—	40	—	116	"	977	473	266	68
16	75	84		M34	111	43	—	—	426	83	C	—	"	4	49	—	80	—	115	"	995	476	251	69
17	75	85		M34	110	43	36	82	457	32	C	—	"	5	50	41	40	77	121	"	1053	475	252	60
18	75	90		M36	113	43	—	—	453	86	C	—	"	7	51	—	41	—	128	"	1010	491	247	52
19	75	93		M36	114	43	—	—	455	88	C	—	"	8	52	—	40	—	130	"	1113	498	268	51
20	77	84		M38	118	43	—	—	436	87	C	—	M19	62	51	—	39	—	117	ACDEFGH	1159	508	232	55
21	77	84		M40	125	41	—	—	461	85	C	—	M21	77	57	—	38	—	117	" "	1756	523	265	55
22	77	79		M37	113	44	30	81	434	88	C	—	M21	80	58	41	38	79	112	" "	1206	524	257	57
23	78	76		M37	112	43	—	—	436	83	C	—	M21	79	50	—	35	—	116	" "	1350	505	286	61
00	78	74		M37	112	45	—	—	421	79	C	—	M21	76	50	—	38	—	112		1167	504	248	60
01	73	94		M38	93	48	—	—	429	77	C	—	M21	82	51	—	29	—	109	" "	1230	490	243	59
02	73	94		M39	120	42	—	—	474	87	C	—	M10	13	51	—	38	—	112	" "	1151	498	241	60
03	75	83		M37	121	41	—	—	425	87	C	—	M10	14	52	—	41	—	107	" "	1068	496	247	51
04	73	90		M37	122	40	27	79	457	89	C	—	M10	14	50	37	37	79	102	" "	1131	492	256	62
05	73	95		M37	122	41	—	—	448	92	C	—	M10	12	50	—	38	—	104	" "	1134	504	242	60
06	73	92		M37	122	40	—	—	463	84	C	—	M10	12	49	—	37	—	102	" "	1089	501	240	67
07	73	94		M33	120	45	—	—	462	75	C	—	M 10	11	46	—	35	—	92	" "	1051	466	221	64
08	73	96		M35	120	44	—	—	422	82	C	—	M 10	17	49	—	36	—	107	ACDGHH	1139	491	208	65

Hr	PLANT FEED			SAG MILL - BALL MILL - CYCLONE CIRCUIT					
	TARGET CONTROL	CV 01 TONNES	CONVEYORS OPERATING	SAG MILL SPEED	SAG MILL POWER	SAG MILL kW	BALL MILL kW	CV01 Density
08	250	249	2-3	198	2775	102	1520	2879	60
09	250	250	2-3	152	2749	102	1500	2832	64
10	250	250	2-3	151	2755	102	1480	2858	66
11	260	264	2-3	139	2734	101	1500	2814	70
12	260	261	2-3	178	2601	101	1500	2858	71
13	270	268	2-3	178	2695	102	1500	2863	69
14	275	276	2-3	181	2770	102	1500	2857	73
15	265	270	2-3	184	2700	101	1500	2861	74
16	250	259	2-3	186	2780	101	1500	2855	79
17	255	252	2-3	180	2711	101	1500	2862	78
18	270	266	2-3	174	2695	102	1500	2878	77
19	280	275	2-3	174	2537	101	1500	2844	66
20	290	290	2-3	172	2715	101	1500	2861	64
21	280	290	2-3	173	2545	102	1500	2829	62
22	265	278	2-3	176	2590	102	1500	2830	72
23	265	265	2-3	174	2599	102	1500	2866	69
00	265	265	2-3	177	2666	102	1500	2861	61
01	255	269	2-3	181	2720	102	1500	2876	60
02	255	253	2-5	180	2655	101	1500	2881	61
03	255	250	2-4	176	2572	102	1500	2843	69
04	255	258	2-4	177	2597	102	1500	2865	63
05	255	255	2-4	180	2695	102	1500	2876	62
06	250	254	2-4	183	2807	102	1500	2862	60
07	240	239	2-4	185	2947	102	1500	2933	52
08	245	240	2-4	175	2591	102	1500	2871	66

PLANT DOWN TIME

START FEED OFF	TIME FEED ON	TOTAL TIME	EQUIPMENT RESPONSIBLE	CAUSE / REASON

CV01 WEIGHTOMETER

				CV01 TOTAL
END OF SHIFT	132824	135022	136972	62.13
START OF SHIFT	130757	132824	135022	
TOTAL	2067	2196	1950	
Short Avg	288 tph	274 tph	244 tph	

CV 04 WEIGHTOMETER

				CV04 TOTAL
END OF SHIFT	106460	107018	107505	160.4
START OF SHIFT	105901	106460	107018	
TOTAL	559	558	487	
Short Avg	70 tph	70 tph	61 tph	

REJECT SCATS CV 04

				SCAT TOTAL
END OF SHIFT	77	77	77	0
START OF SHIFT	77	77	77	
TOTAL	0	0	0	

BALL CONSUMPTION

Size	SAG mm	BM mm
SAG	mm	—
BALL	mm	—
Magnet	kg	1 x 150

	NEW	RECYCLED
BALL	t	1 x R/C
PEBBLE	t	2 x R/C
LINERS	kg	1 x R/C

MILL AVAILABILITY

1440 — Downtime — x 100 — / 1440 = 160 %

CR 82 GAP CHECK

ADJUST (mm)

N	S	E	W

TOTAL MILLED 24 HRS: 6213

Tonnes: 6213 — Rate: 259

Total Buckets of SCATS CV02

N/S	A/S	D/S

FLASH FLOTATION

	Feed Water Addition (cubic)	Reagent Rod Level (%)	Feed Density (g/cc)	Feed Water Addition (cubic)	Reagent Tub Density (%)	Cell Froth Density (%)	Cleaner Cell Level (%)	Cleaner Froth Density (%)
TIME				FT 45			FT 48	
2300	110	78	—	—	—	20	70	—
0200	109	78					71	
0300	108	79				21	70	
0500	109	78					71	
0800	109	78				19	70	
0900	107	78		58		18	70	
1100	106	77					69	
1300	106	78		70		24	70	
1500	109	78		69		20	70	
1700	114	78		—		15	70	
1800	107	78		66		17	70	
2100	105	78		—		—	70	
2300	107	78		70		17	70	

Reversed CV20 to get M weight on a belt.

Ore getting harder, adding more pebbles water to front of SAG and some water to bottom.

07:00 hrs – Changed from FEED C to F, closing feed C

V/G down to 5201 (20.00)

Figure D.7: Module 1 Grinding Logsheet - 11 October 1997

SHIFT COMMUNICATION BOOK

NORTHPARKES

SECTION Grinding I DATE 11/10/97

Night Shift

* Everything that was in Auto is back to manual except PP061.
  - CV305 wouldn't move
  - CV301 has lost it
  - PP004 just ramps up and dawn.
* Increased frother rate by 1% (from 58 mL/min) due to high tonnes
* Cone crusher gap holding well.

Day Shift

* Having trouble keeping mill weight - up to 780 tph and thickening mill up.
* The Sag seems to be sounding the same at 175 m/w as it was yesterday at 181-182, maybe our running m/w range has decreased now we're at 1500 SVC and the Mill has rejected a few more med 150's @ over the week?

Afternoon Shift

* FE03 & 5 keep hanging up, now trying FE04.
* Adjusting CV300 to control m/weight.
* M/w took off big time, cut TPH back on track E.O.S.
* Ok sending to ST01 to help build up ST.
*

NPM24

Figure D.8: Module 1 Shift Communication Book Sheet - 11 October 1997

GRINDING MILLS & CYCLONE CLASSIFICATION MODULE 1

DATE 12/10/97 ORE TYPE/BLEND: SUL O/C/VG.

TECHNICIAN/TEAM LEADER: NS J.M / NS M.Berg.
TECHNICIAN, TEAM LEADER: DS JD / PC / DS Wally TO.
TECHNICIAN TEAM LEADER: AS PC / AS TO.

TIME	SAG MILL			PRIMARY CYCLONES						BALLMILL			SECONDARY CYCLONES							
2300	73	90		M135	120	44	—	—	422	82	C	—	M10	12	49	—	36	—	102	BCDEFGH	1139	491	208	65
2400	73	89		M135	117	44	—	—	448	79	C	—	M10	12	50	—	37	—	108	"	1161	497	223	55
0100	73	91		M135	116	44	—	—	457	82	C	—	M10	11	50	—	36	—	106	"	1185	490	229	56
0200	73	88		M135	117	43	—	—	455	97	C	—	M10	12	48	—	34	—	101	"	1132	493	216	67
0300	73	90		M135	117	46	33	81	461	84	C	—	M10	12	48	24	35	27	95	"	1052	457	217	65
0400	73	86		M135	118	42	—	—	458	86	C	—	M10	11	50	—	35	—	124	BCDEFG	1079	437	232	66
0500	73	79		M135	119	46	—	—	454	82	C	—	M15	40	50	—	36	—	126	"	1109	429	218	56
0600	73	88		M135	118	44	—	—	441	97	C	—	M15	41	50	—	35	—	126	"	1077	476	232	57
0700	73	90		M135	136	442	—	—	463	91	C	—	M15	40	50	—	35	—	130	BCDEFG	1122	493	226	58
0800	73	91		M131	122	41	32	80	410	83	C	—	M15	38	51	28	37	27	132	"	1125	469	235	53
0900	73	93		M130	117	41	—	—	937	84	C	—	M15	37	50	—	38	—	107	BCDEFGH	1217	501	236	54
1000	73	95		M130	118	40	—	—	466	87	C	—	M15	36	50	—	36	—	106	BCDEFGH	1105	385	236	56
1100	73	93		M130	118	39	30	81	492	90	C	—	M15	35	50	41	37	32	109	"	1293	440	242	57
1200	73	92		M130	114	40	—	—	475	89	C	—	M15	34	51	—	36	—	110	"	1266	519	238	55
1300	73	85		M130	113	40	—	—	465	87	C	—	M15	35	50	—	36	—	109	"	1134	447	243	51
1400	72	92		M130	112	41	—	—	484	87	C	—	M15	34	51	—	37	—	111	"	1215	510	240	54
1500	73	94		M130	113	41	—	—	443	82	C	—	M15	34	51	—	38	—	108	"	1270	486	246	54
1600	73	90		M130	113	41	—	—	461	85	C	—	M15	35	51	—	38	—	108	"	1151	478	245	56
1700	73	94		M130	112	41	—	—	448	86	C	—	M15	36	50	—	38	—	103	"	1127	488	244	56
1800	73	94		M130	112	42	27	77	469	91	C	—	M15	35	50	39	37	77	108	"	1241	522	238	61
1900	73	93		M130	112	42	—	—	466	84	C	—	M15	35	51	—	37	—	112	"	1195	525	242	57
2000	73	93		M130	112	42	—	—	451	93	C	—	M15	33	51	—	37	—	113	"	1180	490	246	57
2100	73	92		M130	112	42	—	—	464	93	C	—	M15	33	51	—	37	—	108	"	1201	490	244	58
2200	73	89		M130	112	42	—	—	465	81	C	—	M15	33	50	—	37	—	105	"	1196	498	242	59
2300	73	91		M130	112	42	—	—	4648	82	C	—	M15	33	50	—	37	—	108	BCDEFGH	1170	496	238	57

TIME	PLANT FEED: SAG/BALL CONTROL	PLANT FEED: CY 02 TONNAGE	PLANT FEED: HOURS OPERATING	SAG MILL - BALL MILL - CONE CR02: SAG LOAD WATER	SAG kW	SAG FEED RATE	BALL kW	BALL LOAD	CY04 TONNES
2100	245	200	2.4	175	2591	107	1520	2871	66
2400	240	237	3.4	176	3566	107	1500	2943	61
0100	240	245	2.35	181	2599	104	1500	2846	61
0200	240	244	2.3	186	2890	107	1500	2962	55
0300	240	207	2.3	179	2632	102	1500	2956	67
0400	240	208	2.3	177	2681	107	1500	2958	64
0500	240	238	2.3	176	2649	107	1500	2895	62
0600	240	240	2.3	175	2649	107	1500	2870	58
0700	245	202	2.3	175	2591	104	1500	2837	55
0800	250	246	2.5	176	2530	107	1500	2846	57
0900	250	250	2.5	176	2523	107	1500	2819	59
1000	250	250	2.5	179	2594	103	1500	2829	64
1100	250	252	2.5	175	2596	107	1500	2863	65
1200	250	248	2.5	176	2520	104	1500	2836	62
1300	250	250	2.4	175	2599	107	1500	2843	64
1400	250	249	2.5	179	2598	107	1500	2850	62
1500	255	253	2.5	174	2499	104	1500	2835	61
1600	250	252	2.5	174	2577	104	1500	2883	59
1700	252	252	2.4	175	2495	107	1500	2862	58
1800	252	252	2.4	175	2587	107	1500	2869	61
1900	252	252	2.4	174	2490	107	1500	2871	63
2000	253	253	2.4	176	2477	107	1500	2859	66
2100	250	252	2.4	175	2469	107	1500	2852	62
2200	245	249	2.4	175	2519	107	1500	2874	62
2300	245	245	2.4	175	2454	108	1500	2830	61

PLANT DOWN TIME

TIME FEED OFF	TIME FEED ON	TOTAL TIME	EQUIPMENT RESPONSIBLE	CAUSE/ REASON

CV02 WEIGHTOMETER — CY02 TOTAL 5863

END OF SHIFT	132466	140810	142835
START OF SHIFT	136972	138866	140810
TOTAL	4496	1944	2025
Shift Avg	237	247	257

CV 04 WEIGHTOMETER — CY04 TOTAL 1426

END OF SHIFT	107968	108452	108931
START OF SHIFT	107505	107968	108452
TOTAL	463	485	478
Shift Avg	58	61	60

REJECT SCATS CV 04 — SCAT TOTAL 0

END OF SHIFT	77	77	77
START OF SHIFT	77	77	77
TOTAL	—	0	0

BALL CONSUMPTION

SIZE	SAG TONNES	SAG kW	BALL TONNES	BALL kW
SAG MILL				
BALL MILL		1 x 155		
Weight				

	NEW	RECYCLED
BALL		1 x RIC
MILL		
Kilos		3 x RIC

MILL AVAILABILITY

1440 − Downtime = x 100 / 1440 = 100% %

CR 02 GAP CHECK

ADJUST (mm): N 5 S 11 W 10

TOTAL MILLED (t) SINCE: TONNES 586 3 RATE 244

Total Buckets of SCATS CY02

NS	AS	DS

FLASH FLOTATION

TIME	Flash Mass Addition (tonnes)	Flash Cyc Feed (%Sol)	Flash Cyc Feed Density (t/m³) MEASURED	Flash Cyc Feed (tonnes)	Flash Cyc Tail Density (%solids)	Flash Cyc Tail Density (t/m³)	Flash Cyc Tail Level (t/m³)	Flash Cyc Tail (RLA)
				FT 45			FT 46	
2300	107	78	—	70	—	17	70	—
0200	104	79					70	
0300	106	78				19	70	
0500	107	78					70	
0700	106	78				21	70	
0900	105	77					70	
1100	106	77		62		20	70	
1300	102	78		64		21	70	
1500	104	78		—		—	70	
1700	105	78		—		—	70	
1900	103	78		66		20	70	
2100	102	78		—		—	70	
2300	103	78		70		20	70	

- 21.00hrs.

FEED ON FEED OFF - SLOCKING CONSTANTLY CHECK FOR FEED, RISE UNLOCKING -

538422

Figure D.9: Module 1 Grinding Logsheet - 12 October 1997

SHIFT COMMUNICATION BOOK

NORTHPARKES

SECTION M1 GRINDING DATE 12/10/97

Night Shift

* Persisted with feeders 3 + 5, spent a couple of hours down there until all the big stuff had gone.
  Running 2 + 5 now, 5 has the softer feed but still hangs up occassionally. 3 is OK.
* Cleared build-up around lip of rougher cell a few times. Building up fairly quickly.
* Power + mill weight steady now on 250 tph.

Day Shift

* Spray filters are pretty bad. Need to be acid washed or something. Took one filter out of sag screen spray for now.
* Grind hasn't been too flash all shift.

Load steady now, for once, trouble with FC05, beginning of shift. Rick unblocking for a few hours. Ken changed to FC04, luckily no effect on mill/weight.

Afternoon Shift

* Sag screen sprays still going OK, no evidence of them blocking as yet.
* Cliff has put AS.R OK' on titles on o/s page. (or ASN Event)
* Rougher flush valve is still leaking about the same rate. New rock up there, just incase original blows out.

NPM124

Figure D.10: Module 1 Shift Communication Book Sheet - 12 October 1997

GRINDING MILLS & CYCLONE CLASSIFICATION MODULE 1

DATE: 13/10/97 ORE TYPE/BLEND: SUL O/C

TECHNICIAN: [N/S] ROD - BRIAN - JOHN
TEAM LEADER: [D/S] Hoppa

TECHNICIAN: [N/S] Jay
TEAM LEADER: [N/S] Mick

TECHNICIAN: [A/S] PC
TEAM LEADER: [A/S] [illegible]

HR	SAG MILL: MILL OUTLET WATER CV 20 (m³/h)		COMMENTS	PRIMARY CYCLONES: WATER VALVE TO FEED BOX CV 20 (%)	SLURRY FEED CV 01 (%)	SOLIDS CV 01 (%)	SLURRY SG	FLOW CV 01 (m³/h)	PRESSURE CV 01 (kPa)	SLURRY CV 01	BALLMILL: SWEEP WATER	WATER VALVE TO FEED BOX CV 20 (%)	SLURRY FEED CV 02 (%)	SOLIDS CV 02 (%)	SLURRY SG	SECONDARY CYCLONES: SOLIDS CV 03 (%)	PUMP CONFIGURATION	CYCLONES OPERATING CV 03	FLOW CV 03 (m³/h)	FLOW (%) CV 03	VOLUME TO PLANTS (%)	FLUID HEAD (kPa) CV 03
	m	mm		m³/h	mm			m³/h	kPa		m³/h	m³/h										
18	73	91		120	112	42	—	—	448	82	C	—	M15	33	50	—	37	—	109	BCDEFGH	1170	896	238	57
18	73	91		130	112	42	—	—	460	98	C	—	M15	34	50	—	37	—	105	"	1159	464	236	59
18	73	89		130	117	42	—	—	455	95	C	—	M15	34	50	—	37	—	103	"	1093	490	257	63
18	77	66		133	126	44	32	81	432	83	C	—	M15	30	48	57	36	76	96	BCDEFGH	1063	459	226	67
18	78	64		135	127	43	—	—	427	86	C	—	M15	30	48	—	38	—	117	BCDEFG	899	444	217	66
18	78	64		135	128	42	—	—	431	91	C	—	M15	32	47	—	36	—	115	"	929	466	216	66
18	79	59		135	128	42	—	—	428	81	C	—	M15	31	47	—	36	—	113	"	993	446	217	68
18	79	60		135	128	41	—	—	413	82	C	—	M15	31	47	—	37	—	112	"	988	458	218	68
18	79	60		135	128	42	32	76	449	83	C	—	M15	31	47	56	37	38	112	BCDEFG	985	449	222	66
18	79	61		105	127	42	—	—	417	88	C	—	M15	36	49	—	38	—	114	ABCDEFG	949	435	220	65
18	79	61		135	142	41	29	79	440	92	C	78	M15	28	41	43	32	78	99	ABCDEFG	959	560	249	62
18	78	67		145	125	44	—	—	469	78	C	—	M30	159	49	—	42	—	109	BCDEF	980	487	256	64
18	76	76		45	81	52	24	76	360	58	A	—	M30	83	51	56	35	78	135	BCDEF	1006	481	240	96
18	76	82		131	101	44	—	—	458	77	A	—	M31	150	50	—	38	—	138	ABDEFG	1281	521	251	58
18	76	81		131	102	44	—	—	460	79	A	—	M35	162	51	—	38	—	114	ABDEFGH	1321	491	262	59
18	76	83		134	128	44	26	74	423	75	A	94	M35	160	51	26	28	80	116	BDEFGH	1195	492	264	54
18	78	73		136	128	43	—	—	466	85	A	—	M35	161	51	—	37	—	121	BCDEFGH	1305	456	265	59
18	77	78		134	123	42	—	—	443	77	A	—	M35	162	52	—	37	—	118	" "	1371	538	287	57
18	77	78		136	127	42	—	—	449	75	A	—	M35	163	51	—	38	—	115	" "	1309	532	265	53
18	77	77		136	131	42	—	—	451	82	A	—	M20	93	51	—	37	—	120	" "	1329	548	263	52
18	77	80		137	137	42	—	—	450	80	A	—	M12	32	51	—	39	—	110	" "	1200	510	269	58
18	77	77		137	138	41	—	—	452	86	A	—	M12	39	52	—	39	—	110	" "	1172	520	247	57
18	77	78		137	139	41	24	74	427	86	A	—	M12	34	51	39	31	78	115	ABCDEFG	1311	499	247	59
18	77	74		136	137	42	—	—	440	84	A	—	M12	33	50	—	38	—	112	ABCDEFG	1273	510	261	61
18	77	71		136	137	42	—	—	424	85	A	—	M12	33	50	—	38	—	110	ABCDEFG	1227	503	251	57

4 - FLASH FLOTS OFF LINE AT 0930 - TO CHANGE OUT VALVE.

FEO2 FEEDING ERRATICALLY THEN THINGS UP SWAMPED TO FEO4 / 11 Cg. CONCS O/FEO2, WENT TO A'

* O/S CHECKED AT 0820 @ 17— Reset to [illegible]

PLANT FIXED

HR	SAG MILL CONTROL (kW)	CYCLONES (NUMBER)	PRESSURE (BAR) OPERATING
18	245	245	2·4
18	245	245	2·4
18	240	242	2·4
18	220	225	2·3
18	220	220	2·3
18	220	220	2·3
18	235	233	2·3
18	230	226	2·3
18	230	230	2·3
18	230	230	2·3
18	240	239	2·3
18	260	257	2·3
18	260	260	2·3
18	260	260	2·3
18	260	260	2·3
18	260	260	2·3
18	260	260	2·3
18	260	260	2·3
18	260	260	2·4
18	250	258	2·4
18	240	249	2·4

SAG MILL - BALL MILL - CONE CRS2

SAG MILL LOAD (tonnes)	SAG MILL (kW)	SAG MILL FEED RATE (tph)	SAG MILL SWEEP WATER (m³/h)	BALL MILL (kW)	CYCLONES (NUMBER)
175	2459	107	1500	2880	61
176	2463	108	1500	2854	63
176	2491	107	1500	2839	64
175	2492	107	1500	2833	58
179	2491	108	1500	2805	51
176	2499	108	1500	2791	53
171	2573	107	1500	2964	55
179	2469	107	1500	2981	59
181	2567	107	1500	2915	64
181	2640	107	1500	2899	68
179	2654	107	1500	2875	69
175	2504	107	1500	2857	68
173	2419	107	1500	2951	53
173	2495	108	1500	2943	55
177	2458	107	1500	2934	54
173	2421	107	1500	2915	51
171	2430	107	1500	2929	51
173	2438	107	1500	2825	51
173	2589	108	1500	2831	48
173	2529	108	1500	2863	49
172	2529	108	1500	2863	49
174	2491	108	1500	2836	47
174	2547	108	1500	2862	52
175	2502	108	1500	2864	58
175	2538	108	1500	2891	57
177	2496	107	1500	2880	59

PLANT DOWN TIME

TIME FEED OFF	TIME FEED ON	TOTAL TIME	REQUIREMENT INDISPENSIBLE	CAUSE / REASON

CV02 WEIGHTOMETER

				CV02 TOTAL
END OF SHIFT	144676	146610	148707	5372
START OF SHIFT	142835	144676	146640	
TOTAL	1841	1969	2067	
RUN AVG	230	295	258	

CV04 WEIGHTOMETER

				CV04 TOTAL
END OF SHIFT	109399	109857	110277	1341
START OF SHIFT	108931	109399	109857	
TOTAL	468	458	420	
RUN AVG	59	57	53	

REJECT SCATS CV 04

				REJECT TOTAL
END OF SHIFT	77	77	77	0
START OF SHIFT	77	77	77	
TOTAL	0	—	0	

BALL CONSUMPTION

		NEW	RECYCLED
SAG MILL	M/S		
	A/S	1 x 150	
Weight	M/S		
	A/S	1 x 150	
BALL MILL	M/S		
	A/S		
Weight	M/S		
	A/S		

1 = RECYCLED
5 x R/S

MILL AVAILABILITY

1440 − Downtime = x 100 / 1440 = %

CR 02 GAP CHECK

ADJ/ST (mm) @ 01:30

N 15 E 19 E 12 W 11

TOTAL MILLED 24 HRS

TONNES: 5372
RATE: 245

Total Buckets of SCATS CV02

M/S	A/S	D/S

FLASH FLOTATION

TIME	Flash Water Addition (m³/h)	Reagent Cell Level % TOTAL	Flash Cleaner Cell Level (mm)	Reagent Addition (cm³/min)	Reagent Cell Density % solids	Cell Froth Quality % solids	Cleaner Cell Level % Full	Conc Grade (Cu)
							FT 45	FT 48
2300	103	78		70		20	70	
0100	104	78					70	
0300	104	77				21	70	
0500	104	77					68	
0700	105	78				20	69	
0900	OFF	LINE			OFF	LINE		
1100	100	77				20	70	
1300	102	78	—	40	—	20	69	
1500	101	78					71	
1700	100	78		65		25	71	
1900	112	78		—		20	70	
2100	112	78		—		18	70	
2300	112	78				18	70	

Figure D.11: Module 1 Grinding Logsheet - 13 October 1997

SHIFT COMMUNICATION BOOK

NORTHPARKES

SECTION GRINDING T DATE 13/10/97

Night Shift BOLT ON FEED END OF SAG HAS STARTED TO LEAK E.O.S.

* About 6 leakers by 12:30. Dropped tonnes, thickened mill and change to feeder 3 (coarser) to Stop the bolts leaking.
(Hoping there will be an inspection in the morning.)
Running mill weight between 172 - 176 t over weekend. On high tonnes it all takes off if weight gets over 180 t. Running 73% density to front of mill to get this.

Day Shift CV20 ROCK BOX HAS A HOLE IN IT HUBBO IS FIXING.

* MILL WAT ↑ 181 TONNES ↓ S.O.S. THINNED MILL BY 1%. NO LEAKING BOLTS. TONNES ↑ 10TPH. THINNED MILL BY 1%. NO LEAKING BOLTS. RESET O/SIZE TO 10mm FROM 11 THINNED MILL BY ANOTHER 1%. NO LEAKING BOLTS. TPH ↑ TO 260. MILL WT STEADY AT 174 BUT DECIDED TO DROP AGAIN SO THINNED MILL BY 1%. 77% STILL ORDERS @ 78%. SHUTDOWN CANNED TILL TOMORROW. DUMPED FLASH FLOTS. FIXED VALVE. LOTS OF TROUBLE WITH DENSITY & FLOW TO FLOATS. ALL O.K NOW.

Afternoon Shift RUNNING PRIMARY CYCLONE (A)

- V/G bleeding onto STOR. Then transfer back to STOR at Midnight
- Took out 1 filter on B/Mill sprays, going good so far
- C9'H' bit coarse O/flow swapped with 'A'

Figure D.12: Module 1 Shift Communication Book Sheet - 13 October 1997

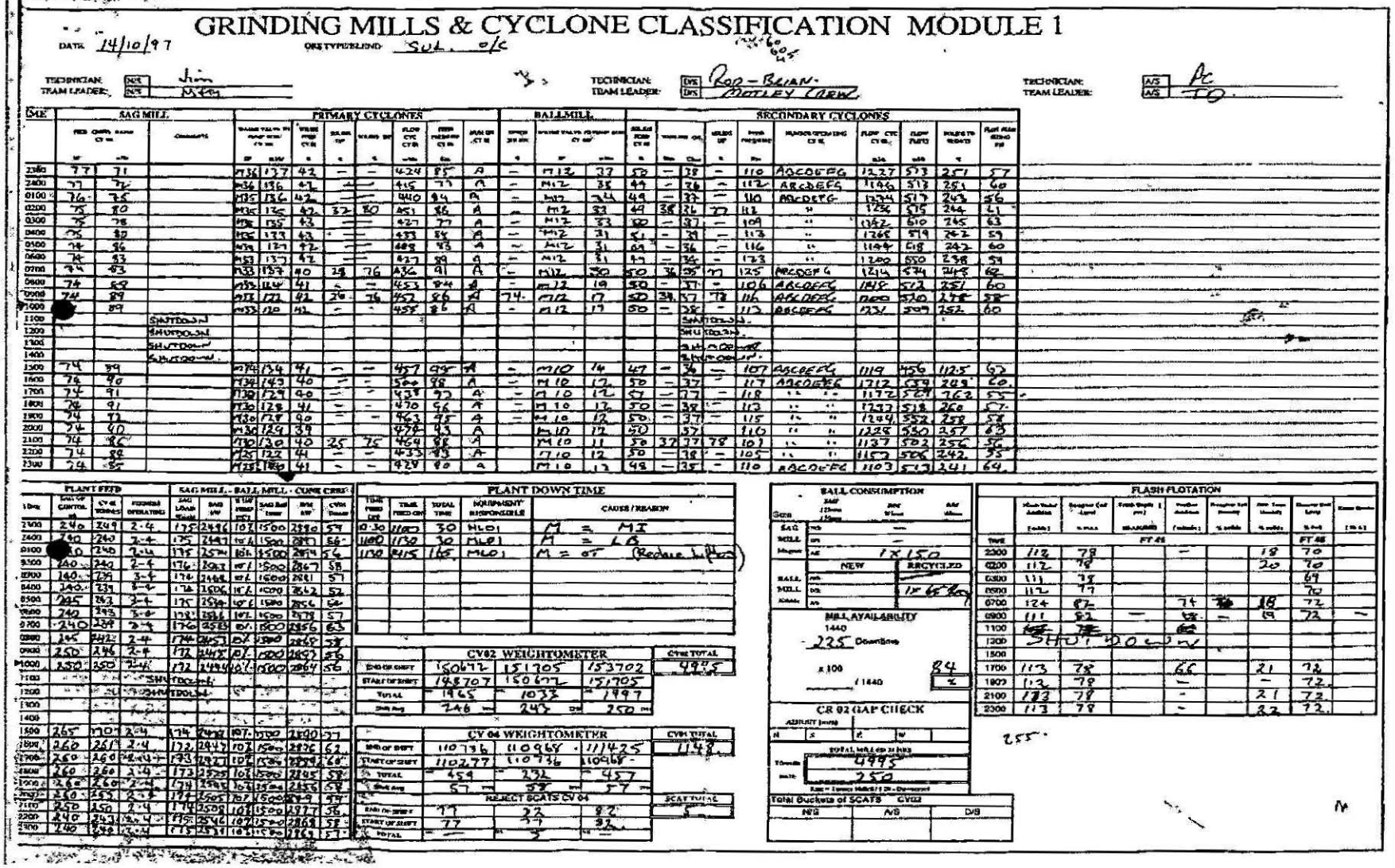

GRINDING MILLS & CYCLONE CLASSIFICATION MODULE 1

DATE: 14/10/97 ORE TYPE/BLEND: SUL. o/c

TECHNICIAN: NS Jim — TEAM LEADER: NS Mac

TECHNICIAN: DS Rod – Brian. — TEAM LEADER: DS Motley Crew

TECHNICIAN: AS Ac — TEAM LEADER: AS Ed.

TIME	SAG MILL			PRIMARY CYCLONES							BALL MILL			SECONDARY CYCLONES						
	FEED CONTROL TPH	FEED CONTROL m³/h	COMMENTS	WATER VALVE % / WATER FLOW m³/h	PRESS CYC kPa	SOLIDS %	WATER m³/h	FLOW CYC m³/h	FEED PRESSURE kPa	RUN OF CYC m	SPEED rpm	WATER VALVE % / WATER FLOW m³/h		SOLIDS TPH	WATER m³/h	SOLIDS %	FEED PRESSURE kPa	NUMBER OF RUNNING CYC	FLOW CYC m³/h	FLOW RATIO	POWER TO MOTORS kW	PLANT FEED SIZING P80
2300	77	71		136	137	42	—	—	424	85	A	—	M12	37	58	—	28	—	110	ABCDEFG	1227	513	251	57
2400	77	74		136	136	41	—	—	415	79	A	—	M12	38	49	—	26	—	112	ABCDEFG	1196	513	251	60
0100	76	75		135	136	42	—	—	440	84	A	—	M12	34	49	—	32	—	110	ABCDEFG	1244	513	243	56
0200	75	80		136	135	43	32	80	451	86	A	—	M12	33	49	38	26	32	111	"	1254	515	244	61
0300	75	78		136	135	43	—	—	427	77	A	—	M12	33	50	—	37	—	109	"	1242	510	245	63
0400	75	80		136	133	43	—	—	433	85	A	—	M12	31	51	—	38	—	113	"	1265	519	262	59
0500	74	86		135	131	42	—	—	408	93	A	—	M12	31	49	—	36	—	116	"	1199	518	242	60
0600	76	83		133	133	42	—	—	427	89	A	—	M12	31	49	—	36	—	123	"	1209	550	238	59
0700	74	93		133	137	40	28	76	436	91	A	—	M12	30	50	36	35	33	125	ABCDEFG	1214	534	245	62
0800	74	89		135	134	41	—	—	453	94	A	—	M12	19	50	—	37	—	106	ABCDEFG	1218	512	251	60
0900	74	89		133	132	41	28	76	457	96	A	74	M12	17	50	38	37	33	116	ABCDEFG	1200	530	238	58
1000		89		133	130	42	—	—	455	86	A	—	M12	17	50	—	38	—	113	ABCDEFG	1231	509	252	60
1100			SHUTDOWN														SHUTDOWN.						
1200			SHUTDOWN														SHUTDOWN.						
1300			SHUTDOWN														SHUTDOWN.						
1400			SHUTDOWN.														SHUTDOWN.						
1500	74	89		134	134	41	—	—	457	95	A	—	M10	14	47	—	34	—	107	ABCDEFG	1119	456	1125	62
1600	74	90		134	143	40	—	—	500	98	A	—	M10	17	50	—	37	—	117	ABCDEFG	1212	489	209	60
1700	74	91		130	129	40	—	—	438	92	A	—	M10	12	47	—	37	—	118	" "	1172	484	262	55
1800	76	91		130	128	41	—	—	470	96	A	—	M10	17	50	—	38	—	113	" "	1227	518	260	57
1900	74	93		130	128	40	—	—	463	95	A	—	M10	12	50	—	37	—	115	" "	1244	552	258	58
2000	74	90		130	129	39	—	—	478	93	A	—	M10	17	50	—	37	—	110	" "	1228	550	257	63
2100	74	86		130	130	40	25	76	464	88	A	—	M10	11	50	32	37	28	103	" "	1137	502	256	56
2200	74	88		125	122	41	—	—	433	85	A	—	M10	12	50	—	38	—	105	" "	1157	526	242	55
2300	74	85		135	130	41	—	—	429	80	A	—	M10	13	48	—	35	—	110	ABCDEFG	1103	513	241	64

TIME	PLANT FEED			SAG MILL - BALL MILL - CONE CIRC							PLANT DOWN TIME				
	SAG FEED CONTROL TPH	SAG FEED CONTROL m³/h	FEEDING OPERATORS	SAG LOAD %	SAG kW	SAG MILL TEMP °C	SAG Ball Tower	BALL kW	CYC FEED kPa		TIME FIXED OFF	TIME FIXED ON	TOTAL TIME	EQUIPMENT RESPONSIBLE	CAUSE / REASON
2300	240	249	2-4	175	2496	107	1500	2990	59		1030	1100	30	ML01	M = MI
2400	240	240	2-4	175	2487	106	1500	2951	56		1100	1130	30	ML01	M = LB
0100	240	240	2-4	175	2574	106	1500	2914	56		1130	1415	165	ML01	M = OT (Reduce Load)
0200	240	240	2-4	176	2583	107	1500	2867	58						
0300	240	239	2-4	176	2488	107	1500	2881	57						
0400	240	239	2-4	176	2506	106	1500	2862	52						
0500	235	243	2-4	175	2534	107	1500	2856	60						
0600	240	243	2-4	173	2584	107	1500	2878	57						
0700	240	239	2-4	176	2585	107	1500	2956	63						
0800	245	242	2-4	176	2457	107	1500	2868	58						
0900	250	246	2-4	177	2445	107	1500	2897	56						
1000	250	250	2-4	172	2496	107	1500	2864	56						
1100			SHUTDOWN												
1200			SHUTDOWN												
1300															
1400															
1500	245	1107	2-4	174	2492	107	1500	2890	57						
1600	260	261	2-4	172	2447	107	1500	2876	62						
1700	260	260	2-4	173	2427	107	1500	2879	60						
1800	260	260	2-4	173	2529	107	1500	2905	58						
1900	260	260	2-4	174	2595	107	1500	2855	58						
2000	250	253	2-4	174	2505	107	1500	2879	59						
2100	250	250	2-4	174	2509	107	1500	2877	56						
2200	240	243	2-4	175	2546	107	1500	2868	58						
2300	240	242	2-4	173	2531	107	1500	2865	57						

CV02 WEIGHTOMETER				CYC TOTAL
END OF SHIFT	150672	151705	153702	4995
START OF SHIFT	148707	150677	151705	
TOTAL	= 1965	= 1028	= 1997	
24HR Avg	246	247	250	

CV 04 WEIGHTOMETER				CYC TOTAL
END OF SHIFT	110736	110968	111425	1148
START OF SHIFT	110277	110736	110968	
TOTAL	= 459	= 232	= 457	
24HR Avg	57	58	57	

REJECT SCATS CV 04				SCAT TOTAL
END OF SHIFT	77	22	82	5
START OF SHIFT	77	77	82	
TOTAL	= —	= 5	= —	

BALL CONSUMPTION

GRIND	2400 / 125mm / 12mm	2000 W/mm	2400
SAG	NO	—	
BALL	NO	—	
Magnet	NO	1X150	

	NEW	RECYCLED
BALL	NO	
MILL	NO	1X 65 Kg
Kibble	NO	

MILL AVAILABILITY

1440

225 Down time

x 100 = 84 %

/ 1440

CR 02 GAP CHECK

ASSAY (mm): N — S — W —

TOTAL MILLED IN 24 HRS

4995

250

Total Buckets of SCATS CV02

N/B	A/S	D/B

FLASH FLOTATION

TIME	Mass Pulled Auxiliary (tonnes)	Reagent Cell Level (% mass)	Froth Depth 1 (mm) (BLANKED)	Froth Depth 2 (mm) (mobile)	Froth Depth 3 (% solids)	Flash Time Variable (% solids)	Flash Feed Solids (% w/w)	Flash Feed Size (FF45)
				FT 45				FT 45
2300	113	78		—		18	70	
0200	112	78				20	70	
0300	111	78					69	
0500	112	77					70	
0700	124	87		74	78	18	72	
0900	111	82	—	58	—	19	73	—
1100	SHUT DOWN							
1300								
1500								
1700	113	78		66		21	74	
1900	113	78		—		—	72	
2100	113	78		—		21	72	
2300	113	78		—		22	72	

255

Figure D.13: Module 1 Grinding Logsheet - 14 October 1997

SHIFT COMMUNICATION BOOK

NORTHPARKES

SECTION GRINDING I DATE 14/10/97.

Night Shift

* Changed back to Feeder 3. Hung up a few times but kept with it. (Until 06:20)
* Feeder 5 is really bad. Will pay to have someone down there and run it through till all the big stuff is gone (took me 2 hours with Feeder 3 the other night)
* Busy with Mod 2 shutdown from 3am → so not much else done.
* Feeders 3+5 both very bad from 0500 onwards.

Day Shift

* SHUTDOWN AT 1030 FOR MILL INSPECTION 2 WORN Lifters & 1 Torn KEO SHELL LINER - Replaced, Retorqued ALL FEED END BOLTS & ALL LOADING DISCHARGE END BOLTS
MILL INSPECTION 17% LOAD & 12% BALL CHARGE

Afternoon Shift

2nd process water pump on (for Mod 2), backed off S.P.'s throughout circuit, including f/flots (cleaner water just finishing, also f/flots is floating it off too good, & cons lifts not handling flow, backed off air in cleaner.
• 23:00 - U/G expecting to hoist within the hour (just me).

NPM2

Figure D.14: Module 1 Shift Communication Book Sheet - 14 October 1997

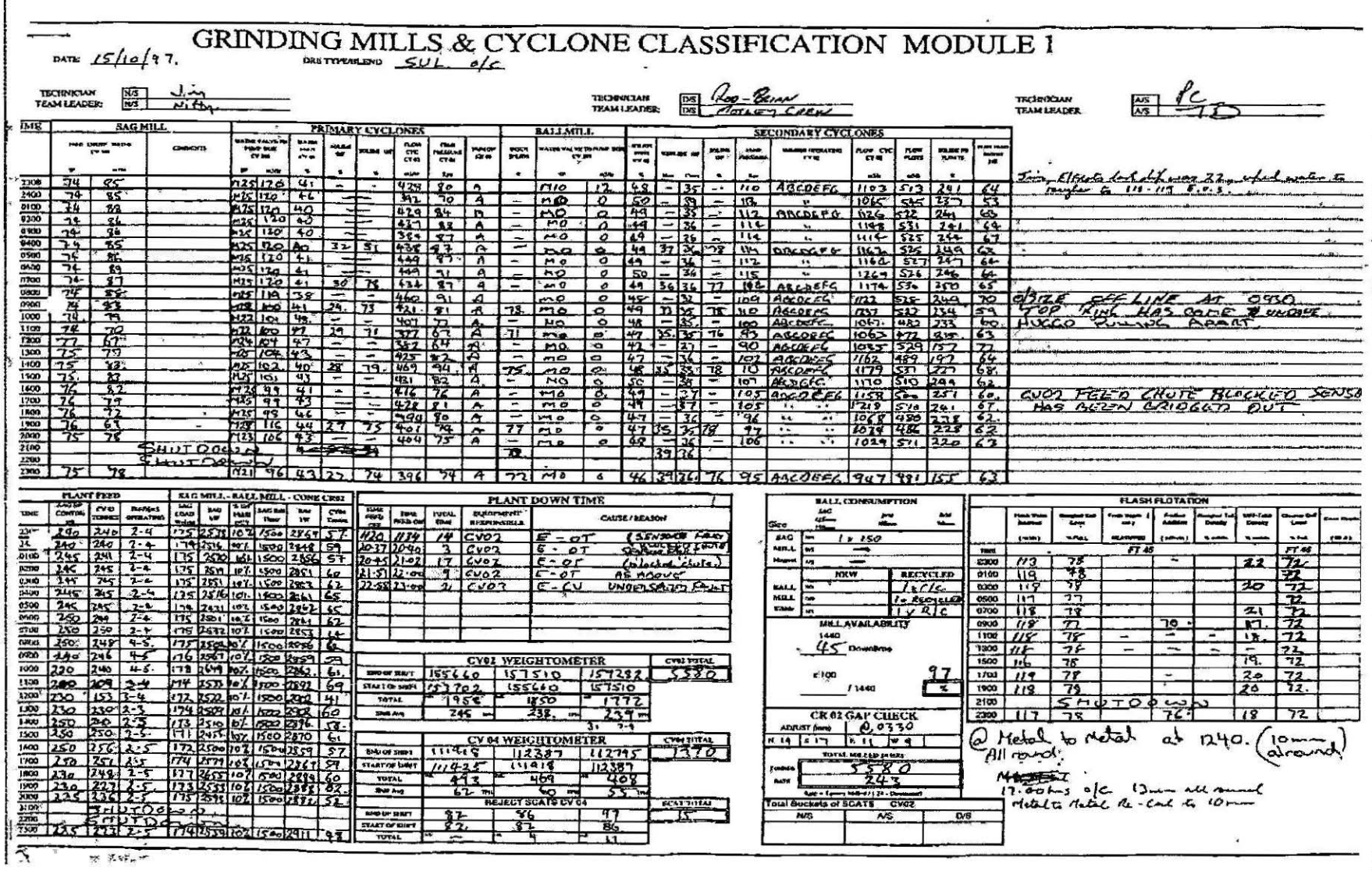

GRINDING MILLS & CYCLONE CLASSIFICATION MODULE 1

DATE: 15/10/97. DRS TYPE/BLEND: SUL. o/c

TECHNICIAN / TEAM LEADER: NS / NS — Jim / Nitty

TECHNICIAN / TEAM LEADER: DS / DS — Rod - Brian / Ashley Chris

TECHNICIAN / TEAM LEADER: A/S / A/S — PC / TD

TIME	SAG MILL			PRIMARY CYCLONES						BALL MILL			SECONDARY CYCLONES						
2300	74	85		M25	176	41	—	—	428	80	A		M10	12	48	—	35	--	110	ABCDEFG	1103	513	241	64
2400	74	85		M25	170	46	—	—	392	70	A		M10	0	50	—	38	—	118	"	1065	525	237	53
0100	74	88		M25	170	40	—	—	429	84	A		M10	0	49	—	35	—	112	ABCDEFG	1026	532	244	66
0200	74	86		M25	170	40	—	—	427	88	A		M10	0	49	—	36	—	114	"	1098	531	241	64
0300	74	86		M25	170	40	—	—	384	87	A		M10	0	49	—	36	—	114	"	1114	525	242	67
0400	74	85		M25	170	40	32	51	438	93	A		M10	0	48	37	36	78	114	ABCDEFG	1162	525	249	62
0500	76	86		M25	170	41	—	—	449	97	A		M10	0	49	—	36	—	112	"	1160	527	247	64
0600	76	89		M25	170	41	—	—	449	91	A		M10	0	50	—	36	—	115	"	1264	526	246	64
0700	74	87		M25	170	41	30	75	434	87	A		M10	0	49	36	36	77	108	ABCDEFG	1174	530	250	65
0800	74	85		M25	118	38	—	—	460	91	A		M10	0	45	—	32	—	109	ABCDEFG	1122	525	249	70
0900	76	93		M28	180	41	24	73	421	81	A	78	M10	0	49	33	35	78	110	ABCDEFG	1057	522	234	59
1000	74	79		M22	101	48	—	—	407	72	A	—	M10	0	48	—	35	—	100	ABCDEFG	1067	483	233	60
1100	78	70		M22	100	49	29	71	377	67	A	71	M10	0	47	35	35	76	93	ABCDEFG	1062	472	235	63
1200	77	67		M24	104	47	—	—	382	64	A	—	M10	0	42	—	27	—	90	ABCDEFG	1035	528	157	77
1300	75	79		M20	104	43	—	—	425	82	A	—	M10	0	47	—	36	—	102	ABCDEFG	1162	489	197	64
1400	75	82		M25	102	40	28	79	469	94	A	75	M10	0	48	33	35	78	110	ABCDEFG	1179	531	227	68
1500	75	82		M25	101	43	—	—	421	82	A	—	M10	0	50	—	36	—	107	ABCDEFG	1170	510	294	62
1600	76	82		M25	99	41	—	—	416	76	A	—	M10	0	49	—	37	—	105	ABCDEFG	1158	500	257	60
1700	76	79		M25	97	43	—	—	428	81	A	—	M10	0	49	—	37	—	105	" "	1219	516	241	67
1800	76	72		M25	98	46	—	—	394	80	A	—	M10	0	47	35	36	78	97	" "	1078	480	228	62
1900	76	69		M25	116	44	27	75	401	74	A	77	M10	0	47	35	36	78	97	" "	1079	486	228	62
2000	75	78		M23	106	43	—	—	404	75	A	—	M10	0	48	—	36	—	106	" "	1029	511	220	63
2100			SHUTDOWN																					
2200			SHUTDOWN																					
2300	75	78		M21	96	43	22	74	396	74	A	72	M10	6	46	39	36	76	95	ABCDEFG	947	981	155	62

Jim, Elfesta left at 1430 hrs, refuel water to maybe 6 1/2 - 11 F.O.S.

0/SIZE EFF LINE AT 0930. TOP RING HAS COME OFF HUGGO SUNDAY AGAIN.

CV07 FEED CHUTE BLOCKED SENSOR HAS BEEN BRIDGED OUT

@ Metal to Metal at 1240. (10mm around). All round. 17.00 hrs o/c 13mm all round Metal to Metal Re-Cal to 10mm

PLANT FEED

TIME	2300 CONTROL	CV01 TONNES	BUCKETS OPERATING	SAG MILL - BALL MILL - CONE CR02					
				SAG LOAD	SAG kW	% SAG MILL Filled	SAG Mill Time	Total kW	CV04 Cones
2300	240	240	2-4	175	2578	10.2	1500	2864	57
24	240	240	2-4	179	2516	10.1	1500	2848	59
0100	245	241	2-4	175	2520	10.1	1500	2866	57
0200	245	245	2-4	175	2519	10.1	1500	2851	60
0300	244	245	2-4	175	2551	10.1	1500	2863	62
0400	244.5	245	2-4	175	2516	10.1	1500	2841	65
0500	245	245	2-4	174	2431	10.2	1500	2842	65
0600	250	248	2-4	175	2501	10.2	1500	2844	62
0700	250	250	2-4	175	2492	10.1	1500	2853	64
0800	250	248	4-5	175	2508	10.1	1500	2886	66
0900	240	246	4-5	176	2567	10.1	1500	2859	58
1000	220	240	4-5	178	2649	10.1	1500	2862	61
1100	200	209	3-4	174	2533	10.1	1500	2892	69
1200	230	153	3-4	172	2532	10.1	1500	2892	41
1300	230	230	2-3	174	2509	10.1	1500	2902	60
1400	250	200	2-3	173	2510	10.1	1500	2896	58
1500	250	250	2-3	171	2495	10.1	1500	2870	61
1600	250	256	2-5	172	2500	10.2	1500	2859	57
1700	250	251	2-5	174	2479	10.2	1500	2867	59
1800	230	244	2-5	177	2455	10.1	1500	2899	60
1900	230	227	2-5	173	2533	10.2	1500	2898	62
2000	225	226	2-5	175	2518	10.1	1500	2872	58
2100			SHUTDOWN						
2200			SHUTDOWN						
2300	225	223	2-5	174	2539	10.2	1500	2911	58

PLANT DOWN TIME

TIME FROM	TIME TO	TOTAL TIME	EQUIPMENT RESPONSIBLE	CAUSE / REASON
1120	1134	14	CV07	E - OT (SENSOR FAULT)
2037	2040	3	CV07	E - OT (SENSOR FAULT)
20+5	21-02	17	CV07	E - OT (blocked chute)
21-51	22-08	9	CV07	E - OT AS ABOVE
22-55	23-06	31	CV07	E - CV UNDER SAFETY PAINT

CV02 WEIGHTOMETER

				CV02 TOTAL
END OF SHIFT	155660	157510	157282	5580
START OF SHIFT	153702	155660	157510	
TOTAL	= 1958	= 1850	= 1772	
Shift Avg	245 tph	238. tph	239 tph	

CV04 WEIGHTOMETER

				CV04 TOTAL
END OF SHIFT	111428	112387	112795	1370
START OF SHIFT	111425	111418	112387	
TOTAL	443	469	408	
Shift Avg	62 tph	60 tph	53 tph	

REJECT SCATS LV 04

				SCATS TOTAL
END OF SHIFT	87	86	97	15
START OF SHIFT	82	87	86	
TOTAL	= 5	= -1	= 11	

BALL CONSUMPTION

Size	SAG	MILL	Magnet
SAG	1 x 150		
MILL	→		
Magnet			

	NKW	RECYCLED
BALL		1 x 150
MILL		1 x RECYCLED
Scats		1 x R | C

MILL AVAILABILITY

1440 − 45 DownTime = 1395

1395 / 1440 = 97 %

CR 02 GAP CHECK

ADJUST from: 0.0330

N 14	E 17	N 11	W 9

TONNES: 5580

RATE: 243

Total Buckets of SCATS CV02

N/S	A/S	D/B

FLASH FLOTATION

TIME	Flash Wash Sandvik (m3/h)	Flash Wash Sandvik (%SOL)	Flash Wash 1 Sandvik (%SOL)	Flash Wash 1 Sandvik (REAGENTS)	Flash Addition Sandvik (ml/min)	Flash Tail Density Sandvik (%SOL)	Flash Tail Density Sandvik (%SOL)	Flash Tail Grind Sandvik (%+45)	Flash Grind Cell Level Sandvik (%SOL)	Flash Froth Depth Sandvik (MM)
TIME	-	FT 46							FT 46	
0000	113	28		-			22		72	
0100	119	28							72	
0200	119	29					20		72	
0500	117	27							72	
0700	118	28					21		72	
0900	118	27		30			17.		72	
1100	118	28	-	-	-		18.		72	
1300	115	26	-	-	-		-		72	
1500	116	28					19.		72	
1700	119	28		-			20		72	
1900	118	29		-			20		72	
2100		SHUTDOWN								
2300	117	28		26			18		72	

Figure D.15: Module 1 Grinding Logsheet - 15 October 1997

SHIFT COMMUNICATION BOOK

NORTHPARKES

SECTION M1 GRINDING DATE 15 / 10 / 97

Night Shift

* GOOD RUN. DIDN'T CHANGE A THING EXCEPT TO INCREASE TONNES BY 10.
* Cons hopper bogged again, "Luckily", the blowers tripped out in float which stopped the bubbles and gave me a chance to really clean it out.
* Topped up ball charger at E.O.S., should now be right all day.
* Running SAG at 74% density but Tim would like it thicker.

Day Shift

* RAN FEEDERS 3 & 5, ~~ONE~~ TWO HANG UP ON 5,
* O/SIZE CRUSHER OFF LINE FROM 0930 TOP Rock Cone undone, HUCCO ROLLING APART TO Replace. V TPH, MILL VAT coming ↑
* O/SIZE BACK ON LINE @ 1130 NEW MANTLE & CONE.
* SHUTDOWN ON FAULTY BLOCKED CHUTE SENSOR (CV02)

NOTE: TOSHI WOULD LIKE 2 BALLMILL DISCHARGE

Afternoon Shift DENSITYS DONE PER SHIFT (AS PER RED BOOK)

* ST01 getting slower pulling in mainly large ore, backing off TPH.
* Tom advises to run sag on the thicker side to minimise after/liner wear. thicker
* Sensor on CV02 feed chute blocked twice, Ronnie seems to have fixed problem. (ITS NOW BRIDGED).
* 12:00 Wally blending with U/G on ST01, expect a change.
* Keep eye on accumulator (leaking oil on CR02)

Figure D.16: Module 1 Shift Communication Book Sheet - 15 October 1997

GRINDING MILLS & CYCLONE CLASSIFICATION MODULE 1

DATE 16/10/97 ORE TYPE/BLEND: SUL O/C / UG.

TECHNICIAN: D/S Rod - Brian
TEAM LEADER: D/S Morris Crew

TECHNICIAN: A/S Rick
TEAM LEADER: A/S Ian

HR	SAG MILL			PRIMARY CYCLONES							BALL MILL			SECONDARY CYCLONES								
01	75	78		1721	96	43	27	74	296	74	A	72	M0	0	46	39	26	76	93	ASCDEFG	947	481	155	63
02	75	79		M21	99	48	—	—	287	70	A	—	M0	0	45	—	34	—	83	"	955	458	105	79
03	75	—		M21	99	45	—	—	307	—	A	—	M0	0	47	—	35	—	95	"	1001	470	209	65
04	75	78		M28	102	44	30	76	303	80	A	—	M0	0	48	37	26	77	99	"	1073	485	223	61
05	75	80		M28	103	42	—	—	311	80	A	—	M0	0	49	—	37	—	103	"	1171	495	227	66
06	75	78		M28	104	43	—	—	306	77	A	—	M0	0	49	—	37	—	101	"	1132	483	233	63
07	75	79		M28	103	43	—	—	311	80	A	—	M0	0	49	—	36	—	105	"	1126	500	234	66
08	75	82		M28	103	45	—	—	317	81	A	—	M0	0	50	—	36	—	108	"	1113	482	232	62
09	75	86		M28	102	44	31	75	310	76	A	—	M0	0	50	38	38	77	107	ABCDEFG	1119	495	235	56
10	75	93		M28	102	44	—	—	330	79	A	—	M0	0	50	—	36	—	108	ABCDEFG	1161	509	239	59
11	75	81		M28	99	44	32	76	323	77	A	75	M0	0	51	38	40	77	106	ABCDEFG	1059	496	249	57
12	75	88		M28	105	43	—	—	340	73	A	—	M0	0	51	—	39	—	99	ABCDEFG	1055	498	248	55
13	75	88		M28	105	43	29	79	327	75	A	78	M0	0	52	36	40	79	103	ABCDEFG	1106	486	256	51
14	77	71		M28	114	47	—	—	302	73	A	—	M0	0	49	—	39	—	110	ABCDEFG	974	402	242	0
15	79	75		M29	119	46	—	—	3281	71	A	—	M0	0	50	—	40	—	114	ABCDEF	1051	483	249	55
16	80	65		M29	114	46	—	—	3269	65	A	—	M0	0	50	—	39	—	110	ABCDEF	1044	464	253	55
17	77	82		M28	117	45	30	78	319	78	A	76	M0	0	50	36	39	78	114	ABCDEF	1082	487	248	58
18																						
19																						
20																						
21																						
22																						
23																						
24																						

HR	PLANT FEED			SAG MILL - BALL MILL - CONE CRS					
	SAG MF Control	CV01 Tonnes	Product Specification	SAG Load	SAG+ SW	% SAG Power Draw	SAG Ball Tons	BM SW	CV01 Tonnes
01	235	223	2-5	178	2533	80%	1500	2911	48
02	235	116	2-3	175	2599	14%	1500	2897	24
03	235	235	2-3	177	2623	16%	1500	2897	52
04	235	205	2-3	177	2639	16%	1500	2915	58
05	235	234	2-5	176	2597	14%	1500	2869	57
06	235	235	2-5	179	2593	18%	1500	2867	57
07	240	239	2-5	178	2577	19%	1500	2824	53
08	245	242	2-5	175	2585	16%	1500	2859	55
09	245	245	2-5	175	2595	16%	1500	2837	58
10	245	248	2-2-5	179	2580	18%	1500	2845	57
11	255	258	2-2-5	180	2576	16%	1500	2852	53
12	265	263	2-5	172	2648	18%	1500	2851	55
13	265	266	2-5	176	2608	16%	1500	2864	58
14	265	261	2-3	172	2593	10%	1500	2874	51
15	265	265	2-3	172	2643	16%	1500	2845	56
16	265	265	2-3	174	2557	16%	1500	2856	59
17	265	265	2-3	172	2598	16%	1500	2845	65
18									
19									
20									
21									
22									
23									
24									

PLANT DOWN TIME

TIME FEED OFF	TIME FEED ON	TOTAL TIME	EQUIPMENT - RESPONSIBLE	CAUSE / REASON
23:00	23:06	6	CV07	E-CV UNDERSIZED FINES
23:10	23:32	22	CV07	AS ABOVE
1123	1128	5	CV02	O = LT

CV02 WEIGHTOMETER — CV02 TOTAL

END OF SHIFT	161085	162142	
START OF SHIFT	159282	161085	1681112
TOTAL	= 1803	= 2057	=
Shift Avg	225 TPH	257 TPH	TPH

??

CV04 WEIGHTOMETER — CV04 TOTAL

END OF SHIFT	113216	113656	
START OF SHIFT	112795	113216	113656
TOTAL	= 421	= 440	=
Shift Avg	53 TPH	55 TPH	TPH

REJECT SCATS CV 04 — SCAT TOTAL

END OF SHIFT	49	102	
START OF SHIFT	47	99	103
TOTAL	= 2	= 3	=

BALL CONSUMPTION

Size	SAG	MILL	Product

	NEW	RECYCLED
BALL MILL		
Kibble		1x Recyc

MILL AVAILABILITY

1440

Downtime

x 100

/ 1440 = %

CR 02 GAP CHECK

ADJUST (mm)

N S E W

TOTAL MILLED in HRS

TONNES

RATE

Total Buckets of SCATS CV02

N/S	A/S	D/S

FLASH FLOTATION

TIME	Feed Water Addition (ml/min)	Feed Density (g/l)	Feed Depth (m)	Product Addition (ml/min)	Reagent Add Density (g/l)	Reagent Add Rate (ml/min)	Product Grind Size (% +106)	Comments (FF1&2)
		FF 1&2					FF 1&2	
2300	117	78		76		18	72	
0100	121	78				19	77	
0300	111	77		74			71	
0500	112	78					73	
0700	113	77				30	72	
0900	107	77	—	68	—	19	71	
1100	106	78	—	—	—	17	71	
1300	105	77	—	—	—	—	72	
1500						15		
1700								
1900								
2100								
2300								

Gap 10 - 11 mm @ 0700

Figure D.17: Module 1 Grinding Logsheet - 16 October 1997

NORTHPARKES

IFT COMMUNICATION BOOK

TION Mt GRINDING DATE 16 / 10 / 97

Shift

- OK run
- Big stuff coming through Feeders 3+5 again - getting worse throughout the shift.
- Cone crusher holding well
- Feeders playing up last ½ hour of shift.
- Accumulator on CVO2 still leaking oil
- Ballmill kW ranging between 2860 - 2900 so no extra balls put in.

Shift

FEEDERS 3-4-5 HANGING UP. 3 & 4 ARE FULL OF FINES TRIED CLEARING 4 OUT WILL GET HALF OF IT OUT.
CVO2 LANYARD TRIP, BIG MOTHERS ON CVO2, SEEM OK NOW,
PRETTY GOOD RUN, JUST CONTROLLING WATER S.P. AT FRONT,

ernoon Shift

NPM24

Figure D.18: Module 1 Shift Communication Book Sheet - 16 October 1997